Theoretical Studies of Unconventional Order in Quantum Many-Particle Systems

Kjetil Børkje

PhD Thesis

NTNU
Norwegian University of
Science and Technology

Preface

This PhD thesis is based on four research articles within the field of condensed matter theory, specifically noncentrosymmetric and high-temperature superconductors. I have made significant contributions to all the articles in all parts of the process, *i.e.* initiating projects, performing calculations and writing articles. The work has been performed at the Norwegian University of Science and Technology (NTNU). My supervisor has been Professor Asle Sudbø, NTNU.

Kjetil Børkje,
Trondheim, January 2008

List of Articles

Article I

K. Børkje and A. Sudbø,

Tunneling between noncentrosymmetric superconductors with significant spin-orbit splitting studied theoretically within a two-band treatment,

Physical Review B **74** 054506 (2006) [cond-mat/0605575]

Tunneling between noncentrosymmetric superconductors with significant spin-orbit splitting is studied theoretically in a two-band treatment of the problem. We find that the critical Josephson current may be modulated by changing the relative angle between the vectors describing absence of inversion symmetry on each side of the junction. The presence of two gaps also results in multiple steps in the quasiparticle current-voltage characteristics. We argue that both these effects may help to determine the pairing states in materials like $CePt_3Si$, UIr, and $Cd_2Re_2O_7$. We propose experimental tests of these ideas, including scanning tunneling microscopy.

Article II

K. Børkje,

Using Josephson junctions to determine the pairing state of superconductors without crystal inversion symmetry,

Physical Review B **76**, 184513 (2007) [0708.3169]

Theoretical studies of a planar tunnel junction between two superconductors with antisymmetric spin-orbit coupling are presented. The half-space Green's function for such a superconductor is determined. This is then used to derive expressions for the dissipative current and the Josephson current of the junction. Numerical results are presented in the case of the Rashba spin-orbit coupling, relevant to the much studied compound $CePt_3Si$. Current-voltage diagrams, differential conductance and the critical Josephson current are presented for different crystallographic orientations and different weights of singlet and triplet components of the pairing state. The main conclusion is that Josephson junctions with different crystallographic orientations may provide a direct connection between unconventional pairing in superconductors of this kind and the absence of inversion symmetry in the crystal.

Article III

K. Børkje, S. Kragset and A. Sudbø,

Instanton correlators and phase transitions in two- and three-dimensional logarithmic plasmas,

Physical Review B **71**, 085112 (2005) [cond-mat/0412281]

The existence of a discontinuity in the inverse dielectric constant of the two-dimensional (2D) Coulomb gas is demonstrated on purely numerical grounds. This is done by expanding the free energy in an applied twist and performing a finite-size scaling analysis of the coefficients of higher-order terms. The phase transition, driven by unbinding of dipoles, corresponds to the Kosterlitz-Thouless transition in the 2D XY model. The method developed is also used for investigating the possibility of a Kosterlitz-Thouless phase transition in a three-dimensional system of point charges interacting with a logarithmic pair-potential, a system related to effective theories of low-dimensional strongly correlated systems. We also contrast the finite-size scaling of the fluctuations of the dipole moments of the two-dimensional Coulomb gas and the three-dimensional logarithmic system to those of the three-dimensional Coulomb gas.

Article IV

K. Børkje and A. Sudbø,

Effective theory of fluctuating orbital currents in high-T_c cuprates,

preprint (2007)

We derive an effective dissipative quantum field theory for fluctuating orbital currents in clean CuO_2 sheets of high-T_c cuprates, based on a three-band model. The Coulomb repulsion term between Cu- and O-sites is decoupled in terms of current operators representing horizontal and vertical parts of circulating currents within each CuO_2 unit cell of the lattice. The model has ordering of currents at finite temperatures. The dissipative kernel in the model is of the form $|\omega|/|\mathbf{q}|$, indicating Landau damping. Applications of the effective theory to other models are also discussed.

Acknowledgements

Many people deserve credit for making me able to achieve a PhD. First and foremost, I would like to thank my supervisor, Asle Sudbø. I am grateful that he gave me the opportunity to start a PhD study. He has also taught me a great deal about phase transitions and critical phenomena, as well as how to attack complicated physics problems in general.

I would also like to thank Professors Zlatko Tešanović, Mats Wallin and Kåre Olaussen for their willingness to serve on my evaluation committee.

In the period of my PhD study, I have been part of a research group with several other PhD students and postdocs, whose help can not be overestimated. I thank Steinar Kragset for a very nice collaboration concerning one of the articles, and for introducing me to Monte Carlo simulations. The former group members Joakim Hove, Jo Smiseth and Eivind Smørgrav deserve credit for always being helpful and answering questions from a fresh group member. I have also enjoyed useful discussions with fellow PhD students Eskil K. Dahl, Martin Grønsleth and Jacob Linder and some amusing conversations with Egor Babaev.

A PhD study involves a lot of frustration and disappointment at the office. However, it was great to be able to take a break from work now and then to enjoy dangerously strong coffee as well as discussions on everything under the sun. In addition to the group members mentioned above, I thank Jan Petter Morten, Anh Kiet Nguyen, Mathieu Taillefumier, Lars Erik Walle, Daniel Huertas-Hernando, Stein Olav Skrøvseth, Terje Røsten, Jan Øystein Haavig Bakke, Christian Andresen, Thomas Ramstad, Henrik Tollefsen and many others for a very pleasant work environment. I have also had a lot of fun with many of them outside the university. Terje and Martin deserve credit for always coming to the rescue whenever I wanted to destroy my computer. Eskil, Terje and Mathieu are also thanked for proofreading this thesis.

I thank other friends outside the physics department for great moments in my spare time. In particular, I would like to thank Odd Marius Aakervik for some memorable years in Elvegata 16.

I have enjoyed several trips to conferences and workshops during the last couple of years, in particular the Nordforsk network meetings on low-dimensional physics. In the summer of 2007, I spent one month at the Centre for Advanced Study at The Norwegian Academy of Science and Letters. I thank the helpful staff there for making it a very pleasant experience.

Finally, I would like to express my gratitude to my parents and the rest of my family, for their unconditional love and support.

Table of Contents

1 Introduction

Newton's law of gravity states that the gravitational force on the Earth from the Sun is proportional to the square of the inverse distance between them. Given this, it is quite easy to describe the motion of the Earth around the Sun. It is what we in physics call a two-body system. However, the moment we include the Moon, we are in trouble. Already in the case of three objects, we have a very complicated problem at our hands.

In a metal, the objects we need to describe are interacting electrons and ions. The number of such particles in a lump of metal is beyond comprehension. For historical reasons, we often compare it to the number of atoms in 12 grams of carbon, which is $6,02 \cdot 10^{23}$. Had the exponent been 22 or 24, it would be just as incomprehensible. Given that we have trouble describing three interacting objects, the task seems insurmountable at first sight. However, we are fortunately not interested in a detailed description of every single electron and ion. We are interested in properties of the system at large, the macroscopic properties. This enables the use of statistical methods to describe such a many-particle system.

A very successful concept in the description of electrons in metals is the Fermi liquid theory, developed by the prominent Soviet physicist Lev D. Landau. The essential idea is that the system of interacting particles conspire to behave as a system of noninteracting particles, called quasiparticles. There are however cases where this picture breaks down. Superconductivity, where the electrical resistance of a material disappears, is one such case. In superconductors, the interactions between electrons lead to a state which has no counterpart in a noninteracting system.

In a superconducting material, electrons form pairs which all behave in the same way. Superconductivity is an example of what we call an ordered state. Another example of an ordered state is ferromagnetism. In a ferromagnet, the intrinsic magnetic moments of the electrons tend to point in the same direction due to interactions. The result is a macroscopic magnetisation. In general, an ordered state is characterised by some sort of systematic behaviour of the interacting objects.

This thesis is based on four research articles, which are all related to the effect of interactions in electron systems. The topic of Article I and II is unconventional superconducting states in a recently discovered class of materials, called noncentrosymmetric superconductors. Article III and IV are related to the high-temperature superconducting cuprates, which has been devoted enormous attention since their discovery in 1986. These materials display unusual properties, also in the phase where they are not superconducting. In Article III and IV, different types of order in the nonsuperconducting phase of these systems are investigated.

The thesis is organised as follows: In Chapter 2, a brief review of basic concepts is presented, with emphasis on topics central to the following chapters and the articles. Chapter 3 provides a concise introduction to superconductivity, where the BCS theory is of special importance. The field of noncentrosymmetric superconductors is introduced in Chapter 4, central to Article I and II of this thesis. Finally, Chapter 5 deals with high-temperature superconducting cuprates, and details concerning Article III and IV.

2 General Concepts

In this chapter, we briefly introduce concepts that are central to the articles presented in this thesis. The subjects introduced are comprehensive and the presentation given here is in no way meant to be a substitute for textbooks. It should rather be viewed as a brief reminder for the already experienced theoretical physicist. Reference to more extensive literature will be given when appropriate.

2.1 Second Quantisation

The most common introduction to quantum mechanics is through the Schrödinger equation, a partial differential equation whose solution is the wavefunction for the system in question. When describing a quantum many-particle system, it is convenient to abandon the language of wavefunctions and differential operators. It is more useful, and sometimes even necessary, to describe the state of the system in an occupation number representation. The operators are then expressed in the so-called second quantised representation. In this section, we will focus on how to move from the description in terms of wavefunctions to the second quantised formalism. The books by Gross *et al* [1], Mahan [2], Negele & Orland [3] or Mandl & Shaw [4] are recommended literature on this subject.

In nonrelativistic quantum mechanics, a single, massive particle in a time-independent, external potential $V_{\text{ext}}(\boldsymbol{r})$ is described by the time-independent Schrödinger equation

$$\left(\frac{\hat{\boldsymbol{p}}^2}{2m} + V_{\text{ext}}(\boldsymbol{r}) \right) \psi_\lambda(\boldsymbol{r}) = \varepsilon_\lambda \, \psi_\lambda(\boldsymbol{r}), \tag{2.1}$$

where m is the mass of the particle and the momentum operator is $\hat{\boldsymbol{p}} = -\mathrm{i}\hbar\nabla$. The solution to this partial differential equation, given proper boundary conditions, provides a description of the system in terms of wavefunctions $\psi_\lambda(\boldsymbol{r})$ corresponding to the energy levels

ε_λ. The wavefunctions are characterised by λ, representing a set of quantum numbers. The wavefunctions constitute a complete set in the single-particle Hilbert space.

We now move on to a system of several identical particles, focusing on fermions. Let us consider a system of N electrons in an external potential, interacting through a Coulomb potential.[1] We neglect the spin degrees of freedom for the moment. The Schrödinger equation becomes

$$\left[\sum_{k=1}^{N}\left(\frac{\hat{\boldsymbol{p}}_k^2}{2m}+V_{\text{ext}}(\boldsymbol{r}_k)\right)+\sum_{k,l,k\neq l}V_{\text{int}}(|\boldsymbol{r}_k-\boldsymbol{r}_l|)\right]\Psi(\boldsymbol{r}_1,\boldsymbol{r}_2,\ldots,\boldsymbol{r}_N)=E\,\Psi(\boldsymbol{r}_1,\boldsymbol{r}_2,\ldots,\boldsymbol{r}_N), \tag{2.2}$$

where the Coulomb interaction is proportional to the inverse distance between two particle coordinates, $V_{\text{int}}(|\boldsymbol{r}_k-\boldsymbol{r}_l|)\sim|\boldsymbol{r}_k-\boldsymbol{r}_l|^{-1}$. Solving this equation analytically and determining the many-particle wavefunction $\Psi(\boldsymbol{r}_1,\boldsymbol{r}_2,\ldots,\boldsymbol{r}_N)$ is in general not possible. However, we know that $\Psi(\boldsymbol{r}_1,\boldsymbol{r}_2,\ldots,\boldsymbol{r}_N)$ may be expressed as a linear combination of so-called Slater-determinants $\Phi_{\lambda_1,\lambda_2,\ldots,\lambda_N}(\boldsymbol{r}_1,\boldsymbol{r}_2,\ldots,\boldsymbol{r}_N)$, since they form a complete basis for the N-particle Hilbert space. An important point is that these Slater-determinants are expressed solely by the single-particle wavefunctions $\psi_\lambda(\boldsymbol{r})$, given a choice of quantum numbers. They are antisymmetric when interchanging two of its arguments. This reflects the Pauli principle, which states that two or more fermions can not occupy the same single-particle quantum state.

In Dirac's general formulation of quantum mechanics, a quantum mechanical state may be described by a state vector $|\lambda\rangle$, characterised by the quantum numbers λ. The wavefunction $\psi_\lambda(\boldsymbol{r})=\langle\boldsymbol{r}|\lambda\rangle$ is the projection of this state onto the eigenvectors of the position operator. The Slater determinants can equivalently be characterised by the state $|\lambda_1,\lambda_2,\ldots,\lambda_N\rangle$, where λ_k is the set of quantum numbers characterising the single-particle state occupied by particle k. The Slater determinants are then $\Phi_{\lambda_1,\lambda_2,\ldots,\lambda_N}(\boldsymbol{r}_1,\boldsymbol{r}_2,\ldots,\boldsymbol{r}_N)=\langle\boldsymbol{r}_1,\boldsymbol{r}_2,\ldots,\boldsymbol{r}_N|\lambda_1,\lambda_2,\ldots,\lambda_N\rangle$.

Next, we introduce the occupation number representation. Let us enumerate[2] the quantum number sets by an upper index, λ^i. If the number of particles occupying the single-particle state with quantum numbers λ^i is n, we denote this n_i. For fermions, n can only take the values 0 or 1. If the single-particle state with quantum numbers λ^i is occupied, we write $|\lambda^i\rangle=|1_i\rangle$. If the state is unoccupied, we write $|0_i\rangle$. In addition, we now let $i_k\equiv\lambda_k^i$ denote that particle k is in the quantum state characterised by the quantum number set λ^i. Consider the example of $N=4$ particles and the Slater-determinant represented by the quantum number sets $|1_1,3_2,4_3,6_4\rangle$. In the occupation-number representation, we write this state as $|1_1,0_2,1_3,1_4,0_5,1_6,0_7,0_8,\ldots.\rangle$, where all occupation numbers not written

[1] We treat the electromagnetic field as classical and assume that we can treat the Coulomb interaction as instantaneous.

[2] The enumeration procedure is arbitrary. Here, we assume that the quantum numbers are countable, but the formalism presented is also applicable to the case of continuous quantum numbers.

explicitly are zero. This representation in terms of so-called Fock states may be used for different particle numbers N.

We will now define operators, c_i and $c_i^\dagger$, that provide a mapping between Slater-determinants of different particle numbers. In the occupation number representation, we define

$$\begin{aligned} c_i \left|n_1, n_2, \ldots, 1_i, \ldots\right\rangle &= (-1)^{\sum_{j<i} n_j} \left|n_1, n_2, \ldots, 0_i, \ldots\right\rangle \\ c_i \left|n_1, n_2, \ldots, 0_i, \ldots\right\rangle &= 0 \\ c_i^\dagger \left|n_1, n_2, \ldots, 1_i, \ldots\right\rangle &= 0 \\ c_i^\dagger \left|n_1, n_2, \ldots, 0_i, \ldots\right\rangle &= (-1)^{\sum_{j<i} n_j} \left|n_1, n_2, \ldots, 1_i, \ldots.\right\rangle. \end{aligned} \tag{2.3}$$

The operators $c_i^\dagger$ and c_i are called *creation and annihilation operators*, respectively, since their effect is to increase or decrease the number of particles by one. From the above properties, one can deduce the important anticommutation relations for fermionic operators,

$$\{c_i, c_j\} = 0 \ , \quad \{c_i^\dagger, c_j^\dagger\} = 0 \ , \quad \{c_i, c_j^\dagger\} = \delta_{i,j} \, , \tag{2.4}$$

where the anticommutator is defined as $\{A, B\} = AB + BA$ and $\delta_{i,j}$ is the Kronecker delta.[3] Similar relations exist for bosonic fields, with the important difference that the anticommutators are replaced by commutators. Note also that $c_i^\dagger c_i \left|n_1, \ldots, n_i, \ldots\right\rangle = n_i \left|n_1, \ldots, n_i, \ldots\right\rangle$, *i.e.* the operator $c_i^\dagger c_i$ is the number operator for the single-particle quantum state characterised by i.

Equation (2.2) contains a differential operator, the Hamiltonian, acting on a multivariate wavefunction $\Psi(\boldsymbol{r}_1, \boldsymbol{r}_2, \ldots, \boldsymbol{r}_N)$. So far, we have argued that the many-particle state can be represented in a different basis, namely occupation number states. In this new basis, the Hamiltonian is not a differential operator, but can be expressed in terms of the creation and annihilation operators. The result is often referred to as *second quantisation* representation of the operators.

From the single-particle Schrödinger equation (2.1), multiplying by $\psi_\lambda^*(\boldsymbol{r})$ and integrating over $\boldsymbol{r}$, one finds

$$\varepsilon_i = \int \mathrm{d}\boldsymbol{r} \, \psi_i^*(\boldsymbol{r}) \, \hat{h}(\boldsymbol{r}) \, \psi_i(\boldsymbol{r}) \ , \tag{2.5}$$

where $\hat{h}(\boldsymbol{r}) = (2m)^{-1} \hat{\boldsymbol{p}}^2 + V_{\text{ext}}(\boldsymbol{r})$ is the single-particle energy operator or Hamiltonian in the basis of position eigenvectors. Equation (2.5) can also be written as

$$\varepsilon_i = \int \mathrm{d}\boldsymbol{r} \int \mathrm{d}\boldsymbol{r}' \, \langle i|\boldsymbol{r}\rangle \langle \boldsymbol{r}|\hat{h}|\boldsymbol{r}'\rangle \langle \boldsymbol{r}'|i\rangle \ , \tag{2.6}$$

where

$$\langle \boldsymbol{r}|\hat{h}|\boldsymbol{r}'\rangle \equiv \hat{h}(\boldsymbol{r}) \, \delta(\boldsymbol{r} - \boldsymbol{r}') \ . \tag{2.7}$$

[3] For continuous quantum numbers, the Kronecker delta is replaced by the Dirac delta distribution.

Exploiting the completeness relation for the position eigenvector basis, one finds

$$\varepsilon_i = \langle i|\hat{h}|i\rangle \ . \tag{2.8}$$

By using the properties of the creation and annihilation operators as well as $|i\rangle = |1_i\rangle$, one can check that $\hat{h} = \sum_i \varepsilon_i c_i^\dagger c_i$ satisfies relation (2.8). This example indicates the criterion for finding the representation of operators in the second quantised formalism, namely that we must require expectation values to be unchanged.

The operator $\sum_{k=1}^N \hat{h}(\boldsymbol{r}_k)$, which is the first term in the many-particle Equation (2.2), is an example of a single-particle operator. It does not couple the coordinates of different particles, but acts on only one particle at the time. In general, for any single-particle operator $\sum_{k=1}^N \hat{T}(\boldsymbol{r}_k)$, the corresponding second quantised representation is

$$\hat{T} = \sum_{i,j} \langle i|\hat{T}|j\rangle \, c_i^\dagger c_j \ , \ \langle i|\hat{T}|j\rangle \equiv \int \mathrm{d}\boldsymbol{r} \, \psi_i^*(\boldsymbol{r}) \, \hat{T}(\boldsymbol{r}) \, \psi_j(\boldsymbol{r}). \tag{2.9}$$

In the above example, we used a choice of quantum numbers where the single-particle Hamiltonian $\hat{h}$ was diagonal. We may also choose quantum numbers where it is not diagonal, and the second quantised representation is then given by Equation (2.9).

The second term in Equation (2.2), the Coulomb interaction, is a two-particle operator, since each term connects two particle coordinates. The operator in the position eigenvector basis can be written $\sum_{k,l,k\neq l} V_{\mathrm{int}}(|\boldsymbol{r}_k - \boldsymbol{r}_l|)$. The corresponding second quantised representation is

$$\hat{V}_{\mathrm{int}} = \sum_{i,j,m,n} \langle i,j|\hat{V}_{\mathrm{int}}|m,n\rangle \, c_i^\dagger \, c_j^\dagger \, c_m \, c_n \tag{2.10}$$

where

$$\langle i,j|\hat{V}_{\mathrm{int}}|m,n\rangle \equiv \int \mathrm{d}\boldsymbol{r} \int \mathrm{d}\boldsymbol{r}' \psi_i^*(\boldsymbol{r}) \, \psi_j^*(\boldsymbol{r}') \, V_{\mathrm{int}}(|\boldsymbol{r} - \boldsymbol{r}'|) \, \psi_m(\boldsymbol{r}) \, \psi_n(\boldsymbol{r}'). \tag{2.11}$$

This is valid for any two-particle operator. One could also imagine higher order operators, but two-particle operators are of most importance in the field of condensed matter theory.

We thus have a recipy for presenting operators corresponding to physical quantities in terms of creation and annihilation operators acting on occupation number states. We have looked at the example of electrons in an external field interacting through a Coulomb potential. However, this procedure of second quantisation representation applies to more general models. We could for instance have included interaction with ions, relevant for describing the physics of solid state materials, or chosen to quantise the electromagnetic field. In all cases, one ends up with a Hamiltonian expressed in terms of fermionic and/or bosonic creation and annihilation operators.

This formalism is relevant not only to condensed matter theory, but is also used in other areas, primarily in elementary particle physics. The formalism is particularly useful in systems where the number of particles is not conserved, or in cases where a description in terms of wavefunctions simply does not exist.

2.2 Statistical Physics

Statistical physics provides the connection between observable, macroscopic properties of a many-particle system and its microscopic constituents. A comprehensive introduction to this field is given by Landau & Lifshitz [5]. The book by Negele & Orland can also be recommended [3].

2.2.1 Classical Statistical Mechanics

In classical statistical mechanics, the probability distribution of the microscopic configurations $\{\psi\}$ of a system of N particles is given by the Boltzmann factor,

$$p_\psi = \frac{\mathrm{e}^{-\beta(H-\mu N)}}{Z} \ , \tag{2.12}$$

where the Hamiltonian H is the energy of the configuration ψ and $\beta = 1/k_\mathrm{B}T$ is proportional to the inverse temperature. The parameter μ is the chemical potential. The *partition function*

$$Z = \sum_{\{\psi\}} \mathrm{e}^{-\beta(H-\mu N)} \tag{2.13}$$

serves here as a normalisation constant. The partition function is however very important, since all thermodynamical quantities can be determined from it. One example is the free energy $F = -k_\mathrm{B}T \ln Z$. The free energy is an important quantity, since the free energy is minimal in an equilibrium system with constant volume and at constant temperature.

The expectation value of a general physical quantity O is

$$\langle O \rangle = \frac{1}{Z} \sum_{\{\psi\}} O \, \mathrm{e}^{-\beta(H-\mu N)}. \tag{2.14}$$

The sums in equations (2.13) and (2.14) run over all microscopic degrees of freedom. For example, in a classical gas the sums symbolise integrals over the momentum and position of every individual particle. In the case of a grand canonical ensemble, *i.e.* a system where the number of particles is not conserved, the sum also runs over all particle numbers N.

2.2.2 Quantum Statistical Mechanics

In a quantum mechanical system, the partition function is defined by

$$Z = \sum_n \langle \Psi_n | \mathrm{e}^{-\beta\left(\hat{H}-\mu\hat{N}\right)} | \Psi_n \rangle \equiv \mathrm{Tr} \left[\mathrm{e}^{-\beta\left(\hat{H}-\mu\hat{N}\right)} \right], \tag{2.15}$$

where the Hamiltonian $\hat{H}$ is now an operator and $|\Psi_n\rangle$ is an arbitrary choice of basis states. All thermodynamical quantities can still be derived from the partition function. The expectation value of a general operator is

$$\langle\hat{O}\rangle = \frac{1}{Z}\sum_n \langle\Psi_n|\hat{O}\,\mathrm{e}^{-\beta\left(\hat{H}-\mu\hat{N}\right)}|\Psi_n\rangle = \frac{1}{Z}\mathrm{Tr}\,\left[\hat{O}\,\mathrm{e}^{-\beta\left(\hat{H}-\mu\hat{N}\right)}\right]. \tag{2.16}$$

Consider a system where the number of particles is fixed and let us assume that we have chosen a basis in which the Hamiltonian is diagonal, *i.e.* $\hat{H}|\Psi_n\rangle = E_n|\Psi_n\rangle$.[4] In that case, Equation (2.16) becomes

$$\langle\hat{O}\rangle = \frac{1}{Z}\sum_n \langle\Psi_n|\hat{O}|\Psi_n\rangle\,\mathrm{e}^{-\beta(E_n-\mu N)}\,. \tag{2.17}$$

At the temperature $T = 0$, which corresponds to $\beta \to \infty$, the leading term in this sum, as well as in the partition function, is the one with lowest energy E_0. This is the energy of the ground state of the system. Thus, the expectation value of an operator at zero temperature becomes

$$\langle\hat{O}\rangle \overset{T=0}{=} \langle\Psi_0|\hat{O}|\Psi_0\rangle, \tag{2.18}$$

simply the quantum mechanical expectation value in the ground state. In systems where there is an energy gap Δ between the ground state and excited states, this relation can also be extended to finite temperatures $k_\mathrm{B}T \ll \Delta$.

2.3 Functional Integral Formulation

A very useful tool when studying quantum many-particle systems is the formulation of the statistical mechanics problem in terms of functional integrals. We will not go into the details of how to achieve this here, but the reader is referred to the book by Negele & Orland [3]. In brief, it enables us to express the partition function (2.15) and expectation values (2.16) as functional integrals over complex variables in the case of bosonic particles or anticommuting Grassman variables in the case of fermionic particles.

The formalism comes about by recognising that the factor $\mathrm{e}^{-\beta\left(\hat{H}-\mu\hat{N}\right)}$ can be viewed as an evolution operator in imaginary time. This can be realised by performing an analytic continuation of the Feynman path integral to imaginary time, through the variable transformation $\tau = \mathrm{i}t$. Furthermore, for Hamiltonians in the second quantised representation, it is convenient to choose coherent states as basis vectors in (2.15). Coherent states $|\phi_i\rangle$ are eigenvectors of the annihilation operator, such that $c_i|\phi_i\rangle = \phi_i|\phi_i\rangle$. The eigenvalues are complex numbers in the case of bosons and Grassman numbers in the case of fermions.

[4] Such a basis always exist, although the actual determination of these basis vectors may not be possible in practice.

The result of this procedure is that the partition function in (2.15) can be written

$$Z = \int_{\phi_i(\beta)=\zeta\phi_i(0)} \mathcal{D}\left[\phi^*, \phi\right] \, \mathrm{e}^{-S[\phi^*,\phi]} \ , \tag{2.19}$$

where, formally

$$\int \mathcal{D}\left[\phi^*, \phi\right] \sim \prod_{i,\tau} \int \mathrm{d}\phi_i^*(\tau)\, \mathrm{d}\phi_i(\tau) \ , \tag{2.20}$$

and the functional $S[\phi^*, \phi]$ is

$$S[\phi^*, \phi] = \int_0^\beta \mathrm{d}\tau \ \left[\sum_i \phi_i^*(\tau) \left(\frac{\partial}{\partial \tau} - \mu \right) \phi_i(\tau) + H(\phi^*, \phi) \right] , \tag{2.21}$$

which is commonly referred to as the *action*. Still, β is proportional to the inverse temperature. The restrictions on the functional integral in (2.19) is given by $\zeta = 1$ in the case of bosons and $\zeta = -1$ for fermions. This means that the boundary conditions for the fields in the imaginary time direction is periodic for bosons and antiperiodic for fermions. In the case of a system of several types of particles, there will be one functional integral for each particle type. The Hamiltonian $H(\phi^*, \phi)$ is simply obtained from the second quantised, normal ordered $\hat{H}$ by replacing the creation and annihilation operators, $c_i^\dagger$ and c_i, by $\phi_i^*(\tau)$ and $\phi_i(\tau)$.

We should note that, for a d-dimensional quantum system, equation (2.19) has the form of the partition function for a classical system, but with an additional finite imaginary time dimension. At zero temperature, the additional dimension becomes infinite, since $\beta \to \infty$. Equation (2.19) may then be viewed as the partition function for a classical system in $d+1$ dimensions. This will be further commented on in Section 2.4.4.

2.3.1 The Hubbard-Stratonovich Decoupling

We will now introduce a technique which is helpful when describing systems of interacting fermions. A more detailed treatment can be found in Ref. [3].

Let us consider an example of an interacting fermion system, described by the second quantised Hamiltonian

$$\hat{H} = \hat{H}_0 + \hat{H}_\mathrm{I} = \sum_i \varepsilon_i \, c_i^\dagger \, c_i + \sum_{i,j,m,n} V_{i,j,m,n} \, c_i^\dagger \, c_j^\dagger \, c_m \, c_n \ . \tag{2.22}$$

The interactions are described by the last term, H_I. In the functional integral formulation, this term can be decoupled by using Gaussian integral identities, such that

$$Z \propto \int \mathcal{D}\left[\phi^*, \phi\right] \mathcal{D}\left[R^*, R\right] \, \mathrm{e}^{-S_0[\phi^*,\phi] - S_\mathrm{I}[\phi^*, \phi, R^*, R]} \ , \tag{2.23}$$

where[5]

$$S_0[\phi^*,\phi] = \int_0^\beta \mathrm{d}\tau \left[\sum_i \phi_i^*(\tau)\,(\partial_\tau - \mu)\,\phi_i(\tau) + H_0(\phi^*,\phi)\right] \tag{2.24}$$

and

$$S_{\mathrm{I}}[\phi^*,\phi,\,R^*,R] = \int_0^\beta \mathrm{d}\tau \left[\sum_{i,j,m,n} R_{i,j}^*(\tau)\,V_{i,m,j,n}^{-1}\,R_{m,n}(\tau) + \sum_{i,j}\left(R_{i,j}^*(\tau)\,\phi_j^*(\tau)\,\phi_i(\tau) + \phi_i^*(\tau)\,\phi_j(\tau)\,R_{i,j}(\tau)\right)\right]. \tag{2.25}$$

The boundary conditions in the imaginary time direction are antiperiodic for the ϕ-field and periodic for the R-field.

Having performed this decoupling, all terms containing the Grassman field ϕ are now quadratic. Of course, there is a price to pay for this. The theory now contains an additional complex field R. We can interpret Equation (2.23) as the partition function for fermions coupled to bosons, where neither the fermions nor bosons interact internally. Here, $R_{j,i}^*(\tau) = R_{i,j}(\tau)$ and $\langle R_{i,j}(\tau)\rangle = -\sum_{m,n} V_{m,i,n,j}\langle\phi_m^*(\tau)\,\phi_n(\tau)\rangle$.[6]

Since the action in (2.23) is quadratic in the fermionic field, the functional integral is Gaussian and can be performed. The result is

$$Z \propto \int \mathcal{D}\,[R^*,R]\ \mathrm{e}^{-S_{\mathrm{eff}}[R^*,R]}\ , \tag{2.26}$$

where the effective action is

$$S_{\mathrm{eff}} = \int_0^\beta \mathrm{d}\tau \left[\sum_{i,j,m,n} R_{i,j}^*(\tau)\,V_{i,m,j,n}^{-1}\,R_{m,n}(\tau) - \mathrm{Tr}\,\ln A(\tau)\right]. \tag{2.27}$$

The abbreviation Tr signifies a trace in the space of quantum numbers and the elements of the matrix A are

$$A_{i,j}(\tau) = [\partial_\tau + (\varepsilon_i - \mu)]\,\delta_{i,j} + R_{i,j}(\tau). \tag{2.28}$$

After the integration over the fermion fields, the theory is no longer quadratic in the field R. Equation (2.26) is thus the partition function for a system of interacting bosons.

To sum up, we have rewritten a theory of interacting fermions as a (complicated) theory of interacting bosons. There is however an important reason for doing this. The saddlepoint approximation is well-defined for integrals over complex numbers R, but has no meaning for

[5] H_0 will contain an additional term from the anticommuting of creation and annihilation operators. This term will ultimately cancel out in physical observables [3]. We neglect it in the following.

[6] This identity may be found from calculating the functional derivative of $\ln Z$ with respect to $(\phi_i^*(\tau)\phi_j(\tau))$ from both Equations (2.19) and (2.23).

integrals over Grassman variables ϕ. Thus, the theories (2.23) or (2.27) are good starting points for doing approximations, such as mean field theory, in cases where perturbation theory is of no use.

One should note that there are different ways of decoupling the interaction $\hat{H}_{\mathrm{I}}$. As long as the theories (2.23) or (2.27) are treated exactly, it does not matter how the interaction is decoupled. However, when approximations are introduced, this no longer holds. The choice of decoupling should then reflect the expected behaviour of the physical system.

2.3.2 Green's Functions

As stated in Section 2.2, thermodynamical quantities can be derived from the partition function Z. However, experiments often learn about physical systems by measuring the response to various external perturbations. A material can for example be studied by applying a voltage to the system, exposing it to electromagnetic radiation or neutron beams, or measuring its response to an external magnetic field. In general, the results of such measurements can be expressed in terms of so-called Green's functions. In quantum field theory, Green's functions are correlation functions of operators at different times.

The simplest example is the single-particle Green's function

$$\mathcal{G}(\lambda^1, t_1; \lambda^2, t_2) = \mathrm{i}\langle T_t \, c_1(t_1) \, c_2^\dagger(t_2)\rangle, \tag{2.29}$$

where T_t is the time-ordering operator. Here, $c_i(t)$ and $c_i^\dagger(t)$ are operators in the Heisenberg picture, where operators are time-dependent and states are time-independent. Specifically, $c_i(t) = \mathrm{e}^{\mathrm{i}\left(\hat{H}-\mu\hat{N}\right)t} \, c_i \, \mathrm{e}^{-\mathrm{i}\left(\hat{H}-\mu\hat{N}\right)t}$. At nonzero temperatures, it is also convenient to define the imaginary time Green's function,

$$\mathcal{G}(\lambda^1, \tau_1; \lambda^2, \tau_2) = -\langle T_\tau \, c_1(\tau_1) \, c_2^\dagger(\tau_2)\rangle, \tag{2.30}$$

where $c_i(\tau) = \mathrm{e}^{\left(\hat{H}-\mu\hat{N}\right)\tau} \, c_i \, \mathrm{e}^{-\left(\hat{H}-\mu\hat{N}\right)\tau}$. The real-time Green's function (2.29) can be obtained from (2.30) by analytic continuation from imaginary to real time.

In the functional integral formalism, the imaginary time, single-particle Green's function becomes

$$\mathcal{G}(\lambda^1, \tau_1; \lambda^2, \tau_2) = -\frac{1}{Z} \int \mathcal{D}\left[\phi^*, \phi\right] \, \phi_1(\tau_1) \, \phi_2^*(\tau_2) \, \mathrm{e}^{-S[\phi^*, \phi]} \, , \tag{2.31}$$

as the functional integral is automatically time-ordering. Again, ϕ_i is the eigenvalue of the annihilation operator in the coherent state basis. The boundary conditions in the imaginary time direction are still periodic for bosons and antiperiodic for fermions.

This method of calculating correlation functions is not restricted to the single-particle Green's function. Let $\hat{A}_i(\tau_i) = \mathrm{e}^{\left(\hat{H}-\mu\hat{N}\right)\tau_i} \hat{A}_i \mathrm{e}^{-\left(\hat{H}-\mu\hat{N}\right)\tau_i}$ be a general operator in the Heisenberg picture at the imaginary time τ_i. The operator can be expressed by the creation and

annihilation operators. A general time-ordered correlation function becomes

$$\langle T_\tau \hat{A}_1(\tau_1)\, \hat{A}_2(\tau_2) \cdots \hat{A}_n(\tau_n) \rangle = \frac{1}{Z} \int \mathcal{D}\left[\phi^*, \phi\right]\; A_1(\tau_1)\, A_2(\tau_2) \cdots A_n(\tau_n)\, \mathrm{e}^{-S[\phi^*,\phi]} \;, \qquad (2.32)$$

where $A_i(\tau_i)$ is obtained by replacing the creation and annihilation operators by their eigenvalues in the coherent basis.

It is often useful to move from a description in terms of τ to a description in terms of Matsubara frequencies, *i.e.* switch to a Fourier representation of the correlation functions. Consult for instance Refs. [2, 6] for details. For nonzero temperatures, the Matsubara frequencies take on discrete values. If we let n and ν denote integers, the Matsubara frequencies are $\omega_n = (2n+1)\pi/\beta$ for anticommuting (fermionic) fields, and $\omega_\nu = 2\nu\pi/\beta$ for periodic (bosonic) fields.

2.4 Phase Transitions

A phase transition is characterised by a sudden change in one or several properties of a physical system when varying a parameter. This parameter may be the temperature, but also other quantities such as pressure or magnetic field. Perhaps the most famous example of a phase transitions is the behaviour of H_2O at 0 °C, where water turns into ice and vice versa. In the strict mathematical sense, a phase transition is defined by a nonanalyticity in the partition function. From equation (2.13), where each term is analytic, it is evident that this can only occur in the limit of an infinite number of configurations, for example an infinite number of interacting particles. However, when the number of configurations becomes large enough, the behaviour of a finite physical system can be well described by the limit of an infinite system, named the *thermodynamic limit*. This limit thus provides a good description of macroscopic systems, such as a glass of water, which contains about 10^{25} H_2O molecules!

There is of course a lot more to be said about phase transitions than will be discussed here. The reader is referred to the textbooks by Landau & Lifshitz [5], Goldenfeld [7] and Anderson [8].

We will limit the discussion to scenarios where the phase transition separates an ordered and a disordered phase. A very important quantity is the *order parameter*, which is zero in the disordered phase and nonzero in the ordered phase. Examples are the magnetisation in a ferromagnet-paramagnet transition and structure functions in solid-liquid transitions. Most phase transitions fall into the categories first order transitions or continuous transitions.

2.4.1 First Order Transitions

A first order phase transition is characterised by the coexistence of two phases at the transition point. This means that the free energy of the ordered and the disordered system are the same at the transition point. One hallmark is that the order parameter drops discontinuously to zero at the transition point, as shown in the left panel of Figure 2.1. Latent heat is also a characteristic of first order transitions, which means that the system either releases or absorbs energy at the transition point. Equivalently, the specific heat capacity diverges as a delta distribution in the thermodynamic limit.

The solid-liquid transition is an example of a first order phase transition. Melting an ice cube requires addition of energy. The energy required is not only to increase the temperature of the ice cube, but one must also add a finite amount of energy at the melting point. The latter is the latent heat.

2.4.2 Continuous Transitions

In a continuous phase transition, the order parameter goes continuously to zero at the phase transition, as in the right panel of Figure 2.1. This class is sometimes referred to as second order phase transitions. The transition point does not feature a coexistence of phases like in the first order scenario. In this case, the ordered and disordered phases become indistinguishable at the transition point. The transition point is referred to as the *critical point*.

A characteristic feature of continuous transitions is the power law behaviour of various quantities close to the critical point. The singular part of the specific heat capacity c is determined by a number α, such that $c \sim |T - T_c|^{-\alpha}$, where T_c is the critical temperature, *i.e.* the temperature at which the phase transition occur. The number α is called a critical exponent. A number of critical exponents can be defined in a similar way for quantities like the order parameter, susceptibility and the correlation length. The critical exponents do not necessarily depend on microscopic details of a system, but depend strongly on the number of spatial dimensions and the symmetry of the order parameter. Consequently, several different systems may have the same set of critical exponents. Continuous phase transitions with the same set of critical exponents are said to belong to the same *universality class*.

At the critical point, the correlation length, which measures the range of correlations in the system, diverges. This divergence is important. It tells us that, at the critical point, the system features scale invariance, *i.e.* it looks similar on all length scales. This property is fundamental for the construction of the renormalisation theory [9], an important tool in the study of continuous phase transitions.

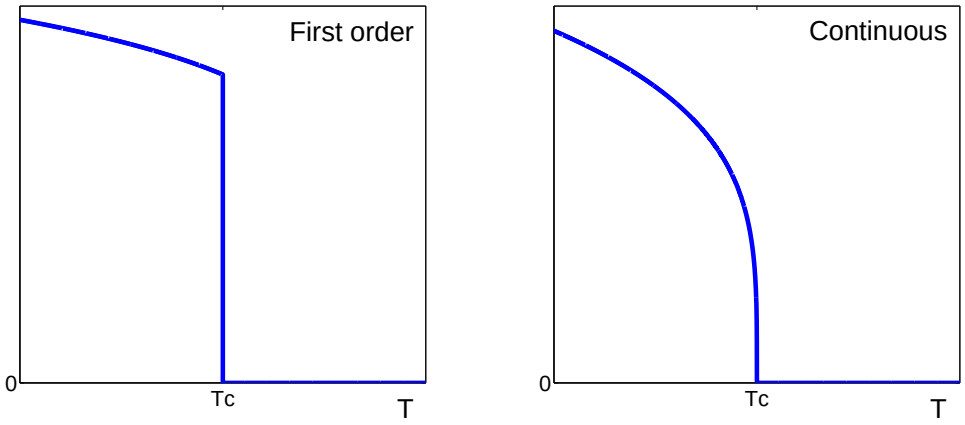

Figure 2.1: The behaviour of the order parameter at first order phase transitions and continuous phase transitions. T_c is the temperature at which the phase transition takes place. The order parameter is zero in the disordered phase above T_c.

A system that features this kind of phase transition is a uniaxial two-dimensional ferromagnet, which can be described by the two-dimensional Ising-model. This model is one of few which has been exactly solved, done by Lars Onsager in 1944 [10]. Experiments on layered materials show agreement with this solution [11].

2.4.3 The Berezinskii-Kosterlitz-Thouless Transition

An exotic phase transition which does not fall into the above two categories is the Berezinskii-Kosterlitz-Thouless transition [12, 13, 14]. We will go a bit into detail on this particular transition, as it is central in Chapter 5 and in Article III.

A model that features this phase transition is the two-dimensional XY-model, which is a two-dimensional model of interacting classical, two-component spins. In a continuum version, the Hamiltonian of this model is

$$H = -J \int \mathrm{d}\boldsymbol{r} \, \cos(\nabla\theta(\boldsymbol{r})) \, , \tag{2.33}$$

where $J > 0$ and the angle $\theta(\boldsymbol{r})$ describes the direction of the spin at coordinate $\boldsymbol{r}$. This model may for example describe the properties of a superfluid film, where the angle $\theta(\boldsymbol{r})$ is interpreted as the complex phase of the macroscopic superfluid wavefunction.

The order-disorder transition in this case can be characterised by the helicity modulus or spin stiffness. The helicity modulus measures the free energy increase due to an infinitesimal twist in the spins across the system. At the transition point, the helicity modulus drops discontinuously to zero. It is not a first order transition, however, since there is no

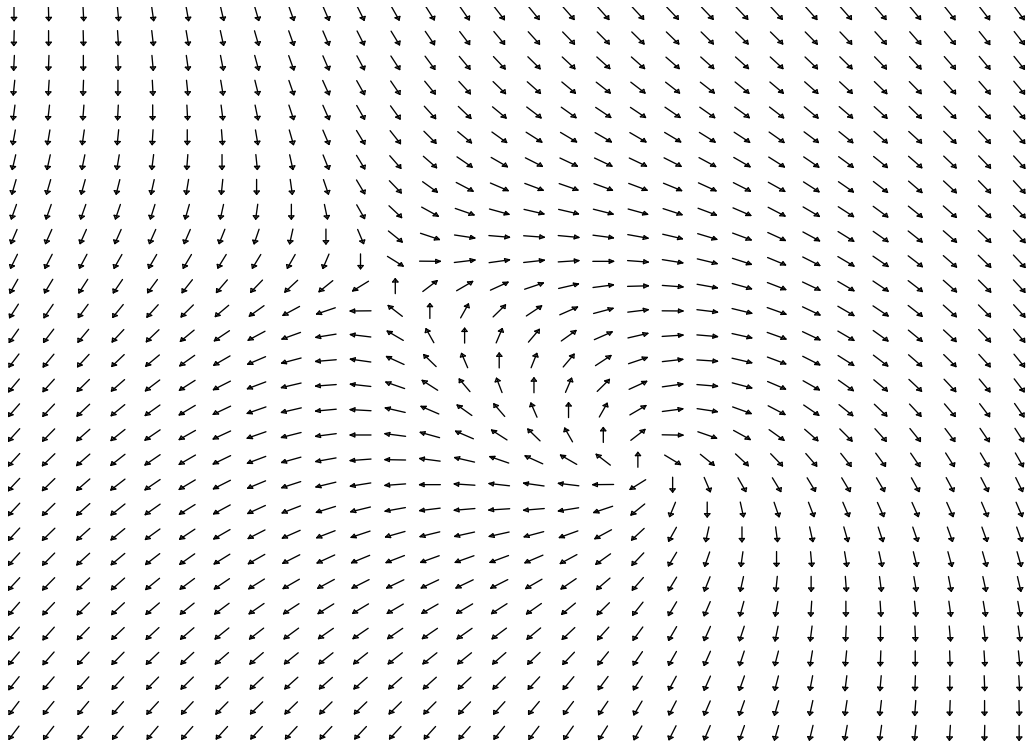

Figure 2.2: A vortex-antivortex pair in the two-dimensional XY-model. In a superfluid film, the direction of the arrows correspond to the complex phase θ of the macroscopic superfluid wavefunction.

latent heat involved. In fact, there is no divergence in the specific heat capacity. In the example of a superfluid film, the helicity modulus is proportional to the superfluid density of the system.

At low temperatures, it is energetically favourable for the spins or phases to more or less point in the same direction. The phase transition is associated with the proliferation of vortices, where the spins/phases spiral around a point. A vortex is defined by the value of the closed path integral

$$\oint \mathrm{d}\boldsymbol{l} \cdot \nabla\theta(\boldsymbol{r}) = 2\pi n \ , \tag{2.34}$$

where the integration path must encircle the centre of the vortex, but is otherwise arbitrary. The integer n characterise the "topological charge" of the vortex. If $n = 1$, we call it a vortex of charge one. If the charge is negative, *e.g.* $n = -1$, we call it an antivortex . An example of a vortex-antivortex pair is shown in Figure 2.2.

The two-dimensional XY-model can be mapped onto the two-dimensional Coulomb gas, which is a gas of point charges interacting through a logarithmic potential. The charges correspond to the vortices in the XY-model. The quantity corresponding to the helicity modulus is then the inverse dielectric constant ε^{-1}. In the low-temperature phase,

charges are bound in dipoles and ε^{-1} is nonzero, *i.e.* the system is dielectric. In the high-temperature phase, the charges are no longer bound in pairs and $\varepsilon^{-1} = 0$, such that the system has infinite polarisability.

As mentioned above, we will return to this type of phase transition in Chapter 5.

2.4.4 Quantum Phase Transitions

A quantum phase transition is a phase transition in a quantum mechanical system at zero temperature. Obviously, such transitions are not driven by a change in temperature, but in other quantitites such as pressure, an external magnetic field, or chemical composition (doping). For example, the high-temperature cuprate superconductors, to be discussed in Chapter 5, seem to exhibit several quantum phase transitions as the degree of doping is changed.

In Section 2.3, we saw that the partition function for a d-dimensional quantum system at zero temperature can be expressed as the partition function of a classical system in $d + 1$ dimensions. This suggests that all we need to do is employ our knowledge of classical phase transitions, only in one more dimension. There are however important reasons that make the study of quantum and classical phase transitions differ [15]. For instance, the imaginary time direction is in general different from the spatial directions, such that time and space scales differently under renormalisation [16]. Furthermore, it has recently been pointed out that a simple analogy to classical systems can break down in a number of important systems [17, 18].

In general, quantum phase transitions are at present not as well understood as their classical counterparts. It continues to be an active field of research and is relevant to a number of strongly correlated electron systems.

2.5 Monte Carlo Simulations

A brief mention of the subject of Monte Carlo simulations, which was used in Article III, is in order. For an introduction to this technique, see *e.g.* the treatment by Landau & Binder [19]. See also Ref. [20] and references therein.

In classical statistical mechanics, the expectation value of a quantity is given by Equation (2.14). As already mentioned, when describing phase transitions, we are interested in the limit of an infinite system. However, already for a modest number of degrees of freedom, the exact calculation of the sum in (2.14) is, in most cases, not possible.

In Monte Carlo integration, one randomly picks out a subset of the terms/configurations

entering this sum, and use them to approximate the expectation value. The concept of *importance sampling* is however central. In short, this ensures that the most important part of configuration space is favoured when picking terms, *i.e.* one picks from a nonuniform distribution. In classical statistical mechanics, this distribution can conveniently be chosen to equal the Boltzmann weight.

3 Superconductivity

A superconducting material displays the striking property of zero resistivity, which means that one can send an electric current through it without energy loss. This property was first observed in mercury (Hg) by Kammerlingh Onnes in 1911, at the very low temperature of 4.2 K ≈ -267 °C. It was later observed in a number of other simple metals, such as aluminium (Al), lead (Pb) and niobium (Nb). However, all these materials become superconducting at very low temperatures. Before 1986, it was believed that superconductivity was restricted to temperatures below about 30 K ≈ -243 °C. However, in 1986 Bednorz and Müller disproved this and broke the world record when observing superconductivity in a cuprate perovskite material. Such materials are now known as high-temperature superconducting cuprates, and are the subject of intense research activity. The world record for superconductivity at standard pressure is at present about 138 K ≈ -135 °C.

The study of a superconductor's response to a magnetic field, reported by Meissner and Ochsenfeld in 1933, showed that superconductivity is something more profound than simply a perfect metal. It is in fact a thermodynamical state, separated from the normal, metallic phase by a phase transition.

All the articles presented in this thesis are related to properties of superconducting materials, although not necessarily in the superconducting phase. It is therefore worthwhile to introduce some essential concepts in the field of superconductivity. For a more extensive introduction to the field, Refs. [21, 22, 23, 24] may be consulted.

3.1 Physical Properties

There are two physical properties which characterise a material in the superconducting state. First of all, the DC electrical resistivity of the material is zero. Secondly, the material is a perfect diamagnet, meaning that the material expels a magnetic field, except

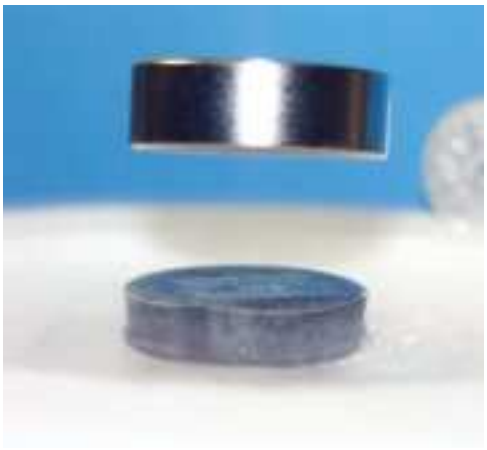

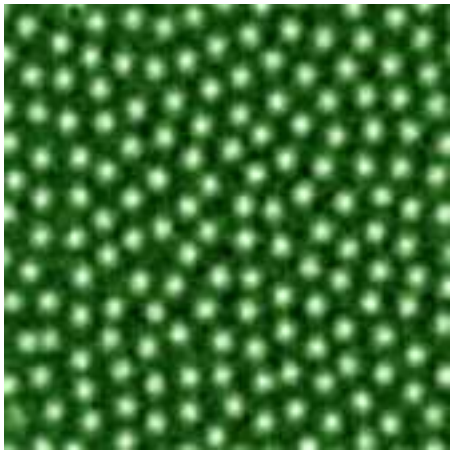

Figure 3.1: *Left panel:* A magnet levitates above a high-temperature superconductor due to the Meissner effect. *Right panel:* A magneto-optical image of vortices in the superconductor $NbSe_2$. The bright dots are places where the magnetic field penetrates the sample. *Credit: Superconductivity Laboratory, University of Oslo, http://www.fys.uio.no/super.*

in a very thin surface layer. This is called the *Meissner effect*. The thickness of the surface layer where the magnetic field is nonzero is called the London penetration depth.

When a material enters the superconducting phase, the electrical resistivity suddenly drops to zero. We should immediately note however, that one can never measure that something is exactly zero. One can nevertheless put bounds on the resistivity by measuring the decay of a current running around in a loop of superconducting material. In fact, the measured decay time indicates that such a current can persist longer than the estimated age of the universe [22], which is about 14 billion years.

The Meissner effect is also a striking property. The left panel of Figure 3.1 shows a picture of a magnet hovering/levitating above a piece of high-temperature superconductor. The superconductor does not allow the magnetic field from the magnet in its interior. This results in a force on the magnet from the superconductor, and hence the magnet levitates.

At a sufficiently large external magnetic field, the Meissner effect breaks down. Superconductors are divided into two categories depending on how this breakdown takes place. In the Type I superconductors, the Meissner effect disappears completely at a critical field H_c and the material is no longer superconducting. Examples from this category are Al and Hg. The scenario for Type II superconductors is however more complicated. At a magnetic field H_{c1}, the superconductor changes to a mixed state, where the magnetic field partially penetrates the material in the form of confined flux lines. At a higher magnetic field H_{c2}, the normal state is reached and the magnetic field penetrates the entire sample. Examples of Type II superconductors are Nb and all the high-temperature cuprates.

The magnetic flux lines in Type II superconductors form a so-called Abrikosov lattice. A

somewhat disordered example of such a lattice is shown in the right panel of Figure 3.1. The flux lines are surrounded by circulating currents, vortices, shielding regions where superconductivity is still intact.

3.2 BCS Theory

In 1957, a microscopic theory of superconductivity was presented by Bardeen, Cooper and Schrieffer [25], hence the name BCS theory. It was argued that the basis for superconductivity is that electrons form pairs, called *Cooper pairs*, due to an effective, *attractive* interaction between them. At low temperatures, the energy of the system is lowered by the Cooper pairs occupying the same two-particle quantum state, similar to the phenomenon of Bose-Einstein condensation.

An effective description of superconductivity had been formulated earlier by Ginzburg and Landau in 1950 [26]. It was based on a complex scalar function $\Psi(\boldsymbol{r})$. At a later stage, it was realised that the interpretation of $\Psi(\boldsymbol{r})$ is the two-particle quantum mechanical wavefunction of the Cooper pairs, where $\boldsymbol{r}$ is the centre of mass coordinate. In 1959, Gor'kov demonstrated the precise connection by deriving the effective Ginzburg-Landau theory from the microscopic BCS theory [27].

In a solid state material, the atoms in the crystal lattice are not completely static, but oscillates about an equilibrium position. In quantum mechanics, these vibrational modes of the lattice are quantised and referred to as phonons. The phonons may be thought of as unconserved, bosonic particles. The electrons moving around in the crystal will scatter off these vibrations, in what is referred to as the electron-phonon coupling.

The origin of effective attractions between electrons in conventional superconductors, such as Al or Pb, is this electron-phonon coupling. The distortion of the ion positions by an electron will affect another electron, which effectively can lead to attraction between the electrons.

There is of course another important source of *repulsive* interactions between electrons in a metal, namely the Coulomb repulsion. The effect of repulsive interactions in electron systems is however not necessarily as dramatic as one might expect. In most cases, the excitations of such an interacting system of fermions are very similar to free-particle excitations, only with a renormalised spectrum and lifetime. The explanation for this is called Landau's *Fermi liquid theory* [6]. The excitations are known as *quasiparticles*, which behave very similar to free electrons. The Fermi liquid theory does however not hold when the interactions are attractive. In that case, the interactions are singular perturbations to the noninteracting system, and their effects are dramatic.

The Hamiltonian considered by Bardeen, Cooper and Schrieffer was

$$\hat{H} - \mu\hat{N} = \sum_{\boldsymbol{k},\sigma} (\varepsilon_{\boldsymbol{k}} - \mu)\, c^\dagger_{\boldsymbol{k},\sigma}\, c_{\boldsymbol{k},\sigma} + \sum_{\boldsymbol{k},\boldsymbol{k}'} V(\boldsymbol{k},\boldsymbol{k}')\, c^\dagger_{-\boldsymbol{k},\downarrow}\, c^\dagger_{\boldsymbol{k},\uparrow}\, c_{\boldsymbol{k}',\uparrow}\, c_{-\boldsymbol{k}',\downarrow}\ , \tag{3.1}$$

The Hamiltonian is written down in the spirit of retaining only the important part of the interactions. The operators $c^\dagger_{\boldsymbol{k},\sigma}$ and $c_{\boldsymbol{k},\sigma}$ creates or annihilates fermionic quasiparticles, in the language of Fermi liquid theory. However, we will often refer to them as electron operators. The quantum numbers $\boldsymbol{k}$ and σ signify momentum and spin, respectively. In the absence of the last term, the energy μ separates the occupied states from the unoccupied states at zero temperature. This is called the Fermi energy.

The last term in (3.1) describes the scattering of a pair of particles from single-particle states with opposite momenta $\boldsymbol{k}$ and $-\boldsymbol{k}$ into another pair of states with momenta $\boldsymbol{k}'$ and $-\boldsymbol{k}'$. This process is governed by the negative matrix element $V(\boldsymbol{k},\boldsymbol{k}')$. Only pairs of states with opposite spin have been included here. This is sufficient in most superconductors, but extensions will be discussed below. Note that equation (3.1) applies also to other pairing mechanisms than phonons.

Bardeen, Cooper and Schrieffer found that the many-particle eigenstate of the above Hamiltonian is a coherent state, a product of linear combinations of occupied and unoccupied pairs of opposite momentum states. For more details on this point, and on BCS theory in general, Refs. [21, 28] are particularly recommended.

Next, we introduce the mean field approximation. One way to arrive at this is to Hubbard-Stratonovich decouple the interaction term in (3.1) in a particular way, and then apply the saddlepoint/mean field approximation to the auxiliary bosonic field. The result is

$$\hat{H} - \mu\hat{N} = \sum_{\boldsymbol{k},\sigma} (\varepsilon_{\boldsymbol{k}} - \mu)\, c^\dagger_{\boldsymbol{k},\sigma}\, c_{\boldsymbol{k},\sigma} + \sum_{\boldsymbol{k}} \left(\Delta_{\boldsymbol{k}}\, c^\dagger_{\boldsymbol{k},\uparrow}\, c^\dagger_{-\boldsymbol{k},\downarrow} + \Delta^*_{\boldsymbol{k}}\, c_{-\boldsymbol{k},\downarrow}\, c_{\boldsymbol{k},\uparrow} \right). \tag{3.2}$$

plus a constant term which we ignore. Here, the complex expectation value $\Delta_{\boldsymbol{k}} = -\sum_{\boldsymbol{k}'} V(\boldsymbol{k},\boldsymbol{k}')\langle c_{\boldsymbol{k}',\uparrow}\, c_{-\boldsymbol{k}',\downarrow}\rangle$ is known as the *pair potential* or the *gap function*. It should be determined self-consistently by demanding the free energy of the system to be minimised.

One can diagonalise[1] Equation (3.2) to obtain the spectrum of excitations of a superconductor, *i.e.* the energy spectrum above the ground state. The excitations of the system are fermionic particles and their energy spectrum is given by

$$E_{\boldsymbol{k}} = \sqrt{(\varepsilon_{\boldsymbol{k}} - \mu)^2 + |\Delta_{\boldsymbol{k}}|^2}\ . \tag{3.3}$$

We observe that even for momenta such that $\varepsilon_{\boldsymbol{k}} \sim \mu$, there is a gap $|\Delta_{\boldsymbol{k}}|$ between the Fermi energy and the excited states. In fact, a single-particle excitation, *i.e* a normal

[1] This is known as the Bogolyubov-Valatin transformation.

scattering process where one removes an electron from one particular single-particle state with momentum $\boldsymbol{k}$ and place it in another with momentum $\boldsymbol{k}'$, has a minimum energy cost of $|\Delta_{\boldsymbol{k}}| + |\Delta_{\boldsymbol{k}'}|$. The energy gap $|\Delta_{\boldsymbol{k}}|$ is actually the secret behind the property of zero resistivity in superconductors. Although we have not discussed the current-carrying state, where Cooper pairs have a nonzero net momentum, an *energy gap to excited states* is what protects the current from normal scattering processes and thus from dissipation.

The BCS theory also explains the Meissner effect, but we will not go into the details here. The short explanation is that an external magnetic field will induce surface currents in the material, creating a magnetic field that cancels the external field inside the material.

3.2.1 Singlet and Triplet Pairing

In the previous section, we assumed that the net momentum of a Cooper pair is zero. This is not necessarily the case in the presence of an external magnetic field or when the system is in a current-carrying state.[2] Consequently, the pair potential or gap function $\Delta_{\boldsymbol{k},\boldsymbol{q}}$ is in general not only a function of the relative momentum $\boldsymbol{k}$, but also on the net momentum $\boldsymbol{q}$. By Fourier transforming to real-space, the gap function would be $\Delta(\boldsymbol{r}_{\text{rel}}, \boldsymbol{r}_{\text{CM}})$, where $\boldsymbol{r}_{\text{CM}}$ is the centre of mass-coordinate. The gap function may be thought of as a two-particle quantum mechanical wave function.[3] When deriving the above mentioned Ginzburg-Landau theory, the relative coordinate is integrated out and one is left with a function of $\boldsymbol{r}_{\text{CM}}$ [6]. However, let us now assume that the total momentum of the Cooper pairs are zero, such that we can choose a coordinate system where $\boldsymbol{r}_{\text{CM}} = 0$ and thereby suppress this coordinate.

A two-particle wavefunction of two spin-1/2 particles is not only dependent on the coordinates of the particles, but also on their spin. In most cases, the wavefunction factorise into a product of a spatial part and a spin part, *i.e.* $\Psi(\boldsymbol{r}_1 - \boldsymbol{r}_2, \sigma_1, \sigma_2) = \phi(\boldsymbol{r}_1 - \boldsymbol{r}_2)\chi(\sigma_1, \sigma_2)$, where σ_i is the spin projection of particle i along a particular quantisation axis. Due to the Pauli principle, the wavefunction $\Psi(\boldsymbol{r}_1 - \boldsymbol{r}_2, \sigma_1, \sigma_2)$ must be antisymmetric when interchanging $(\boldsymbol{r}_1, \sigma_1)$ and $(\boldsymbol{r}_2, \sigma_2)$. Thus, if $\phi(\boldsymbol{r}_1 - \boldsymbol{r}_2)$ is symmetric, $\chi(\sigma_1, \sigma_2)$ must be antisymmetric, and vice versa. For the spin part, it is well known that there is one configuration which is antisymmetric, the *singlet* state with total spin $S = 0$, and three which are symmetric, the *triplet* states with total spin $S = 1$.

In Equation (3.1), we included only scattering of pairs with opposite spins. This is sufficient in most materials, where the Cooper pairs form spin singlets. In the case of spin singlets, the pair potential is an even function of the relative coordinate, which in momentum space means $\Delta_{-\boldsymbol{k}} = \Delta_{\boldsymbol{k}}$. However, spin triplet Cooper pairs are not only of academic interest. They appear in *superfluid* ^{3}He [28], and have recently been claimed observed in

[2] One can also imagine equilibrium situations where the Cooper pairs have nonzero momenta. See Refs. [29].

[3] We neglect the issue of normalisation here.

the superconductors UPt_3 [30] and Sr_2RuO_4 [31]. To include other types of pairing, one must consider a spin-generalised version of the BCS Hamiltonian [32, 33]. In the mean field approximation, it becomes

$$\hat{H} - \mu\hat{N} = \sum_{\boldsymbol{k},\sigma} (\varepsilon_{\boldsymbol{k}} - \mu)\, c^\dagger_{\boldsymbol{k},\sigma}\, c_{\boldsymbol{k},\sigma} + \frac{1}{2} \sum_{\boldsymbol{k},\sigma,\sigma'} \left(\Delta_{\boldsymbol{k},\sigma\sigma'}\, c^\dagger_{\boldsymbol{k},\sigma}\, c^\dagger_{-\boldsymbol{k},\sigma'} + \Delta^*_{\boldsymbol{k},\sigma\sigma'}\, c_{-\boldsymbol{k},\sigma'}\, c_{\boldsymbol{k},\sigma} \right). \quad (3.4)$$

The gap function is now a matrix in spin space. In the singlet case, the elements of this matrix may be expressed as $\Delta_{\boldsymbol{k},\sigma\sigma'} = g_{\boldsymbol{k}}(\mathrm{i}\sigma_y)_{\sigma\sigma'}$, where $g_{-\boldsymbol{k}} = g_{\boldsymbol{k}}$. For triplet pairing, the matrix elements can be written as $\Delta_{\boldsymbol{k},\sigma\sigma'} = \boldsymbol{d}_{\boldsymbol{k}} \cdot (\boldsymbol{\sigma}\, \mathrm{i}\sigma_y)_{\sigma\sigma'}$, where the vector $\boldsymbol{d}_{\boldsymbol{k}}$ has the property $\boldsymbol{d}_{-\boldsymbol{k}} = -\boldsymbol{d}_{\boldsymbol{k}}$. The vector $\boldsymbol{\sigma}$ consists of the three Pauli matrices.

In systems with spatial inversion symmetry, the gap function, *i.e.* the wavefunction of Cooper pairs, must have a definite spatial parity, which means either a spin singlet or spin triplet state [33]. This is also the case when spin-orbit coupling is important, but the pairing is then between so-called pseudospin states [32]. However, if spatial inversion symmetry is absent and spin-orbit coupling is present, the gap function no longer has a definite spatial parity. We will consider such systems in Chapter 4.

In an isotropic material, the functions $g_{\boldsymbol{k}}$ and $\boldsymbol{d}_{\boldsymbol{k}}$ can be expressed in terms of spherical harmonics $Y_{lm}(\hat{\boldsymbol{k}})$ [33]. The symmetry of the gap functions are usually designated by the orbital angular momentum number l. In the singlet case, l is even, whereas in the triplet case, l is odd. In analogy with atomic orbitals, these numbers are represented by letters, such that $l = 0$ is called s-wave, $l = 1$ is called p-wave, and $l = 2$ is d-wave. In an anisotropic crystal, $g_{\boldsymbol{k}}$ and $\boldsymbol{d}_{\boldsymbol{k}}$ may be expressed by irreducible representations of the point symmetry group of the crystal [33]. Nevertheless, the superconducting states are usually approximated by spherical harmonics. As mentioned before, most superconductors have singlet pairing. In the conventional superconductors such as aluminium, the gap is an anisotropic s-wave. Note that nonmagnetic impurities in the crystal can cause isotropisation of the gap [34]. The high-temperature cuprate superconductors also have singlet pairing, but the gap there is of d-wave nature [35]. The most famous example of a system with a p-wave pairing state is superfluid ^{3}He. Note that when the gap symmetry is different from s-wave, the size of the gap can be zero at special regions on the Fermi surface. Such regions are called *gap nodes*. If the region is simply a point, we call it a point node. If the region is a line, we call it a line node.

3.3 The Josephson Effects

Only five years after the breakthrough of BCS theory, Brian D. Josephson used the theory to study the charge transport between two superconductors separated by a thin, insulating layer [36]. The insulating layer acts as an energy barrier between the superconductors, but electrons can still pass from one side to the other by quantum mechanical tunnelling. A

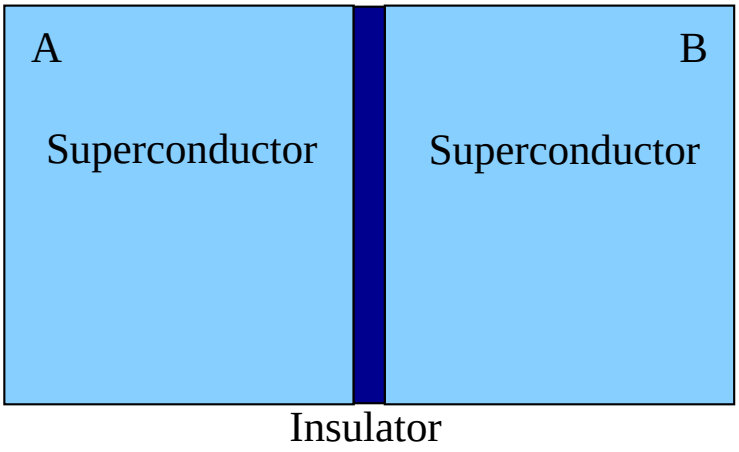

Figure 3.2: A schematic view of a Josephson junction. Two superconductors are separated by a thin, insulating layer. Note that this is only one of several ways to construct a weak link between two superconductors.

schematic view of the junction, now called a Josephson junction, is shown in Figure 3.2. Josephson predicted some astonishing effects, which were experimentally verified in the following years.

Let us briefly mention that in a similar junction between two normal metals, the current is typically proportional to the voltage. In the early 1960's, Giaever studied the current-voltage characteristics of junctions of one normal metal and one superconductor, and junctions of two superconductors [37]. These measurements directly probed the presence of an energy gap in the superconductors, and hence served as one of many verifications of BCS theory.

In order to appreciate the Josephson effect, one should remember that the Cooper pair wavefunction, $\Psi(\boldsymbol{r}) = |\Psi(\boldsymbol{r})|e^{i\theta(\boldsymbol{r})}$ in the language of Ginzburg and Landau, is a complex quantity. The superconducting state is characterised by macroscopic phase coherence, meaning that the variations in $\theta(\boldsymbol{r})$ are small over a large distance, called the phase coherence length. The value of this phase is dependent on the choice of coordinate system in the complex plane, which means that no observable quantity can depend on it alone. However, in the case of the Josephson junction of Figure 3.2, the *phase difference* between the superconductors, $\theta_B - \theta_A$, is not dependent on the choice of coordinate system.

Josephson's first prediction was that in the case of two superconductors, it is possible to send an electric current through the junction in the absence of a voltage difference between the two sides. This is known as the *DC Josephson effect*. The current depends on the above mentioned phase difference, such that

$$I = I_c \sin(\theta_B - \theta_A) \ . \tag{3.5}$$

The constant I_c is the critical or maximal Josephson current. This means that a current

of size I, where $I < I_c$, can flow through the junction without an applied voltage. This is called a supercurrent, since it is a dissipationless current of Cooper pairs. A very useful property of the DC Josephson current is that the critical current I_c is very sensitive to an external magnetic field, displaying a so-called Fraunhofer modulation pattern as the strength of the magnetic field is varied.

Josephson's second prediction was that, in the presence of an applied voltage V, the Cooper pair current would become alternating, with a frequency given by $f = eV/(\pi\hbar)$, where e is the electron charge and $\hbar$ the Planck constant. This is the *AC Josephson effect*. Such a high-frequency AC current would average out in a simple measurement of current and voltage, which would only show the dissipative, single-particle DC current. The effect was however experimentally verified by the use of microwave radiation.

The Josephson effects are very useful for doing very precise or very sensitive measurements. There is also a potential for utilising this effect in high-frequency electronics.

4 Superconductors without Crystal Inversion Symmetry

In Section 3.2.1, the symmetry properties of the superconducting gap function were discussed. In the conventional, spin singlet superconductors, such as aluminium and lead, the gap functions have s-wave symmetry. The high-temperature superconducting cuprates are also of spin singlet type, but with a d-wave symmetry of the gap function. Spin triplet pairing is more unusual, but is also realised in nature. The prime example of a system with triplet pairing is superfluid ^{3}He [28]. Later, triplet pairing states have been proposed to be relevant for so-called heavy-fermion superconductivity, first observed in 1979 in the material $CeCu_2Si_2$ [38]. The name heavy-fermion superconductors refers to the fact that the quasiparticles forming Cooper pairs have a strongly renormalised mass, which can be several orders of magnitude larger than the bare electron mass. The most promising candidate for displaying triplet pairing is the compound Sr_2RuO_4[31].

A complicating issue in the heavy-fermion superconductors compared to the ^{3}He system is the *spin-orbit coupling* due to the Coulomb potential from the crystal lattice [39, 40]. Spin-orbit coupling is a relativistic effect which couples orbital and spin degrees of freedom in the presence of an electric field. It is usually expected to be significant in compounds containing atoms with a high atomic number Z, which many of the heavy-fermion superconductors do.

When discussing spin-orbit coupling in superconductors, we will need to distinguish between crystals with and without a *centre of inversion*. Imagine that one mirrors the entire crystal through an arbitrary point. If the crystal structure looks the same, we say that the crystal has a centre of inversion or that it is centrosymmetric. If it looks different, we say that it lacks inversion symmetry and is noncentrosymmetric. A simple, two-dimensional example of a crystal without inversion symmetry is shown in Figure 4.1. Examples of materials where the noncentrosymmetric crystal structure is important are the ferroelectrics. In these materials, which are insulators, a phase transition where the inversion symmetry is

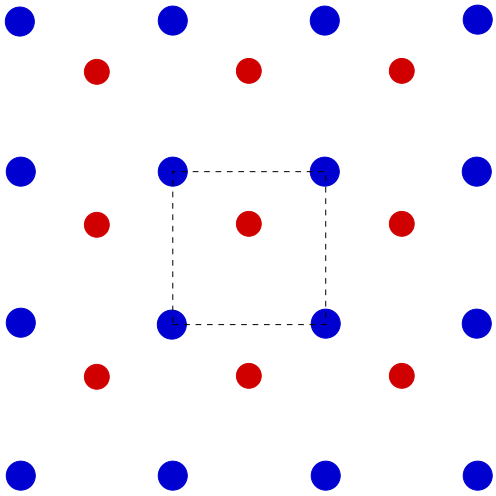

Figure 4.1: A simple, two-dimensional example of a noncentrosymmetric crystal lattice. One choice of unit cell is indicated by the dashed square. The red atom is displaced from the centre of the unit cell.

lost is associated with the appearance of a macroscopic electric field.

The result of spin-orbit coupling is that the single-particle/quasiparticle states are no longer eigenstates of the spin operator. In crystals with inversion symmetry, Cooper pairing is then between so-called *pseudospin* states [32, 41], which are linear combination of the eigenstates of the spin operator. The name pseudospin refers to the fact that the transformation properties of these states are closely related to the spin eigenstates [32]. In crystals with inversion symmetry, the single-particle (pseudospin) bands are still doubly degenerate in the presence of spin-orbit coupling. This means that the spatial part of the superconducting gap function can still be classified as either symmetric (singlet) or antisymmetric (triplet), but where singlet and triplet refers to pseudospin rather than spin [32, 41]. Although the pairing symmetry is unaffected by dealing with pseudospin states, it can however lead to other important differences. This will be further mentioned in Section 4.2.

The effect of spin-orbit coupling in noncentrosymmetric crystals is however qualitatively different. The degeneracy of the single-particle bands is destroyed by spin-orbit coupling in that case, and the states forming Cooper pairs are not pseudospin states. The result is that the spatial part of the superconducting gap function can no longer be classified as either symmetric or antisymmetric [42, 43]. Recently, superconductivity has been discovered in a number of noncentrosymmetric materials where spin-orbit coupling is expected to be strong. This has led to much theoretical work on such systems, including Article I and II of this thesis. The purpose of Article I and II was to investigate transport measurement signatures of the unconventional pairing states allowed in these systems.

In this Chapter, we will first discuss the experimental motivation for studying superconductivity in the absence of inversion symmetry. We then discuss how to include spin-

orbit coupling in a second quantised Hamiltonian and point out differences between the centrosymmetric and the noncentrosymmetric case. We also present the model employed in Article I and II, as well as in many other studies, to describe superconductivity in these systems.

4.1 Motivation

The recent upturn in experiments on superconductivity in the absence of spatial inversion symmetry was initiated by the discovery of superconductivity in the noncentrosymmetric compound $CePt_3Si$. Several similar materials have since been discovered, such as UIr, $CeRhSi_3$, $CeIrSi_3$, Li_2Pd_3B, Li_2Pt_3B, $Cd_2Re_2O_7$ and KOs_2O_6. Some of these fall into the category heavy-fermion superconductors, others do not.

The most studied of these compounds is the heavy-fermion superconductor $CePt_3Si$. Experiments on this material have produced unusual results, which have been attributed to the presence of strong antisymmetric spin-orbit coupling [44, 45, 46]. The observation of antiferromagnetic order in this particular compound is however a complicating issue.

The symmetry of the pairing state in $CePt_3Si$ has been subject to both experimental and theoretical investigations. Experiments showed power law behaviour in both the London penetration depth and the heat conductance at low temperatures [47]. This is compatible with the presence of line nodes in the gap. However, a so-called Hebel-Slichter peak in the nuclear spin-lattice relaxation rate was also observed [48], which is indicative of a conventional, fully-gapped superconductor. One explanation of this apparent paradox is that the gap function is a combination of spin singlet and spin triplet components, which could have accidental line nodes in the gap [49]. This combination of singlet and triplet parts is possible due to antisymmetric spin-orbit coupling. The singlet component would then be responsible for the observed Hebel-Slichter peak. Other explanations have been put forth. One proposal is that the line nodes could be induced by coupling to the static antiferromagnetic order [50]. Another explanation of the line nodes is that, in the presence of antisymmetric spin-orbit coupling, they naturally arise from expressing the gap function in terms of irreducible representations of the crystal point group [51].

The response to an external, magnetic field has also attracted attention both by experimentalists [48, 52, 53] and theorists [42, 43, 54, 55, 56, 57]. The critical field H_{c2} is unusually large in $CePt_3Si$ [52, 53]. It also seems to be almost isotropic, in contrast to theoretical predictions [44, 57]. In addition, some exotic effects of a magnetic field have been predicted, such as magnetoelectric effects [42, 58] and a helical vortex phase [54, 55]. The latter has been suggested to explain the nearly isotropic H_{c2}.

Let us briefly return to the issue of pairing state in noncentrosymmetric superconductors with spin-orbit coupling. As mentioned above, some experiments have indicated that the

possibility of the pairing state being a mix of spin singlet and spin triplet parts can be realised. Historically, tunnelling spectroscopy and the study of Josephson currents have been important probes of the pairing state of superconductors. The purpose of Article I and II was therefore to study possible signatures of this exotic pairing state in tunnelling experiments on noncentrosymmetric superconductors.

4.2 Spin-Orbit Coupling

We will now consider how spin-orbit coupling enters a second quantised Hamiltonian, and how the absence of inversion symmetry affects this. The discussion follows closely the treatment in the Appendix of Ref. [57].

Let us consider the wave equation for a single particle in a *periodic* crystal potential $V(\boldsymbol{r})$,

$$\left[\frac{\hat{\boldsymbol{p}}^2}{2m} + V(\boldsymbol{r}) + \frac{\hbar}{4m^2c^2}\left(\nabla V(\boldsymbol{r}) \times \hat{\boldsymbol{p}}\right) \cdot \boldsymbol{\sigma}\right] \psi(\boldsymbol{r}) = \varepsilon\, \psi(\boldsymbol{r}) \ , \tag{4.1}$$

where $\hat{\boldsymbol{p}} = -\mathrm{i}\hbar\nabla$, $\boldsymbol{\sigma}$ is the Pauli matrix vector and c is the speed of light. The last term is a relativistic correction to the Schrödinger equation (2.1), and can be derived from the Dirac equation by considering the nonrelativistic limit. The last term obviously couples spin and momentum and is the origin of the spin-orbit coupling. In the absence of the spin-orbit coupling, the solutions/eigenstates of the above equation are Bloch spinors,

$$\psi_{\boldsymbol{k},\mu,\sigma}(\boldsymbol{r}) = u_{\boldsymbol{k},\mu}(\boldsymbol{r})\, \mathrm{e}^{\mathrm{i}\boldsymbol{k}\cdot\boldsymbol{r}}\, \chi_\sigma \ , \tag{4.2}$$

where

$$\chi_\uparrow = \begin{pmatrix} 1 \\ 0 \end{pmatrix} \ , \ \chi_\downarrow = \begin{pmatrix} 0 \\ 1 \end{pmatrix} . \tag{4.3}$$

The index $\boldsymbol{k}$ refers to momentum, μ is a band index, and σ denote the spin projection along a quantisation axis. The spatial parts are modulated plane wave states. These do not depend on spin, since the Hamiltonian in the absence of spin-orbit coupling is spin-independent. The energy of a state with momentum $\boldsymbol{k}$ in band μ is $\varepsilon_{\mu,\boldsymbol{k}}$. Time-reversal symmetry ensures that $\varepsilon_{\mu,-\boldsymbol{k}} = \varepsilon_{\mu,\boldsymbol{k}}$. The Bloch spinors will serve as our basis states, and $c^\dagger_{\boldsymbol{k},\mu,\sigma}$ and $c_{\boldsymbol{k},\mu,\sigma}$ will be the associated creation and annihilation operators.

According to Equation (2.9), the way to represent the spin-orbit term in second quantisation is

$$\hat{H}_{\mathrm{SO}} = \sum_{\boldsymbol{k}_1,\boldsymbol{k}_2} \sum_{\mu_1,\mu_2} \sum_{\sigma_1,\sigma_2} \langle \boldsymbol{k}_1,\mu_1,\sigma_1|\hat{H}_{\mathrm{SO}}|\boldsymbol{k}_2,\mu_2,\sigma_2\rangle\, c^\dagger_{\boldsymbol{k}_1,\mu_1,\sigma_1} c_{\boldsymbol{k}_2,\mu_2,\sigma_2} \ , \tag{4.4}$$

where the matrix element is

$$\langle \boldsymbol{k}_1,\mu_1,\sigma_1|\hat{H}_{\mathrm{SO}}|\boldsymbol{k}_2,\mu_2,\sigma_2\rangle = \int \mathrm{d}\boldsymbol{r}\, \psi^*_{\boldsymbol{k}_1,\mu_1,\sigma_1}(\boldsymbol{r}) \left[\frac{\hbar}{4m^2c^2}\left(\nabla V(\boldsymbol{r}) \times \hat{\boldsymbol{p}}\right) \cdot \boldsymbol{\sigma}\right] \psi_{\boldsymbol{k}_2,\mu_2,\sigma_2}(\boldsymbol{r}) \ . \tag{4.5}$$

Inserting the Bloch spinors (4.2), gives

$$\begin{aligned}&\langle \boldsymbol{k}_1,\mu_1,\sigma_1|\hat{H}_{\mathrm{SO}}|\boldsymbol{k}_2,\mu_2,\sigma_2\rangle\\&=\frac{\hbar}{4m^2c^2}\,\boldsymbol{\sigma}_{\sigma_1\sigma_2}\cdot\int \mathrm{d}\boldsymbol{r}\, u^*_{\boldsymbol{k}_1,\mu_1}(\boldsymbol{r})\,\mathrm{e}^{\mathrm{i}(\boldsymbol{k}_2-\boldsymbol{k}_1)\cdot\boldsymbol{r}}\Big[\nabla V(\boldsymbol{r})\times(-\mathrm{i}\hbar\nabla+\boldsymbol{k}_2)\Big]u_{\boldsymbol{k}_2,\mu_2}(\boldsymbol{r})\;.\end{aligned}\tag{4.6}$$

Since the potential $V(\boldsymbol{r})$ and the functions $u_{\boldsymbol{k},\mu}(\boldsymbol{r})$ are lattice-periodic functions, the integral is nonzero only if $\boldsymbol{k}_1$ and $\boldsymbol{k}_2$ differ by a reciprocal lattice vector. Since $\boldsymbol{k}_1$ and $\boldsymbol{k}_2$ are in the first Brillouin zone (the unit cell in reciprocal space), the only possibility is $\boldsymbol{k}_1=\boldsymbol{k}_2$. Thus, the second quantised representation of the single-particle Hamiltonian appearing in Equation (4.1) becomes

$$\hat{H}_{\mathrm{N}}=\sum_{\boldsymbol{k},\mu,\sigma}\varepsilon_{\mu,\boldsymbol{k}}\,c^\dagger_{\boldsymbol{k},\mu,\sigma}c_{\boldsymbol{k},\mu,\sigma}+\sum_{\boldsymbol{k}}\sum_{\mu_1,\mu_2}\sum_{\sigma_1,\sigma_2}\boldsymbol{B}_{\boldsymbol{k},\mu_1\mu_2}\cdot\boldsymbol{\sigma}_{\sigma_1\sigma_2}\,c^\dagger_{\boldsymbol{k},\mu_1,\sigma_1}c_{\boldsymbol{k},\mu_2,\sigma_2}\;,\tag{4.7}$$

where the vector

$$\boldsymbol{B}_{\boldsymbol{k},\mu_1\mu_2}=\frac{\hbar}{4m^2c^2}\int \mathrm{d}\boldsymbol{r}\, u^*_{\boldsymbol{k},\mu_1}(\boldsymbol{r})\Big[\nabla V(\boldsymbol{r})\times(-\mathrm{i}\hbar\nabla+\boldsymbol{k})\Big]u_{\boldsymbol{k},\mu_2}(\boldsymbol{r})\tag{4.8}$$

was introduced.

Some properties of the vector $\boldsymbol{B}_{\boldsymbol{k},\mu_1\mu_2}$ may be deduced from symmetry arguments. The Hamiltonian should be hermitian, which gives $\boldsymbol{B}_{\boldsymbol{k},\mu_1\mu_2}=\boldsymbol{B}^*_{\boldsymbol{k},\mu_2\mu_1}$. Furthermore, it should be invariant under point group operations of the crystal and under time reversal. The time reversed Hamiltonian is obtained by complex conjugation and $c^\dagger_{\boldsymbol{k},\mu,\sigma}\to-\sigma c^\dagger_{-\boldsymbol{k},\mu,-\sigma}$, $c_{\boldsymbol{k},\mu,\sigma}\to-\sigma c_{-\boldsymbol{k},\mu,-\sigma}$. Hermiticity and time reversal invariance thus leads to the conditions

$$\boldsymbol{B}_{\boldsymbol{k},\mu_1\mu_2}=\boldsymbol{B}^*_{\boldsymbol{k},\mu_2\mu_1}\;,\quad \boldsymbol{B}_{\boldsymbol{k},\mu_1\mu_2}=-\boldsymbol{B}^*_{-\boldsymbol{k},\mu_1\mu_2}\;.\tag{4.9}$$

To analyse this further, we will distinguish between crystals with and without inversion symmetry.

In a *centrosymmetric* crystal, the vector $\boldsymbol{B}_{\boldsymbol{k},\mu_1\mu_2}$ must have the property $\boldsymbol{B}_{\boldsymbol{k},\mu_1\mu_2}=\boldsymbol{B}_{-\boldsymbol{k},\mu_1\mu_2}$. By combining the above arguments, this gives $\boldsymbol{B}_{\boldsymbol{k},\mu_1\mu_2}=-\boldsymbol{B}^*_{\boldsymbol{k},\mu_1\mu_2}$ and

$$\boldsymbol{B}_{\boldsymbol{k},\mu_1\mu_1}=0\;.\tag{4.10}$$

Thus, the inclusion of at least two bands is necessary to describe spin-orbit coupling in a centrosymmetric crystal.

In a *noncentrosymmetric* crystal, the constraint (4.10) is absent and the band-diagonal elements does not vanish. Then, the spin-orbit coupling enters already at the one-band level. By considering only one band, the single-particle Hamiltonian becomes

$$\hat{H}_{\mathrm{N}}=\sum_{\boldsymbol{k},\sigma}\varepsilon_{\boldsymbol{k}}\,c^\dagger_{\boldsymbol{k},\sigma}c_{\boldsymbol{k},\sigma}+\sum_{\boldsymbol{k}}\sum_{\sigma,\sigma'}\boldsymbol{B}_{\boldsymbol{k}}\cdot\boldsymbol{\sigma}_{\sigma\sigma'}\,c^\dagger_{\boldsymbol{k},\sigma}c_{\boldsymbol{k},\sigma'}\;,\tag{4.11}$$

where the band index has been neglected. The vector $\boldsymbol{B}_{\boldsymbol{k}}$ is real and antisymmetric, *i.e.* $\boldsymbol{B}_{\boldsymbol{k}} = -\boldsymbol{B}_{-\boldsymbol{k}}$. In principle, one could calculate its dependence on the momentum from (4.8), but this is in general difficult. However, one may obtain important properties from $\boldsymbol{B}_{\boldsymbol{k}} = g\boldsymbol{B}_{g^{-1}\boldsymbol{k}}$, where g is an operation in the crystal point group.

The single-particle Hamiltonian (4.11) has been used extensively in the description of noncentrosymmetric superconductors by various authors [44, 45, 46, 59] and in Article I and II of this thesis. It is also commonly used to describe spin-orbit coupling in semiconductors where inversion may be absent due to the crystal structure [60] or external fields [61].

However, we should note that the reduction to a one-band model is an approximation, and that the effect of spin-orbit coupling is in general not only the *antisymmetric*, intra-band term in Equation (4.11). Fujimoto has argued that, in the case of heavy-fermion noncentrosymmetric superconductors such as $CePt_3Si$, the presence of a strong *symmetric* spin-orbit coupling dictates that the Hamiltonian should be expressed by pseudospin basis states [45]. The form of the antisymmetric spin-orbit coupling, as well as the Zeeman-coupling, is unchanged by using pseudospin basis states. Thus, it will in most cases not lead to any qualitative changes.

In the case of a heterostructure of different materials, it might nevertheless be important whether the indices in (4.11) refer to spin or pseudospin. For instance, in the transfer Hamiltonian formalism, it would affect the interpretation of the spin-dependence of the tunnelling matrix elements. It is well known that, even for nonmagnetic interfaces, the tunnelling matrix elements between a (centrosymmetric) heavy-fermion superconductor and a conventional superconductor may be nondiagonal [32, 62]. The reason is that the "spin" indices in the heavy-fermion superconductor are really pseudospin indices, due to strong spin-orbit coupling.

The interpretation of the indices in Equation (4.11) as pseudospin could therefore be of importance in tunnel junctions containing *e.g.* $CePt_3Si$. One might worry that this would affect the results of Article I and II when applying the theory to *e.g.* $CePt_3Si$. However, the examples considered in Article I and II will not suffer from this. The reason is that we considered systems of identical superconductors with the crystallographic orientation only differing by noncentrosymmetricity. The tunnelling and the reflection from the barrier would then conserve pseudospin as well, as long as one considers so-called specular reflection and tunnelling. The theory could also be modified to include "pseudospin-active" barriers, to allow the study of other crystallographic orientations in cases where the symmetric spin-orbit coupling is important.

4.3 Model

In BCS theory, superconductivity arises due to Cooper pairing of the long-lived excitations of the normal, nonsuperconducting phase, *i.e.* the quasiparticles. In most cases, the pairing is between states that are mapped onto each other by time reversal [34, 63]. Here, we take the point of view that the normal phase can be described by the single-particle Hamiltonian (4.11). By diagonalising this, one arrives at

$$\hat{H}_{\mathrm{N}} = \sum_{\lambda=\pm,\boldsymbol{k}} \tilde{\varepsilon}_{\lambda,\boldsymbol{k}} \tilde{c}^{\dagger}_{\lambda,\boldsymbol{k}} \tilde{c}_{\lambda,\boldsymbol{k}} \ , \quad \tilde{\varepsilon}_{\lambda,\boldsymbol{k}} = \varepsilon_{\boldsymbol{k}} + \lambda |\boldsymbol{B}_{\boldsymbol{k}}| \ . \tag{4.12}$$

We observe that if the crystal lacks inversion symmetry, the spin-orbit coupling leads to nondegenerate bands except at high-symmetry points where $\boldsymbol{B}_{\boldsymbol{k}} = 0$. This is in contrast to the inversion symmetric case, where spin-orbit coupling does not destroy the doubly degenerate band structure. The operator $\tilde{c}^{\dagger}_{\lambda,\boldsymbol{k}}$ are linear combinations of spin-up and spin-down creation operators, where the coefficients depend on momentum through the vector $\boldsymbol{B}_{\boldsymbol{k}}$. The spin in a state in the plus(minus) bands points along(opposite) the vector $\boldsymbol{B}_{\boldsymbol{k}}$. While the operators in the spin basis transform as $c^{\dagger}_{\boldsymbol{k},\mu,\sigma} \to -\sigma c^{\dagger}_{-\boldsymbol{k},\mu,-\sigma}$ under time reversal, the new operators transform as $\tilde{c}^{\dagger}_{\lambda,\boldsymbol{k}} \to t_{\lambda,\boldsymbol{k}} \tilde{c}^{\dagger}_{\lambda,-\boldsymbol{k}}$ [63]. In other words, time reversed states are in the same band. This means that we may not interpret the index λ in (4.12) as a pseudospin index [46]. The phase factor $t_{\lambda,\boldsymbol{k}}$ is antisymmetric in $\boldsymbol{k}$ and depends both on the nature of $\boldsymbol{B}_{\boldsymbol{k}}$ and the choice of spin quantisation axis.

To get a feel of the effect of the antisymmetric spin-orbit coupling, let us consider the much studied Rashba spin-orbit coupling [61]. In that case, we have $\boldsymbol{B}_{\boldsymbol{k}} = \alpha(\hat{\boldsymbol{n}} \times \boldsymbol{k})$. This is relevant to crystals where a mirror plane with normal vector $\hat{\boldsymbol{n}}$ is absent, such as in $CePt_3Si$. In addition, it is relevant to asymmetric potential wells in semiconductor heterostructures, *i.e.* two-dimensional electron gases. The band splitting results in two Fermi surfaces. A cut through these Fermi surfaces is shown in Figure 4.2, where $\hat{\boldsymbol{n}} = \hat{\boldsymbol{z}}$. The red(blue) arrows show the direction of the spins in the plus(minus) band. The splitting of the bands compared to the Fermi wavevector has been hugely exaggerated in Figure 4.2. It is also useful to plot the dispersion relations of the two bands. Figure 4.3 shows the $\tilde{\varepsilon}_{\pm,\boldsymbol{k}}$ along a particular direction in the (k_x, k_y)-plane. The energy ε_{F} indicate the Fermi energy. Observe that the spins in opposite momentum states within a band point in opposite directions.

Returning to the general case, we wish to add a BCS term to the Hamiltonian to describe superconductivity. If the energy splitting of the new bands, depicted in Figure 4.3, is large compared to the superconducting gap, we may consider only intraband Cooper pairs in opposite momentum states [46]. This is a valid limit in several noncentrosymmetric superconductors [46, 63, 64]. We express the BCS term by the long-lived excitations of the normal phase, such that

$$\hat{H}_{\mathrm{SC}} = \frac{1}{2} \sum_{\lambda,\mu} \sum_{\boldsymbol{k},\boldsymbol{k}'} V_{\lambda,\mu}(\boldsymbol{k},\boldsymbol{k}') \, \tilde{c}^{\dagger}_{\lambda,-\boldsymbol{k}} \tilde{c}^{\dagger}_{\lambda,\boldsymbol{k}} \tilde{c}_{\mu,\boldsymbol{k}'} \tilde{c}_{\mu,-\boldsymbol{k}'} \ . \tag{4.13}$$

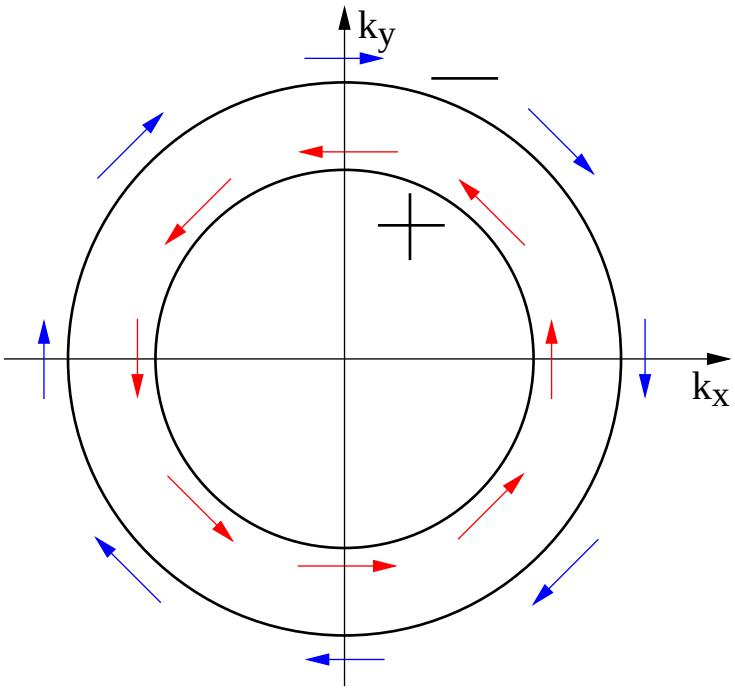

Figure 4.2: A cut through the Fermi surfaces in the case of Rashba spin-orbit coupling, where $\hat{\boldsymbol{n}} = \hat{\boldsymbol{z}}$. The inner(outer) circle represents the Fermi surface of the plus(minus) band. The arrows indicate how the spin depends on momentum. Note that the band splitting is extremely exaggerated compared to the Fermi wavevector.

We do not speculate on the pairing mechanism responsible for the attractive interactions. In the mean field approximation, the above term turns into

$$\hat{H}_{\mathrm{SC}} = \frac{1}{2}\sum_{\lambda}\sum_{\boldsymbol{k}}\left(\tilde{\Delta}_{\lambda,\boldsymbol{k}}\tilde{c}^{\dagger}_{\lambda,\boldsymbol{k}}\tilde{c}^{\dagger}_{\lambda,-\boldsymbol{k}} + \tilde{\Delta}^{*}_{\lambda,\boldsymbol{k}}\tilde{c}_{\lambda,-\boldsymbol{k}}\tilde{c}_{\lambda,\boldsymbol{k}}\right) \tag{4.14}$$

plus a constant term. Using the fermionic anticommutation relations, one can deduce that the gap function $\tilde{\Delta}_{\lambda,\boldsymbol{k}}$ is antisymmetric in $\boldsymbol{k}$. It can be written $\tilde{\Delta}_{\lambda,\boldsymbol{k}} = t_{\lambda,\boldsymbol{k}}\chi_{\lambda,\boldsymbol{k}}$, where $\chi_{\lambda,\boldsymbol{k}} = \chi_{\lambda,-\boldsymbol{k}}$ can be expressed by even basis functions of the irreducible representations of the space group [63].

We are dealing with two superconducting gaps on the two spin-orbit split Fermi surfaces. Since $\tilde{c}^{\dagger}_{\lambda,\boldsymbol{k}} \rightarrow t_{\lambda,\boldsymbol{k}}\tilde{c}^{\dagger}_{\lambda,-\boldsymbol{k}}$ under time-reversal, one may view the gap functions $\chi_{\lambda,\boldsymbol{k}}$ as the pair potential for time reversed states. Even though the two bands are decoupled at the mean field level in Equation (4.14), they are not independent. The gaps in a two-band mean field superconductor are in general related through a self-consistency relation [65]. Another example of a two-band superconductor is the much studied MgB_2. However, the bands in that case are of a different nature than here.

As mentioned above, the operator $\tilde{c}^{\dagger}_{\lambda,\boldsymbol{k}}$ are linear combinations of the creation operators in a spin basis. By inserting this relation into Equation (4.14), we arrive at the BCS term in

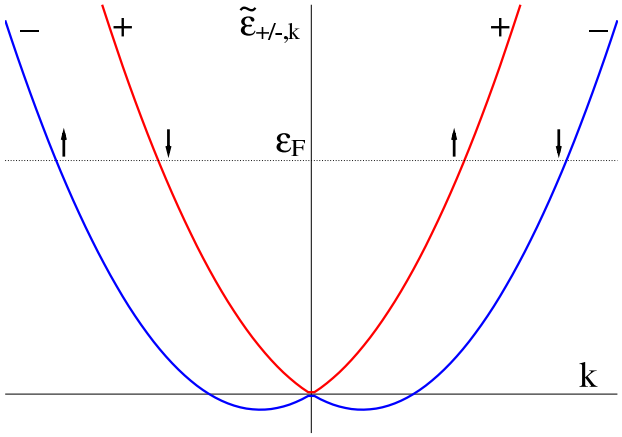

Figure 4.3: The dispersion relations $\tilde{\varepsilon}_{\pm,\boldsymbol{k}}$ in the case of Rashba spin-orbit coupling, where a simple, quadratic $\varepsilon_{\boldsymbol{k}}$ was used. The splitting of the bands have been strongly exaggerated.

a spin basis,

$$\hat{H}_{\mathrm{SC}} = \frac{1}{2}\sum_{\boldsymbol{k},\sigma,\sigma'}\left(\Delta_{\boldsymbol{k},\sigma\sigma'}\, c^{\dagger}_{\boldsymbol{k},\sigma}\, c^{\dagger}_{-\boldsymbol{k},\sigma'} + \Delta^{*}_{\boldsymbol{k},\sigma\sigma'}\, c_{-\boldsymbol{k},\sigma'}\, c_{\boldsymbol{k},\sigma}\right) \tag{4.15}$$

The gap function is then a matrix in spin space, which relates to the gaps $\chi_{\lambda,\boldsymbol{k}}$ by

$$\Delta_{\boldsymbol{k}} = \eta_{\boldsymbol{k},\mathrm{S}}\,(-\mathrm{i}\sigma_y) + \eta_{\boldsymbol{k},\mathrm{T}}(\hat{\boldsymbol{B}}_{\boldsymbol{k}}\cdot\boldsymbol{\sigma})\,(-\mathrm{i}\sigma_y), \tag{4.16}$$

where

$$\begin{aligned}\eta_{\boldsymbol{k},\mathrm{S}} &= \frac{1}{2}\left(\chi_{+,\boldsymbol{k}} + \chi_{-,\boldsymbol{k}}\right),\\ \eta_{\boldsymbol{k},\mathrm{T}} &= \frac{1}{2}\left(\chi_{+,\boldsymbol{k}} - \chi_{-,\boldsymbol{k}}\right)\ .\end{aligned} \tag{4.17}$$

We observe that the gap function in a spin basis is in general not a pure spin singlet or spin triplet. The first term in Equation (4.16) has the structure of a spin singlet gap, whereas the last term has spin triplet structure. Comparing with Section 3.2.1, the singlet part is given by $g_{\boldsymbol{k}} = -\eta_{\boldsymbol{k},\mathrm{S}}$ and the triplet by $\boldsymbol{d}_{\boldsymbol{k}} = -\eta_{\boldsymbol{k},\mathrm{T}}\hat{\boldsymbol{B}}_{\boldsymbol{k}}$, where $\hat{\boldsymbol{B}}_{\boldsymbol{k}}$ is a unit vector.

In Article I and II, we considered tunnelling currents between two noncentrosymmetric superconductors described by the model discussed above. This particular system was chosen since it offers a direct connection between the unconventional pairing and signatures in the dissipative current and the Josephson current. This is a result of the combination of spin conservation when electrons tunnel between the systems and that the spin structure of the bands is determined by the noncentrosymmetricity through $\boldsymbol{B}_{\boldsymbol{k}}$. Note that a study of tunnelling between a normal metal and a superconductor of this kind was reported in Ref. [66].

A complicating issue when studying heterostructures of these materials is that the spin-orbit split bands (plus and minus) could be strongly mixed by the reflection of a surface

or barrier. The presence of a spin triplet component could also lead to deviation of the gap from its value in the bulk of the material. This is well studied in the case of triplet superconductivity and superfluidity [67, 68]. In addition, sign changes in the gap function over the Fermi surface can lead to so-called surface Andreev bound states, which are states with energies below the bulk value of the superconducting gap. Such states have been well studied in the context of high-temperature superconductors [69, 70]. These matters where taken into account in Article II.

We will not go through the actual calculation of tunnelling currents here. The reader is referred to Article II, which is rich on details.

5 High-Temperature Superconductors

The discovery of high-temperature superconducting cuprates by Bednorz and Müller initiated an intense hunt for new materials with even higher critical temperatures. An important breakthrough was the discovery of superconductivity in the compound abbreviated YBCO with a critical temperature of 90 K [71]. For the first time, one could observe superconductivity by using liquid nitrogen (which boils at 77 K) as a cooler. Even higher critical temperatures have been obtained, but the dream of room-temperature superconductivity has not yet been fulfilled.

The superconducting state is different in these systems compared to the conventional superconductors. The superconductivity still involves Cooper pair formation. Important differences from the conventional superconductors are however that the gap function has d-wave symmetry, and that the pairing glue between electrons does not seem to be phonons. Furthermore, experiments in the nonsuperconducting region of the phase diagram have also revealed very unusual and unique properties. In other words, these materials do not behave like ordinary metals outside the superconducting phase.

Beside the experimental efforts, a tremendous amount of theoretical work has been devoted to the high-temperature superconductors. The BCS theory does not provide a satisfactory description of the metal-superconductor transition in these systems, although it can be used well inside the superconducting phase. The anomalous properties of the nonsuperconducting phase have also attracted the attention of many theoreticians. At present, there is no consensus on a microscopic theory for these systems. However, some key features of such a theory are generally agreed upon, summed up by Leggett in Ref. [72].

This Chapter starts with a discussion of the general features of high-temperature superconducting cuprates in Sections 5.1 and 5.2, whereas Sections 5.3 and 5.4 deals with the motivation and contents of Article III and Article IV, respectively.

5.1 Crystal Structure

The crystal structure of the high-temperature superconducting cuprates is in most cases complicated and can differ from compound to compound. The most important feature, which they all have in common, is the copper-oxide/CuO_2-planes, shown in Figure 5.1. The crystal has a layered structure, where the two-dimensional CuO_2-layers are separated

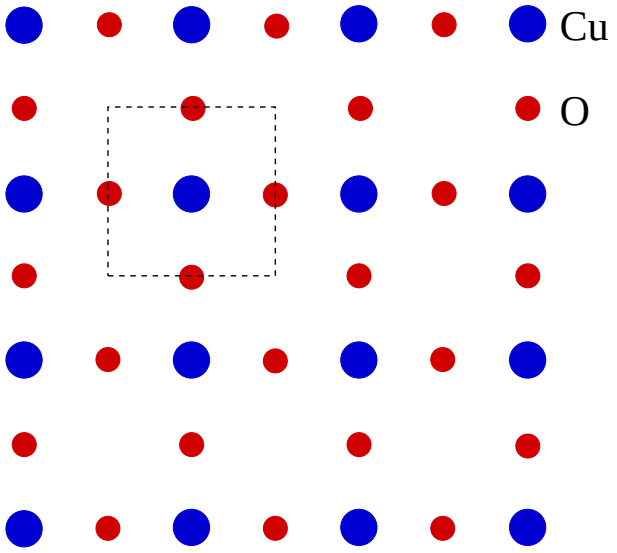

Figure 5.1: The crystal structure of the CuO_2-planes in high-temperature superconducting cuprates. The blue and red dots indicate copper and oxygen atoms, respectively. The dashed square is one particular choice of unit cell.

by other structures, specific to the compound in question. A very important property of these systems is the ability to accommodate chemical substitutions. By replacing atoms in the region between the CuO_2-planes, electrons can be added (electron doping) or taken away (hole doping) from the CuO_2-planes. This kind of doping leads to superconductivity and many other surprising effects, to be discussed in section 5.2.

The high-T_c cuprates are insulators at zero doping and become metallic at finite doping. Due to the layered structure, the electrical conductivity is very anisotropic. The conductivity perpendicular to the CuO_2-planes is much smaller than the in-plane conductivity. It was quickly realised [73] that the essential structure to consider to explain superconductivity and other phenomena is the CuO_2-plane, since the coupling between different layers is weak. The cuprates are therefore said to be quasi-two-dimensional. However, the inter-layer coupling may be important in some cases, since dimensionality is very important when it comes to phase transitions and critical phenomena.

5.2 Phase Diagram

The conduction band in the CuO_2-planes is the antibonding combination of the $3d_{x^2-y^2}$-orbital of copper and the $2p_x$- and $2p_y$-orbitals of oxygen. At zero doping, this band is half-filled. Naively, one would then expect the system to be metallic. However, due to interactions between electrons, it is actually an antiferromagnetic insulator. The common explanation for this is discussed in Section 5.3.1.

The doping is usually quantified by x, which is the number of added charge carriers (holes or electrons) divided by the number of Cu-lattice sites. The hole doped compounds have been much more studied than the electron doped materials, mainly due to experimental problems. Electron doped materials are briefly discussed in Ref. [74]. We will focus on hole doping here, which means that electrons are removed from the conduction band through chemical substitution.

As mentioned earlier, the properties of the high-T_c-cuprates depends strongly on doping. A schematic phase diagram in terms of doping x and temperature T is shown in Figure 5.2. This phase diagram seems to be applicable to all the hole-doped cuprates, although

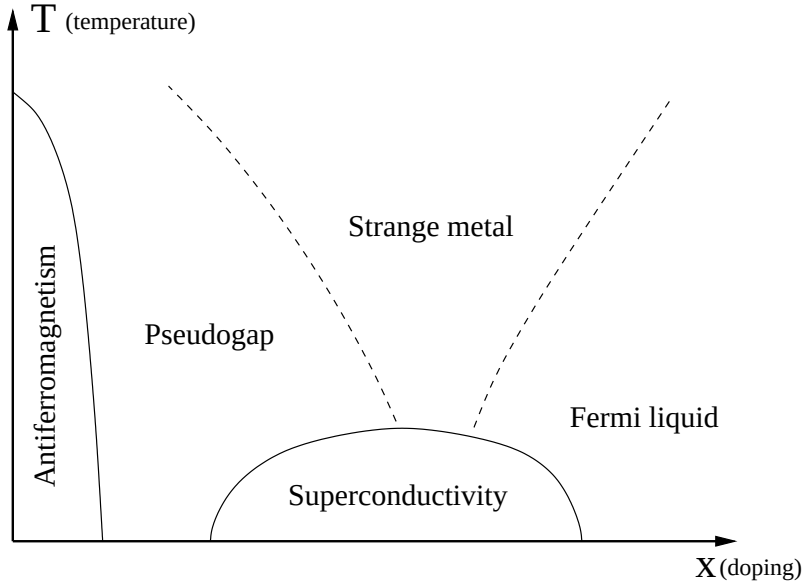

Figure 5.2: A schematic phase diagram for the hole-doped high-temperature superconducting cuprates, where T is temperature and x is the deviation from a half-filled conduction band.

small modifications occur from material to material. The dashed lines may or may not be associated with phase transitions. This is a heavily debated subject. We will now discuss some of the experimental features of the various parts of the phase diagram. For more details and references to experimental and theoretical work, consult *e.g.* Refs. [74, 75, 76, 77].

The superconducting dome in Figure 5.2 is usually centred around $x \approx 0.15$, the optimal doping value. The region to the left(right) of optimal doping is said to be underdoped(overdoped). The superconducting gap has spin singlet, d-wave symmetry, as was established by Josephson current measurements in tricrystal grain boundary experiments [78]. This means that the gap has four point nodes on the two-dimensional Fermi surface. The mechanism of Cooper pair formation is not known. It does not seem to be phonons, however, due to a lack of the so-called isotope effect. The superconductivity in the cuprates is also characterised by a very small coherence length, which is the distance over which the electrons are correlated in opposite momentum and spin states, *i.e.* the "size" of a Cooper pair. This has the consequence that they are extreme type II superconductors. Superconductivity is destroyed by transverse phase fluctuations in the Cooper pair wavefunction [24, 79, 80, 81]. The temperatures at which Cooper pairs form and where superconductivity sets in are not the same, at least in the underdoped region. This is supported by the observation of vortices, an indication of Cooper pairs, above the critical temperature for superconductivity [82]. The transition on the overdoped side seems to be more in line with standard BCS theory.

The *pseudogap* region in the phase diagram 5.2 has been and still is a subject of much debate. The presence of an energy gap in the quasiparticle density of states was first indicated by measurements of nuclear spin lattice relaxation rates and of the so-called Knight shift. Later, the existence of a gap on the Fermi surface has been well established by angle-resolved photoemission spectroscopy (ARPES) and tunnelling spectroscopy. For a review, see Refs. [75, 76]. The name pseudogap refers to the fact that there are regions in momentum space where gapless excitations exist, commonly named *Fermi arcs*. The gap is in other words very anisotropic and does not cover the entire Fermi surface. The origin of the pseudogap state is controversial and much debated. One point of view is to interpret the pseudogap state as a precursor to the superconducting state, where the pseudogap is a remnant of the superconducting gap, but where phase coherence is lost. The observation of vortices and hence Cooper pairs above the critical temperature for superconductivity supports this scenario [82]. Another point of view is that the pseudogap state is characterised by some sort of long range order, such as charge modulation (stripes) or orbital currents. A phase transition at the pseudogap line would have to be of a subtle kind, since no thermodynamic singularities have been reported there. Recently, different experiments [83, 84, 85, 86] have indicated signatures of long range order onset near the pseudogap line, supporting this line of thought. It might also be that these two viewpoints need to be combined to fully understand this region of the phase diagram.

In the early days of high-T_c superconductivity, a lot of experiments were performed near optimal doping. It turned out that the properties in the region above the superconducting dome, named *strange metal*, where not as one would expect from a normal metal. The reader may *e.g.* consult Ref. [87] and references therein for details. The easiest example is resistivity, which shows a linear temperature dependence over a large temperature range [88]. This does not comply with the Fermi liquid paradigm, where the resistivity of a normal

metal would display a T^2-dependence. The non-Fermi liquid behaviour is something very unusual and poses a theoretical challenge. We will return to the strange metal region in Section 5.4.1.

5.3 Phase Transitions in Logarithmic Plasmas

In Article III, we performed Monte Carlo simulations on two- and three-dimensional systems of point charges interacting via a logarithmic potential. The purpose was to study alleged exotic phase transitions in these systems. The motivation for considering this problem will be discussed below, before we move on to a concise presentation of the particular method used and its potential extensions.

5.3.1 Motivation

As noted previously, the essential systems to consider when describing the high-temperature cuprates are the almost independent CuO_2-planes [73]. Early on, it was also argued that the description of these planes may be reduced to a one-band Hubbard model on the quadratic Cu-lattice [73, 74, 89, 90]. This band, the antibonding combination of the copper $3d_{x^2-y^2}$- and the oxygen $2p_x$- and $2p_y$-orbitals, is half-filled at zero doping. The reduction of the problem to a one-band model is not generally agreed upon, however [91, 92]. We will return to this in section 5.4.

The Hubbard Model

The one-band Hubbard model consists of a kinetic energy term (hopping) and an on-site repulsion term,

$$\hat{H} = -t \sum_{\langle \boldsymbol{r},\boldsymbol{r}'\rangle,\sigma} c^\dagger_{\boldsymbol{r},\sigma} c_{\boldsymbol{r}',\sigma} + U \sum_{\boldsymbol{r}} n_{\boldsymbol{r},\uparrow} n_{\boldsymbol{r},\downarrow} \ . \tag{5.1}$$

The bracket $\langle \boldsymbol{r}, \boldsymbol{r}'\rangle$ indicates summation over nearest neighbours. The repulsion is governed by the parameter U and $n_{\boldsymbol{r},\sigma}$ is the number operator at site $\boldsymbol{r}$ for spin σ. If the on-site repulsion is strong, one can consider the $U \to \infty$ limit, which results in the so-called $t-J$ model,

$$\hat{H} = -t \sum_{\langle \boldsymbol{r},\boldsymbol{r}'\rangle,\sigma} c^\dagger_{\boldsymbol{r},\sigma} c_{\boldsymbol{r}',\sigma} + J \sum_{\langle \boldsymbol{r},\boldsymbol{r}'\rangle} \boldsymbol{S}_{\boldsymbol{r}} \cdot \boldsymbol{S}_{\boldsymbol{r}'} \ . \tag{5.2}$$

Here, the spin operator is $\boldsymbol{S}_{\boldsymbol{r}} = \frac{1}{2} \sum_{\sigma,\sigma'} c^\dagger_{\boldsymbol{r},\sigma} \boldsymbol{\sigma}_{\sigma\sigma'} c_{\boldsymbol{r},\sigma'}$ and J is positive. Equation (5.2) is subject to the no-double-occupancy constraint, which means that at most one electron can occupy any lattice site.

As mentioned above, at zero doping the band is half-filled, *i.e.* the number of charge carriers equals the number of Cu lattice sites. Due to the no-double-occupancy constraint, each lattice site is then occupied by exactly one electron. This means that the system is a so-called Mott insulator, where the electron interactions are responsible for the insulating behaviour. In addition, the energy is minimised by adjacent electrons having opposite spins, since $J > 0$. One can thus conclude that the ground state is an antiferromagnetic insulator at zero doping.

The mean field (x, T) phase diagram of the $t - J$-model, where x is the deviation from half-filling and T is temperature, has several interesting features in connection with the high-T_c cuprates, reviewed in Refs. [74, 90]. One sector of the proposed phase diagram, the spin-gap phase, is meant to correspond to the pseudogap phase mentioned earlier. A peculiar feature of this phase is the concept of spin-charge separation, which means that spin and charge degrees of freedom decouple at the quasiparticle level. Obviously, the bare electrons are intact. It is the excitations of the many-particle systems that can display such properties.

Studying this model beyond mean field is a complicated task. A common way of attacking this problem is a reformulation in terms of gauge theories [90, 93, 94, 95, 96, 97]. The no-double-occupancy constraint is normally dealt with by the slave-boson method, where electrons are represented as composite particles of spinons and holons. The spinons are chargeless spin-1/2 fermions (spins), whereas the holons are spinless bosons with positive charge (holes). The constraint can then be expressed by an operator identity and is incorporated in the theory by introducing an auxiliary field, a Lagrange multiplier at every space-time point. Furthermore, a Hubbard-Stratonovich decoupling of the spin interaction term introduces additional auxiliary fields. Under certain conditions, these auxiliary fields behave as compact gauge fields. This means that, besides the local gauge symmetries, the effective action is periodic in the fields. Nagaosa and Lee [95] arrived at a theory where the emergent compact gauge field is what connects the spinons and the holons. The issue of spin-charge separation is thus connected to a *confinement-deconfinement transition* in the compact gauge theory [97]. However, note that this point of view has been questioned [98].

The essential point of the above discussion is that compact gauge fields can emerge from a theory of strongly correlated electrons. The resulting gauge theories obtained from this procedure are complicated and difficult to analyse. To gain some insight, one possibility is to study simpler models that contain the same key features [97]. One such simplified model is the compact Abelian Higgs model.

The Compact Abelian Higgs Model

The compact Abelian Higgs model is a theory of a phase-fluctuating, bosonic field coupled to a compact $U(1)$ gauge field. It is of interest both in condensed matter physics and in high-energy physics [99, 100]. In connection to the high-T_c cuprates, it should be studied in $(2+1)$ dimensions, referring to the two spatial dimensions of the CuO_2-sheets and the infinite imaginary time direction at zero temperature. In the continuum, the partition function is

$$Z = \int \mathcal{D}\theta \int \mathcal{D}\boldsymbol{A}\, \mathrm{e}^{-S[\theta,\boldsymbol{A}]} \tag{5.3}$$

$$S\left[\theta,\boldsymbol{A}\right] = -\int \mathrm{d}\boldsymbol{r}\left[\kappa\,\cos(\nabla\theta(\boldsymbol{r}) - q\boldsymbol{A}(\boldsymbol{r})) + \lambda\,\cos(\nabla\times\boldsymbol{A}(\boldsymbol{r}))\right] \tag{5.4}$$

The field θ is the phase of the complex bosonic field, whereas $\boldsymbol{A}$ is the gauge field. Both these fields are compact, defined on the interval $[-\pi,\pi)$, and living in three dimensions. The properties of the model are determined by the value of the parameters κ, λ and q.

There are two types of topological excitations in this model [99]. The θ-field can contain vortices, which are three-dimensional versions of the ones discussed in section 2.4.3. The compact gauge field, however, can contain another type of defect, determined by

$$\oint_{\mathcal{S}} \mathrm{d}\boldsymbol{a}\cdot(\nabla\times\boldsymbol{A}) = 4\pi m\ , \tag{5.5}$$

where m is an integer and the surface integrated over surrounds the defect. This type of defect is referred to as a *magnetic monopole*, since Equation (5.5) can be interpreted as a Gauss' law for a "magnetic field" $\nabla\times\boldsymbol{A}$, in analogy with electrodynamics. These topological defects are also called *instantons*, since they are localised point charges in space-time.

Since Equation (5.3) is a compact gauge theory, the value of the charge q must be quantised [100]. In the $q=0$ case, the two fields are decoupled and one is left with a three-dimensional XY-model and a free, compact gauge theory. The XY-sector features a well-studied [24] continuous phase transition, whereas the free gauge sector does not display a phase transition [101]. The model has been extensively studied for $q\geq 2$ [100, 102].

The model (5.3) at $q=1$, called the fundamental charge [100], is of importance in connection with the high-T_c cuprates [97]. It has been established that the phase diagram of this model does not contain an ordinary phase transition (first order or continuous) [97, 100, 103]. Nevertheless, Kleinert *et al* [104] proposed that the model displays a phase transition similar to the Berezinskii-Kosterlitz-Thouless (BKT) transition discussed in Section 2.4.3. This transition is connected to proliferation of magnetic monopoles, very similar to the proliferation of vortices in the two-dimensional XY-model.

As mentioned above, in the pure gauge theory without the matter field θ, there is no phase transition [101]. The magnetic monopoles effectively interact through a $1/r$-potential and

are always in a plasma phase, *i.e.* they are proliferated for all values of the parameter λ. In the presence of matter fields and with $q = 1$, however, the effective interaction between monopoles changes to a logarithmic potential $-\ln r$ [105]. Kleinert *et al* claimed [104] that in the case of $q = 1$, the essential system to study is a three-dimensional gas of point charges (monopoles) interacting via a logarithmic potential, and that this model features a phase transition similar to the BKT-transition. This means that, in contrast to the pure gauge theory, there should exist a phase where the monopoles are tightly bound in pairs. The latter point has however been subject to extensive discussions. It has been argued that the system will always be in the plasma phase [106], whereas Monte Carlo simulations directly on the model (5.3) seem to support a phase where monopoles are bound in pairs [103]. One should also note that the legitimacy of an effective theory of a monopole gas with only pairwise interactions has been questioned [107].

The presence or absence of a BKT-transition in a three-dimensional logarithmic plasma is the topic of Article III. Given the amount of handwaving in the above discussion, there is little chance of a direct connection between this system and the properties of the copper-oxide planes of high-temperature superconductors. Although the logarithmic gas is of academic interest, one can, in all honesty, only hope that it is relevant to physical systems.

5.3.2 Logarithmic Plasmas

A model of point charges on a periodic lattice interacting via a logarithmic potential in d dimensions (2 or 3) can be described by the Hamiltonian

$$H = \frac{1}{2} \sum_{\boldsymbol{r},\boldsymbol{r}'} m(\boldsymbol{r}) V(\boldsymbol{r} - \boldsymbol{r}') m(\boldsymbol{r}') \ . \tag{5.6}$$

Here, $m(\boldsymbol{r})$ is an integer charge field and the potential is defined by

$$V(\boldsymbol{r}) = \frac{4\pi^2}{L^d} \sum_{\boldsymbol{q}} \frac{\mathrm{e}^{-\mathrm{i}\boldsymbol{q}\cdot\boldsymbol{r}}}{[2\,(d - \sum_i \cos q_i)\,]^{d/2}} \ . \tag{5.7}$$

L^d is the number of lattice points of the system. For $|\boldsymbol{r}| \ll L$, this potential has a logarithmic behaviour, $V(\boldsymbol{r}) = -c(d)\,\ln(|\boldsymbol{r}|/r_0)$, where r_0 is a short-distance cut-off. The divergence of $V(0)$ demands that only neutral configurations contribute [108], enabling the potential to be replaced by $V(\boldsymbol{r}) - V(0)$. $c(d)$ is a dimension-dependent constant.

Renormalisation analysis

For $d = 2$, the model (5.6) is nothing but the lattice version of the two-dimensional Coulomb gas.[1] As mentioned in Section 2.4.3, the two-dimensional XY-model can be mapped onto

[1] The Coulomb potential is defined as the Green's function of the Poisson equation.

this model, where the charges represent vortices. In a mean field renormalisation procedure, Kosterlitz and Thouless [13, 14] showed that this model features a phase transition from a low temperature phase, where charges are bound in dipoles, to a high-temperature plasma phase. The hallmark of this dissociation of dipoles is a universal jump in the inverse dielectric constant ε^{-1}.

In Ref. [104], it was argued that the renormalisation procedure also holds in the three-dimensional case, such that the corresponding phase transition in the $q = 1$ compact Abelian Higgs model corresponds to proliferation of magnetic monopoles. Let us briefly consider the renormalisation argument in d dimensions, following Refs [104, 109, 110]. It is based on the assumption that one can define a length-dependent dielectric constant $\varepsilon(r)$, such that

$$\varepsilon(r) = 1 + \kappa\,\beta\,\frac{z^2}{r_0^{2d}}\int_{r_0}^{r} \mathrm{d}s\; s^{d+1}\mathrm{e}^{\beta\,U(s)} \;, \quad \frac{\partial U(r)}{\partial r} = -\frac{c(d)}{\varepsilon(r)\,r} \;. \tag{5.8}$$

The expression for $\varepsilon(r)$ is only valid at low charge densities. The integral is over the square of the dipole moment multiplied by the pair distribution function in the low density limit [110]. The potential $U(r)$ is the effective, screened potential between two charges. It corresponds to a logarithmic potential in the unscreened case ($\varepsilon(r) = 1$). The parameter z is the fugacity,[2] β is the inverse temperature and κ is an unimportant constant. By introducing a logarithmic length scale, $r = r_0\mathrm{e}^l$, these equations can be transformed to

$$\frac{\partial K^{-1}}{\partial l} = \Big[y(l)\Big]^2 \;, \quad \frac{\partial y}{\partial l} = 2y(l)\Big[d + 2 - c(d)K(l)\Big] \;, \tag{5.9}$$

where $K(l) = \beta/\varepsilon(r_0\mathrm{e}^l)$ and

$$y(l) = \left[\frac{\kappa z^2}{r_0^{d-2}}\,\mathrm{e}^{\beta\,U(r_0\mathrm{e}^l)+(d+2)l}\right]^{\frac{1}{2}} \tag{5.10}$$

can be viewed as a length-dependent fugacity. By analysing these equations [24, 104, 110], one finds that there is a line of zero-fugacity fixed points terminating at the value $K^* = (d+2)/c(d)$. One may conclude that, at the transition temperature, the ratio between $\varepsilon^{-1} \equiv \lim_{l\to\infty}\varepsilon^{-1}(r_0\mathrm{e}^l)$ and the temperature T_c drops from[3]

$$\frac{\varepsilon^{-1}}{T_c} = \frac{d+2}{c(d)} \;, \tag{5.11}$$

to zero. Obviously, this jump depends on the strength of the potential. For the potential defined in Equation (5.7), we have $c(2) = 2\pi$ and $c(3) = 2$. Thus, this analysis predicts

[2] The fugacity is related to the chemical potential and the temperature, $z = \mathrm{e}^{\beta\,\mu}$ [110]. For an ideal gas, the fugacity equals the density.

[3] We set the Boltzmann constant k_B to unity.

that the size of the inverse dielectric constant at the transition temperature is determined by

$$\begin{aligned} \varepsilon^{-1} &= \frac{2}{\pi}\, T_c \quad , \quad d = 2 \\ \varepsilon^{-1} &= \frac{5}{2}\, T_c \quad , \quad d = 3 \ . \end{aligned} \tag{5.12}$$

Although this analysis is very simple, it seems to fit well with experiments when $d = 2$ [111, 112]. Article III was an attempt to verify whether or not this renormalisation analysis and the consequential jump in ε^{-1} also holds in $d = 3$. Unfortunately, this remains an open question.

Numerical Detection of a Discontinuity

Kragset *et al* [113] studied the model (5.6) by Monte Carlo simulations. They considered the scaling of the mean square dipole moment with increasing system size. The results clearly indicated that a low-temperature phase exists also in three dimensions. The similarity to the two-dimensional case was emphasised.

Although the results of Ref. [113] indicated the existence of two phases in the three-dimensional case, the character of the phase transition was not determined. The attempt to verify the BKT-transition in the three-dimensional logarithmic gas became the subject of Article III. The goal was to detect a discontinuity in the inverse dielectric constant by using Monte Carlo simulations.

The method employed in Article III was inspired by Minnhagen & Kim's numerical establishement of the discontinuity in the helicity modulus of the two-dimensional XY-model [114]. The method is based on studying the response of the system to an external, infinitesimal perturbation of the charge field, $m(\boldsymbol{r}) \to m(\boldsymbol{r}) + \delta(\boldsymbol{r})$. If charges are bound in dipoles in the low-temperature phase, which Ref. [113] strongly indicates, the system will not be able to screen a long-wavelength charge perturbation $\delta(\boldsymbol{r})$. This implies that the difference in free energy $F = -T \ln Z$ between the perturbed and the unperturbed system should be positive,

$$F(\delta(\boldsymbol{r}) \neq 0) - F(\delta(\boldsymbol{r}) = 0) \geq 0 \ , \tag{5.13}$$

at least for temperatures $T \leq T_c$. In Article III, we chose to use the (charge neutral) perturbation $\delta(\boldsymbol{r}) = -2\pi\Delta L^{-1-\eta} \cos(2\pi y/L)$, where the parameter Δ is infinitesimal. The exponent η is determined by demanding the energy difference (5.13) not to scale with system size, giving $\eta = d - 1$ in the logarithmic case.[4] Note that one could also choose to perturb the system with a dipole of point charges with the maximal separation $\sqrt{d}\, L/2$. However, when averaging over the positions of these test charges, one arrives at similar results as in Article III.

[4] In the case of a potential $V_{\boldsymbol{q}} \sim q^{-\alpha}$ in Fourier space, $\eta = (d + \alpha - 2)/2$.

By the rescaling $\Delta \to \Delta/(\sqrt{2}\pi)$, the free energy difference, when expanded in the parameter Δ, becomes[5]

$$F(\delta(\boldsymbol{r}) \neq 0) - F(\delta(\boldsymbol{r}) = 0) = \frac{\Delta^2}{2}\,\varepsilon^{-1}(\boldsymbol{k}) + \frac{\Delta^4}{4!}\,3\,\varepsilon_4(\boldsymbol{k}) + \mathcal{O}(\Delta^6)\ . \tag{5.14}$$

The wavevector $\boldsymbol{k} = 2\pi/L\,\hat{\boldsymbol{y}}$ is the smallest, nonzero wavevector in the finite system. The function appearing in the second order term is the inverse dielectric response function in Fourier space,

$$\varepsilon^{-1}(\boldsymbol{k}) = 1 - \frac{V_{\boldsymbol{k}}}{L^d T}\langle m(\boldsymbol{k})\, m(-\boldsymbol{k})\rangle\ . \tag{5.15}$$

However, since the inverse dielectric constant is $\varepsilon^{-1} = \lim_{\boldsymbol{k}\to 0}\varepsilon^{-1}(\boldsymbol{k})$ and $\boldsymbol{k} \to 0$ as $L \to \infty$, the second order term in (5.15) should become proportional to the inverse dielectric constant in the limit of infinite system size.

The fourth order term is proportional to

$$\varepsilon_4(\boldsymbol{k}) = \frac{1}{T^3}\left(\langle m(\boldsymbol{k})\, m(-\boldsymbol{k})\rangle^2 - \frac{1}{2}\langle\,(m(\boldsymbol{k})\, m(-\boldsymbol{k}))^2\,\rangle\right)\ . \tag{5.16}$$

The Monte Carlo simulations in Article III showed that, both in $d = 2$ and $d = 3$, this quantity is *negative* and has a dip in the temperature region where $\varepsilon^{-1}(\boldsymbol{k})$ goes to zero. If the depth of $\varepsilon_4(\boldsymbol{k})$ remains finite in the limit $L \to \infty$, Equation (5.13) implies that ε^{-1} must be nonzero at the phase transition point T_c. However, since ε^{-1} is zero in the high-temperature plasma phase, it necessarily must experience a discontinuity at T_c, in agreement with the renormalisation argument. Article III showed that the negative fourth order term remains finite as $L \to \infty$ in $d = 2$. However, such a conclusion could not be drawn in $d = 3$. One should also note that, even if $\varepsilon_4(\boldsymbol{k})$ goes to zero at T_c, this does not exclude a discontinuity in the inverse dielectric constant. Clearly, this inability to falsify the renormalisation arguments is a weakness of this method.

Direct Probe of the Zero Wavevector Response

In the previous section, we assumed that the behaviour of the quantity $\varepsilon^{-1}(\boldsymbol{k})$ as $L \to \infty$ corresponds to taking the limit $\lim_{\boldsymbol{k}\to 0}\varepsilon^{-1}(\boldsymbol{k})$. Strictly speaking, one should take the limit $\boldsymbol{k} \to 0$ before $L \to \infty$. However, in a system with periodic boundary conditions, this is not possible. In the two-dimensional case, a method of directly probing the $\boldsymbol{k} = 0$ response of the system nevertheless exists [115, 116].[6] In fact, a rigorous dualisation [116] of the two-dimensional XY-model with periodic boundary conditions gives an additional

[5] Terms odd in Δ vanish. This is natural, since the energy difference should be unaffected by the sign of Δ.

[6] A similar method can be used to measure the $\boldsymbol{k} = 0$ helicity modulus in a three-dimensional superconductor [117].

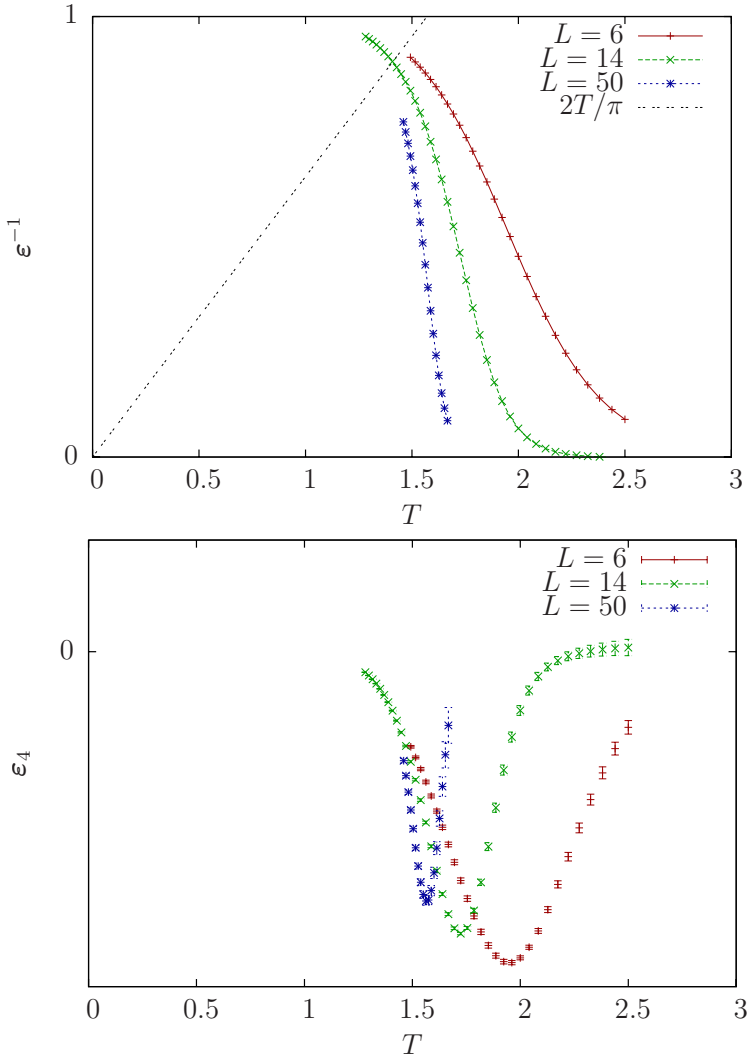

Figure 5.3: Monte Carlo results for a $d = 2$ logarithmic gas for three system sizes $L = 6$, $L = 14$ and $L = 50$. *Upper panel:* The inverse dielectric constant ε^{-1} as a function of temperature T getting steeper as L increases. The dashed line corresponds to the universality criterion of Kosterlitz and Thouless (see Equation (5.12)). *Lower panel:* The fourth order term ε_4 in the free energy expansion as a function of T, which has a negative dip.

term $2\pi^2 \boldsymbol{P}^2$ in Equation (5.6), where $\boldsymbol{P} = \boldsymbol{w} + L^{-1} \sum_{\boldsymbol{r}} m(\boldsymbol{r})\, \boldsymbol{r}$ is the polarisation of the system.[7] The global vector $\boldsymbol{w}$ keeps track of the winding number as charges move across the boundaries. This modification of the model allows measurements of the response to an external, constant electric field $\boldsymbol{D}$ [115]. The same reasoning as in the previous section

[7]The additional term can be viewed as a modification of the potential, such that it no longer obeys periodic boundary conditions [116].

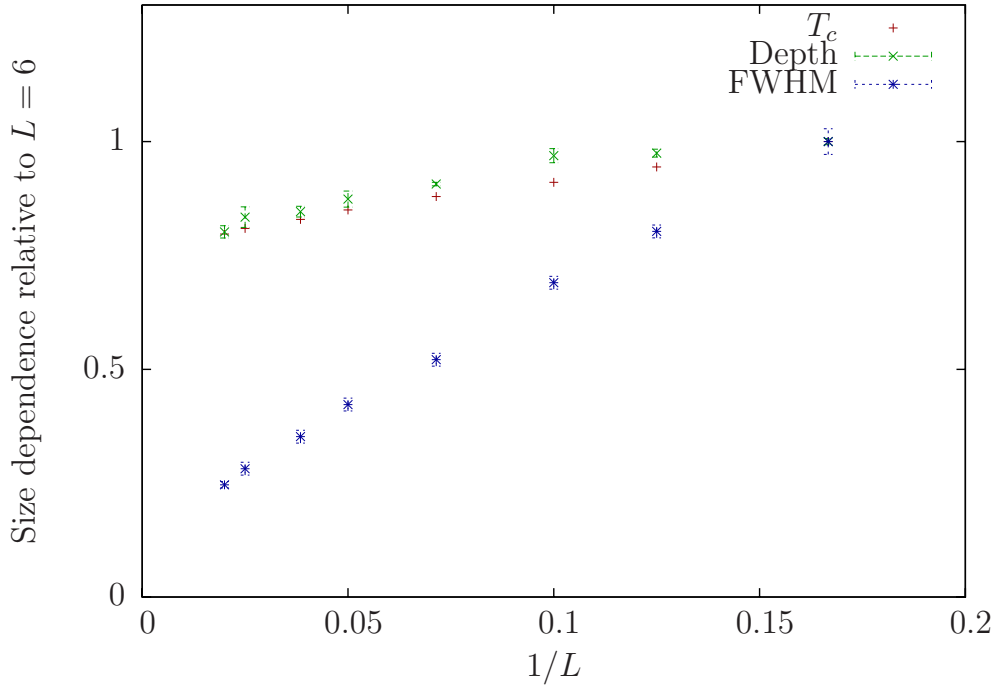

Figure 5.4: The dependence on inverse system size $(1/L)$ of the position T_c, the depth, and the width (FWHM) of the dip in ε_4 for system sizes from $L = 6$ to $L = 50$. The values are given relative to the $L = 6$ values. Note that the system size dependencies of the depth and the position are qualitatively different from the size dependence of the width.

then gives a second order term in the difference in free energy, proportional to

$$\varepsilon^{-1} = 1 - \frac{2\pi^2}{T}\langle \boldsymbol{P}^2 \rangle \ . \tag{5.17}$$

This is nothing but the inverse dielectric constant. A plot of this quantity in $d = 2$ for the system sizes $L = 6$, $L = 14$ and $L = 50$ are shown in Figure 5.3(a), showing the sharp drop as the system size increases. In Figure 5.3(b), the corresponding fourth-order term ε_4 is plotted. It is indeed negative and has a dip at a temperature associated with the decline in ε^{-1}.

The depth of the dip in ε_4 at different system sizes are shown in Figure 5.4. In addition, the position of the dip (T_c) and the width of the dip (FWHM) are displayed. An important point is the qualitative difference between the system size dependence of the depth and T_c compared to the FWHM-value. These results clearly indicate that the depth and position of the dip in ε_4 remains nonzero as $L \to \infty$, whereas the width seems to be a finite size effect. The results for $d = 2$ in Article III are thus confirmed.

To apply this method to the three-dimensional case is however not straightforward. First of all, it is not clear how the model should be modified in order to enable a response to an external electric field. Secondly, it is important to remember that the external field should

not obey ordinary electrostatics. One should consider an external electric field in a world where the potential from a point charge is logarithmic. In ordinary electrostatics, one would use a plate condensator to construct a constant electric field. In this world, however, this does not work. In fact, the energy of the field from an ordinary plate condensator diverges. The electric field from a line charge will be constant in magnitude, but not in direction. Thus, the very existence of a constant electric field in such a world seems to be ill-defined. The application of the above mentioned method to $d = 3$ hence seems difficult and remains an unsolved problem.

5.4 Effective Theory of Fluctuating Orbital Currents

This section deals with the effective theory of orbital currents in high-T_c cuprates presented in Article IV. We start by considering the experimental motivation for studying this problem. Then, since Article IV is scarce on details concerning the derivation of the effective theory, we will include a fair amount of the details here.

5.4.1 Motivation

As mentioned earlier, not long after the discovery of the high-T_c cuprates, it was realised that the region above the superconducting dome in the phase diagram contains puzzling properties. A number of different experiments display anomalous results in this *strange metal* region, such as measurements of resistivity, nuclear lattice relaxation rate, Raman scattering and photoemission. See Ref. [87] and references therein for details.

These anomalous normal-state properties led Varma *et al* to propose the *Marginal Fermi Liquid* hypothesis. They showed that the anomalous properties may be explained by a phenomenological assumption. The assumption was that the electrons are interacting with bosonic excitations with a particular kind of fluctuation spectrum, given by the susceptibility[8]

$$\operatorname{Im}\chi(\boldsymbol{q},\omega,T) \propto \begin{cases} \omega/T\ , & \omega \ll T \\ \text{const.}\ , & T \ll \omega \ll \omega_c \end{cases} . \tag{5.18}$$

Here, T is temperature, $\boldsymbol{q}$ is momentum, ω is frequency (energy) and ω_c is a cut-off. By calculating the electron self-energy given this assumption, they argued that the anomalous experimental results could be explained. It was also noted that multiplying Equation (5.18) by a smooth function of $\boldsymbol{q}$ does not change the qualitative results. The name Marginal Fermi Liquid is related to the fact that the quasiparticle weight in the single-particle Green's function vanish logarithmically at the Fermi surface. In other words, the system is only just a Fermi liquid.

[8] $\chi(\boldsymbol{q},\omega,T)$ is the Fourier transform of a correlation function of the bosonic field.

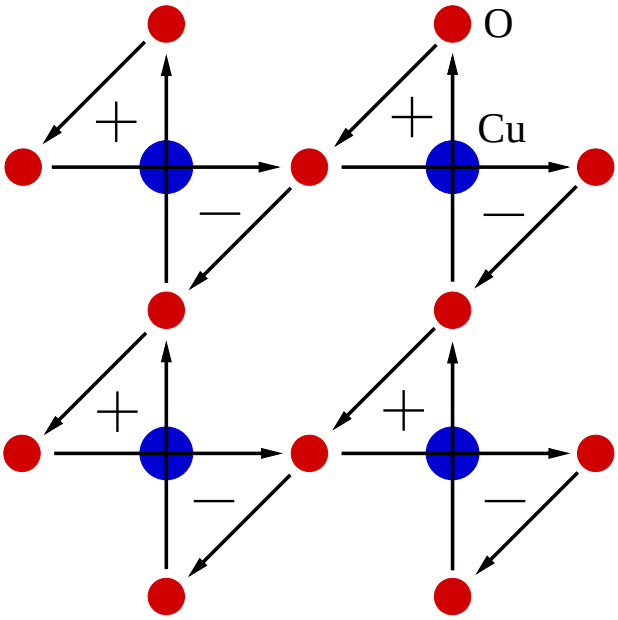

Figure 5.5: The proposed current pattern in the CuO_2-planes of high-T_c cuprates. Blue and red dots indicate copper and oxygen atoms, respectively. The plus and minus signs indicate the magnetic moments produced by the circulating currents. Three other equivalent patterns exist, which is realised by reversing one or both of the horizontal and vertical currents and closing the loops by the diagonal *O*-*O*-currents.

The spectrum (5.18) was written down on pure phenomenological grounds. The question is then: What is the fluctuating quantity? Varma has proposed that this spectrum is associated with the breakup of a subtle order, involving *circulating currents* within the CuO_2 unit cell [91, 92]. Figure 5.5 shows the proposed current pattern. The idea is that the pseudogap line in the phase diagram describes a true phase transition, and that the current loops are ordered in the pseudogap region and fluctuates in the strange metal region. The proposed order is based on a three-band, microscopic model of the CuO_2-planes. It has been shown that this model supports a phase with ordered current loops. Clearly, this type of order would not show up in the single-band Hubbard model discussed in section 5.3.1. In addition, it is claimed [91] that this type of order leads to a Fermi surface instability and consequently an anisotropic gap,[9] which is then interpreted as the pseudogap.

An important thing to notice in Figure 5.5 is that the current pattern does not break the translation symmetry of the CuO_2-lattice. In fact, the model contains two types of translational invariant current patterns. However, experiments (see below) seem to support only one of these, which should also have a higher transition temperature [91].

[9] According to Varma, the Fermi surface is composed of four points at zero temperature, but that the regions in momentum space where a gap can be detected shrinks with increasing temperature, leading to the observed Fermi arcs.

Recently, a magnetic signal consistent with the current pattern in Figure 5.5 has been observed in polarised neutron scattering experiments [83, 84]. In particular, the experiments indicate order respecting the translational symmetry of the lattice. In addition, ARPES experiments with circularly polarised photons support this state [85]. These experimental results are interesting and justifies a continued study of the model and the type of order proposed by Varma. We should however note that the neutron scattering experiments measures a magnetic moment which is significantly canted, *i.e.* it does not point perpendicular to the CuO_2 lattice.[10] Also, other experiments have indicated a magnetic signal with a period of twice the unit cell [119], seemingly supporting another type of staggered current pattern [120]. Let us also mention that recent numerical studies of the three-band model of the CuO_2-system do not support the scenario advocated by Varma [121]. In other words, even though we choose to study the particular type of order proposed by Varma, we should bear in mind that there might be more to the story.

The question is now whether or not the fluctuations associated with the breakup of the current pattern in the proposed model have a spectrum of the form (5.18). In addition, one should check that the phase transition in the proposed model is consistent with the apparent lack of thermodynamic singularities at the pseudogap line. To try to answer these questions, Aji & Varma [122] has studied a conjectured effective field theory for the circulating currents, from which they claim that the fluctuation spectrum (5.18) follows. In Article IV, we *derived* an effective theory for the currents from the microscopic model shown by Varma [91] to support ordering of current loops. Our results do not seem to agree with the conjectured model used in Ref. [122].

5.4.2 Model

We will consider the microscopic model used by Varma in Refs. [91, 92]. It is based on the copper $3d_{x^2-y^2}$-orbital and the oxygen $2p_x$- and $2p_y$-orbitals. The orbital wavefunctions are products of a radial part and a linear combination of spherical harmonics. For a particular choice of phases of these wavefunctions, we have

$$\psi_{3d_{x^2-y^2}}(\boldsymbol{r}) \propto \frac{x^2-y^2}{|\boldsymbol{r}|^2} \ , \quad \psi_{2p_x}(\boldsymbol{r}) \propto \frac{x}{|\boldsymbol{r}|} \ , \quad \psi_{2p_y}(\boldsymbol{r}) \propto \frac{y}{|\boldsymbol{r}|} \ . \tag{5.19}$$

Figure 5.6 shows a schematic view of the unit cell with the orbital wavefunctions indicated. The model contains hopping between these atomic orbitals, in addition to Coulomb repulsion between electrons. The hopping matrix elements are overlap integrals of the wavefunctions and the Coulomb potential from the ions. The hopping between d- and p-orbitals is governed by t_{pd}, whereas the matrix element for *direct hopping* between p-orbitals is t_{pp}. The distance between Cu-atoms is denoted a.

[10] This has been attempted explained by spin-orbit coupling [118].

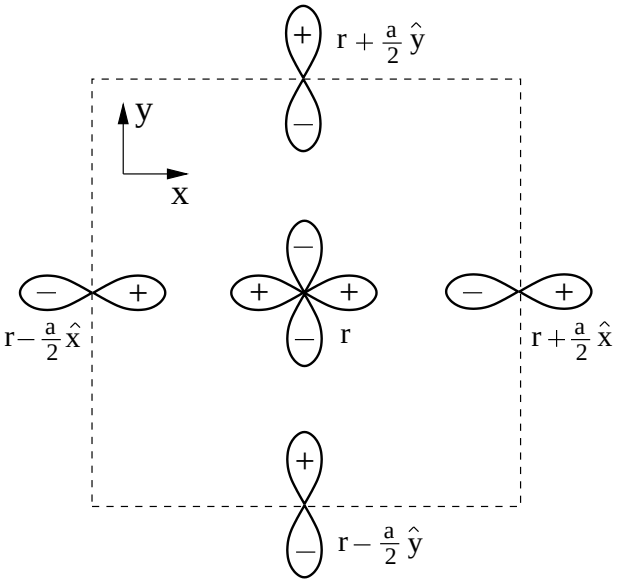

Figure 5.6: A choice of unit cell in the CuO_2-plane. The $3d_{x^2-y^2}$-orbital in the middle belongs to the copper atom, whereas the surrounding $2p_x$- and $2p_y$-orbitals belong to the oxygen atoms. The plus and minus signs indicate a particular choice of relative phases of the orbital wavefunctions.

The Hamiltonian we consider is[11]

$$H = \varepsilon_d \sum_{\boldsymbol{r},\sigma} d^\dagger_{\boldsymbol{r},\sigma} d_{\boldsymbol{r},\sigma} + K_{pd} + K_{pp} + H^{(1)}_{\text{int}} + H^{(2)}_{\text{int}} \ . \tag{5.20}$$

The coordinate $\boldsymbol{r}$ will refer to the Cu-lattice, and σ denotes spin. We let $d_{\boldsymbol{r},\sigma}$ be the annihilation operator for an electron in a d-orbital state in the copper atom at $\boldsymbol{r}$, and $p_{x,\boldsymbol{r}\pm\frac{a}{2}\hat{\boldsymbol{x}},\sigma}$ and $p_{y,\boldsymbol{r}\pm\frac{a}{2}\hat{\boldsymbol{y}},\sigma}$ the electron annihilation operators for p-orbital states in the oxygen atoms. The operators respect the ordinary fermionic anticommutation relations. The vacuum is defined as empty $d_{x^2-y^2}$-, p_x- and p_y-orbitals. The parameter ε_d is the energy difference between the copper and oxygen orbitals, which means that energy is measured relative to the oxygen level. The kinetic energy operators are

$$\begin{aligned} K_{pd} &= t_{pd} \sum_{\boldsymbol{r},\sigma} \left[d^\dagger_{\boldsymbol{r},\sigma} (p_{x,\boldsymbol{r}+\frac{a}{2}\hat{\boldsymbol{x}},\sigma} - p_{x,\boldsymbol{r}-\frac{a}{2}\hat{\boldsymbol{x}},\sigma} - p_{y,\boldsymbol{r}+\frac{a}{2}\hat{\boldsymbol{y}},\sigma} + p_{y,\boldsymbol{r}-\frac{a}{2}\hat{\boldsymbol{y}},\sigma}) + \text{h.c.} \right] \ , \\ K_{pp} &= -t_{pp} \sum_{\boldsymbol{r},\sigma} \left[(p^\dagger_{x,\boldsymbol{r}+\frac{a}{2}\hat{\boldsymbol{x}},\sigma} - p^\dagger_{x,\boldsymbol{r}-\frac{a}{2}\hat{\boldsymbol{x}},\sigma})(p_{y,\mathbf{r}+\frac{a}{2}\hat{\boldsymbol{y}},\sigma} - p_{y,\boldsymbol{r}-\frac{a}{2}\hat{\boldsymbol{y}},\sigma}) + \text{h.c.} \right] \ . \end{aligned} \tag{5.21}$$

The abbreviation h.c. means hermitian conjugation. The sign differences in the hopping terms are related to the sign changes in the orbital wavefunctions (5.19) and may be understood by inspection of Figure 5.6.

[11] We skip hats on operators from now on. Hats will be used to indicate unit vectors.

The interaction part of the Hamiltonian can be formulated by the number operators $n_{d,\boldsymbol{r},\sigma} = d^\dagger_{\boldsymbol{r},\sigma} d_{\boldsymbol{r},\sigma}$, $n_{p_x,\boldsymbol{r}\pm\frac{a}{2}\hat{\boldsymbol{x}},\sigma} = p^\dagger_{x,\boldsymbol{r}\pm\frac{a}{2}\hat{\boldsymbol{x}},\sigma} p_{x,\boldsymbol{r}\pm\frac{a}{2}\hat{\boldsymbol{x}},\sigma}$ and $n_{p_y,\boldsymbol{r}\pm\frac{a}{2}\hat{\boldsymbol{y}},\sigma} = p^\dagger_{y,\boldsymbol{r}\pm\frac{a}{2}\hat{\boldsymbol{y}},\sigma} p_{y,\boldsymbol{r}\pm\frac{a}{2}\hat{\boldsymbol{y}},\sigma}$. The term

$$\begin{aligned} H^{(1)}_{\text{int}} &= U_d \sum_{\boldsymbol{r},\sigma} n_{d,\boldsymbol{r},\sigma} n_{d,\boldsymbol{r},-\sigma} \\ &\quad + U_p \sum_{\boldsymbol{r},\sigma} \left(n_{p_x,\boldsymbol{r}+\frac{a}{2}\hat{\boldsymbol{x}},\sigma} n_{p_x,\boldsymbol{r}+\frac{a}{2}\hat{\boldsymbol{x}},-\sigma} + n_{p_y,\boldsymbol{r}+\frac{a}{2}\hat{\boldsymbol{y}},\sigma} n_{p_y,\boldsymbol{r}+\frac{a}{2}\hat{\boldsymbol{y}},-\sigma} \right) \end{aligned} \tag{5.22}$$

describes local (on-site) repulsion between electrons, whereas

$$H^{(2)}_{\text{int}} = V \sum_{\boldsymbol{r},\sigma,\sigma'} \sum_{\gamma=\pm} n_{d,\boldsymbol{r},\sigma} \left(n_{p_x,\boldsymbol{r}+\gamma\frac{a}{2}\hat{\boldsymbol{x}},\sigma'} + n_{p_y,\boldsymbol{r}+\gamma\frac{a}{2}\hat{\boldsymbol{y}},\sigma'} \right) \tag{5.23}$$

represents Coulomb interactions between nearest neighbour copper and oxygen atoms. We could also include Coulomb interactions between oxygen atoms by including the term

$$H^{(3)}_{\text{int}} = W \sum_{\boldsymbol{r},\sigma,\sigma'} \sum_{\gamma,\eta=\pm} n_{p_x,\boldsymbol{r}+\gamma\frac{a}{2}\hat{\boldsymbol{x}},\sigma} n_{p_y,\boldsymbol{r}+\eta\frac{a}{2}\hat{\boldsymbol{y}},\sigma} \ . \tag{5.24}$$

This is usually assumed small and neglected. This will also be done here, but we will comment on its effect at the end of the derivation.

Like Varma [91], we will assume that the effects of the on-site repulsions $H^{(1)}_{\text{int}}$ are to renormalise the hopping parameters, $\bar{t}_{pd} = |x| t_{pd} \to t_{pd}$ and $\bar{t}_{pp} = |x| t_{pp} \to t_{pp}$, where $|x|$ is the deviation from half-filling. This approximation is supposed to be valid in the limit $(U_d, U_p) \gg (t_{pd}, t_{pp})$ and when $|x|$ is small [91]. In the following, we therefore only consider the nearest neighbour interaction $H^{(2)}_{\text{int}}$ explicitly.

It is convenient to transform to a wavevector basis. Formally, we may write

$$\begin{aligned} d_{\boldsymbol{k},\sigma} &= \frac{1}{\sqrt{N}} \sum_{\boldsymbol{r}} d_{\boldsymbol{r},\sigma} \, \mathrm{e}^{\mathrm{i}\boldsymbol{k}\cdot\boldsymbol{r}} \ , \quad d_{\boldsymbol{r},\sigma} = \frac{1}{\sqrt{N}} \sum_{\boldsymbol{k}} d_{\boldsymbol{k},\sigma} \, \mathrm{e}^{-\mathrm{i}\boldsymbol{k}\cdot\boldsymbol{r}} \ , \\ p_{x,\boldsymbol{k},\sigma} &= \frac{1}{\sqrt{N}} \sum_{\boldsymbol{r}} p_{x,\boldsymbol{r}\pm\frac{a}{2}\hat{\boldsymbol{x}},\sigma} \, \mathrm{e}^{\mathrm{i}\boldsymbol{k}\cdot\left(\boldsymbol{r}\pm\frac{a}{2}\hat{\boldsymbol{x}}\right)} \ , \quad p_{x,\boldsymbol{r}\pm\frac{a}{2}\hat{\boldsymbol{x}},\sigma} = \frac{1}{\sqrt{N}} \sum_{\boldsymbol{k}} p_{x,\boldsymbol{k},\sigma} \, \mathrm{e}^{-\mathrm{i}\boldsymbol{k}\cdot\left(\boldsymbol{r}\pm\frac{a}{2}\hat{\boldsymbol{x}}\right)} \end{aligned} \tag{5.25}$$

and similarly for $p_{y,\boldsymbol{k},\sigma}$. N is the number of copper lattice sites. Using $N^{-1/2}$ as a prefactor ensures that the Fourier space operators also respect the usual anticommutation relations. We also introduce the abbreviations

$$s_{x,k} \equiv \sin\left(\frac{k_x a}{2}\right) \ , \quad c_{x,k} \equiv \cos\left(\frac{k_x a}{2}\right) \ , \tag{5.26}$$

and similarly for k_y.

Writing the Hamiltonian as $H - \mu N \equiv (H_0 - \mu N) + H_{\text{int}}^{(2)}$, we arrive at

$$\begin{aligned} H_0 - \mu N = \sum_{\boldsymbol{k},\sigma} \Big[& (\varepsilon_d - \mu)\, n_{d,\boldsymbol{k},\sigma} - \mu \left(n_{p_x,\boldsymbol{k},\sigma} + n_{p_y,\boldsymbol{k},\sigma} \right) \\ & - 2\mathrm{i} t_{pd} s_{x,k} \left(d_{\boldsymbol{k},\sigma}^\dagger p_{x,\boldsymbol{k},\sigma} - p_{x,\boldsymbol{k},\sigma}^\dagger d_{\boldsymbol{k},\sigma} \right) + 2\mathrm{i} t_{pd} s_{y,k} \left(d_{\boldsymbol{k},\sigma}^\dagger p_{y,\boldsymbol{k},\sigma} - p_{y,\boldsymbol{k},\sigma}^\dagger d_{\boldsymbol{k},\sigma} \right) \\ & - 4 t_{pp} s_{x,k} s_{y,k} \left(p_{x,\boldsymbol{k},\sigma}^\dagger p_{y,\boldsymbol{k},\sigma} + p_{y,\boldsymbol{k},\sigma}^\dagger p_{x,\boldsymbol{k},\sigma} \right) \Big] \end{aligned} \tag{5.27}$$

and

$$H_{\text{int}}^{(2)} = \frac{2V}{N} \sum_{\boldsymbol{k},\boldsymbol{k}',\boldsymbol{q}} \sum_{\sigma,\sigma'} d_{\boldsymbol{k},\sigma}^\dagger d_{\boldsymbol{k}',\sigma} \left[c_{x,k-k'}\, p_{x,\boldsymbol{k}'-\boldsymbol{q},\sigma'}^\dagger p_{x,\boldsymbol{k}-\boldsymbol{q},\sigma'} + c_{y,k-k'}\, p_{y,\boldsymbol{k}'-\boldsymbol{q},\sigma'}^\dagger p_{y,\boldsymbol{k}-\boldsymbol{q},\sigma'} \right] . \tag{5.28}$$

Note that, by choosing other momentum variables, there are many ways of writing the latter expression. However, this way will be convenient in the following.

5.4.3 Derivation of the Effective Theory

We will now go through the basics steps in the procedure of deriving an effective theory in terms of the horizontal and vertical currents $J_{\boldsymbol{r}}^x$ and $J_{\boldsymbol{r}}^y$ in Figure 5.5, which are supposed to order in the circulating current phase proposed by Varma [91].

Rewriting the Interaction Term

The strategy for deriving this theory is to decouple the interaction term $H_{\text{int}}^{(2)}$ in the manner sketched in section 2.3.1. As mentioned there, the choice of decoupling should be motivated by the expected behaviour of the physical system. Thus, we need to write the interaction term in a different way, inspired by Ref. [91]. Let us define the operators

$$A_{\boldsymbol{q},\sigma,\sigma'}^{(i)} = \frac{1}{\sqrt{N}} \sum_{\boldsymbol{k}} \left(a_{x,k-q}^{(i)} p_{x,\boldsymbol{k}-\boldsymbol{q},\sigma'}^\dagger d_{\boldsymbol{k},\sigma} + a_{y,k-q}^{(i)} p_{y,\boldsymbol{k}-\boldsymbol{q},\sigma'}^\dagger d_{\boldsymbol{k},\sigma} \right) , \tag{5.29}$$

where $i = 1, 2, 3, 4$ and the prefactors are

$$a_{x,k}^{(i)} = \begin{cases} s_{x,k} \ , & i = 1, 2 \\ c_{x,k} \ , & i = 3, 4 \end{cases} \quad , \quad a_{y,k}^{(i)} = \begin{cases} (-1)^{i+1} s_{y,k} \ , & i = 1, 2 \\ (-1)^{i+1} c_{y,k} \ , & i = 3, 4 \end{cases} . \tag{5.30}$$

By using the fermionic anticommutation relations, one may show that

$$H_{\text{int}}^{(2)} = -V \sum_{\boldsymbol{q}} \sum_{\sigma,\sigma'} \sum_{i=1}^{4} A_{\boldsymbol{q},\sigma,\sigma'}^{(i)\,\dagger} A_{\boldsymbol{q},\sigma,\sigma'}^{(i)} + 8V \sum_{\boldsymbol{k},\sigma} n_{d,\boldsymbol{k},\sigma} . \tag{5.31}$$

The last term may be included in H_0 through the renormalisation $\varepsilon_d + 8V \to \varepsilon_d$. Ref. [91] contains a discussion of $\langle A^{(i)}_{0,\sigma,\sigma'}\rangle$ as potential order parameters in the high-T_c cuprates. The reason for considering $\boldsymbol{q} = 0$ is to search for order parameters that do not break the translational symmetry of the lattice. The $i = 2$ part transforms like the kinetic energy in H_0 and hence can not lead to a broken symmetry. Order in the $i = 1$ and $i = 3, 4$ parts may give rise to different current patterns.

Let us investigate the $i = 3, 4$ part more closely. First, one should notice that $A^{(3),(4)}_{\boldsymbol{q},\sigma,\sigma'}$ can be written

$$A^{(3),(4)}_{\boldsymbol{q},\sigma,\sigma'} = \frac{1}{2\sqrt{N}} \sum_{\boldsymbol{r}} \left[\left(p^\dagger_{x,\boldsymbol{r}+\frac{a}{2}\hat{\boldsymbol{x}},\sigma'} + p^\dagger_{x,\boldsymbol{r}-\frac{a}{2}\hat{\boldsymbol{x}},\sigma'} \right) \pm \left(p^\dagger_{y,\boldsymbol{r}+\frac{a}{2}\hat{\boldsymbol{y}},\sigma'} + p^\dagger_{y,\boldsymbol{r}-\frac{a}{2}\hat{\boldsymbol{y}},\sigma'} \right) \right] d_{\boldsymbol{r},\sigma}\, \mathrm{e}^{\mathrm{i}\boldsymbol{q}\cdot\boldsymbol{r}} \ , \tag{5.32}$$

where the upper(lower) sign refers to 3(4). Next, we define the four operators

$$\begin{aligned}
\kappa^x_{\boldsymbol{r},\sigma,\sigma'} &= \frac{1}{2}\left[d^\dagger_{\boldsymbol{r},\sigma} \left(p_{x,\boldsymbol{r}+\frac{a}{2}\hat{\boldsymbol{x}},\sigma'} + p_{x,\boldsymbol{r}-\frac{a}{2}\hat{\boldsymbol{x}},\sigma'} \right) + \text{h.c.} \right] \\
j^x_{\boldsymbol{r},\sigma,\sigma'} &= \frac{\mathrm{i}}{2}\left[d^\dagger_{\boldsymbol{r},\sigma} \left(p_{x,\boldsymbol{r}+\frac{a}{2}\hat{\boldsymbol{x}},\sigma'} + p_{x,\boldsymbol{r}-\frac{a}{2}\hat{\boldsymbol{x}},\sigma'} \right) - \text{h.c.} \right] \\
\kappa^y_{\boldsymbol{r},\sigma,\sigma'} &= -\frac{1}{2}\left[d^\dagger_{\boldsymbol{r},\sigma} \left(p_{y,\boldsymbol{r}+\frac{a}{2}\hat{\boldsymbol{y}},\sigma'} + p_{y,\boldsymbol{r}-\frac{a}{2}\hat{\boldsymbol{y}},\sigma'} \right) + \text{h.c.} \right] \\
j^y_{\boldsymbol{r},\sigma,\sigma'} &= -\frac{\mathrm{i}}{2}\left[d^\dagger_{\boldsymbol{r},\sigma} \left(p_{y,\boldsymbol{r}+\frac{a}{2}\hat{\boldsymbol{y}},\sigma'} + p_{y,\boldsymbol{r}-\frac{a}{2}\hat{\boldsymbol{y}},\sigma'} \right) - \text{h.c.} \right] \ .
\end{aligned} \tag{5.33}$$

These definitions enable us to write

$$\begin{aligned}
A^{(3),(4)}_{\boldsymbol{q},\sigma,\sigma'} &= \frac{1}{2\sqrt{N}} \sum_{\boldsymbol{r}} \left[\kappa^x_{\boldsymbol{r},\sigma,\sigma'} + \mathrm{i} j^x_{\boldsymbol{r},\sigma,\sigma'} \mp \left(\kappa^y_{\boldsymbol{r},\sigma,\sigma'} + \mathrm{i} j^y_{\boldsymbol{r},\sigma,\sigma'} \right) \right] \mathrm{e}^{\mathrm{i}\boldsymbol{q}\cdot\boldsymbol{r}} \\
&= \frac{1}{2}\left[\kappa^x_{\boldsymbol{q},\sigma,\sigma'} + \mathrm{i} j^x_{\boldsymbol{q},\sigma,\sigma'} \mp \left(\kappa^y_{\boldsymbol{q},\sigma,\sigma'} + \mathrm{i} j^y_{\boldsymbol{q},\sigma,\sigma'} \right) \right] \ .
\end{aligned} \tag{5.34}$$

Let us try to interpret the operator $j^x_{\boldsymbol{r},\sigma,\sigma'}$ in Equations (5.33). From the Heisenberg equation of motion, one may show that the operator $j^x_{\mathrm{R},\boldsymbol{r},\sigma}$ for a particle current with spin σ *from* a copper atom in $\boldsymbol{r}$ *to* the oxygen in $\boldsymbol{r} + \frac{a}{2}\hat{\boldsymbol{x}}$ is

$$j^x_{\mathrm{R},\boldsymbol{r},\sigma} = -\mathrm{i}t_{pd} \left(p^\dagger_{x,\boldsymbol{r}+\frac{a}{2}\hat{\boldsymbol{x}},\sigma} d_{\boldsymbol{r},\sigma} - \text{h.c.} \right) \ . \tag{5.35}$$

In addition, the current $j^x_{\mathrm{L},\boldsymbol{r},\sigma}$ *from* the oxygen in $\boldsymbol{r} - \frac{a}{2}\hat{\boldsymbol{x}}$ *to* the copper in $\boldsymbol{r}$ is

$$j^x_{\mathrm{L},\boldsymbol{r},\sigma} = \mathrm{i}t_{pd} \left(d^\dagger_{\boldsymbol{r},\sigma} p_{x,\boldsymbol{r}-\frac{a}{2}\hat{\boldsymbol{x}},\sigma} - \text{h.c.} \right) \ . \tag{5.36}$$

The sign difference is a consequence of the wavefunction signs indicated in Figure 5.6. In the current pattern depicted in Figure 5.5, these operators will have equal, nonzero expectation values. Thus, a suitable operator for the horizontal current of particles with spin σ *across the unit cell* from the oxygen in $\boldsymbol{r} - \frac{a}{2}\hat{\boldsymbol{x}}$ to the oxygen in $\boldsymbol{r} + \frac{a}{2}\hat{\boldsymbol{x}}$ is $t_{pd}(j^x_{\mathrm{L},\boldsymbol{r},\sigma} + j^x_{\mathrm{R},\boldsymbol{r},\sigma})/2$. This

is nothing but the spin-diagonal version of $j^x_{\boldsymbol{r},\sigma,\sigma'}$. In the same way, one may argue that spin-diagonal elements of $j^y_{\boldsymbol{r},\sigma,\sigma'}$ are currents from the lower to the upper oxygen in the unit cell. We also note that the off-diagonal elements represent spin-flip currents, not believed to be relevant to the cuprates. Finite expectation values of the operators $\kappa^{x(y)}_{\boldsymbol{r},\sigma,\sigma'}$ would lead to alterations of the point group symmetry, so-called Landau-Pomeranchuk instabilities. These are also not expected to be relevant, at least not in the circulating current phase we intend to describe.

One can also express the operators $A^{(1),(2)}_{\boldsymbol{q},\sigma,\sigma'}$ in a similar way. The current operators in that case would have finite expectation values in a different current pattern. See Ref. [91] for details. We do not investigate this further here, since both the ARPES [85] and the neutron scattering experiments [83, 84] are consistent with the current pattern arising from the $i = 3, 4$-part. Note also that an effective theory for the $i = 1$-part was considered in Ref. [123].

The Hubbard-Stratonovich Decoupling

We proceed by expressing the theory in the functional integral formulation. The fermion operators are then replaced by Grassman variables. However, to avoid complicated notation, we will keep the same symbols, such that $d_{\boldsymbol{k},\sigma}$ hereafter refers to a Grassman variable. The interaction term $H^{(2)}_{\text{int}}$ is then Hubbard-Stratonovich-decoupled,

$$\begin{aligned}
&\mathrm{e}^{-\int_0^\beta \mathrm{d}\tau\, H^{(2)}_{\text{int}}(\tau)} = \mathrm{e}^{V\int_0^\beta \mathrm{d}\tau \sum_{\boldsymbol{q},\sigma,\sigma',i} A^{(i)\,*}_{\boldsymbol{q},\sigma,\sigma'}(\tau) A^{(i)}_{\boldsymbol{q},\sigma,\sigma'}(\tau)} \\
&\propto \int \mathcal{D}[R^*, R] \mathrm{e}^{-\int_0^\beta \mathrm{d}\tau \sum_{\boldsymbol{q},\sigma,\sigma',i} \left(\frac{1}{V} R^{(i)\,*}_{\boldsymbol{q},\sigma,\sigma'}(\tau) R^{(i)}_{\boldsymbol{q},\sigma,\sigma'}(\tau) + R^{(i)\,*}_{\boldsymbol{q},\sigma,\sigma'}(\tau) A^{(i)}_{\boldsymbol{q},\sigma,\sigma'}(\tau) + A^{(i)\,*}_{\boldsymbol{q},\sigma,\sigma'}(\tau) R^{(i)}_{\boldsymbol{q},\sigma,\sigma'}(\tau) \right)} \ , \quad (5.37)
\end{aligned}$$

where the boundary conditions on the R-fields are periodic, *i.e.* they are bosonic fields. Note that $*$ now simply means complex conjugation. Let us for a while return to real space, where $\langle R^{(i)}_{\boldsymbol{r},\sigma,\sigma'}(\tau)\rangle = -V\langle A^{(i)}_{\boldsymbol{r},\sigma,\sigma'}(\tau)\rangle$. In correspondence with Equation (5.34), we define

$$R^{(3),(4)}_{\boldsymbol{r},\sigma,\sigma'}(\tau) = -\frac{1}{2}\left[K^x_{\boldsymbol{r},\sigma,\sigma'} + \mathrm{i}J^x_{\boldsymbol{r},\sigma,\sigma'} \mp \left(K^y_{\boldsymbol{r},\sigma,\sigma'} + \mathrm{i}J^y_{\boldsymbol{r},\sigma,\sigma'}\right)\right] \ . \quad (5.38)$$

Again, the upper(lower) sign refer to $i = 3(4)$. The fields $K^{x(y)}_{\boldsymbol{r},\sigma,\sigma'}$ and $J^{x(y)}_{\boldsymbol{r},\sigma,\sigma'}$ are real, such that the number of degrees of freedom is conserved. This definition gives $\langle K^x_{\boldsymbol{r},\sigma,\sigma'}(\tau)\rangle = V\langle \kappa^x_{\boldsymbol{r},\sigma,\sigma'}(\tau)\rangle$ and $\langle J^x_{\boldsymbol{r},\sigma,\sigma'}(\tau)\rangle = V\langle j^x_{\boldsymbol{r},\sigma,\sigma'}(\tau)\rangle$ and similarly for y. As stated earlier, the current pattern in Figure 5.5 is characterised by nonzero expectation values of the spin-diagonal current operators $j^x_{\boldsymbol{r},\sigma,\sigma'}\delta_{\sigma,\sigma'}$ and $j^y_{\boldsymbol{r},\sigma,\sigma'}\delta_{\sigma,\sigma'}$. Thus, we retain only the auxiliary fields $J^x_{\boldsymbol{r},\sigma,\sigma'}\delta_{\sigma,\sigma'} \equiv J^x_{\boldsymbol{r}}\,\delta_{\sigma,\sigma'}$ and $J^y_{\boldsymbol{r},\sigma,\sigma'}\delta_{\sigma,\sigma'} \equiv J^y_{\boldsymbol{r}}\,\delta_{\sigma,\sigma'}$ in the following.[12] The rest of the auxiliary fields, $R^{(1)}$, $R^{(2)}$, K^x, K^y and the spin-flip currents, are set to zero, since we do not consider ordering nor fluctuations in these quantities. An important point to remember is that the fields $J^x_{\boldsymbol{r}}$ and $J^y_{\boldsymbol{r}}$ *transform as vectors* under a change of coordinate system.

[12] Here, we make the natural assumption that the current expectation values are the same for both spins.

At this point, we transform from imaginary time to Matsubara frequencies. In general, for bosonic fields $b(\tau)$ and fermionic fields $f(\tau)$, the transformations are defined by

$$\begin{aligned} b(\mathrm{i}\omega_\nu) &= \frac{1}{\sqrt{\beta}} \int_0^\beta \mathrm{d}\tau\, b(\tau)\, \mathrm{e}^{\mathrm{i}\omega_\nu \tau} \ , \quad b(\tau) = \frac{1}{\sqrt{\beta}} \sum_{\omega_\nu} b(\mathrm{i}\omega_\nu)\, \mathrm{e}^{-\mathrm{i}\omega_\nu \tau} \ , \quad \omega_\nu = \frac{2\nu\pi}{\beta} \\ f(\mathrm{i}\omega_n) &= \frac{1}{\sqrt{\beta}} \int_0^\beta \mathrm{d}\tau\, f(\tau)\, \mathrm{e}^{\mathrm{i}\omega_n \tau} \ , \quad f(\tau) = \frac{1}{\sqrt{\beta}} \sum_{\omega_n} f(\mathrm{i}\omega_n)\, \mathrm{e}^{-\mathrm{i}\omega_n \tau} \ , \quad \omega_n = \frac{(2n+1)\pi}{\beta} \ , \end{aligned} \tag{5.39}$$

where ν and n are integers. Furthermore, it is convenient to perform the variable transformations $p_{x,\boldsymbol{k},\sigma} \rightarrow \mathrm{i}p_{x,\boldsymbol{k},\sigma}$ and $p_{y,\boldsymbol{k},\sigma} \rightarrow -\mathrm{i}p_{y,\boldsymbol{k},\sigma}$. Let us also define the vector $\Phi_{\boldsymbol{k},\sigma}(\mathrm{i}\omega_n)$ through its adjoint (complex conjugate and transpose),

$$\Phi^\dagger_{\boldsymbol{k},\sigma}(\mathrm{i}\omega_n) = \left[d^*_{\boldsymbol{k},\sigma}(\mathrm{i}\omega_n), p^*_{x,\boldsymbol{k},\sigma}(\mathrm{i}\omega_n), p^*_{y,\boldsymbol{k},\sigma}(\mathrm{i}\omega_n) \right] . \tag{5.40}$$

We are then ready to write the partition function for the system as

$$Z \propto \int \mathcal{D}[R^*, R] \mathcal{D}[\Phi^\dagger, \Phi]\, \mathrm{e}^{-S[R^*, R, \Phi^\dagger, \Phi]} \ , \tag{5.41}$$

where the action is

$$\begin{aligned} S[R^*, R, \Phi^\dagger, \Phi] &= \frac{1}{2V} \sum_{\boldsymbol{q}, \omega_\nu} \left[J^x_{\boldsymbol{q}}(\mathrm{i}\omega_\nu) J^x_{-\boldsymbol{q}}(-\mathrm{i}\omega_\nu) + J^y_{\boldsymbol{q}}(\mathrm{i}\omega_\nu) J^y_{-\boldsymbol{q}}(-\mathrm{i}\omega_\nu) \right] \\ &+ \sum_{\boldsymbol{k}_1, \boldsymbol{k}_2} \sum_{\sigma_1, \sigma_2} \sum_{\omega_{n_1}, \omega_{n_2}} \Phi^\dagger_{\boldsymbol{k}_1, \sigma_1}(\mathrm{i}\omega_{n_1}) \left[\mathcal{G}_0^{-1} + \Sigma \right]_{\boldsymbol{k}_1, \boldsymbol{k}_2, \sigma_1, \sigma_2} (\mathrm{i}\omega_{n_1}, \mathrm{i}\omega_{n_2})\, \Phi_{\boldsymbol{k}_2, \sigma_2}(\mathrm{i}\omega_{n_2}) \ . \end{aligned} \tag{5.42}$$

Here, $\mathcal{G}_0^{-1}$ and Σ are matrices in momentum space, spin space, frequency space and the space of atomic orbitals. Their elements are given by

$$\mathcal{G}^{-1}_{0,\boldsymbol{k}_1 \boldsymbol{k}_2, \sigma_1 \sigma_2}(\mathrm{i}\omega_{n_1}, \mathrm{i}\omega_{n_2}) = \delta_{\boldsymbol{k}_1, \boldsymbol{k}_2} \delta_{n_1, n_2} \delta_{\sigma_1, \sigma_2} \begin{pmatrix} -\mathrm{i}\omega_{n_1} + \varepsilon_d - \mu & 2t_{pd} s_{x,k_1} & 2t_{pd} s_{y,k_1} \\ 2t_{pd} s_{x,k_1} & -\mathrm{i}\omega_{n_1} - \mu & 4t_{pp} s_{x,k_1} s_{y,k_1} \\ 2t_{pd} s_{y,k_1} & 4t_{pp} s_{x,k_1} s_{y,k_1} & -\mathrm{i}\omega_{n_1} - \mu \end{pmatrix} \tag{5.43}$$

and

$$\Sigma_{\boldsymbol{k}_1 \boldsymbol{k}_2, \sigma_1 \sigma_2}(\mathrm{i}\omega_{n_1}, \mathrm{i}\omega_{n_2}) = \frac{\delta_{\sigma_1 \sigma_2}}{\sqrt{\beta N}} \begin{pmatrix} 0 & c_{x,k_2} J^x_{\boldsymbol{k}_{12}}(\mathrm{i}\omega_{12}) & c_{y,k_2} J^y_{\boldsymbol{k}_{12}}(\mathrm{i}\omega_{12}) \\ c_{x,k_1} J^x_{\boldsymbol{k}_{12}}(\mathrm{i}\omega_{12}) & 0 & 0 \\ c_{y,k_1} J^y_{\boldsymbol{k}_{12}}(\mathrm{i}\omega_{12}) & 0 & 0 \end{pmatrix} , \tag{5.44}$$

where $\boldsymbol{k}_{12} \equiv \boldsymbol{k}_1 - \boldsymbol{k}_2$ and $\omega_{12} \equiv \omega_{n_1} - \omega_{n_2}$. Note that $J^{x\,*}_{\boldsymbol{k}_{12}}(\mathrm{i}\omega_{12}) = J^x_{-\boldsymbol{k}_{12}}(-\mathrm{i}\omega_{12})$. The decoupling of the interaction term has rendered the integrals over the fermionic fields Gaussian. Performing the integral over the fermionic fields gives the action

$$S[R^*, R] = \frac{1}{2V} \sum_{\boldsymbol{q}, \omega_\nu} \left[J^x_{\boldsymbol{q}}(\mathrm{i}\omega_\nu) J^x_{-\boldsymbol{q}}(-\mathrm{i}\omega_\nu) + J^y_{\boldsymbol{q}}(\mathrm{i}\omega_\nu) J^y_{-\boldsymbol{q}}(-\mathrm{i}\omega_\nu) \right] - \mathrm{Tr}\, \ln \left[\mathcal{G}_0^{-1} + \Sigma \right] \ , \tag{5.45}$$

The trace denotes a sum over the diagonal elements in momentum, spin, frequency and orbital space.

We now have an effective theory in terms of the current fields J^x and J^y. However, the last term in Equation (5.45) is very complicated, such that the theory in this form is not of much use. To get further, we first note that $\mathrm{Tr}\,\ln\left[\mathcal{G}_0^{-1}+\Sigma\right] = \mathrm{Tr}\,\ln\mathcal{G}_0^{-1} + \mathrm{Tr}\,\ln\left[1+\mathcal{G}_0\Sigma\right]$. The first term $\mathrm{Tr}\,\ln\mathcal{G}_0^{-1}$ is simply the negative of the free energy of the noninteracting system and is independent of the currents J^x and J^y. Thus, it goes outside the functional integral as an uninteresting constant. At this point, it is customary [16] to expand the logarithm in the last term in powers of J^x and J^y, and then truncate the expansion. Furthermore, since it is the long-wavelength and low-frequency fluctuations that is important near the phase transition, the coefficients in the expansion may then be expanded in small $|\boldsymbol{q}|$ and $|\omega_\nu|$. Even though there might not be an appropriate smallness parameter, this procedure is often expected to produce a theory with the correct properties.

A word of caution is however in order at this point. It has recently been pointed out [17] that in the case of a $|\boldsymbol{q}|=0$ order parameter coupled to gapless fermions, like in the example considered here, this procedure might not be appropriate at $T=0$. It could lead to singular coefficients in all orders of the expansion. This will for example make the theory unsuited for renormalisation group analysis. However, it is believed that this procedure is safer at $T>0$ [17]. With this in mind, we will in the following nevertheless expand the logarithm as sketched above. After all, it is ultimately the fluctuation spectrum at nonzero temperatures above the superconducting phase we are interested in.

Deriving the Coefficients

To find the terms in the expansion $\mathrm{Tr}\,\ln\left[1+\mathcal{G}_0\Sigma\right] = \mathrm{Tr}\,\left[\mathcal{G}_0\Sigma\right] - \frac{1}{2}\mathrm{Tr}\,\left[\mathcal{G}_0\Sigma\right]^2 + \mathcal{O}(J^3)$, one needs to obtain the inverse of the matrix $\mathcal{G}_0^{-1}$. The result is given by $\mathcal{G}_{0,\boldsymbol{k}_1,\boldsymbol{k}_2,\sigma_1,\sigma_2}(\mathrm{i}\omega_{n_1},\mathrm{i}\omega_{n_2}) \equiv \mathcal{G}_{0,\boldsymbol{k}_1}(\mathrm{i}\omega_{n_1})\delta_{\boldsymbol{k}_1,\boldsymbol{k}_2}\delta_{n_1,n_2}\delta_{\sigma_1,\sigma_2}$, where

$$\mathcal{G}_{0,\boldsymbol{k}}(\mathrm{i}\omega_n) = -\sum_{\lambda=\pm,0}\begin{pmatrix} K_{\lambda,\boldsymbol{k}} & L_{x,\lambda,\boldsymbol{k}} & L_{y,\lambda,\boldsymbol{k}} \\ L_{x,\lambda,\boldsymbol{k}} & M_{xx,\lambda,\boldsymbol{k}} & M_{xy,\lambda,\boldsymbol{k}} \\ L_{y,\lambda,\boldsymbol{k}} & M_{xy,\lambda,\boldsymbol{k}} & M_{yy,\lambda,\boldsymbol{k}} \end{pmatrix}\frac{G_{\lambda,\boldsymbol{k}}(\mathrm{i}\omega_n)}{\mathcal{N}_{\lambda,\boldsymbol{k}}}\ . \tag{5.46}$$

Several quantities need to be introduced. $G_{\lambda,\boldsymbol{k}}(\mathrm{i}\omega_n)$ are the Green's functions for the bands obtained by diagonalising the noninteracting fermionic theory, denoted by the band index $\lambda=(-,0,+)$. The Green's functions are

$$G_{\lambda,\boldsymbol{k}}(\mathrm{i}\omega_n) = \frac{1}{\mathrm{i}\omega_n - (E_{\lambda,\boldsymbol{k}}-\mu)}\ . \tag{5.47}$$

The dispersion relations for the bands $E_{\lambda,\boldsymbol{k}}$ are determined by the equation

$$E_{\lambda,\boldsymbol{k}}^3 - \varepsilon_d E_{\lambda,\boldsymbol{k}}^2 - 4\left(t_{pd}^2 s_{xy,k}^2 + 4t_{pp}^2 s_{x,k}^2 s_{y,k}^2\right)E_{\lambda,\boldsymbol{k}} - 16t_{pp}\,s_{x,k}^2 s_{y,k}^2\left(2t_{pd}^2 - \varepsilon_d t_{pp}\right) = 0\ . \tag{5.48}$$

The abbreviation $s^2_{xy,k} = s^2_{x,k} + s^2_{y,k}$ has been introduced. Note that $E_{\lambda,\boldsymbol{k}}$ is even in both k_x and k_y. The explicit solutions to Equation (5.48) are complicated, but they are not really needed to determine the structure of the theory. At half-filling, the upper band (+) is partially filled, whereas the other bands are full. In other words, the energy μ lies in the (+)-band, the antibonding band. The explicit expressions for the band dispersions simplify in the special case $t_{pp} = 0$, giving

$$E_{\pm,\boldsymbol{k}} = \frac{\varepsilon_d}{2} \pm \sqrt{\left(\frac{\varepsilon_d}{2}\right)^2 + 4t^2_{pd} s^2_{xy,k}} \ , \qquad E_{0,\boldsymbol{k}} = 0 \ . \tag{5.49}$$

This provides a qualitative picture of the band structure when t_{pp} is small. A nonzero t_{pp} is however crucial to make nonzero currents J^x and J^y energetically favourable [91]. Furthermore, we have defined

$$\mathcal{N}_{\lambda,\boldsymbol{k}} = \left(E_{\bar{\lambda}_1,\boldsymbol{k}} - E_{\lambda,\boldsymbol{k}}\right)\left(E_{\bar{\lambda}_2,\boldsymbol{k}} - E_{\lambda,\boldsymbol{k}}\right) \ , \qquad \bar{\lambda}_i \neq \lambda \ , \ \bar{\lambda}_1 \neq \bar{\lambda}_2 \tag{5.50}$$

i.e. it is the product of the energy differences to the other two bands. This means that $\mathcal{N}_{\pm,\boldsymbol{k}} > 0$ and $\mathcal{N}_{0,\boldsymbol{k}} < 0$. Finally, the remaining quantities appearing in the matrix in (5.46) are[13]

$$\begin{aligned}
K_{\lambda,\boldsymbol{k}} &= \left(E^2_{\lambda,\boldsymbol{k}} - 16t^2_{pp} s^2_{x,k} s^2_{y,k}\right) \ , \\
L_{x,\lambda,\boldsymbol{k}} &= 2t_{pd} s_{x,k}\left(E_{\lambda,\boldsymbol{k}} + 4t_{pp} s^2_{y,k}\right) \ , \\
L_{y,\lambda,\boldsymbol{k}} &= 2t_{pd} s_{y,k}\left(E_{\lambda,\boldsymbol{k}} + 4t_{pp} s^2_{x,k}\right) \ , \\
M_{xx,\lambda,\boldsymbol{k}} &= \left(E^2_{\lambda,\boldsymbol{k}} - \varepsilon_d E_{\lambda,\boldsymbol{k}} - 4t^2_{pd} s^2_{y,k}\right) \ , \\
M_{yy,\lambda,\boldsymbol{k}} &= \left(E^2_{\lambda,\boldsymbol{k}} - \varepsilon_d E_{\lambda,\boldsymbol{k}} - 4t^2_{pd} s^2_{x,k}\right) \ , \\
M_{xy,\lambda,\boldsymbol{k}} &= 4 s_{x,k} s_{y,k}\left[\left(E_{\lambda,\boldsymbol{k}} - \varepsilon_d\right) t_{pp} + t^2_{pd}\right] \ .
\end{aligned} \tag{5.51}$$

The most important things to notice here are the symmetry properties in momentum space of the various expressions.

We may now calculate the various terms in the expansion of the logarithm. Consider the first order term,

$$\mathrm{Tr}\,[\mathcal{G}_0\Sigma] = -\frac{4}{\sqrt{\beta N}} \sum_{\boldsymbol{k},\omega_n} \sum_{\lambda=\pm,0} \left[L_{x,\lambda,\boldsymbol{k}} c_{x,k} J^x_0(0) + L_{y,\lambda,\boldsymbol{k}} c_{y,k} J^y_0(0)\right] G_{\lambda,\boldsymbol{k}}(\mathrm{i}\omega_n) = 0. \tag{5.52}$$

This is zero since $L_{x,\lambda,\boldsymbol{k}}$ and $L_{y,\lambda,\boldsymbol{k}}$ are odd in k_x and k_y, respectively. In fact, all odd order terms in $J^{x,y}$ will be zero, which ensures that the effective theory is time-reversal

[13] One can express these in different ways by exploiting Equation (5.48). By doing that, one may show that $M_{xx,\lambda,\boldsymbol{k}} \propto s^2_{x,k}$ and $M_{yy,\lambda,\boldsymbol{k}} \propto s^2_{y,k}$, which is useful when deriving the dissipation term.

symmetric. We swiftly move on to the second order term, which becomes[14]

$$\begin{aligned}
\mathrm{Tr}\,[\mathcal{G}_0\Sigma]^2 = \frac{2}{\beta N}\sum_{\boldsymbol{k}_1,\boldsymbol{k}_2}\sum_{\omega_{n_1},\omega_{n_2}}\sum_{\lambda,\rho}\frac{G_{\lambda,\boldsymbol{k}_1}(\mathrm{i}\omega_{n_1})G_{\rho,\boldsymbol{k}_2}(\mathrm{i}\omega_{n_2})}{\mathcal{N}_{\lambda,\boldsymbol{k}_1}\mathcal{N}_{\rho,\boldsymbol{k}_2}} \\
\times\Bigg[\Big(2L_{x,\lambda,\boldsymbol{k}_1}L_{x,\rho,\boldsymbol{k}_2}c_{x,k_1}c_{x,k_2}+K_{\lambda,\boldsymbol{k}_1}M_{xx,\rho,\boldsymbol{k}_2}c^2_{x,k_2}+K_{\rho,\boldsymbol{k}_2}M_{xx,\lambda,\boldsymbol{k}_1}c^2_{x,k_1}\Big) \\
\times J^x_{\boldsymbol{k}_{12}}(\mathrm{i}\omega_{12})J^x_{-\boldsymbol{k}_{12}}(-\mathrm{i}\omega_{12}) \\
+\Big(2L_{y,\lambda,\boldsymbol{k}_1}L_{y,\rho,\boldsymbol{k}_2}c_{y,k_1}c_{y,k_2}+K_{\lambda,\boldsymbol{k}_1}M_{yy,\rho,\boldsymbol{k}_2}c^2_{y,k_2}+K_{\rho,\boldsymbol{k}_2}M_{yy,\lambda,\boldsymbol{k}_1}c^2_{y,k_1}\Big) \\
\times J^y_{\boldsymbol{k}_{12}}(\mathrm{i}\omega_{12})J^y_{-\boldsymbol{k}_{12}}(-\mathrm{i}\omega_{12}) \\
+\Big(L_{x,\lambda,\boldsymbol{k}_1}L_{y,\rho,\boldsymbol{k}_2}c_{x,k_1}c_{y,k_2}+L_{y,\lambda,\boldsymbol{k}_1}L_{x,\rho,\boldsymbol{k}_2}c_{y,k_1}c_{x,k_2} \\
+K_{\lambda,\boldsymbol{k}_1}M_{xy,\rho,\boldsymbol{k}_2}c_{x,k_2}c_{y,k_2}+K_{\rho,\boldsymbol{k}_2}M_{xy,\lambda,\boldsymbol{k}_1}c_{x,k_1}c_{y,k_1}\Big) \\
\times\Big(J^x_{\boldsymbol{k}_{12}}(\mathrm{i}\omega_{12})J^y_{-\boldsymbol{k}_{12}}(-\mathrm{i}\omega_{12})+J^y_{\boldsymbol{k}_{12}}(\mathrm{i}\omega_{12})J^x_{-\boldsymbol{k}_{12}}(-\mathrm{i}\omega_{12})\Big)\Bigg]
\end{aligned} \tag{5.53}$$

Keep in mind that we are interested in long-wavelength and low-frequency fluctuations of the fields J^x and J^y, which means that we can expand the coefficients in $\boldsymbol{q}\equiv\boldsymbol{k}_{12}$ and $\omega_\nu\equiv\omega_{12}$. It is therefore convenient to introduce the variable changes

$$\boldsymbol{k}_1=\boldsymbol{k}\ ,\quad \boldsymbol{k}_2=\boldsymbol{k}-\boldsymbol{q}\ ,\quad \omega_{n_1}=\omega_n\ ,\quad \omega_{n_2}=\omega_n-\omega_\nu\ , \tag{5.54}$$

and expand the coefficients in $\boldsymbol{q}$ and ω_ν.

The last term in (5.53) couples the J^x- and J^y-fields. Notice that when $\boldsymbol{q}=0$, which means $\boldsymbol{k}_1=\boldsymbol{k}_2$, the summation over momentum in this term gives zero due to the symmetry properties of the quantities in Equations (5.51). This means that the coefficient of this term vanish when $\boldsymbol{q}=0$. This is expected, since the fields transform as vectors. However, the $\boldsymbol{q}\neq 0$ coefficients do not vanish. Terms of the form $q_xq_yJ^x_{\boldsymbol{q}}(\mathrm{i}\omega_\nu)J^y_{-\boldsymbol{q}}(-\mathrm{i}\omega_\nu)$ are invariant under coordinate transformations and do indeed appear in the expansion.

After the variable changes (5.54), we can perform the sum over the fermionic Matsubara frequency, which becomes

$$\frac{1}{\beta}\sum_{\omega_n}G_{\lambda,\boldsymbol{k}}(\mathrm{i}\omega_n)G_{\rho,\boldsymbol{k}-\boldsymbol{q}}(\mathrm{i}\omega_n-\mathrm{i}\omega_\nu)=\frac{f(E_{\rho,\boldsymbol{k}-\boldsymbol{q}}-\mu)-f(E_{\lambda,\boldsymbol{k}}-\mu)}{\mathrm{i}\omega_\nu+E_{\rho,\boldsymbol{k}-\boldsymbol{q}}-E_{\lambda,\boldsymbol{k}}}\ , \tag{5.55}$$

where $f(x)=(1+\mathrm{e}^{\beta x})^{-1}$ is the Fermi-Dirac distribution. Since the chemical potential μ lies in the upper band $(+)$, we assume that $f(E_{\lambda,\boldsymbol{k}}-\mu)\approx 1$ when $\lambda=\{-1,0\}$. This means that, even though there are 9 terms in the sums over λ,ρ, only 5 of them will

[14] It is possible to simplify this by changing variables in some of the terms. However, the expression presented here makes the symmetries clearer.

contribute. Moreover, of the 5 terms, only 3 are different. Thus, we need only consider $\lambda = 1$ and $\rho = \{-1, 0, 1\}$. Let us look at the cases $\rho = \{-1, 0\}$ first. The energy difference $E_{\lambda,\boldsymbol{k}} - E_{\rho,\boldsymbol{k}-\boldsymbol{q}}$ in the denominator will then be nonzero in the contributing terms of the $\boldsymbol{k}$-sum in Equation (5.53). We may then safely neglect the $\boldsymbol{q}$-dependence in Equation (5.55) and in $\mathcal{N}_{\rho,\boldsymbol{k}-\boldsymbol{q}}$, since we are to take the limit $\boldsymbol{q} \to 0$. Furthermore, since we consider $\omega_\nu \to 0$, we can expand the denominator in the quantity $\omega_\nu/(E_{\lambda,\boldsymbol{k}} - E_{\rho,\boldsymbol{k}})$. Ultimately, when combining this with the rest of the $\boldsymbol{q}$-dependent expression and investigating its symmetry properties, this will result in ω_ν-independent terms as well as terms proportional to ω_ν^2.

The $(\rho = \lambda = +)$-term is a bit more complicated. This term represents the coupling of the currents J^x and J^y to the gapless particle-hole excitations on the Fermi surface. For simplicity, we discuss this term in the limit $t_{pp} = 0$. The qualitative picture is not significantly changed by a finite t_{pp}. In this case, when expanding in small $(\omega_\nu, \boldsymbol{q})$, the $(\rho = \lambda = +)$-term in (5.53) becomes proportional to

$$\begin{aligned}
&\frac{t_{pd}^2}{N} \sum_{\boldsymbol{q},\omega_\nu} \sum_{\boldsymbol{k}} \frac{\partial f(E_{+,\boldsymbol{k}} - \mu)}{\partial E_{+,\boldsymbol{k}}} \frac{(\boldsymbol{v}_{\boldsymbol{k}} \cdot \boldsymbol{q})^2}{\omega_\nu^2 + (\boldsymbol{v}_{\boldsymbol{k}} \cdot \boldsymbol{q})^2} \frac{E_{+,\boldsymbol{k}}^2}{\mathcal{N}_{+,\boldsymbol{k}}^2} \\
&\quad \times \Bigg[\Big(s_{x,k}^2 c_{x,k}^2 + \mathcal{O}(q^2) \Big) J_{\boldsymbol{q}}^x(\mathrm{i}\omega_\nu) J_{-\boldsymbol{q}}^x(-\mathrm{i}\omega_\nu) + \Big(s_{y,k}^2 c_{y,k}^2 + \mathcal{O}(q^2) \Big) J_{\boldsymbol{q}}^y(\mathrm{i}\omega_\nu) J_{-\boldsymbol{q}}^y(-\mathrm{i}\omega_\nu) \\
&\qquad + \Big(s_{x,k} c_{x,k} s_{y,k} c_{y,k} + \mathcal{O}(q^2) \Big) \Big(J_{\boldsymbol{q}}^x(\mathrm{i}\omega_\nu) J_{-\boldsymbol{q}}^y(-\mathrm{i}\omega_\nu) + J_{\boldsymbol{q}}^y(\mathrm{i}\omega_\nu) J_{-\boldsymbol{q}}^x(-\mathrm{i}\omega_\nu) \Big) \Bigg] \,. \qquad (5.56)
\end{aligned}$$

Here, the vector $\boldsymbol{v}_{\boldsymbol{k}} = \nabla_{\boldsymbol{k}} E_{+,\boldsymbol{k}}$ has been defined. Keep in mind that we consider the limits $\boldsymbol{q} \to 0$ and $\omega_\nu \to 0$. Note that, in the limit $|\omega_\nu|/|\boldsymbol{q}| \gg 1$, the above term vanishes. Thus, we consider the opposite limit, where $|\omega_\nu|/|\boldsymbol{q}| \ll 1$. The terms of $\mathcal{O}(q^2)$ will not contribute to the terms containing ω_ν, since $(\boldsymbol{q}, \omega_\nu) \to 0$.

At low temperatures, we can replace the derivative of the Fermi-Dirac distribution by a delta distribution, $-\delta(E_{+,\boldsymbol{k}} - \mu)$, such that the $\boldsymbol{k}$-sum reduces to a line integral over the Fermi curve.[15] In addition, it is helpful to realise that $s_{x,k} c_{x,k} = v_{\boldsymbol{k},x}(2E_{+,k} - \varepsilon_d)/(8t_{pd}^2)$ and $s_{y,k} c_{y,k} = v_{\boldsymbol{k},y}(2E_{+,k} - \varepsilon_d)/(8t_{pd}^2)$. Then, by approximating $|\boldsymbol{v}_{\boldsymbol{k}}| \approx v_\mathrm{F}$ by a constant over the entire Fermi curve and parametrising the line integral by $\cos\theta \equiv \hat{\boldsymbol{v}}_{\boldsymbol{k}} \cdot \hat{\boldsymbol{q}}$,[16] the integral becomes tractable. The result is ω_ν-independent terms and terms in the small parameter $|\omega_\nu|/|\boldsymbol{q}|$. To zeroth order in t_{pp} and first order in $|\omega_\nu|/|\boldsymbol{q}|$, the latter terms become proportional to

$$\begin{aligned}
&\sum_{\boldsymbol{q},\omega_\nu} \frac{|\omega_\nu|}{v_\mathrm{F}|\boldsymbol{q}|} \Bigg[\hat{q}_y^2 J_{\boldsymbol{q}}^x(\mathrm{i}\omega_\nu) J_{-\boldsymbol{q}}^x(-\mathrm{i}\omega_\nu) + \hat{q}_x^2 J_{\boldsymbol{q}}^y(\mathrm{i}\omega_\nu) J_{-\boldsymbol{q}}^y(-\mathrm{i}\omega_\nu) \\
&\qquad - \hat{q}_x \hat{q}_y \Big(J_{\boldsymbol{q}}^x(\mathrm{i}\omega_\nu) J_{-\boldsymbol{q}}^y(-\mathrm{i}\omega_\nu) + J_{\boldsymbol{q}}^y(\mathrm{i}\omega_\nu) J_{-\boldsymbol{q}}^x(-\mathrm{i}\omega_\nu) \Big) \Bigg] \,. \qquad (5.57)
\end{aligned}$$

[15] In 3D, it would be a surface integral over the Fermi surface.

[16] The hats denote unit vectors.

These terms describe how the gapless particle-hole excitations at the Fermi surface result in dissipation in the effective fields J^x and J^y. The singular dissipation kernel $|\omega_\nu|/(v_\mathrm{F}|\boldsymbol{q}|)$ is a hallmark of so-called *Landau damping*, a term used in the description of damping of longitudinal charge waves in a plasma. The modifications for small, nonzero t_{pp} are not important. We neglect them in the following.

The remaining expansions in $\boldsymbol{q}$ are straightforward, so we need not dwell on them here. Thus, we are ready to write down the effective action when the expansion of the logarithm is truncated at second order. The resulting action is $S = S_\mathrm{C} + S_\mathrm{Q}$

$$\begin{aligned} S_\mathrm{C} &= \sum_{\boldsymbol{q},\omega_\nu} \sum_{i,j=x,y} G^{-1}_{\mathrm{C},ij}\, J^i_{\boldsymbol{q}}(i\omega_\nu) J^j_{-\mathbf{q}}(-i\omega_\nu), \\ S_\mathrm{Q} &= \sum_{\boldsymbol{q},\omega_\nu} \sum_{i,j=x,y} G^{-1}_{\mathrm{Q},ij}\, J^i_{\boldsymbol{q}}(i\omega_\nu) J^j_{-\mathbf{q}}(-i\omega_\nu), \end{aligned} \tag{5.58}$$

with

$$\begin{aligned} G^{-1}_{\mathrm{C},xx} &= \alpha_c + \alpha_l\, q_x^2 + \alpha_t\, q_y^2\ , \quad G^{-1}_{\mathrm{Q},xx} = \alpha_0\, \omega_\nu^2 + \alpha_d \frac{|\omega_\nu|}{|\boldsymbol{q}|} \hat{q}_y^2\ , \\ G^{-1}_{\mathrm{C},yy} &= \alpha_c + \alpha_l\, q_y^2 + \alpha_t\, q_x^2\ , \quad G^{-1}_{\mathrm{Q},yy} = \alpha_0\, \omega_\nu^2 + \alpha_d \frac{|\omega_\nu|}{|\boldsymbol{q}|} \hat{q}_x^2\ , \\ G^{-1}_{\mathrm{C},xy} &= G^{-1}_{\mathrm{C},yx} = \alpha_{xy}\, q_x q_y\ , \quad G^{-1}_{\mathrm{Q},xy} = G^{-1}_{\mathrm{Q},yx} = -\alpha_d \frac{|\omega_\nu|}{|\boldsymbol{q}|} \hat{q}_x \hat{q}_y\ . \end{aligned} \tag{5.59}$$

The expressions for the coefficients α_i are obviously complicated and not very useful, although we should note that α_d is positive. It is however the structure of the effective theory that is important.

A common way to analyse a theory like this is to include fourth order terms in J, where all momentum and frequency dependence in the coefficients are usually neglected [16]. One can then perform a renormalisation group analysis on the theory. An important quantity when studying a $T = 0$ quantum critical phenomenon by renormalisation group analysis is the dynamical critical exponent z [16]. It relates the scaling of the frequency ω to the scaling of momenta, such that if the momenta are rescaled by $q' = q\,\mathrm{e}^l$, the frequency is rescaled by $\omega' = \omega\,\mathrm{e}^{zl}$. In the above model, the (bare) dynamical critical exponent is 3 when neglecting the ω^2-terms. This value is usually slightly modified by higher order terms in J^x and J^y. We should also bear in mind that the expansion of the logarithm in some cases can lead to a nonrenormalisable theory [17].

When reverting to a real-space Cu-lattice formulation, q_x and q_y gives rise to difference operators, whereas the singular dissipation term gives rise to a nonlocal interaction in both space and imaginary time. For details, the reader is referred to Article IV. The real-space theory presented there is well suited for Monte Carlo simulations. One should also note that the theory derived here seemingly does not agree with the conjectured effective theory employed in Ref. [122].

Including O-O Coulomb Repulsion

The proposed current pattern in Figure 5.5 is such that there is no current between the unit cells due to the diagonal O-O-currents. This information is not included in the above derivation, and one might worry that this could influence the effective theory. However, by including the O-O-repulsion $H_{\text{int}}^{(3)}$ and decomposing it in terms of direct O-O-currents, this constraint can be taken care of. Using relations between expectation values of the fermionic particle currents, one may then express the auxiliary fields representing O-O-currents by the horizontal J^x and the vertical J^y. In that case, the Σ-matrix becomes

$$\Sigma_{\boldsymbol{k}_1\boldsymbol{k}_2,\sigma_1\sigma_2}(\mathrm{i}\omega_{n_1},\mathrm{i}\omega_{n_2}) = \frac{\delta_{\sigma_1\sigma_2}}{\sqrt{\beta N}} \begin{pmatrix} 0 & c_{x,k_2} J^x_{\boldsymbol{k}_{12}}(\mathrm{i}\omega_{12}) & c_{y,k_2} J^y_{\boldsymbol{k}_{12}}(\mathrm{i}\omega_{12}) \\ c_{x,k_1} J^x_{\boldsymbol{k}_{12}}(\mathrm{i}\omega_{12}) & 0 & \tilde{w} F_{xy} \\ c_{y,k_1} J^y_{\boldsymbol{k}_{12}}(\mathrm{i}\omega_{12}) & \tilde{w} F_{yx} & 0 \end{pmatrix} , \tag{5.60}$$

where $F_{ij} = \big(c_{i,k_1} s_{j,k_2} J^i_{\boldsymbol{k}_{12}}(\mathrm{i}\omega_{12}) + s_{i,k_1} c_{j,k_2} J^j_{\boldsymbol{k}_{12}}(\mathrm{i}\omega_{12})\big)$ and the constant $\tilde{w} \equiv (W t_{pd})/(V t_{pp})$. Clearly, this modification can not change the terms already derived, since they are controlled by the parameter $\tilde{w}$. Furthermore, it is easy to check that the additional terms will only modify the coefficients α_i.

Bibliography

[1] E. K. U. Gross, E. Runge, and O. Heinonen, *Many-Particle Theory* (Adam Hilger, 1991).

[2] G. D. Mahan, *Many-Particle Physics* (Plenum Publishing Corp., 1990).

[3] J. W. Negele and H. Orland, *Quantum Many-Particle Systems* (Addison-Wesley Publishing Company, 1988).

[4] F. Mandl and G. Shaw, *Quantum Field Theory* (John Wiley & Sons, 1993).

[5] L. D. Landau and E. M. Lifshitz, *Statistical Physics* (Elsevier Ltd., 1980).

[6] A. A. Abrikosov, L. P. Gor'kov, and I. Y. Dzyaloshinskii, *Quantum Field Theoretical Methods in Statistical Physics* (Pergamon Press, 1965).

[7] N. Goldenfeld, *Lectures on Phase Transitions and the Renormalization Group* (Addison-Wesley Publishing Company, 1992).

[8] P. W. Anderson, *Basics of Condensed Matter Physics* (Benjamin-Cummings Publishing Company, 1984).

[9] K. G. Wilson, Rev. Mod. Phys. **47**, 773 (1975).

[10] L. Onsager, Phys. Rev. **65**, 117 (1944).

[11] E. J. Samuelsen, Phys. Rev. Lett. **31**, 936 (1973).

[12] V. Berezinskii, Sov. Phys. JETP **32**, 493 (1970).

[13] J. M. Kosterlitz and D. J. Thouless, J. Phys. C **6**, 1181 (1973).

[14] J. M. Kosterlitz, J. Phys. C **10**, 3753 (1977).

[15] S. Sachdev, *Quantum Phase Transitions* (Cambridge University Press, 1999).

[16] J. A. Hertz, Phys. Rev. B **14**, 1165 (1976).

[17] D. Belitz, T. R. Kirkpatrick, and T. Vojta, Rev. Mod. Phys. **77**, 579 (2005).

[18] D. Belitz and T. R. Kirkpatrick, Nat. Phys. **3**, 15 (2007).

[19] D. P. Landau and K. Binder, *A guide to Monte Carlo Simulations in Statistical Physics* (Cambridge University Press, 2000).

[20] S. Kragset, *Phase transitions in effective lattice models for strongly correlated systems*, PhD thesis, NTNU, 2006.

[21] J. R. Schrieffer, *Theory of Superconductivity* (W. A. Benjamin, Inc., 1964).

[22] M. Tinkham, *Introduction to Superconductivity* (McGraw-Hill, 199).

[23] P. G. de Gennes, *Superconductivity of Metals and Alloys* (W. A. Benjamin, Inc., 1966).

[24] K. Fossheim and A. Sudbø, *Superconductivity: Physics and Applications* (John Wiley & Sons, 2004).

[25] J. Bardeen, L. N. Cooper, and J. R. Schrieffer, Phys. Rev. **108**, 1175 (1957).

[26] V. L. Ginzburg and L. D. Landau, Zh. Eksp. Teor. Fiz. **20**, 1064 (1950).

[27] L. P. Gor'kov, Sov. Phys. JETP **36**, 1364 (1959).

[28] A. J. Leggett, Rev. Mod. Phys. **47**, 331 (1975).

[29] A. I. Larkin and Yu. N. Ovchinnikov, Sov. Phys. JETP **20**, 762 (1965); P. Fulde and R. A. Ferrell, Phys. Rev. **135**, 550 (1964).

[30] H. Tou *et al*, Phys. Rev. Lett. **80**, 3129 (1998).

[31] K. Ishida *et al*, Nature **396**, 658 (1998).

[32] M. Sigrist and K. Ueda, Rev. Mod. Phys. **63**, 239 (1991).

[33] V. P. Mineev and K. V. Samokhin, *Introduction to Unconventional Superconductivity* (Gordon and Breach Science Publishers, 1998).

[34] P. W. Anderson, J. Phys. Chem. Solids **11**, 26 (1959).

[35] C. C. Tsuei and J. R. Kirtley, Rev. Mod. Phys. **72**, 969 (2000).

[36] B. D. Josephson, Phys. Lett. **1**, 251 (1962).

[37] I. Giaever, Phys. Rev. Lett. **5**, 147 (1960); *ibid.* **5**, 464 (1960).

[38] F. Steglich *et al*, Phys. Rev. Lett. **43**, 1892 (1979).

[39] G. E. Volovik and L. P. Gor'kov, JETP Lett. **39**, 674 (1984).

[40] P. W. Anderson, Phys. Rev. B **30**, 4000 (1984).

[41] K. Ueda and T. M. Rice, Phys. Rev. B **31**, 7114 (1985).

[42] V. M. Edelstein, JETP **68**, 1244 (1989); Phys. Rev. Lett. **75**, 2004 (1995).

[43] L. P. Gor'kov and E. I. Rashba, Phys. Rev. Lett. **87**, 037004 (2001).

[44] M. Sigrist *et al.*, J. Magn. Magn. Mat. **310**, 536 (2007).

[45] S. Fujimoto, J. Phys. Soc. Jpn. **76**, 051008 (2007).

[46] K. V. Samokhin, E. S. Zijlstra and S. K. Bose, Phys. Rev. B **69**, 094514 (2004); *ibid* **70**, 069902(E) (2004).

[47] I. Bonalde, W. Brämer-Escamilla, and E. Bauer, Phys. Rev. Lett. **94**, 207002 (2005); K. Izawa, Y. Kasahara, Y. Matsuda, K. Behnia, T. Yasuda, R. Settai and Y. Onuki, Phys. Rev. Lett. **94**, 197002 (2005).

[48] M. Yogi *et al*, Phys. Rev. Lett. **93**, 027003 (2004); M. Yogi *et al*, J. Phys. Soc. Jpn. **75**, 013709 (2006).

[49] N. Hayashi, K. Wakabayashi, P. A. Frigeri, and M. Sigrist, Phys. Rev. B **73**, 092508 (2006).

[50] S. Fujimoto, J. Phys. Soc. Jpn. **75**, 083704 (2006).

[51] K. V. Samokhin, Phys. Rev. B **72**, 054514 (2005).

[52] E. Bauer *et al.*, Phys. Rev. Lett. **92**, 027003 (2004).

[53] T. Yasuda *et al*, J. Phys. Soc. Jpn. **73**, 1657 (2004).

[54] K. V. Samokhin, Phys. Rev. B **70**, 104521 (2004).

[55] R. P. Kaur, D. F. Agterberg, and M. Sigrist, Phys. Rev. Lett. **94**, 137002 (2005).

[56] S. Fujimoto, Phys. Rev. B **72**, 024515 (2005).

[57] K. V. Samokhin, Phys. Rev. B **76**, 094516 (2007).

[58] S. K. Yip, Phys. Rev. B **65**, 144508 (2002).

[59] P. A. Frigeri, D. F. Agterberg, A. Koga, and M. Sigrist, Phys. Rev. Lett. **92**, 097001 (2004).

[60] G. Dresselhaus, Phys. Rev. **100**, 580 (1955).

[61] E. I. Rashba, Sov. Phys. Solid State **2**, 1109 (1960).

[62] V. B. Geshkenbein and A. I. Larkin, JETP Lett. **43**, 395 (1986).

[63] I. A. Sergienko and S. H. Curnoe, Phys. Rev. B **70**, 214510 (2004).

[64] K.-W. Lee and W. E. Pickett, Phys. Rev. B **72**, 174505 (2005).

[65] H. Suhl, B. T. Matthias, and L. R. Walker, Phys. Rev. Lett. **3**, 552 (1959).

[66] C. Iniotakis *et al.*, Phys. Rev. B **76**, 012501 (2007).

[67] V. Ambegaokar, P. G. de Gennes, and D. Rainer, Phys. Rev. A **9**, 2676 (1974).

[68] L. J. Buchholtz and G. Zwicknagl, Phys. Rev. B **23**, 5788 (1981).

[69] C. R. Hu, Phys. Rev. Lett. **72**, 1526 (1994).

[70] S. Kashiwaya and Y. Tanaka, Rep. Prog. Phys. **63**, 1641 (2000).

[71] N. K. Wu *et al*, Phys. Rev. Lett. **58**, 908 (1987).

[72] A. J. Leggett, Nat. Phys. **2**, 134 (2006).

[73] P. W. Anderson, Science **235**, 1196 (1987).

[74] M. R. Norman and C. Pepin, Rep. Prog. Phys. **66**, 1547 (2003).

[75] Ø. Fischer *et al*, Rev. Mod. Phys. **79**, 353 (2007).

[76] T. Timusk and B. Statt, Rep. Prog. Phys. **62**, 61 (1999).

[77] E. Dagotto, Rev. Mod. Phys. **66**, 763 (1994).

[78] C. C. Tsuei *et al.*, Science **271**, 329 (1996).

[79] V. J. Emery and S. A. Kivelson, Nature **374**, 434 (1995).

[80] Z. Tešanović, Phys. Rev. B **51**, 16204 (1995); *ibid.* **59**, 6449 (1999).

[81] A. K. Nguyen and A. Sudbø, Phys. Rev. B **60**, 15307 (1999).

[82] Z. A. Xu *et al*, Nature **406**, 486 (2000).

[83] B. Fauqué *et al.*, Phys. Rev. Lett. **96**, 197001 (2006).

[84] H. A. Mook *et al*, Talk at Aspen Center for Physics, August 2007.

[85] A. Kaminski *et al*, Nature **416**, 610 (2002).

[86] J. Xia *et al*, preprint, arXiv:0711.2494 (2007).

[87] C. M. Varma, P. B. Littlewood, S. Schmitt-Rink, E. Abrahams, and A. E. Ruckenstein, Phys. Rev. Lett. **63**, 1996 (1989).

[88] M. Gurvitch and A. T. Fiory, Phys. Rev. Lett. **59**, 1337 (1987).

[89] F. C. Zhang and T. M. Rice, Phys. Rev. B **37**, 3759 (1988).

[90] P. A. Lee, N. Nagaosa, and X.-G. Wen, Rev. Mod. Phys. **78**, 17 (2006).

[91] C. M. Varma, Phys. Rev. B **73**, 155113 (2006).

[92] C. M. Varma, Phys. Rev. Lett. **83**, 3538 (1999); Phys. Rev. B **55**, 14554 (1997).

[93] G. Baskaran and P. W. Anderson, Phys. Rev. B **37**, 580 (1988).

[94] L. B. Ioffe and A. I. Larkin, Phys. Rev. B **39**, 8988 (1989).

[95] N. Nagaosa and P. A. Lee, Phys. Rev. Lett. **64** 2450 (1990); P. A. Lee and N. Nagaosa, Phys. Rev. B **46** 5621 (1992).

[96] G. Mudry and E. Fradkin, Phys. Rev. B **49**, 5200 (1994); *ibid.* **50**, 11409 (1994).

[97] N. Nagaosa and P. A. Lee, Phys. Rev. B **61**, 9166 (2000).

[98] C. Nayak, Phys. Rev. Lett. **85**, 178 (2000); *ibid.* **86**, 943 (2001).

[99] M. B. Einhorn and R. Savit, Phys. Rev. D **17**, 2583 (1978); *ibid.* **19** 1198 (1979).

[100] E. Fradkin and S. Shenker, Phys. Rev. D **19**, 3682 (1979).

[101] A. M. Polyakov, Nucl. Phys. B **120**, 429 (1977).

[102] J. Smiseth *et al*, Phys. Rev. B **67**, 205104 (2003).

[103] M. N. Chernodub, E.-M. Ilgenfritz and A. Schiller, Phys. Lett. B **547**, 269 (2002); *ibid.* **555**, 206 (2003).

[104] H. Kleinert, F. S. Nogueira, and A. Sudbø, Phys. Rev. Lett. **88** 232001 (2002); Nucl. Phys. B **666** 361-395 (2003).

[105] I. F. Herbut and Z. Tešanović, Phys. Rev. Lett. **76**, 4588 (1996).

[106] I. F. Herbut and B. H. Seradjeh, Phys. Rev. Lett. **91**, 171601 (2003); I. F. Herbut, B. H. Seradjeh, S. Sachdev and G. Murthy, Phys. Rev B **68**, 195110 (2003); M. J. Case, B. H. Seradjeh and I. F. Herbut, Nucl. Phys. B **676**, 572-586 (2004); T. Senthil *et al*, Phys. Rev. B **70**, 144407 (2004).

[107] M. Hermele *et al.*, Phys. Rev. B **70**, 214437 (2004).

[108] J. Lidmar and M. Wallin, Phys. Rev. B **55**, 522 (1997).

[109] A. P. Young, Phys. Rev. B **19**, 1855 (1982).

[110] E. H. Hauge, *Go Critical!* (Lecture notes, Phase Transitions and Critical Phenomena, NTNU, 2001).

[111] D. J. Bishop and J. D. Reppy, Phys. Rev. Lett. **40**, 1727 (1978).

[112] G. Agnolet, D. F. McQueeney, and J. D. Reppy, Phys. Rev. B **39**, 8934 (1989).

[113] S. Kragset, F. S. Nogueira, and A. Sudbø, Phys. Rev. Lett. **92** 186403 (2004).

[114] P. Minnhagen and B. J. Kim, Phys. Rev. B **67**, 172509 (2003).

[115] A. Vallat and H. Beck, Phys. Rev. B **50**, 4015 (1994).

[116] P. Olsson, Phys. Rev. B **46**, 14598 (1992); *ibid.* **52**, 4511 (1995).

[117] J. Lidmar and M. Wallin, Phys. Rev. B **59**, 8451 (1999).

[118] V. Aji and C. M. Varma, Phys. Rev. B **75**, 224511 (2007).

[119] H. A. Mook *et al*, Phys. Rev. B **66**, 144513 (2002); H. A. Mook *et al*, Phys. Rev. B **69**, 134509 (2004).

[120] S. Chakravarty, R. B. Laughlin, D. K. Morr, and C. Nayak, Phys. Rev. B **63**, 094503 (2001).

[121] M. Greiter and R. Thomale, Phys. Rev. Lett. **99**, 027005 (2007).

[122] V. Aji and C. M. Varma, Phys. Rev. Lett. **99**, 067003 (2007).

[123] H. C. Lee and H.-Y. Choi, Phys. Rev. B **64**, 094508 (2001).

Article I

Tunneling between noncentrosymmetric superconductors with significant spin-orbit splitting studied theoretically within a two-band treatment

Physical Review B **74**, 054506 (2006)

Tunneling between noncentrosymmetric superconductors with significant spin-orbit splitting studied theoretically within a two-band treatment

K. Børkje and A. Sudbø
Department of Physics, Norwegian University of Science and Technology, N-7491 Trondheim, Norway
(Received 4 July 2006; published 11 August 2006)

Tunneling between noncentrosymmetric superconductors with significant spin-orbit splitting is studied theoretically in a two-band treatment of the problem. We find that the critical Josephson current may be modulated by changing the relative angle between the vectors describing absence of inversion symmetry on each side of the junction. The presence of two gaps also results in multiple steps in the quasiparticle current-voltage characteristics. We argue that both these effects may help to determine the pairing states in materials like $CePt_3Si$, UIr, and $Cd_2Re_2O_7$. We propose experimental tests of these ideas, including scanning tunneling microscopy.

DOI: 10.1103/PhysRevB.74.054506 PACS number(s): 74.50.+r, 71.70.Ej, 74.20.Rp, 74.70.Tx

Superconductors where inversion symmetry is absent and spin-orbit splitting is significant have recently attracted considerable attention.[1–8] Much of this interest was initiated by the discovery of superconductivity in $CePt_3Si$ (Ref. 9) and UIr.[10] In addition to not having an inversion center, band structure calculations on $CePt_3Si$ (Ref. 3) have shown that spin-orbit coupling splits otherwise degenerate bands by 50–200 meV near the Fermi level. This is much larger than k_BT_c, where T_c is the critical temperature for superconductivity. This must be taken into account when describing superconductivity in these systems. These materials also order magnetically, which could influence the nature of the superconducting state. However, at least for $CePt_3Si$, there seems to be little communication between superconductivity and magnetic order.[11]

Another superconductor of interest in this context is $Cd_2Re_2O_7$. This material has a structural phase transition where a center of symmetry is lost.[12] When certain ions in the unit cell are displaced throughout the lattice, internal electric fields are induced, giving rise to spin-orbit splitting of spin-degenerate states. Calculations and photoemission studies[13] have indicated that this splitting will have a significant influence on the electronic band structure. Thus, $Cd_2Re_2O_7$ is similar to the materials mentioned above, although simpler, since it shows no sign of magnetic order.[14] Another pyrochlore superconductor that might fall into this category is KOs_2O_6.[15]

The spin-orbit splitting of otherwise degenerate bands demands a two-band description of superconductivity in these materials. An exotic feature of noncentrosymmetric superconductors with large spin-orbit splitting is the possible absence of a definite parity of the superconducting state.[1,2,6] Experiments have indicated that $CePt_3Si$ might be in such a pairing state, a linear combination of spin-singlet and spin-triplet states, and that the gap may contain line nodes.[8] $Cd_2Re_2O_7$ and KOs_2O_6 seem to be nodeless, however.[14,15]

In the present study, we will investigate tunneling currents between two superconductors where a two-band description is necessary in both systems. Junctions involving one superconductor with spin-orbit split bands have been studied in Refs. 5 and 16. We will restrict ourselves to intraband Cooper pairing without specifying the microscopic mechanism responsible for this. See Ref. 17 for related work on MgB_2 junctions. Our main focus will be on noncentrosymmetric superconductors with spin-orbit split bands and we will specialize to this case when needed. We find that the critical Josephson current may be modulated by changing the angle between the vectors describing absence of inversion symmetry on each side. This effect is analogous to tunneling magnetoresistance in ferromagnetic tunnel junctions.[18] We also calculate the quasiparticle current. For temperatures close to zero, the current-voltage diagram may contain several discontinuities determined by the relative size of the two gaps. We claim that both these results may help to determine the properties of the superconducting state in materials like $CePt_3Si$, UIr, and $Cd_2Re_2O_7$.

The Hamiltonian considered is $H=H_N+H_{SC}$, where H_{SC} describes superconductivity. The normal state Hamiltonian is

$$H_N = \sum_{\boldsymbol{k}} \phi_{\boldsymbol{k}}^{\dagger}(\varepsilon_{\boldsymbol{k}} + \boldsymbol{B}_{\boldsymbol{k}} \cdot \boldsymbol{\sigma})\phi_{\boldsymbol{k}}, \tag{1}$$

where $\phi_{\boldsymbol{k}}^{\dagger}=(c_{\boldsymbol{k}\uparrow}^{\dagger}, c_{\boldsymbol{k}\downarrow}^{\dagger})$, $\varepsilon_{\boldsymbol{k}}$ is the band dispersion, and the vector $\boldsymbol{\sigma}$ consists of the three Pauli matrices. We name the spin quantization axis the z axis. The vector $\boldsymbol{B}_{\boldsymbol{k}}$ removes the spin degeneracy from the band $\varepsilon_{\boldsymbol{k}}$. By a transformation to a basis $\tilde{\phi}_{\boldsymbol{k}}^{\dagger}=(\tilde{c}_{+,\boldsymbol{k}}^{\dagger}, \tilde{c}_{-,\boldsymbol{k}}^{\dagger})$ where (1) is diagonal, one finds $H_N=\Sigma_{\lambda=\pm,\boldsymbol{k}}\tilde{\varepsilon}_{\lambda,\boldsymbol{k}}\tilde{c}_{\lambda,\boldsymbol{k}}^{\dagger}\tilde{c}_{\lambda,\boldsymbol{k}}$. The quasiparticle spectrum is $\tilde{\varepsilon}_{\pm,\boldsymbol{k}}=\varepsilon_{\boldsymbol{k}}\pm|\boldsymbol{B}_{\boldsymbol{k}}|$. We define $B_{\boldsymbol{k},\pm}=B_{\boldsymbol{k},x}\pm iB_{\boldsymbol{k},y}=B_{\boldsymbol{k},\perp}e^{\pm i\varphi_{\boldsymbol{k}}}$.

The vector $\boldsymbol{B}_{\boldsymbol{k}}$ has the property $\boldsymbol{B}_{-\boldsymbol{k}}=-\boldsymbol{B}_{\boldsymbol{k}}$,[4] where $\boldsymbol{B}_{\boldsymbol{k}}$ characterizes the absence of inversion symmetry in the crystal. The origin may be that ions are removed from high-symmetry positions, as in ferroelectrics,[12] leading to internal electric fields and thus increased spin-orbit coupling.[19,20] To establish the form of $\boldsymbol{B}_{\boldsymbol{k}}$, point group symmetry considerations may be employed[4] and $\boldsymbol{B}_{\boldsymbol{k}}$ will depend on the direction in which the ions are displaced.

An electron with momentum $\boldsymbol{k}$ will align its spin parallel or antiparallel to $\boldsymbol{B}_{\boldsymbol{k}}$. In a free electron model with the Rashba interaction,[19] the one-dimensional (1D) density of states for the + and − band at the Fermi level are equal.[21] Still, we allow these to be unequal, which is the general case.

Let us now turn to the term responsible for superconduc-

 ©2006 The American Physical Society

tivity, H_{SC}. We write down the interaction in terms of the long-lived excitations in the normal state

$$H_{SC} = \frac{1}{2}\sum_{\lambda\mu,\boldsymbol{k}\boldsymbol{k}'} V_{\lambda\mu}(\boldsymbol{k},\boldsymbol{k}')\tilde{c}^{\dagger}_{\lambda,-\boldsymbol{k}}\tilde{c}^{\dagger}_{\lambda,\boldsymbol{k}}\tilde{c}_{\mu,\boldsymbol{k}'}\tilde{c}_{\mu,-\boldsymbol{k}'}. \quad (2)$$

This model contains only intraband Cooper pairing. Interband Cooper pairs are strongly suppressed if the spin-orbit splitting is much larger than the superconducting gaps, even though the two bands may touch at some isolated points on the Fermi surface.[3] This is the limit we are investigating. Defining $\Delta_{\lambda,\boldsymbol{k}} = -\Sigma_{\mu,\boldsymbol{k}'} V_{\lambda\mu}(\boldsymbol{k},\boldsymbol{k}')\langle\tilde{c}_{\mu,\boldsymbol{k}'}\tilde{c}_{\mu,-\boldsymbol{k}'}\rangle$, the standard mean field approach gives the total Hamiltonian

$$H = \sum_{\lambda,\boldsymbol{k}}\left[\tilde{\varepsilon}_{\lambda,\boldsymbol{k}}\tilde{c}^{\dagger}_{\lambda,\boldsymbol{k}}\tilde{c}_{\lambda,\boldsymbol{k}} + \frac{1}{2}(\Delta_{\lambda,\boldsymbol{k}}\tilde{c}^{\dagger}_{\lambda,\boldsymbol{k}}\tilde{c}^{\dagger}_{\lambda,-\boldsymbol{k}} + \text{H.c.})\right]. \quad (3)$$

Note that $\Delta_{\lambda,-\boldsymbol{k}} = -\Delta_{\lambda,\boldsymbol{k}}$ follows from the fermionic anticommutation relations. In Eq. (3), the two bands are decoupled, resulting in Green's functions diagonal in the band indices. This is a result of the mean field approximation. $\Delta_{\pm,\boldsymbol{k}}$ are in general not independent, but related through the self-consistency equations due to the possibility of interband pair scattering.[7]

The relation $\boldsymbol{B}_{-\boldsymbol{k}} = -\boldsymbol{B}_{\boldsymbol{k}}$ ensures that states with opposite momenta within a band have opposite spins. For a spin-1/2 state, the time-reversal operator is $\mathcal{K} = -i\sigma_y\mathcal{K}_0$, where $\mathcal{K}_0$ denotes complex conjugation. Let the original operators transform according to $\mathcal{K}: c^{\dagger}_{\boldsymbol{k},\sigma} = -\sigma c^{\dagger}_{-\boldsymbol{k},-\sigma}$ under time reversal. The effect of time reversal on the new operators then becomes $\mathcal{K}: \tilde{c}^{\dagger}_{\lambda,\boldsymbol{k}} = t_{\lambda,\boldsymbol{k}}\tilde{c}^{\dagger}_{\lambda,-\boldsymbol{k}}$, where $t_{\lambda,\boldsymbol{k}} = e^{-\lambda i\varphi_{\boldsymbol{k}}}$. This means that if $\chi_{\lambda,\boldsymbol{k}}$ is the order parameter for pairs of time-reversed states, one finds $\Delta_{\lambda,\boldsymbol{k}} = t_{\lambda,\boldsymbol{k}}\chi_{\lambda,\boldsymbol{k}}$. This gives $\chi_{\lambda,\boldsymbol{k}} = \chi_{\lambda,-\boldsymbol{k}}$. Thus, $\chi_{\lambda,\boldsymbol{k}}$ may be expanded in terms of even basis functions of irreducible representations of the space group.[5]

Define the matrix $\Delta_{\boldsymbol{k}}$ whose elements are the gap functions $\Delta_{\boldsymbol{k},\sigma\sigma'}$ in the original basis where spin is quantized along the z axis. This may be written as

$$\Delta_{\boldsymbol{k}} = \eta_{\boldsymbol{k},S}g + \eta_{\boldsymbol{k},T}(\hat{\boldsymbol{B}}_{\boldsymbol{k}}\cdot\boldsymbol{\sigma})g, \quad (4)$$

where $g = -i\sigma_y$. The first term is symmetric in momentum space and antisymmetric in spin space, whereas the opposite is the case for the last term. Thus, in the absence of spatial inversion symmetry, the order parameters in a spin basis have no definite parity, but is in general a linear combination of singlet (S) and triplet (T) parts.[1,2,6] The singlet and triplet components are determined by $\eta_{\boldsymbol{k},S} = (\chi_{+,\boldsymbol{k}} + \chi_{-,\boldsymbol{k}})/2$ and $\eta_{\boldsymbol{k},T} = (\chi_{+,\boldsymbol{k}} - \chi_{-,\boldsymbol{k}})/2$, respectively. *This means that knowledge of $\chi_{\pm,\boldsymbol{k}}$ and $\boldsymbol{B}_{\boldsymbol{k}}$ could help determine the gap structure and the symmetry of the pairing state*. For noncentrosymmetric materials like $CePt_3Si$, this is currently a matter of intense study.[3–6,8]

The normal and anomalous Green's functions for each band are $\mathcal{G}_{\lambda}(\boldsymbol{k},\omega_n) = -(i\omega_n + \xi_{\lambda,\boldsymbol{k}})/(\omega_n^2 + \xi_{\lambda,\boldsymbol{k}}^2 + |\chi_{\lambda,\boldsymbol{k}}|^2)$ and $\mathcal{F}_{\lambda}(\boldsymbol{k},\omega_n) = t_{\lambda,\boldsymbol{k}}\chi_{\lambda,\boldsymbol{k}}/(\omega_n^2 + \xi_{\lambda,\boldsymbol{k}}^2 + |\chi_{\lambda,\boldsymbol{k}}|^2)$, respectively. These are defined in the standard way, see, e.g., Ref. 5. ω_n is a fermion Matsubara frequency, $\xi_{\lambda,\boldsymbol{k}} = \tilde{\varepsilon}_{\lambda,\boldsymbol{k}} - \mu$ and μ is the chemical potential.

Consider tunneling between two such superconductors, A and B. Let system A be described by the Hamiltonian (3). The Hamiltonian of system B is defined equivalently, only with $c_{\boldsymbol{k}\sigma}, \tilde{c}_{\lambda,\boldsymbol{k}} \to d_{\boldsymbol{p}\sigma}, \tilde{d}_{\rho,\boldsymbol{p}}$. Moreover, we allow $\boldsymbol{B}^{\mathrm{A}}_{\boldsymbol{k}}$ and $\boldsymbol{B}^{\mathrm{B}}_{\boldsymbol{p}}$ to be different. Consequently, even if $\boldsymbol{k} = \boldsymbol{p}$, the spin in a state + or − may be different on sides A and B. The tunneling Hamiltonian is $H_T = \Sigma_{\lambda\rho,\boldsymbol{k}\boldsymbol{p}}(\tilde{T}^{\lambda\rho}_{\boldsymbol{k}\boldsymbol{p}}\tilde{c}^{\dagger}_{\lambda,\boldsymbol{k}}\tilde{d}_{\rho,\boldsymbol{p}} + \tilde{T}^{\lambda\rho *}_{\boldsymbol{k}\boldsymbol{p}}\tilde{d}^{\dagger}_{\rho,\boldsymbol{p}}\tilde{c}_{\lambda,\boldsymbol{k}})$. The tunneling matrix elements $\tilde{T}^{\lambda\rho}_{\boldsymbol{k}\boldsymbol{p}}$ depends strongly on the *direction* of $\boldsymbol{k}$ and $\boldsymbol{p}$.[22] Tunneling is much more probable for a momentum normal to the interface rather than parallel to it.[22–24] If we assume that spin is conserved in the tunneling process, i.e., $H_T = \Sigma_{\boldsymbol{k}\boldsymbol{p},\sigma}T_{\boldsymbol{k}\boldsymbol{p}}c^{\dagger}_{\boldsymbol{k}\sigma}d_{\boldsymbol{p}\sigma} + \text{H.c.}$, we find $|\tilde{T}^{\lambda\rho}_{\boldsymbol{k}\boldsymbol{p}}|^2 = |T_{\boldsymbol{k}\boldsymbol{p}}|^2(1 + \lambda\rho\hat{\boldsymbol{B}}^{\mathrm{A}}_{\boldsymbol{k}}\cdot\hat{\boldsymbol{B}}^{\mathrm{B}}_{\boldsymbol{p}})/2$.

The number operator for band λ in system A is $N^{\mathrm{A}}_{\lambda} = \Sigma_{\boldsymbol{k}}\tilde{c}^{\dagger}_{\lambda,\boldsymbol{k}}\tilde{c}_{\lambda,\boldsymbol{k}}$. We define $\dot{N}^{T}_{\lambda} = i[H_T, N^{\mathrm{A}}_{\lambda}]$, such that the charge current is $I(t) = -e\Sigma_{\lambda}\langle\dot{N}^{T}_{\lambda}\rangle$. To lowest order in the tunneling matrix elements, standard theory gives $I(t) = I_{\mathrm{qp}} + I_J(t)$, where $I_{\mathrm{qp}} = -2e\Sigma_{\lambda}\mathrm{Im}\,\Phi_{\lambda}(eV)$ and $I_J(t) = 2e\Sigma_{\lambda}\mathrm{Im}[\Psi_{\lambda}(eV)e^{2ieVt}]$. The voltage is $eV = \mu_{\mathrm{A}} - \mu_{\mathrm{B}}$. In the Matsubara formalism, we have

$$\Phi_{\lambda}(\omega_{\nu}) = \frac{1}{\beta}\sum_{\substack{\boldsymbol{k}\boldsymbol{p}\\ \rho,\omega_n}} |\tilde{T}^{\lambda\rho}_{\boldsymbol{k}\boldsymbol{p}}|^2\mathcal{G}^{\mathrm{A}}_{\lambda}(\boldsymbol{k},\omega_n - \omega_{\nu})\mathcal{G}^{\mathrm{B}}_{\rho}(\boldsymbol{p},\omega_n),$$

$$\Psi_{\lambda}(\omega_{\nu}) = \frac{1}{\beta}\sum_{\substack{\boldsymbol{k}\boldsymbol{p}\\ \rho,\omega_n}} \tilde{T}^{\lambda\rho}_{\boldsymbol{k}\boldsymbol{p}}\tilde{T}^{\lambda\rho}_{-\boldsymbol{k},-\boldsymbol{p}}\mathcal{F}^{\mathrm{A}*}_{\lambda}(\boldsymbol{k},\omega_n - \omega_{\nu})\mathcal{F}^{\mathrm{B}}_{\rho}(\boldsymbol{p},\omega_n), \quad (5)$$

where $\omega_{\nu} \to eV + i0^+$ is a boson Matsubara frequency. We have assumed that the bulk Green's functions may be used, neglecting boundary effects. Such effects could however be of importance in these systems,[16] due to the possibility of subgap surface bound states or distortions of the order parameters close to the surface.

Time-reversal symmetry of H_T gives $\tilde{T}^{\lambda\rho}_{-\boldsymbol{k},-\boldsymbol{p}} = \tilde{T}^{\lambda\rho *}_{\boldsymbol{k}\boldsymbol{p}}t^{\mathrm{A}}_{\lambda,\boldsymbol{k}}t^{\mathrm{B}*}_{\rho,\boldsymbol{p}}$.[5] These phase factors will cancel the ones from the anomalous Green's functions in Eq. (5), which shows that each band λ may behave as a singlet superconductor with gap function $\chi_{\lambda,\boldsymbol{k}}$.[2,5]

We take the continuum limit[25] and assume that $\mathcal{N}_{\lambda}(\xi,\Omega)$, the angle-resolved density of states in band λ in the nonsuperconducting phase, is constant.

The gap $\chi_{\lambda}(\xi,\Omega)$ depends on both energy and the direction of momentum. Neglecting the energy dependence is standard.[26,27] The tunneling matrix elements ensures that momenta approximately perpendicular to the interface will dominate.[22–24] We therefore let $\chi_{\lambda}(\xi,\Omega) \approx \chi_{\lambda}$, the value at the Fermi level and directions normal to the interface (remember that $\chi_{\lambda,\boldsymbol{k}} = \chi_{\lambda,-\boldsymbol{k}}$). This is exact if the gaps are isotropic or if the tunneling is strictly one dimensional. It could also be a good approximation if the variations of χ_+ and χ_- are small in the region around normal incidence. We define $\chi_{\lambda} = |\chi_{\lambda}|e^{i\vartheta_{\lambda}}$.

The energy dependence of the tunneling matrix elements may be neglected. We will need the quantity $\tau_{\lambda\rho} = \int d\Omega^{\mathrm{A}}\int d\Omega^{\mathrm{B}}|\tilde{T}^{\lambda\rho}(\Omega^{\mathrm{A}},\Omega^{\mathrm{B}})|^2$. Let us look at a specific example, where $|T_{\boldsymbol{k}\boldsymbol{p}}|^2 \sim |T|^2\hat{k}_{\perp}\hat{p}_{\perp}\Theta(\hat{k}_{\perp}\hat{p}_{\perp})$.[28] In addition, we

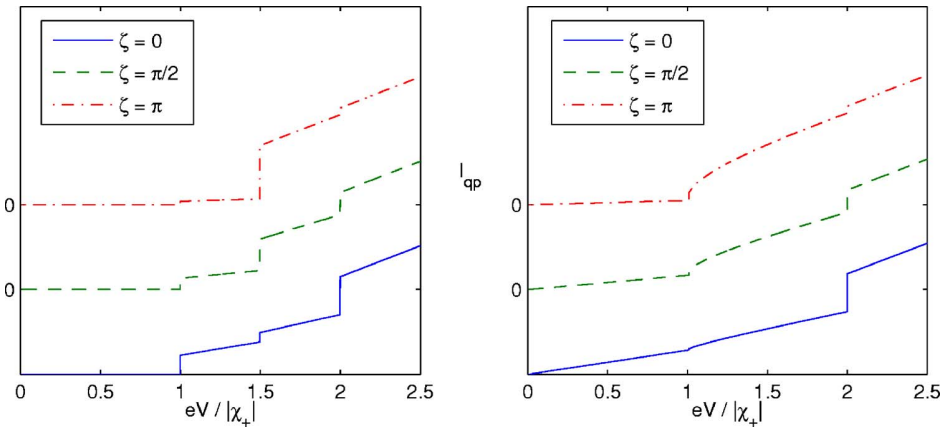

FIG. 1. (Color online) The quasiparticle current-voltage diagram at $T=0$ for angles $\zeta=0,\pi/2,\pi$, $x=0.7$, and $d=1$. The graphs are displaced in the vertical direction for clarity. Left-hand panel, $|\chi_-|/|\chi_+|=0.5$. Right-hand panel, $|\chi_-|/|\chi_+|=0.01$.

choose the Rashba interaction $\boldsymbol{B}_{\boldsymbol{k}}^{\mathrm{A}}=\alpha(\hat{\boldsymbol{n}}^{\mathrm{A}}\times\boldsymbol{k})$.[19] We let $\hat{\boldsymbol{n}}^{\mathrm{A}}$ and $\hat{\boldsymbol{n}}^{\mathrm{B}}$, and consequently the nodes of $\boldsymbol{B}_{\boldsymbol{k}}^{\mathrm{A}}$ and $\boldsymbol{B}_{\boldsymbol{p}}^{\mathrm{B}}$, point parallel to the interface. The Rashba interaction appears to be an appropriate choice for $CePt_3Si$ (Ref. 4) and $Cd_2Re_2O_7$.[5] Define the angle ζ by $\cos\zeta=\hat{\boldsymbol{n}}^{\mathrm{A}}\cdot\hat{\boldsymbol{n}}^{\mathrm{B}}$. This gives

$$\tau_{\lambda\rho}=\frac{|T|^2}{2}(1+x\lambda\rho\cos\zeta), \tag{6}$$

with $x\approx 0.6$.[29] Numerical integration indicates that Eq. (6) is a very good approximation also when parallel momentum is conserved.[30] In general, it seems reasonable that if mostly electrons near normal incidence contribute to the current, Eq. (6) is applicable with $\cos\zeta\equiv\hat{\boldsymbol{B}}_{\boldsymbol{q}_\perp}^{\mathrm{A}}\cdot\hat{\boldsymbol{B}}_{\boldsymbol{q}_\perp}^{\mathrm{B}}$ where $\boldsymbol{q}_\perp$ is perpendicular to the interface. $x\in[0,1]$ is in fact an experimentally accessible quantity. This will be discussed below.

The conductance in the normal phase is given by $G_N\equiv I_N/V=2e^2\pi\Sigma_{\lambda\rho}\mathcal{N}_\lambda^{\mathrm{A}}\mathcal{N}_\rho^{\mathrm{B}}\tau_{\lambda\rho}$. Define $r_N(\zeta)\equiv G_N(\zeta)/G_N(\pi/2)$. Using Eq. (6), we find $r_N(\zeta)=1+(1-d)^2/(1+d)^2x\cos\zeta$ where $d\equiv\mathcal{N}_-/\mathcal{N}_+$ is the ratio of the densities of states. The dependence on the angle ζ is similar to tunneling magnetoresistance between ferromagnets[18] and vanishes if $\mathcal{N}_+=\mathcal{N}_-$.

In the superconducting phase, the quasiparticle current for $T\to 0$ becomes $I_{\mathrm{qp}}=\pi e\Sigma_{\lambda\rho}\mathcal{N}_\lambda^{\mathrm{A}}\mathcal{N}_\rho^{\mathrm{B}}\tau_{\lambda\rho}\gamma_{\lambda\rho}^{\mathrm{AB}}$, where

$$\gamma_{\lambda\rho}^{\mathrm{AB}}=\Theta[|eV|-(|\chi_\lambda^{\mathrm{A}}|+|\chi_\rho^{\mathrm{B}}|)]eV\sqrt{1-\delta_{\lambda\rho}^2}\times\left[2E\left(\frac{1-\sigma_{\lambda\rho}^2}{1-\delta_{\lambda\rho}^2}\right)-\frac{\sigma_{\lambda\rho}^2-\delta_{\lambda\rho}^2}{1-\delta_{\lambda\rho}^2}K\left(\frac{1-\sigma_{\lambda\rho}^2}{1-\delta_{\lambda\rho}^2}\right)\right]. \tag{7}$$

$K(m)$ and $E(m)$ are the complete elliptic integrals of the first and second kind, respectively.[31] We have defined $\sigma_{\lambda\rho}=(|\chi_\lambda^{\mathrm{A}}|+|\chi_\rho^{\mathrm{B}}|)/eV$ and $\delta_{\lambda\rho}=(|\chi_\lambda^{\mathrm{A}}|-|\chi_\rho^{\mathrm{B}}|)/eV$. This is a two-band generalization of the one-band s-wave expression.[27] *The usual one-band threshold at* $eV=\chi^{\mathrm{A}}+\chi^{\mathrm{B}}$ *is replaced by at most four discontinuities.*

At zero voltage difference, the Josephson current becomes $I_{\mathrm{J}}=4\pi e\Sigma_{\lambda\rho}\mathcal{N}_\lambda^{\mathrm{A}}\mathcal{N}_\rho^{\mathrm{B}}\tau_{\lambda\rho}\Gamma_{\lambda\rho}^{\mathrm{AB}}\sin(\vartheta_\rho^{\mathrm{B}}-\vartheta_\lambda^{\mathrm{A}})$, where

$$\Gamma_{\lambda\rho}^{\mathrm{AB}}=\frac{|\chi_\lambda^{\mathrm{A}}||\chi_\rho^{\mathrm{B}}|}{|\chi_\lambda^{\mathrm{A}}|+|\chi_\rho^{\mathrm{B}}|}K\left(\frac{(|\chi_\lambda^{\mathrm{A}}|-|\chi_\rho^{\mathrm{B}}|)^2}{(|\chi_\lambda^{\mathrm{A}}|+|\chi_\rho^{\mathrm{B}}|)^2}\right). \tag{8}$$

This is a general two-band s-wave expression valid when interband Cooper pairs are absent. It is a straightforward generalization of the standard one-band result.[26,27]

We now consider the case of spin-orbit split bands. Usually, for equal systems one could let $|\chi_\pm^{\mathrm{A}}|=|\chi_\pm^{\mathrm{B}}|\equiv|\chi_\pm|$. This might not always be justified in our model, since the direction dependence of the gaps might depend on the nature of $\boldsymbol{B}_{\boldsymbol{k}(\boldsymbol{p})}^{\mathrm{A(B)}}$. However, let us again turn to the example above, where $\hat{\boldsymbol{n}}^{\mathrm{A}}$ and $\hat{\boldsymbol{n}}^{\mathrm{B}}$ point parallel to the interface. This makes $\boldsymbol{k},\boldsymbol{p}\sim\boldsymbol{q}_\perp$ equivalent directions even though $\hat{\boldsymbol{n}}^{\mathrm{A}}\neq\hat{\boldsymbol{n}}^{\mathrm{B}}$, at least in the isotropic approximation. The above assumption should then be justified and will be used below. In addition, since the model (2) contains interband pair scattering, we consider phase-locked bands where $\vartheta_+=\vartheta_-+n\pi$ and n is zero or one. We do not investigate the possibility of small oscillations of the interband phase difference.[32]

Whenever $|\chi_+|=|\chi_-|$ and $\mathcal{N}_+=\mathcal{N}_-$, I_{qp} becomes independent of ζ and equals the one-band result. In the case of unequal gaps, extra discontinuities should appear in the current-voltage characteristics. Figure 1 shows the quasiparticle current at $T=0$ as function of voltage for the three angles $\zeta=0$, $\pi/2$ and π with $x=0.7$ and $d=1$. The graphs are displaced in the vertical direction for clarity. Note that as $x\to 0$ all cases approach the $\zeta=\pi/2$ graph. In the left-hand panel, $|\chi_-|/|\chi_+|=0.5$. Discontinuities appear at $eV=2|\chi_-|$, $(|\chi_+|+|\chi_-|)$, and $2|\chi_+|$. In the right-hand panel, where $|\chi_-|/|\chi_+|=0.01$, current can flow also for small voltages, although this almost vanishes as $\zeta\to\pi$. Smearing of the steps due to interband scattering of quasiparticles should be negligible as long as the gap difference is well above k_BT. This breaks down in the limit of equal gaps, but then the current-voltage diagram collapse to the one-band result anyway. Anisotropic gaps, gap nodes, and nonzero temperature may in general also lead to smearing. At nonzero temperatures, logarithmic singularities in I_{qp} at $eV=||\chi_+|-|\chi_-||$ may show up.[33]

Define $|\chi_M|=\max(|\chi_+|,|\chi_-|)$ and $|\chi_m|=\min(|\chi_+|,|\chi_-|)$. The ratio $F\equiv|\chi_m|/|\chi_M|$ is easily found from the position of the first and last discontinuity. In addition, if $D_{\lambda\rho}$ denotes the jump in I_{qp} at $eV=(|\chi_\lambda|+|\chi_\rho|)$, one finds $d^2F=D_{mm}/D_{MM}$, where $d\equiv\mathcal{N}_m/\mathcal{N}_M$. These methods for finding F and d^2F are independent of ζ and x. Furthermore, x may be determined from $x\cos\zeta=(2\sqrt{D_{mm}D_{MM}}-D_{+-})/(2\sqrt{D_{mm}D_{MM}}+D_{+-})$, for any angle ζ.

The critical Josephson current $I_{J,c}$ will also depend on ζ. There is a close analogy to tunneling magnetoresistance.[18] Define $a=(-1)^n8\mathcal{N}_+\mathcal{N}_-\Gamma_{+-}/\pi(\mathcal{N}_+^2|\chi_+|+\mathcal{N}_-^2|\chi_-|)$, where

$|a|=|a|(F,d)$ is monotonically increasing for $F\leq 1$, $|a|(0,d)=0$ and $|a|(1,d)=2d/(1+d^2)\leq 1$. We find that $a=-1$ results in $I_{J,c}(\pi/2)=0$. For $a\neq -1$, we define

$$r_J(\zeta)\equiv\frac{I_{J,c}(\zeta)}{I_{J,c}\left(\frac{\pi}{2}\right)}=\left|1+\frac{1-a}{1+a}x\cos\zeta\right|, \tag{9}$$

showing the possible modulation of the critical Josephson current with ζ. In addition, $a=[1-r_J(0)+x]/[r_J(0)-1+x]$. The sign of a determines n and hence the relative sign between $\chi_{+,\boldsymbol{q}_\perp}$ and $\chi_{-,\boldsymbol{q}_\perp}$. *One may then determine the ratio between the singlet and triplet components of the order parameters in a spin basis, since* $|\eta_{\boldsymbol{q}_\perp,S}|/|\eta_{\boldsymbol{q}_\perp,T}|=[1+(-1)^nF]/[1-(-1)^nF]$.

Note that if $|\chi_+|=|\chi_-|$ and $n=0$, $r_J(\zeta)=r_N(\zeta)$. If in addition $d=1$, $I_{J,c}$ becomes independent of ζ and the one-band result [26] is recovered. A modulation may be a result of unequal gaps ($F\neq 1$), unequal densities of states ($d\neq 1$) or both. In addition, no modulation of $r_J(\zeta)$ could be interpreted both as $x=0$ and $a=1$. Both these ambiguities should be distinguishable through the quasiparticle current-voltage characteristics. Consistency demands that $|a|(F,d)$ found from the Josephson current fits F and d found from the quasiparticle current.

To determine that the jumps in the quasiparticle current arise from spin-orbit split bands due to breakdown of inversion symmetry along a certain axis, several junctions with different relative orientations of those axes would be needed.[34] The synthesis and manipulation of such junctions thus represents a considerable experimental challenge. However, building Josephson junctions with controllable crystallographic orientations was essential to proving the d-wave symmetry of the order parameter in the high-T_c cuprates.[35] Also, the presence of two gaps may be possible to detect in other experiments, such as scanning tunneling microscopy.

In conclusion, we predict possible effects in the tunneling current between noncentrosymmetric superconductors with significant spin-orbit splitting. Spin conservation in the tunneling barrier may then result in a modulation of the critical Josephson current when varying the relative angle between the vectors describing absence of inversion symmetry on each side. We have also shown that several discontinuities may appear in the quasiparticle current. We have argued that both these phenomena might help to determine the possibly exotic gap symmetry and pairing state of noncentrosymmetric superconductors.

The authors thank Thomas Tybell for valuable discussions. This work was supported by the Research Council of Norway, Grants Nos. 158518/431, 158547/431, and 167498/V30 (NANOMAT).

[1] V. M. Edelstein, Zh. Eksp. Teor. Fiz. **95**, 2151 (1989) [Sov. Phys. JETP **68**, 1244 (1989)]; V. M. Edelstein, Phys. Rev. Lett. **75**, 2004 (1995).
[2] L. P. Gor'kov and E. I. Rashba, Phys. Rev. Lett. **87**, 037004 (2001).
[3] K. V. Samokhin, E. S. Zijlstra, and S. K. Bose, Phys. Rev. B **69**, 094514 (2004).
[4] P. A. Frigeri, D. F. Agterberg, A. Koga, and M. Sigrist, Phys. Rev. Lett. **92**, 097001 (2004).
[5] I. A. Sergienko and S. H. Curnoe, Phys. Rev. B **70**, 214510 (2004).
[6] S. Fujimoto, Phys. Rev. B **72**, 024515 (2005); N. Hayashi, K. Wakabayashi, P. A. Frigeri, and M. Sigrist, *ibid.* **73**, 092508 (2006).
[7] V. P. Mineev, Int. J. Mod. Phys. B **18**, 2963 (2004).
[8] I. Bonalde, W. Brämer-Escamilla, and E. Bauer, Phys. Rev. Lett. **94**, 207002 (2005); M. Yogi, H. Mukuda, Y. Kitaoka, S. Hashimoto, T. Yasuda, R. Settai, T. D. Matsuda, Y. Haga, Y. Onuki, P. Rogl, and E. Bauer, J. Phys. Soc. Jpn. **75**, 013709 (2006); K. Izawa, Y. Kasahara, Y. Matsuda, K. Behnia, T. Yasuda, R. Settai, and Y. Onuki, Phys. Rev. Lett. **94**, 197002 (2005).
[9] E. Bauer, G. Hilscher, H. Michor, C. Paul, E. W. Scheidt, A. Gribanov, Y. Seropegin, H. Noel, M. Sigrist, and P. Rogl, Phys. Rev. Lett. **92**, 027003 (2004).
[10] T. Akazawa, H. Hidaka, T. Fujiwara, T. C. Kobayashi, E. Yamamoto, Y. Haga, R. Settai, and Y. Onuki, J. Phys.: Condens. Matter **16**, L29 (2004).
[11] A. Amato, E. Bauer, and C. Baines, Phys. Rev. B **71**, 092501 (2005).
[12] I. A. Sergienko *et al.*, Phys. Rev. Lett. **92**, 065501 (2004).
[13] R. Eguchi, T. Yokoya, T. Baba, M. Hanawa, Z. Hiroi, N. Kamakura, Y. Takata, H. Harima, and S. Shin, Phys. Rev. B **66**, 012516 (2002).
[14] O. Vyaselev, K. Arai, K. Kobayashi, J. Yamazaki, K. Kodama, M. Takigawa, M. Hanawa, and Z. Hiroi, Phys. Rev. Lett. **89**, 017001 (2002); M. D. Lumsden, S. R. Dunsiger, J. E. Sonier, R. I. Miller, R. F. Kiefl, R. Jin, J. He, D. Mandrus, S. T. Bramwell, and J. S. Gardner, *ibid.* **89**, 147002 (2002).
[15] T. Shibauchi *et al.*, cond-mat/0603309 (unpublished).
[16] T. Yokoyama, Y. Tanaka, and J. Inoue, Phys. Rev. B **72**, 220504(R) (2005).
[17] A. Brinkman, A. A. Golubov, H. Rogalla, O. V. Dolgov, J. Kortus, Y. Kong, O. Jepsen, and O. K. Andersen, Phys. Rev. B **65**, 180517(R) (2002); D. F. Agterberg, E. Demler, and B. Janko, *ibid.* **66**, 214507 (2002).
[18] M. Julliere, Phys. Lett. **54A**, 225 (1975); J. C. Slonczewski, Phys. Rev. B **39**, 6995 (1989).
[19] E. I. Rashba, Sov. Phys. Solid State **2**, 1109 (1960).
[20] G. Dresselhaus, Phys. Rev. **100**, 580 (1955).
[21] L. W. Molenkamp, G. Schmidt, and G. E. W. Bauer, Phys. Rev. B **64**, 121202(R) (2001).
[22] C. Bruder, A. van Otterlo, and G. T. Zimanyi, Phys. Rev. B **51**, 12904 (1995).
[23] C. B. Duke, *Tunneling in Solids*, Solid State Physics, Suppl. 10 (Academic, New York, 1969).
[24] W. A. Harrison, Phys. Rev. **123**, 85 (1961); D. J. Scalapino, J. R. Schrieffer, and J. W. Wilkins, *ibid.* **148**, 263 (1966).

[25] $\Sigma_{\boldsymbol{k}} f_\lambda(\boldsymbol{k}) \to \int d\xi \int_{S(\xi)} d\Omega \mathcal{N}_\lambda(\xi,\Omega) f_\lambda(\boldsymbol{k}(\xi,\Omega))$. $S(\xi)$ is a constant energy surface in momentum space. $\mathcal{N}_\lambda(\xi,\Omega)$ is the density of states.

[26] V. Ambegaokar and A. Baratoff, Phys. Rev. Lett. **10**, 486 (1963).

[27] N. R. Werthamer, Phys. Rev. **147**, 255 (1966).

[28] The Heaviside function Θ ensures that the momentum perpendicular to the interface does not change sign (Ref. 22).

[29] We find $x=[2\int_0^1 dy\sqrt{1-y}K(y)/\pi]^2 \approx 0.6$, where $K(y)$ is the complete elliptic integral of the first kind (Ref. 31).

[30] $|T_{\boldsymbol{kp}}|^2 \sim |T|^2 \hat{k}_\perp \delta_{\boldsymbol{k},\boldsymbol{p}}$ gives the same qualitative result. Refraction effects are not included, but this is negligible whenever $(|\boldsymbol{k}_{F,-}|+|\boldsymbol{k}_{F,+}|)/2 \gg \|\boldsymbol{k}_{F,-}|-|\boldsymbol{k}_{F,+}\| \sim \alpha$, at least in the important region, i.e., close to normal incidence.

[31] M. Abramowitz and I. A. Stegun, *Handbook of Mathematical Functions* (Dover, New York, 1972).

[32] A. J. Leggett, Prog. Theor. Phys. **36**, 901 (1966).

[33] A. Barone and G. Paterno, *Physics and Applications of the Josephson Effect* (Wiley, New York, 1982).

[34] In our model, this amounts to controlling the angle between $\hat{\boldsymbol{n}}^A$ and $\hat{\boldsymbol{n}}^B$.

[35] C. C. Tsuei, J. R. Kirtley, M. Rupp, J. Z. Sun, A. Gupta, M. B. Ketchen, C. A. Wang, Z. F. Ren, J. H. Wang, and M. Bhushan, Science **271**, 329 (1996).

Article II

Using Josephson junctions to determine the pairing state of superconductors without crystal inversion symmetry

Physical Review B **76**, 184513 (2007)

Using Josephson junctions to determine the pairing state of superconductors without crystal inversion symmetry

K. Børkje
Department of Physics, Norwegian University of Science and Technology, N-7491 Trondheim, Norway
(Received 23 August 2007; published 14 November 2007)

Theoretical studies of a planar tunnel junction between two superconductors with antisymmetric spin-orbit coupling are presented. The half-space Green's function for such a superconductor is determined. This is then used to derive expressions for the dissipative current and the Josephson current of the junction. Numerical results are presented in the case of the Rashba spin-orbit coupling, relevant to the much studied compound $CePt_3Si$. Current-voltage diagrams, differential conductance and the critical Josephson current are presented for different crystallographic orientations and different weights of singlet and triplet components of the pairing state. The main conclusion is that Josephson junctions with different crystallographic orientations may provide a direct connection between unconventional pairing in superconductors of this kind and the absence of inversion symmetry in the crystal.

DOI: 10.1103/PhysRevB.76.184513 PACS number(s): 74.50.+r, 71.70.Ej, 74.20.Rp, 74.70.Tx

I. INTRODUCTION

The question of how parity violation affects superconductivity has until recently not been subject to much experimental studies. In recent years, however, superconductivity has been discovered in several materials with a noncentrosymmetric crystal structure. This offers an arena for the study of superconductivity in the absence of inversion symmetry. Theoretical studies of such systems have predicted several exotic features, reviewed in Refs. 1 and 2. The absence of inversion symmetry allows an antisymmetric spin-orbit coupling in the Hamiltonian. This has, among other things, the consequence that the pairing state of the superconductor may not be classified as a spin singlet or a spin triplet state.[3,4]

The most famous and studied example of the noncentrosymmetric superconductors is the heavy fermion compound $CePt_3Si$, which possesses several interesting properties.[1,2,5,6] For instance, the pairing state of $CePt_3Si$ seems to contain line nodes[5] even though NMR measurements are of the kind expected for a conventional superconductor.[6] Several theories have been put forward to explain this.[7–9] Other examples of noncentrosymmetric superconductors are UIr, Li_2Pd_3B, Li_2Pt_3B, $Cd_2Re_2O_7$, and possibly KOs_2O_6. The absence of inversion symmetry in these materials destroys spin degeneracy through antisymmetric spin-orbit coupling. This is expected to be strong in some of the materials mentioned above,[10,11] especially in compounds containing atoms with a large atomic number. Line nodes also seem to appear in the pairing state of Li_2Pt_3B,[12,13] whereas $Cd_2Re_2O_7$, Li_2Pd_3B, and KOs_2O_6 appear to be nodeless.[12,14,15]

The experiments performed on these materials so far mostly concern quantities such as specific heat, magnetic penetration depth, and the nuclear spin-lattice relaxation rate. They are all important in order to determine the pairing state of a superconductor. However, tunneling spectroscopy and experiments on Josephson junctions are also a very useful tool in this respect, both in conventional and high-T_c superconductors.[16–18]

Recently, theoretical studies of transport in a junction between a normal metal and a noncentrosymmetric superconductor were performed.[19,20] These kinds of transport measurements do not probe bulk properties directly but will depend on how the pairing state is affected by the surface. Due to the possible triplet component, one may expect the gap to deviate from its bulk value[21,22] and formation of Andreev bound states near the surface.[17,23]

The transport properties of a Josephson junction consisting of two noncentrosymmetric superconductors have been investigated in Ref. 24. Given particular pairing states, it was noted that both the quasiparticle current and the critical Josephson current would depend on the relative crystal orientation of the superconductors. Similar effects may appear with the two-band superconductor MgB_2.[25,26] However, in Ref. 24, the bulk density of states was used, neglecting the effect of surface scattering. One might therefore question the validity of these results, since the effect of surface reflection was not considered.

In this paper, the effect of surface scattering is taken into account when determining the transport properties of the above mentioned Josephson junction. It is shown that the effects predicted in Ref. 24 may still appear, even though the surface provides a strong coupling between the spin-orbit split bands. Thus, in some cases, one may expect qualitative changes in the differential conductance for different relative crystal orientations of the two superconductors. In addition, quantitative changes in the critical Josephson current may be expected. This could make it easier to establish a direct connection between the unconventional pairing and the absence of inversion symmetry. This paper is hence an attempt to motivate experimental work on such junctions.

The paper is organized as follows. In Sec. II, we define the model containing a general antisymmetric spin-orbit coupling. The Green's function is then established, first in the bulk case and then in a half-space or semi-infinite scenario. Expressions for the tunneling currents are presented in Sec. III. In Sec. IV, numerical results using the Rashba spin-orbit coupling are presented to exemplify the predicted effects.

II. MODEL

We will start by considering the bulk properties of a clean superconductor with spin-orbit split bands. The model will

 ©2007 The American Physical Society

be written down in the continuum limit. Having established the bulk Green's function, we move on to derive the Green's function in the presence of a reflecting surface.

A. Bulk properties

Let the Hamiltonian consist of two terms, $H=H_N+H_{SC}$, a normal part and a part describing superconductivity. In the bulk, the normal part is

$$H_N = \int d\boldsymbol{k}\,\phi_{\boldsymbol{k}}^\dagger[(\varepsilon_{\boldsymbol{k}}-\mu)\mathbb{1}+\boldsymbol{B}_{\boldsymbol{k}}\cdot\boldsymbol{\sigma}]\phi_{\boldsymbol{k}}, \tag{1}$$

where $\phi_{\boldsymbol{k}}^\dagger=(c_{\boldsymbol{k}\uparrow}^\dagger,c_{\boldsymbol{k}\downarrow}^\dagger)$, $\varepsilon_{\boldsymbol{k}}$ is the band dispersion, and μ is the chemical potential. The vector $\boldsymbol{\sigma}$ consists of the three Pauli matrices.

The vector $\boldsymbol{B}_{\boldsymbol{k}}$ describes the antisymmetric spin-orbit coupling. It removes the spin degeneracy from the band $\varepsilon_{\boldsymbol{k}}$. The absence of inversion symmetry is reflected in the property $\boldsymbol{B}_{-\boldsymbol{k}}=-\boldsymbol{B}_{\boldsymbol{k}}$. An electron in a state with momentum $\boldsymbol{k}$ will align its spin parallel or antiparallel to $\boldsymbol{B}_{\boldsymbol{k}}$. The symmetries of $\boldsymbol{B}_{\boldsymbol{k}}$ may be determined from point group symmetry considerations.[27]

Diagonalization of Eq. (1) gives $H_N=\Sigma_{\lambda=\pm,\boldsymbol{k}}\xi_{\lambda,\boldsymbol{k}}\tilde{c}_{\lambda,\boldsymbol{k}}^\dagger\tilde{c}_{\lambda,\boldsymbol{k}}$, where $\xi_{\pm,\boldsymbol{k}}=\varepsilon_{\boldsymbol{k}}-\mu\pm|\boldsymbol{B}_{\boldsymbol{k}}|$. The spin of an electron in a state with momentum $\boldsymbol{k}$ will point parallel (antiparallel) to $\boldsymbol{B}_{\boldsymbol{k}}$ in band + (−).

We write down the term responsible for superconductivity in terms of the long-lived excitations in the normal state, i.e.,

$$H_{SC}=\frac{1}{2}\sum_{\lambda\mu}\int d\boldsymbol{k}d\boldsymbol{k}'V_{\lambda\mu}(\boldsymbol{k},\boldsymbol{k}')\tilde{c}_{\lambda,-\boldsymbol{k}}^\dagger\tilde{c}_{\lambda,\boldsymbol{k}}^\dagger\tilde{c}_{\mu,\boldsymbol{k}'}\tilde{c}_{\mu,-\boldsymbol{k}'}. \tag{2}$$

We will consider the limit where the spin-orbit splitting is much larger than the superconducting gaps. This is a relevant limit, at least for the materials $CePt_3Si$ (Ref. 10) and $Cd_2Re_2O_7$.[11] In that case, interband Cooper pairs are strongly suppressed, even though the two bands may touch at some isolated points on the Fermi surface.[10] Thus, model (2) contains only intraband Cooper pairing. However, it does include an internal Josephson coupling, i.e., scattering of Cooper pairs between the bands.

The standard mean field approach gives

$$H_{SC}=\frac{1}{2}\sum_{\lambda}\int d\boldsymbol{k}(\tilde{\Delta}_{\lambda,\boldsymbol{k}}\tilde{c}_{\lambda,\boldsymbol{k}}^\dagger\tilde{c}_{\lambda,-\boldsymbol{k}}^\dagger+\tilde{\Delta}_{\lambda,\boldsymbol{k}}^*\tilde{c}_{\lambda,-\boldsymbol{k}}\tilde{c}_{\lambda,\boldsymbol{k}}), \tag{3}$$

where $\tilde{\Delta}_{\lambda,\boldsymbol{k}}=-\Sigma_\mu\int d\boldsymbol{k}'V_{\lambda\mu}(\boldsymbol{k},\boldsymbol{k}')\langle\tilde{c}_{\mu,\boldsymbol{k}'}\tilde{c}_{\mu,-\boldsymbol{k}'}\rangle$. $\tilde{\Delta}_{\lambda,-\boldsymbol{k}}=-\tilde{\Delta}_{\lambda,\boldsymbol{k}}$ follows from the fermionic anticommutation relations. One should note that the two bands are decoupled in the mean field approximation. However, the gaps $\tilde{\Delta}_{\pm,\boldsymbol{k}}$ are, in general, not independent but related through the self-consistency equations due to the above mentioned possibility of interband pair scattering.[28]

Let $\mathcal{K}$ denote the time-reversal operator, whose effect on the operators in the spin basis is $\mathcal{K}:c_{\boldsymbol{k},\sigma}^\dagger=-\sigma c_{-\boldsymbol{k},-\sigma}^\dagger$. It may be derived that $\mathcal{K}:\tilde{c}_{\lambda,\boldsymbol{k}}^\dagger=t_{\lambda,\boldsymbol{k}}\tilde{c}_{\lambda,-\boldsymbol{k}}^\dagger$, where $t_{\lambda,\boldsymbol{k}}=-t_{\lambda,-\boldsymbol{k}}$ is a gauge-dependent phase factor. One may write $\tilde{\Delta}_{\lambda,\boldsymbol{k}}=t_{\lambda,\boldsymbol{k}}\chi_{\lambda,\boldsymbol{k}}$, where $\chi_{\lambda,\boldsymbol{k}}$ is the order parameter for pairs of time reversed states on which observable quantities will depend. Thus, $\chi_{\lambda,\boldsymbol{k}}=\chi_{\lambda,-\boldsymbol{k}}$ may be expanded in terms of even basis functions of irreducible representations of the space group.[29]

Define the matrix $\Delta_{\boldsymbol{k}}$ whose elements are the gap functions $\Delta_{\boldsymbol{k},\sigma\sigma'}$ in a spin basis. By transforming Eq. (3), one arrives at

$$\Delta_{\boldsymbol{k}}=\eta_{\boldsymbol{k},S}(-i\sigma_y)+\eta_{\boldsymbol{k},T}(\hat{\boldsymbol{B}}_{\boldsymbol{k}}\cdot\boldsymbol{\sigma})(-i\sigma_y). \tag{4}$$

Thus, in the absence of spatial inversion symmetry, the order parameter in a spin basis has no definite parity but is, in general, a linear combination of a singlet (S) and a triplet (T) part.[3,4,8,30] The singlet and triplet components are determined by

$$\eta_{\boldsymbol{k},S}=\frac{1}{2}(\chi_{+,\boldsymbol{k}}+\chi_{-,\boldsymbol{k}}),$$

$$\eta_{\boldsymbol{k},T}=\frac{1}{2}(\chi_{+,\boldsymbol{k}}-\chi_{-,\boldsymbol{k}}). \tag{5}$$

There is no need to specify the momentum dependence of the gaps $\chi_{\lambda,\boldsymbol{k}}$ at this point.

In the bulk, the Green's functions are diagonal in momentum space due to translational symmetry. In the imaginary time formalism, define the normal and anomalous Green's functions as $\mathcal{G}_{b,\sigma\sigma'}(\boldsymbol{k},\tau)=-\langle T_\tau c_{\boldsymbol{k}\sigma}(\tau)c_{\boldsymbol{k}\sigma'}^\dagger(0)\rangle$ and $\mathcal{F}_{b,\sigma\sigma'}(\boldsymbol{k},\tau)=\langle T_\tau c_{\boldsymbol{k}\sigma}(\tau)c_{-\boldsymbol{k}\sigma'}(0)\rangle$, respectively, where the subscript b denotes bulk. It is convenient to transform to fermionic Matsubara frequencies $\omega_n=(2n+1)\pi/\beta$, where β is the inverse temperature. The bulk Green's function in spin $\times$ particle-hole space,

$$\mathbb{G}_b(\boldsymbol{k},i\omega_n)=\begin{pmatrix}\mathcal{G}_b(\boldsymbol{k},i\omega_n) & -\mathcal{F}_b(\boldsymbol{k},i\omega_n)\\ -\mathcal{F}_b^\dagger(\boldsymbol{k},i\omega_n) & -\mathcal{G}_b^t(-\boldsymbol{k},-i\omega_n)\end{pmatrix}, \tag{6}$$

is found by solving the Gor'kov equations [Eq. (A1)] presented in Appendix A. The components are matrices in spin space, given by

$$\mathcal{G}_b(\boldsymbol{k},i\omega_n)=\frac{1}{2}\sum_{\lambda=\pm}\sigma_{\hat{\boldsymbol{B}}_{\boldsymbol{k}}}^\lambda G_\lambda(\boldsymbol{k},i\omega_n),$$

$$\mathcal{F}_b(\boldsymbol{k},i\omega_n)=-\frac{i}{2}\sum_{\lambda=\pm}\sigma_{\hat{\boldsymbol{B}}_{\boldsymbol{k}}}^\lambda\sigma_y F_\lambda(\boldsymbol{k},i\omega_n), \tag{7}$$

in terms of the complex scalar functions

$$G_\lambda(\boldsymbol{k},i\omega_n)=-\frac{i\omega_n+\xi_{\lambda,\boldsymbol{k}}}{\omega_n^2+\xi_{\lambda,\boldsymbol{k}}^2+|\chi_{\lambda,\boldsymbol{k}}|^2},$$

$$F_\lambda(\boldsymbol{k},i\omega_n)=\frac{\chi_{\lambda,\boldsymbol{k}}}{\omega_n^2+\xi_{\lambda,\boldsymbol{k}}^2+|\chi_{\lambda,\boldsymbol{k}}|^2}, \tag{8}$$

and the matrices

$$\sigma_{\hat{\boldsymbol{B}}_{\boldsymbol{k}}}^\lambda=\mathbb{1}+\lambda\hat{\boldsymbol{B}}_{\boldsymbol{k}}\cdot\boldsymbol{\sigma}. \tag{9}$$

B. Half-space Green's function

The bands + and − defined in the previous section has the property that reversing the direction of an electron's mo-

mentum while preserving its spin requires a change of bands. Thus, one would expect that the independence of bands + and − could be vulnerable to scattering, e.g., from impurities. In fact, it has been shown that a small concentration of nonmagnetic impurities does not change the picture of independent bands in the mean field approximation.[31] A perfectly reflecting surface should, however, lead to a severe mixing of the bands. This needs to be taken into account when describing transport in heterostructures containing these materials.

The presence of a surface will make the Hamiltonian and the Green's function nondiagonal in momentum space. Still, due to the nature of the spin-orbit coupling, it is convenient to work in a plane wave basis. We will assume that the surface is perfectly smooth. Of course, any real surface will have some roughness, which may very well modify the results of this paper. However, at least for not too rough surfaces, this model is an appropriate starting point. We will also assume that the surface is spin inactive, i.e., nonmagnetic.

Consider the simplest case of a perfectly smooth surface at $x=0$, such that the electrons are confined to $x<0$. We seek the Green's function $\mathbb{G}(\boldsymbol{k}_1,\boldsymbol{k}_2,\tau)$ whose elements are

$$\mathcal{G}_{\sigma\sigma'}(\boldsymbol{k}_1,\boldsymbol{k}_2,\tau) \equiv -\langle T_\tau c_{\boldsymbol{k}_1,\sigma}(\tau) c^\dagger_{\boldsymbol{k}_2,\sigma'}(0)\rangle,$$

$$\mathcal{F}_{\sigma\sigma'}(\boldsymbol{k}_1,\boldsymbol{k}_2,\tau) \equiv \langle T_\tau c_{\boldsymbol{k}_1,\sigma}(\tau) c_{-\boldsymbol{k}_2,\sigma'}(0)\rangle, \tag{10}$$

where $c_{\boldsymbol{k}_1,\sigma}$ is the annihilation operator for a *plane wave* state. In the presence of a scattering surface, these correlation functions will not be diagonal in momentum space.

Due to translational invariance in the y and z directions, it is natural to introduce the 4×4 Green's function in spin$\times$particle-hole space in a mixed representation, $\tilde{\mathbb{G}}(x_1,x_2,\boldsymbol{k}_\parallel,i\omega_n)$. We have defined $\boldsymbol{k}_\parallel=k_y\hat{\boldsymbol{y}}+k_z\hat{\boldsymbol{z}}$. The normal and anomalous components are $\tilde{\mathcal{G}}_{\sigma\sigma'}(x_1,x_2,\boldsymbol{k}_\parallel,\tau) = -\langle T_\tau c_{x_1,\boldsymbol{k}_\parallel,\sigma}(\tau) c^\dagger_{x_2,\boldsymbol{k}_\parallel,\sigma'}(0)\rangle$ and $\tilde{\mathcal{F}}_{\sigma\sigma'}(x_1,x_2,\boldsymbol{k}_\parallel,\tau) = \langle T_\tau c_{x_1,\boldsymbol{k}_\parallel,\sigma}(\tau) c_{x_2,-\boldsymbol{k}_\parallel,\sigma'}(0)\rangle$, respectively. The Green's function is determined by the Gor'kov [Eq. (A3)], which are presented in Appendix A. The boundary conditions are

$$\tilde{\mathbb{G}}(x_1,x_2,\boldsymbol{k}_\parallel,i\omega_n)=0, \quad x_1=0 \quad \text{or } x_2=0. \tag{11}$$

The pair potential in this mixed basis, $\Delta(x_1,x_2,\boldsymbol{k}_\parallel)$, should be determined self-consistently. Even though it may deviate significantly from the bulk near surfaces,[21,22] we will approximate it by its bulk value. This approximation is expected to give qualitatively correct results.[17,20] In Appendix A, it is shown that this approximation enables us to express the half-space Green's function in terms of bulk Green's functions. This may be realized by treating the surface as a wall of nonmagnetic impurities of infinite strength.[32] The momentum space Green's function then becomes

$$\begin{aligned}\mathbb{G}(\boldsymbol{k}_1,\boldsymbol{k}_2,i\omega_n) &= [\mathbb{G}_b(\boldsymbol{k}_1,i\omega_n)\delta(k_{1,x}-k_{2,x}) \\ &\quad - \mathbb{G}_b(\boldsymbol{k}_1,i\omega_n)\tilde{\mathbb{G}}_b^{-1}(0,0,\boldsymbol{k}_\parallel,i\omega_n)\mathbb{G}_b(\boldsymbol{k}_2,i\omega_n)]\delta(\boldsymbol{k}_{1,\parallel}-\boldsymbol{k}_{2,\parallel}).\end{aligned} \tag{12}$$

To determine this, we need the inverse of the matrix

$$\tilde{\mathbb{G}}_b(0,0,\boldsymbol{k}_\parallel,i\omega_n) = \int_{-\infty}^{\infty} dk_x \mathbb{G}_b(\boldsymbol{k},i\omega_n). \tag{13}$$

Let us now define $\boldsymbol{k}\equiv(k_x,\boldsymbol{k}_\parallel)$ and $\bar{\boldsymbol{k}}\equiv(-k_x,\boldsymbol{k}_\parallel)$. From the previous Section, we saw that the gaps $\chi_{\pm,\boldsymbol{k}}$ were unchanged upon reversal of the momentum. At this point, we restrict ourselves to surfaces such that the gaps are unchanged also when reversing the component of the momentum perpendicular to the surface only, i.e., $\chi_{\lambda,\bar{\boldsymbol{k}}}=\chi_{\lambda,\boldsymbol{k}}$. Although this is not a necessary requirement to determine the Green's function, it will simplify the calculations and be sufficient for the scenarios considered here. We will also assume $\xi_{\lambda,\bar{\boldsymbol{k}}}=\xi_{\lambda,\boldsymbol{k}}$. Using these approximations, the properties $G_\lambda(\bar{\boldsymbol{k}},i\omega_n)=G_\lambda(\boldsymbol{k},i\omega_n)$ and $F_\lambda(\bar{\boldsymbol{k}},i\omega_n)=F_\lambda(\boldsymbol{k},i\omega_n)$ follow from Eqs. (8). We now convert the k_x-integral in Eq. (13) to an energy integral. The integrand will be strongly peaked about the Fermi level. Thus, we apply the quasiclassical approximation of replacing all momentum-dependent quantities by their value at the Fermi level.[33] We introduce the notation

$$\boldsymbol{k}_F \equiv (k_{F,x},\boldsymbol{k}_\parallel), \quad \bar{\boldsymbol{k}}_F \equiv (-k_{F,x},\boldsymbol{k}_\parallel), \tag{14}$$

where $k_{F,x}\geqslant 0$ is determined by $\xi_{\boldsymbol{k}_F}=0$ given $\boldsymbol{k}_\parallel$. We define the quasiclassical or ξ-integrated Green's functions by

$$g_\lambda(\boldsymbol{k}_F,i\omega_n) = -\frac{i\omega_n}{\sqrt{\omega_n^2+|\chi_{\lambda,\boldsymbol{k}_F}|^2}},$$

$$f_\lambda(\boldsymbol{k}_F,i\omega_n) = \frac{\chi_{\lambda,\boldsymbol{k}_F}}{\sqrt{\omega_n^2+|\chi_{\lambda,\boldsymbol{k}_F}|^2}}. \tag{15}$$

The integral over the normal Green's function in matrix (13) is found using

$$\frac{1}{2}\int_{-\infty}^{\infty} dk_x \sigma^\lambda_{\hat{\boldsymbol{B}}_{\boldsymbol{k}}} G_\lambda(\boldsymbol{k},i\omega_n) = \pi N^x_{\lambda,\boldsymbol{k}_F}\sigma^\lambda_{\boldsymbol{b}_{\boldsymbol{k}_\parallel}} g_\lambda(\boldsymbol{k}_F,i\omega_n), \tag{16}$$

where $N^x_{\lambda,\boldsymbol{k}_F}$ is $|\partial_{k_x}\xi_{\lambda,\boldsymbol{k}}|^{-1}$ taken at $\boldsymbol{k}_F$. The vector

$$\boldsymbol{b}_{\boldsymbol{k}_\parallel} = \frac{1}{2}(\hat{\boldsymbol{B}}_{\boldsymbol{k}_F}+\hat{\boldsymbol{B}}_{\bar{\boldsymbol{k}}_F}) \tag{17}$$

has the property $\boldsymbol{b}_{-\boldsymbol{k}_\parallel}=-\boldsymbol{b}_{\boldsymbol{k}_\parallel}$ but is not a unit vector. Similarly, the integral over the anomalous Green's function is obtained from

$$\frac{1}{2}\int_{-\infty}^{\infty} dk_x \sigma^\lambda_{\hat{\boldsymbol{B}}_{\boldsymbol{k}}} F_\lambda(\boldsymbol{k},i\omega_n) = \pi N^x_{\lambda,\boldsymbol{k}_F}\sigma^\lambda_{\boldsymbol{b}_{\boldsymbol{k}_\parallel}} f_\lambda(\boldsymbol{k}_F,i\omega_n). \tag{18}$$

We now assume that the difference in the density of states of the two spin-orbit split bands is small and may be neglected. Consequently, we also let $N^x_{+,\boldsymbol{k}_F}=N^x_{-,\boldsymbol{k}_F}\equiv N^x_{\boldsymbol{k}_F}$.[34] This is not a necessary step in order to proceed, but it simplifies the calculations.

The inverse of matrix (13) is then

$$\tilde{\mathbb{G}}_b^{-1}(0,0,\boldsymbol{k}_\parallel,i\omega_n) = \frac{1}{\pi K(\boldsymbol{k}_F,i\omega_n)N^x_{\boldsymbol{k}_F}} \times \sum_{\rho=\pm} \begin{pmatrix} \sigma^\rho_{\hat{\boldsymbol{b}}_{\boldsymbol{k}_\parallel}} g^*_\rho(\boldsymbol{k}_F,i\omega_n) & i\sigma^\rho_{\hat{\boldsymbol{b}}_{\boldsymbol{k}_\parallel}}\sigma_y f_\rho(\boldsymbol{k}_F,i\omega_n) \\ -i\sigma_y\sigma^\rho_{\hat{\boldsymbol{b}}_{\boldsymbol{k}_\parallel}} f^*_\rho(\boldsymbol{k}_F,i\omega_n) & -\sigma_y\sigma^\rho_{\hat{\boldsymbol{b}}_{\boldsymbol{k}_\parallel}}\sigma_y g_\rho(\boldsymbol{k}_F,i\omega_n) \end{pmatrix}. \tag{19}$$

We have introduced the function

$$K(\boldsymbol{k}_F,i\omega_n) = 2\left[b_{+,\boldsymbol{k}_\parallel} + b_{-,\boldsymbol{k}_\parallel} \frac{\omega_n^2 + \mathrm{Re}(\chi_{+,\boldsymbol{k}_F}\chi^*_{-,\boldsymbol{k}_F})}{\sqrt{\omega_n^2+|\chi_{+,\boldsymbol{k}_F}|^2}\sqrt{\omega_n^2+|\chi_{-,\boldsymbol{k}_F}|^2}} \right], \tag{20}$$

where $b_{\pm,\boldsymbol{k}_\parallel} = 1 \pm |\boldsymbol{b}_{\boldsymbol{k}_\parallel}|^2$. Later, it will be apparent that zeros in $K(\boldsymbol{k}_F,i\omega_n)$ will correspond to surface bound states.

Introduce the simplified notation $G_{\lambda,1} \equiv G_\lambda(\boldsymbol{k}_1,i\omega_n)$, $F_{\mu,2} \equiv F_\mu(\boldsymbol{k}_2,i\omega_n)$, and $g_\rho \equiv g_\rho(\boldsymbol{k}_F,i\omega_n)$. No momentum index is needed on the latter since it depends only on the parallel momentum and $\boldsymbol{k}_{1,\parallel}=\boldsymbol{k}_{2,\parallel}\equiv\boldsymbol{k}_\parallel$. We are then ready to write down the half-space Green's function. The normal and anomalous parts, defined in Eq. (10), are

$$\mathcal{G}(\boldsymbol{k}_1,\boldsymbol{k}_2,i\omega_n) = \frac{1}{2}\Bigg\{ \sum_\lambda \sigma^\lambda_{\hat{\boldsymbol{B}}_{\boldsymbol{k}}} G_{\lambda,1}\delta(k_{1,x}-k_{2,x}) - \frac{1}{2\pi K(\boldsymbol{k}_F,i\omega_n)N^x_{\boldsymbol{k}_F}} \sum_{\lambda\rho\mu} \tilde{\sigma}^{\lambda\rho\mu}_{\boldsymbol{k}_1,\boldsymbol{k}_2} \times [G_{\lambda,1}(g^*_\rho G_{\mu,2} + f_\rho F^*_{\mu,2}) + F_{\lambda,1}(f^*_\rho G_{\mu,2} - g_\rho F^*_{\mu,2})] \Bigg\} \times \delta(\boldsymbol{k}_{1,\parallel}-\boldsymbol{k}_{2,\parallel}) \tag{21}$$

and

$$\mathcal{F}(\boldsymbol{k}_1,\boldsymbol{k}_2,i\omega_n) = -\frac{i}{2}\Bigg\{ \sum_\lambda \sigma^\lambda_{\hat{\boldsymbol{B}}_{\boldsymbol{k}}}\sigma_y F_{\lambda,1}\delta(k_{1,x}-k_{2,x}) - \frac{1}{2\pi K(\boldsymbol{k}_F,i\omega_n)N^x_{\boldsymbol{k}_F}} \sum_{\lambda\rho\mu} \tilde{\sigma}^{\lambda\rho\mu}_{\boldsymbol{k}_1,\boldsymbol{k}_2}\sigma_y \times [G_{\lambda,1}(g^*_\rho F_{\mu,2} - f_\rho G^*_{\mu,2}) + F_{\lambda,1}(f^*_\rho F_{\mu,2} + g_\rho G^*_{\mu,2})] \Bigg\} \delta(\boldsymbol{k}_{1,\parallel}-\boldsymbol{k}_{2,\parallel}), \tag{22}$$

respectively. These functions are found by inserting Eqs. (6) and (19) into Eq. (12).

We have defined the matrix

$$\tilde{\sigma}^{\lambda\rho\mu}_{\boldsymbol{k}_1,\boldsymbol{k}_2} = \sigma^\lambda_{\hat{\boldsymbol{B}}_{\boldsymbol{k}_1}}\sigma^\rho_{\hat{\boldsymbol{b}}_{\boldsymbol{k}_\parallel}}\sigma^\mu_{\hat{\boldsymbol{B}}_{\boldsymbol{k}_2}} \equiv \beta^{\lambda\rho\mu}_{\boldsymbol{k}_1,\boldsymbol{k}_2}\mathbb{1} + \boldsymbol{\alpha}^{\lambda\rho\mu}_{\boldsymbol{k}_1,\boldsymbol{k}_2}\cdot\boldsymbol{\sigma}, \tag{23}$$

where the expressions for the scalar $\beta^{\lambda\rho\mu}_{\boldsymbol{k}_1,\boldsymbol{k}_2}$ and the vector $\boldsymbol{\alpha}^{\lambda\rho\mu}_{\boldsymbol{k}_1,\boldsymbol{k}_2}$ are given in Appendix B.

III. CALCULATION OF TUNNELING CURRENTS

Let us now consider a planar tunnel junction between two superconductors with spin-orbit split bands. We name the systems A and B and let the x axis point perpendicular to the junction. In addition, we use the letter c for operators and $\boldsymbol{k}$ for momenta on side A, and d and $\boldsymbol{p}$ for the corresponding quantities on side B. The spin-orbit coupling is described by the vectors $\boldsymbol{B}^{\mathrm{A}}_{\boldsymbol{k}}$ and $\boldsymbol{B}^{\mathrm{B}}_{\boldsymbol{p}}$ on each side. These vectors are not necessarily equal. Let us briefly exemplify this by considering the Rashba spin-orbit coupling, $\boldsymbol{B}_{\boldsymbol{k}}=\alpha(\hat{\boldsymbol{n}}\times\boldsymbol{k})$, even though we will work with a general $\boldsymbol{B}_{\boldsymbol{k}}$. Here, the vector $\hat{\boldsymbol{n}}$ describes the direction of broken inversion symmetry of the crystal. This means that if the crystallographic orientation on side B is different from side A, $\boldsymbol{B}^{\mathrm{A}}_{\boldsymbol{k}}$ and $\boldsymbol{B}^{\mathrm{B}}_{\boldsymbol{p}}$ will point in different directions even when $\boldsymbol{k}=\boldsymbol{p}$.

The tunneling process is described by

$$H_T = \sum_{\sigma\sigma'} \int d\boldsymbol{k}d\boldsymbol{p}(\mathcal{T}_{\boldsymbol{k}\boldsymbol{p},\sigma\sigma'}c^\dagger_{\boldsymbol{k}\sigma}d_{\boldsymbol{p}\sigma'} + \mathcal{T}^*_{\boldsymbol{k}\boldsymbol{p},\sigma\sigma'}d^\dagger_{\boldsymbol{p}\sigma'}c_{\boldsymbol{k}\sigma}). \tag{24}$$

The validity of results using perturbation theory in the tunneling Hamiltonian formalism has been shown by Prange.[35]

We emphasize that the systems are described in terms of plane wave states. Thus, $\mathcal{T}_{\boldsymbol{k}\boldsymbol{p},\sigma\sigma'}$ is the transfer amplitude from an incoming plane wave state with momentum $\boldsymbol{p}$ on side B to an outgoing plane wave state with momentum $\boldsymbol{k}$ on side A. When scattering a plane wave on a barrier, the perpendicular momentum of the transmitted wave points in the same direction as the incoming wave. In addition, we assume that the tunneling process conserves spin. These properties result in

$$\mathcal{T}_{\boldsymbol{k}\boldsymbol{p},\sigma\sigma'} \equiv T_{\boldsymbol{k},\boldsymbol{p}}\Theta[k_x p_x]\delta_{\sigma,\sigma'}, \tag{25}$$

where $\Theta[x]$ is the Heaviside step function. Time-reversal symmetry also demands $T^*_{-\boldsymbol{k},-\boldsymbol{p}}=T_{\boldsymbol{k},\boldsymbol{p}}$.

Of course, there is also an amplitude for the incoming plane wave being reflected. However, when treating Eq. (24) as a perturbation, the current will be expressed as Green's functions of the unperturbed systems A and B. Thus, the reflection is taken into account by using the half-space Green's functions obtained in the previous section.

The current from side B to side A is defined as $I(t) = -e\langle\dot{\mathcal{N}}_{\mathrm{A}}\rangle$, where $\mathcal{N}_{\mathrm{A}}$ is the total charge operator on side A and the operator $\dot{\mathcal{N}}_{\mathrm{A}}$ is given by the Heisenberg equation $\dot{\mathcal{N}}_{\mathrm{A}} = i[H_{\mathrm{T}},\mathcal{N}_{\mathrm{A}}]$. Treating the tunneling Hamiltonian as a perturbation, the Kubo formula gives $I(t)=I_{\mathrm{qp}}+I_J(t)$,[36] where

$$I_{\mathrm{qp}} = -2e\ \mathrm{Im}\,\Phi(eV),$$

$$I_J(t) = 2e\ \mathrm{Im}[e^{-2ieVt}\Psi(eV)]. \tag{26}$$

In the imaginary time formalism, when defining $M(\tau) \equiv \Sigma_{\sigma\sigma'}\int d\boldsymbol{k}d\boldsymbol{p}c^\dagger_{\boldsymbol{k}\sigma}(\tau)d_{\boldsymbol{p}\sigma'}(\tau)$, we have

$$\Phi(i\omega_\nu) = -\int_0^\beta d\tau e^{i\omega_\nu\tau}\langle T_\tau M(\tau)M^\dagger(0)\rangle,$$

$$\Psi(i\omega_\nu) = -\int_0^\beta d\tau e^{i\omega_\nu \tau}\langle T_\tau M(\tau)M(0)\rangle. \tag{27}$$

The time dependence of the operators are given by the unperturbed Hamiltonian, and the expectation values are to be taken in the unperturbed state. The voltage is defined by $eV=\mu_A-\mu_B$. The bosonic Matsubara frequency is $\omega_\nu = 2\nu\pi/\beta$, which will be subjected to $i\omega_\nu \to eV+i0^+$.

Equations (27) may be written as

$$\Phi(i\omega_\nu) = \frac{1}{\beta}\int d\boldsymbol{k}_1 d\boldsymbol{k}_2 d\boldsymbol{p}_1 d\boldsymbol{p}_2 T_{\boldsymbol{k}_1,\boldsymbol{p}_1} T^*_{\boldsymbol{k}_2,\boldsymbol{p}_2} \sum_{\omega_n} \times \mathrm{Tr}[\mathcal{G}_A(\boldsymbol{k}_2,\boldsymbol{k}_1,i\omega_n - i\omega_\nu)\mathcal{G}_B(\boldsymbol{p}_1,\boldsymbol{p}_2,i\omega_n)] \tag{28}$$

and

$$\Psi(i\omega_\nu) = \frac{1}{\beta}\int d\boldsymbol{k}_1 d\boldsymbol{k}_2 d\boldsymbol{p}_1 d\boldsymbol{p}_2 T_{\boldsymbol{k}_1,\boldsymbol{p}_1} T^*_{\boldsymbol{k}_2,\boldsymbol{p}_2} \sum_{\omega_n} \times \mathrm{Tr}[\mathcal{F}^\dagger_A(\boldsymbol{k}_2,\boldsymbol{k}_1,i\omega_n - i\omega_\nu)\mathcal{F}_B(\boldsymbol{p}_1,\boldsymbol{p}_2,i\omega_n)], \tag{29}$$

where the components of the Green's functions are defined in Eq. (10) and Tr denotes a trace in spin space.

As before, when converting the momentum integrals to energy integrals, we replace all momentum-dependent quantities by their value on the Fermi level. The density of states $N(\boldsymbol{k}_F)$ at the Fermi level is assumed equal in both bands. In addition, we assume $N(\bar{\boldsymbol{k}}_F)=N(\boldsymbol{k}_F)$ and $T_{\bar{\boldsymbol{k}}_F,\bar{\boldsymbol{p}}_F}=T_{\boldsymbol{k}_F,\boldsymbol{p}_F}$.

A. Quasiparticle current

Inserting the Green's function (21) in Eq. (28), one arrives at

$$\Phi(i\omega_\nu) = \frac{\pi^2}{4}\int' d\hat{\boldsymbol{k}}\int' d\hat{\boldsymbol{p}}|T_{\boldsymbol{k}_F,\boldsymbol{p}_F}|^2 N^A(\boldsymbol{k}_F)N^B(\boldsymbol{p}_F) \times\Big\{ A_1^{\lambda\gamma}(\boldsymbol{k}_F,\boldsymbol{p}_F)S_1^{\lambda\gamma}(\boldsymbol{k}_F,\boldsymbol{p}_F,i\omega_\nu) - \frac{1}{2}A_2^{\lambda\gamma\eta\nu}(\boldsymbol{k}_F,\boldsymbol{p}_F)S_2^{\lambda\gamma\eta\nu}(\boldsymbol{k}_F,\boldsymbol{p}_F,i\omega_\nu) - \frac{1}{2}A_3^{\lambda\rho\mu\gamma}(\boldsymbol{k}_F,\boldsymbol{p}_F)S_3^{\lambda\rho\mu\gamma}(\boldsymbol{k}_F,\boldsymbol{p}_F,i\omega_\nu) + \frac{1}{4}A_4^{\lambda\rho\mu\gamma\eta\nu}(\boldsymbol{k}_F,\boldsymbol{p}_F)S_4^{\lambda\rho\mu\gamma\eta\nu}(\boldsymbol{k}_F,\boldsymbol{p}_F,i\omega_\nu)\Big\}, \tag{30}$$

where *repeated Greek indices are to be summed over*. The prime indicates that the integrals over the Fermi surfaces are restricted to positive $\hat{k}_x,\hat{p}_x$. The A_i's are defined by[37]

$$A_1^{\lambda\gamma}(\boldsymbol{k},\boldsymbol{p}) = \mathrm{Tr}\,\sigma^\lambda_{\hat{\boldsymbol{B}}^A_{\boldsymbol{k}}}\sigma^\gamma_{\hat{\boldsymbol{B}}^B_{\boldsymbol{p}}} + \mathrm{Tr}\,\sigma^\lambda_{\hat{\boldsymbol{B}}^A_{\bar{\boldsymbol{k}}}}\sigma^\gamma_{\hat{\boldsymbol{B}}^B_{\bar{\boldsymbol{p}}}},$$

$$A_2^{\lambda\gamma\eta\nu}(\boldsymbol{k},\boldsymbol{p}) = \mathrm{Tr}\,\sigma^\lambda_{\hat{\boldsymbol{B}}^A_{\boldsymbol{k}}}\tilde{\sigma}^{\gamma\eta\nu}_{\boldsymbol{p},\boldsymbol{p}} + \mathrm{Tr}\,\sigma^\lambda_{\hat{\boldsymbol{B}}^A_{\bar{\boldsymbol{k}}}}\tilde{\sigma}^{\gamma\eta\nu}_{\bar{\boldsymbol{p}},\bar{\boldsymbol{p}}},$$

$$A_3^{\lambda\rho\mu\gamma}(\boldsymbol{k},\boldsymbol{p}) = \mathrm{Tr}\,\tilde{\sigma}^{\lambda\rho\mu}_{\boldsymbol{k},\boldsymbol{k}}\sigma^\gamma_{\hat{\boldsymbol{B}}^B_{\boldsymbol{p}}} + \mathrm{Tr}\,\tilde{\sigma}^{\lambda\rho\mu}_{\bar{\boldsymbol{k}},\bar{\boldsymbol{k}}}\sigma^\gamma_{\hat{\boldsymbol{B}}^B_{\bar{\boldsymbol{p}}}},$$

$$A_4^{\lambda\rho\mu\gamma\eta\nu}(\boldsymbol{k},\boldsymbol{p}) = \mathrm{Tr}\,\tilde{\sigma}^{\lambda\rho\mu}_{\boldsymbol{k},\boldsymbol{k}}\tilde{\sigma}^{\gamma\eta\nu}_{\boldsymbol{p},\boldsymbol{p}} + \mathrm{Tr}\,\tilde{\sigma}^{\lambda\rho\mu}_{\bar{\boldsymbol{k}},\bar{\boldsymbol{k}}}\tilde{\sigma}^{\gamma\eta\nu}_{\bar{\boldsymbol{p}},\bar{\boldsymbol{p}}} + \mathrm{Tr}\,\tilde{\sigma}^{\lambda\rho\mu}_{\bar{\boldsymbol{k}},\boldsymbol{k}}\tilde{\sigma}^{\gamma\eta\nu}_{\boldsymbol{p},\bar{\boldsymbol{p}}} + \mathrm{Tr}\,\tilde{\sigma}^{\lambda\rho\mu}_{\boldsymbol{k},\bar{\boldsymbol{k}}}\tilde{\sigma}^{\gamma\eta\nu}_{\bar{\boldsymbol{p}},\boldsymbol{p}}. \tag{31}$$

These quantities depend on $\hat{\boldsymbol{B}}^A_{\boldsymbol{k}}$, $\hat{\boldsymbol{B}}^A_{\bar{\boldsymbol{k}}}$, $\hat{\boldsymbol{B}}^B_{\boldsymbol{p}}$, and $\hat{\boldsymbol{B}}^B_{\bar{\boldsymbol{p}}}$, and explicit expressions are given in Appendix B. The S_i's depend on the momenta through the gaps and are defined as

$$S_1^{\lambda\gamma}(\boldsymbol{k},\boldsymbol{p},i\omega_\nu) = \frac{1}{\beta}\sum_{\omega_n} g^A_\lambda(\boldsymbol{k},i\omega_n - i\omega_\nu)g^B_\gamma(\boldsymbol{p},i\omega_n),$$

$$S_2^{\lambda\gamma\eta\nu}(\boldsymbol{k},\boldsymbol{p},i\omega_\nu) = \frac{1}{\beta}\sum_{\omega_n} g^A_\lambda(\boldsymbol{k},i\omega_n - i\omega_\nu)\Gamma^B_{\gamma\eta\nu}(\boldsymbol{p},i\omega_n),$$

$$S_3^{\lambda\rho\mu\gamma}(\boldsymbol{k},\boldsymbol{p},i\omega_\nu) = \frac{1}{\beta}\sum_{\omega_n} \Gamma^A_{\lambda\rho\mu}(\boldsymbol{k},i\omega_n - i\omega_\nu)g^B_\gamma(\boldsymbol{p},i\omega_n),$$

$$S_4^{\lambda\rho\mu\gamma\eta\nu}(\boldsymbol{k},\boldsymbol{p},i\omega_\nu) = \frac{1}{\beta}\sum_{\omega_n} \Gamma^A_{\lambda\rho\mu}(\boldsymbol{k},i\omega_n - i\omega_\nu)\Gamma^B_{\gamma\eta\nu}(\boldsymbol{p},i\omega_n). \tag{32}$$

The function $g_\lambda(\boldsymbol{k},i\omega_n)$ was defined in Eq. (15). The function $\Gamma_{\lambda\rho\mu}(\boldsymbol{k},i\omega_n)$ is

$$\Gamma_{\lambda\rho\mu}(\boldsymbol{k},i\omega_n) = \frac{g_\lambda[g^*_\rho g_\mu + f_\rho f^*_\mu] + f_\lambda[f^*_\rho g_\mu - g_\rho f^*_\mu]}{K(\boldsymbol{k},i\omega_n)}, \tag{33}$$

where the arguments of the g's and f's were omitted for clarity. Note that $\Gamma_{\lambda\rho\mu}(\boldsymbol{k}_F,i\omega_n)$ does not depend on $N^x_{\boldsymbol{k}_F}$.

In Eq. (30), we have reached the point at which the current I_{qp} is expressed as two surface integrals over half of the Fermi surface on each side. In addition, one is left with the Matsubara sums which may be converted to energy integrals. To get further, one must insert the appropriate angular dependence of the quantities $\chi_{\lambda,\boldsymbol{k}_F}$, $\hat{\boldsymbol{B}}_{\boldsymbol{k}_F}$, and $N(\boldsymbol{k}_F)$ on each side as well as $|T_{\boldsymbol{k}_F,\boldsymbol{p}_F}|$. In most cases, the remaining integrals need to be performed numerically. Both the energy and angle integrands contain integrable singularities which must be handled with care.

We will now assume that the two gaps $\chi_{\pm,\boldsymbol{k}}$ are phase locked due to the internal Josephson coupling. We write out the phase explicitly, such that $\chi^A_{\pm,\boldsymbol{k}} \to \chi^A_{\pm,\boldsymbol{k}}e^{i\vartheta^A}$. $\chi^A_{+,\boldsymbol{k}}$ and $\chi^A_{-,\boldsymbol{k}}$ are real from now on, but not necessarily of the same sign. Obviously, the same also applies to the gaps on side B.

To obtain the current I_{qp}, we need $\mathrm{Im}\,\Phi(i\omega_\nu)$. Since the A_i's are real (see Appendix B), the only complex parts are contained in the Matsubara sums. By converting the sums to contour integrals in the complex plane and deforming the contour, one finds that $\mathrm{Im}\,S_i(eV+i0^+)$ may be expressed as energy integrals containing the functions $\mathrm{Im}\,g_\lambda(\boldsymbol{k},E+i0^+)$, $\mathrm{Im}\,\Gamma_{\lambda\rho\mu}(\boldsymbol{k},E+i0^+)$, and the Fermi-Dirac distribution $n_F(E)$. Details of this procedure and the choice of appropriate branch cuts are found in Appendix C. The first function is proportional to the usual bulk density of states

$$\mathrm{Im}\, g_\lambda(\boldsymbol{k}, E+i0^+) = -\Theta[|E|-|\chi_{\lambda,\boldsymbol{k}}|]\frac{|E|}{\sqrt{E^2-|\chi_{\lambda,\boldsymbol{k}}|^2}}. \quad (34)$$

As before, $\Theta[x]$ is the Heaviside step function. The second function is somewhat complicated but may be written as

$$\begin{aligned}\mathrm{Im}\,\Gamma_{\lambda\rho\mu}(\boldsymbol{k}, E+i0^+) &= \Theta[|E|-|\chi_{m,\boldsymbol{k}}|]P_{\lambda\rho\mu}(E) \\ &+ \Theta[|\chi_{m,\boldsymbol{k}}|-|E|]\Theta[-\chi_{+,\boldsymbol{k}}\chi_{-,\boldsymbol{k}}]\bar{P}_{\lambda\rho\mu}(E)\delta(|E|-E_{0,\hat{\boldsymbol{k}}}),\end{aligned} \quad (35)$$

where $|\chi_{m,\boldsymbol{k}}| \equiv \min(|\chi_{+,\boldsymbol{k}}|, |\chi_{-,\boldsymbol{k}}|)$. The functions $P_{\lambda\rho\mu}(E)$ and $\bar{P}_{\lambda\rho\mu}(E)$ are even functions of E and may be found by using Eqs. (C2) and (C3) in Appendix C. If one interprets $\mathrm{Im}\,\Gamma_{\lambda\rho\mu}(\boldsymbol{k}, E+i0^+)$ as a density of states, the first term describes a continuum above the smallest gap. However, the second term describes *additional discrete states below the smallest gap*. These are the Andreev bound states induced by the reflection from the surface. Note that they appear only when the signs of the two gaps differ, as was also noted in Ref. 20. The energy $E_{0,\hat{\boldsymbol{k}}}$ is the positive solution to the equation

$$b_{-,\boldsymbol{k}_\parallel}(\chi_{+,\boldsymbol{k}}\chi_{-,\boldsymbol{k}} - E_{0,\hat{\boldsymbol{k}}}^2) + b_{+,\boldsymbol{k}_\parallel}\sqrt{|\chi_{+,\boldsymbol{k}}|^2 - E_{0,\hat{\boldsymbol{k}}}^2}\sqrt{|\chi_{-,\boldsymbol{k}}|^2 - E_{0,\hat{\boldsymbol{k}}}^2} = 0 \quad (36)$$

and is measured relative to the Fermi level. Thus, we get a band of low energy surface bound states in the part of momentum space where $\chi_{+,\boldsymbol{k}}\chi_{-,\boldsymbol{k}} < 0$. Equation (36) corresponds to Eq. (14) of Ref. 20, but here we have made no assumption of the particular form of $\boldsymbol{B}_{\boldsymbol{k}}$.

Let us also comment on what happens in the limit of a singlet superconductor. From Eq. (5), we see that this limit corresponds to $\chi_{+,\boldsymbol{k}} = \chi_{-,\boldsymbol{k}}$. In that case, there are obviously no Andreev bound states and $\Gamma_{\lambda\rho\mu}(\boldsymbol{k}, i\omega_n) = g_+(\boldsymbol{k}, i\omega_n)/4 = g_-(\boldsymbol{k}, i\omega_n)/4$. The current I_{qp} then equals the result obtained using bulk Green's function.[36,38]

Whereas the limit $\chi_{+,\boldsymbol{k}} = \chi_{-,\boldsymbol{k}}$ corresponds to a singlet superconductor, setting the gaps to zero corresponds to a normal metal. The current will, in those cases, not depend on the nature of the spin-orbit coupling vector $\boldsymbol{B}_{\boldsymbol{k}}$. The reader may wonder why there are no remnants of the spin-orbit coupling in these limits. This is a consequence of the approximation of equal densities of states for the two bands.

B. Josephson current

The two-particle current is found by inserting the Green's function (22) in Eq. (29), giving

$$\begin{aligned}\Psi(i\omega_\nu) = \frac{\pi^2}{4}\int' d\hat{\boldsymbol{k}}\int' d\hat{\boldsymbol{p}}|T_{\boldsymbol{k}_F,\boldsymbol{p}_F}|^2 N^{\mathrm{A}}(\boldsymbol{k}_F)N^{\mathrm{B}}(\boldsymbol{p}_F) \\ \times\Big\{A_1^{\lambda\gamma}(\boldsymbol{k}_F,\boldsymbol{p}_F)\tilde{S}_1^{\lambda\gamma}(\boldsymbol{k}_F,\boldsymbol{p}_F,i\omega_\nu) \\ -\frac{1}{2}A_2^{\lambda\gamma\eta\nu}(\boldsymbol{k}_F,\boldsymbol{p}_F)\tilde{S}_2^{\lambda\gamma\eta\nu}(\boldsymbol{k}_F,\boldsymbol{p}_F,i\omega_\nu) \\ -\frac{1}{2}A_3^{\lambda\rho\mu\gamma}(\boldsymbol{k}_F,\boldsymbol{p}_F)\tilde{S}_3^{\lambda\rho\mu\gamma}(\boldsymbol{k}_F,\boldsymbol{p}_F,i\omega_\nu) \\ +\frac{1}{4}A_4^{\lambda\rho\mu\gamma\eta\nu}(\boldsymbol{k}_F,\boldsymbol{p}_F)\tilde{S}_4^{\lambda\rho\mu\gamma\eta\nu}(\boldsymbol{k}_F,\boldsymbol{p}_F,i\omega_\nu)\Big\}.\end{aligned} \quad (37)$$

As before, the integrals are restricted to positive $\hat{k}_x$ and $\hat{p}_x$ and repeated Greek indices are summed over. The $\tilde{S}_i$'s are defined as

$$\begin{aligned}\tilde{S}_1^{\lambda\gamma}(\boldsymbol{k},\boldsymbol{p},i\omega_\nu) &= \frac{1}{\beta}\sum_{\omega_n} f_\lambda^{*\mathrm{A}}(\boldsymbol{k}, i\omega_n - i\omega_\nu)f_\gamma^{\mathrm{B}}(\boldsymbol{p}, i\omega_n), \\ \tilde{S}_2^{\lambda\gamma\eta\nu}(\boldsymbol{k},\boldsymbol{p},i\omega_\nu) &= \frac{1}{\beta}\sum_{\omega_n} f_\lambda^{*\mathrm{A}}(\boldsymbol{k}, i\omega_n - i\omega_\nu)\Lambda_{\gamma\eta\nu}^{\mathrm{B}}(\boldsymbol{p}, i\omega_n), \\ \tilde{S}_3^{\lambda\rho\mu\gamma}(\boldsymbol{k},\boldsymbol{p},i\omega_\nu) &= \frac{1}{\beta}\sum_{\omega_n} \Lambda_{\lambda\rho\mu}^{*\mathrm{A}}(\boldsymbol{k}, i\omega_n - i\omega_\nu)f_\gamma^{\mathrm{B}}(\boldsymbol{p}, i\omega_n), \\ \tilde{S}_4^{\lambda\rho\mu\gamma\eta\nu}(\boldsymbol{k},\boldsymbol{p},i\omega_\nu) &= \frac{1}{\beta}\sum_{\omega_n} \Lambda_{\lambda\rho\mu}^{*\mathrm{A}}(\boldsymbol{k}, i\omega_n - i\omega_\nu)\Lambda_{\gamma\eta\nu}^{\mathrm{B}}(\boldsymbol{p}, i\omega_n).\end{aligned} \quad (38)$$

The function $f_\lambda(\boldsymbol{k}, i\omega_n)$ is defined in Eq. (15) and $\Lambda_{\lambda\rho\mu}(\boldsymbol{k}, i\omega_n)$ is

$$\Lambda_{\lambda\rho\mu}(\boldsymbol{k}, i\omega_n) = \frac{g_\lambda(g_\rho^* f_\mu - f_\rho g_\mu^*) + f_\lambda(f_\rho^* f_\mu + g_\rho g_\mu^*)}{K(\boldsymbol{k}, i\omega_n)}. \quad (39)$$

As in the previous section, we assume that the gaps are phase locked, i.e., $\chi_{\pm,\boldsymbol{k}}^{\mathrm{A}} \to \chi_{\pm,\boldsymbol{k}}^{\mathrm{A}} e^{i\vartheta^{\mathrm{A}}}$, and treat $\chi_{\pm,\boldsymbol{k}(\boldsymbol{p})}^{\mathrm{A(B)}}$ as real.

In the limit of a singlet superconductor, $\Lambda_{\lambda\rho\mu}(\boldsymbol{k}, i\omega_n) = f_+(\boldsymbol{k}, i\omega_n)/4 = f_-(\boldsymbol{k}, i\omega_n)/4$. The Josephson current reduces to the result found using bulk Green's functions.[39]

It should be noted that Eq. (37) is a tunneling limit expression. Thus, it may not capture all the unusual phenomena that arise when Andreev bound states contribute to Josephson currents.[40]

IV. RESULTS

In this section, we consider a junction consisting of two equal superconductors and present numerical results on the quasiparticle and Josephson currents. We choose to study the Rashba interaction

$$\boldsymbol{B}_{\boldsymbol{k}} = \alpha(\hat{\boldsymbol{n}} \times \boldsymbol{k}), \quad (40)$$

both because of its simplicity and its relevance to real materials such as $CePt_3Si$ (Ref. 27) and $Cd_2Re_2O_7$ (Ref. 29). The vector $\hat{\boldsymbol{n}}$ represents the direction of broken inversion symmetry of the crystal.

We restrict ourselves to junctions where $\hat{\boldsymbol{n}}^{\mathrm{A}}$ and $\hat{\boldsymbol{n}}^{\mathrm{B}}$ are perpendicular to the tunneling direction, i.e., $\hat{\boldsymbol{n}}^{\mathrm{A(B)}} \cdot \hat{\boldsymbol{x}} = 0$. The angle ζ is defined by

$$\cos\zeta \equiv \hat{\boldsymbol{n}}^{\mathrm{A}} \cdot \hat{\boldsymbol{n}}^{\mathrm{B}}. \quad (41)$$

Of course, from an experimental point of view, only discrete values of the angle ζ may be realizable.

The variation of the current with ζ is a result of the facts that $\hat{\boldsymbol{n}}$ determines the spin structure of the spin-orbit split bands and that spin is conserved in the tunneling process. It should be noted that replacing one of the superconductors by a ferromagnet with magnetization $\boldsymbol{M}^{\mathrm{B}}$ and varying $\hat{\boldsymbol{n}}^{\mathrm{A}}\cdot\boldsymbol{M}^{\mathrm{B}}$ would not necessarily give similar conductance variations.[41]

A. Quasiparticle current

We now present numerical results on the quasiparticle current I_{qp} given by Eq. (30). In addition to the choice of Rashba spin-orbit coupling, we also need the angular dependence of the gaps $\chi_{\pm,\boldsymbol{k}}$. As before, we write the phase explicitly, such that $\chi_{+,\boldsymbol{k}}$ and $\chi_{-,\boldsymbol{k}}$ are real.

We consider the same gaps as in Refs. 8 and 20, given by $\eta_{\boldsymbol{k},S}=\Psi$ and $\eta_{\boldsymbol{k},T}=\Delta|\hat{\boldsymbol{n}}\times\hat{\boldsymbol{k}}|$. The singlet and triplet components, $\eta_{\boldsymbol{k},S}$ and $\eta_{\boldsymbol{k},T}$, are defined in Eqs. (4) and (5). Ψ and Δ are treated as constants for simplicity. We also assume that $\Psi\geqslant 0$ and $\Delta\geqslant 0$ without loss of generality. The gaps in the spin-orbit split bands are then

$$\chi_{\pm,\boldsymbol{k}}=\Psi\pm\Delta|\hat{\boldsymbol{n}}\times\hat{\boldsymbol{k}}|. \tag{42}$$

Let us define $q=\Psi/\Delta$. Whereas $\chi_{+,\boldsymbol{k}}$ is fully gapped if $q>0$, the gap $\chi_{-,\boldsymbol{k}}$ contains line nodes if $0<q<1$. See Ref. 8 for details. At this point, we should mention that other explanations of line nodes in $CePt_3Si$ have been put forward.[7,9]

It is also for $q<1$ that we may expect Andreev bound states at the surface, since $\chi_{+,\boldsymbol{k}}\chi_{-,\boldsymbol{k}}<0$ on a part of the Fermi surface in that case. However, one should note that formation of Andreev bound states does not depend on the presence of gap nodes. Isotropic $\chi_{\pm,\boldsymbol{k}}$ with different signs will also result in subgap surface bound states.

For simplicity, we assume a spherical Fermi surface and let the density of states be constant over the Fermi surface, $N(\boldsymbol{k}_F)=N$. Let us introduce spherical coordinates by $\hat{\boldsymbol{k}}=(\cos\phi\sin\theta,\sin\phi\sin\theta,\cos\theta)$. As mentioned before, the x axis is perpendicular to the junction. In addition, we let $\hat{\boldsymbol{n}}^{\mathrm{A}}$ and $\hat{\boldsymbol{n}}^{\mathrm{B}}$ point along or opposite to the $\hat{\boldsymbol{z}}$ direction. The gaps are then given by $\chi_{\pm,\boldsymbol{k}}/\Delta=q\pm\sin\theta$. For $q<1$, Andreev bound states are formed for momenta with $\arcsin(q)<\theta<\pi-\arcsin(q)$. As mentioned in Sec. III A, these surface bound states form below the smallest gap, i.e., below $|\chi_{-,\boldsymbol{k}}|/\Delta=|q-\sin\theta|$. Figure 1 shows the spectrum of Andreev bound states $E_{0,\hat{\boldsymbol{k}}}$ in the case $q=0$. The dependence on the azimuthal angle ϕ is shown for three different polar angles θ. We see that $E_{0,\hat{\boldsymbol{k}}}\to 0$ as $\phi\to 0$, which corresponds to $k_y=0$ and thus $|\boldsymbol{b}_{\boldsymbol{k}_\parallel}|=0$. The maximal value of $E_{0,\hat{\boldsymbol{k}}}$ is given by $|q-\sin\theta|$.

The tunneling matrix element, defined in Eqs. (24) and (25), will typically favor momenta with a large component in the tunneling direction. Also, in the case of a smooth barrier, the parallel momentum is conserved in the tunneling process. Thus, we assume that

$$|T_{\boldsymbol{k}_F,\boldsymbol{p}_F}|^2=t\hat{k}_x\hat{p}_x\delta(\hat{\boldsymbol{k}}_\parallel-\hat{\boldsymbol{p}}_\parallel) \tag{43}$$

will capture the qualitative features of the tunneling matrix element, where t is a constant.[42]

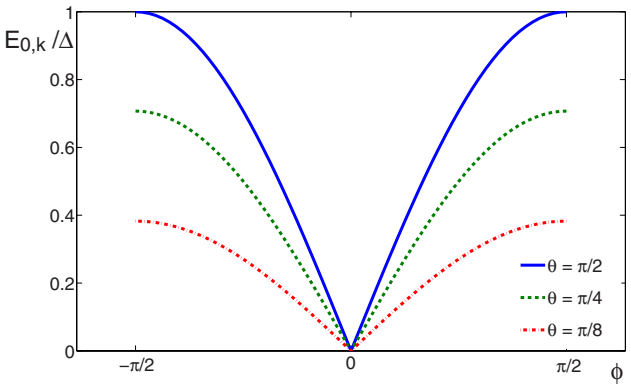

FIG. 1. (Color online) Energy spectrum for the bound states $E_{0,\hat{\boldsymbol{k}}}$ in the case $q=0$. The dependence on the azimuthal angle ϕ is shown for three different polar angles θ.

One may show that the variation of the current with the angle ζ disappears when only perpendicular momenta contribute. In other words, the effect is dependent on a finite tunneling cone, where also nonzero parallel momenta contribute to the current.

Tunneling spectroscopy on superconductors are interesting at low temperatures. At higher temperatures, sharp features giving information on pairing states may be smeared out. Thus, we investigate the limit of zero temperature here. However, for $q<1$, the current at low voltage is dominated by resonant transport between Andreev bound states. This is contained in the sum $S_4^{\lambda\rho\mu\gamma\eta\nu}(\boldsymbol{k}_F,\boldsymbol{p}_F,i\omega_\nu)$, where a product of two delta distributions enters. At zero temperature, this leads to a discontinuity at $V=0$, where the current jumps from zero to a finite value. The discontinuity disappears for nonzero temperatures and a sharp zero bias conductance peak appears. To get realistic current-voltage diagrams, we therefore retain a small temperature $(T/\Delta=0.015)$ in this particular term, such that this discontinuity at zero voltage is smeared out. Such a small temperature will have no significant effect on the other terms.

The current-voltage diagrams for several q are now presented, where we have defined $i_{\mathrm{qp}}\equiv -I_{\mathrm{qp}}/(2e\pi^2t^2N^2)$. We consider the cases of $\zeta=0$ and $\zeta=\pi$, i.e., equal and opposite directions of broken inversion symmetry. In addition, we present the differential conductance $G(eV)\equiv di_{\mathrm{qp}}/d(eV)$, which may be directly accessible in experiments. The latter has been obtained through a Savitzky-Golay smoothing filter[43] to remove noise from the numerical integration.

We start by considering the $q=0$ case, which corresponds to a pure spin triplet state. The gaps $\chi_{+,\boldsymbol{k}}$ and $\chi_{-,\boldsymbol{k}}$ are then of opposite signs on the entire Fermi surface except at $\hat{\boldsymbol{k}}_F=\pm\hat{\boldsymbol{n}}$, where they have point nodes. Figure 2 shows the current-voltage diagram when $q=0$. The differential conductance is presented in Fig. 3. The large current at small voltages is due to transport between Andreev bound states on each side. This gives rise to a zero bias conductance peak followed by negative differential conductance. Similar phenomena appear in some d-wave junctions.[40] We observe that there is no difference between the cases $\zeta=0$ and $\zeta=\pi$ in the pure triplet case. As stated before, this is also the case for the

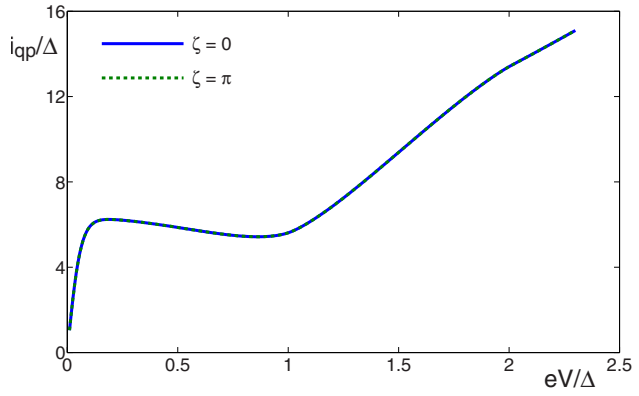

FIG. 2. (Color online) Current-voltage diagram in a Josephson junction when $q=\Psi/\Delta=0$. Transport between Andreev bound states dominates for small voltages. There is no dependence on ζ in this pure triplet case.

pure singlet case, $q\to\infty$.[44] However, we will see that this changes for finite q when the gap is a mixture of singlet and triplet.

Figure 4 shows the current-voltage diagram in the case $q=0.4$. In this case, $\chi_{+,k}$ is fully gapped (although anisotropic), whereas the gap $\chi_{-,k}$ has got line nodes at $\theta \approx 23.6°$ and $\theta \approx 66.4°$. Andreev bound states exist between these angles. Observe that the cases $\zeta=0$ and $\zeta=\pi$ differ. This becomes clearer when studying the differential conductance in Fig. 5. We do not attempt to explain every feature in this figure, as this depends on the particular pairing state chosen. In addition, some of these features might also be smeared out in experimental results. However, the important thing to notice, which might be observable, is the qualitative difference of a junction with equal $\hat{\boldsymbol{n}}$ vectors ($\zeta=0$) and one with opposite $\hat{\boldsymbol{n}}$ vectors ($\zeta=\pi$).

The next current-voltage diagram, presented in Fig. 6, is for $q=1$. Then, the line nodes have moved to the equator ($\theta=\pi/2$) and will disappear for $q>1$. Now, there is no part of the Fermi surface where $\chi_{+,k}\chi_{-,k}<0$, such that there are

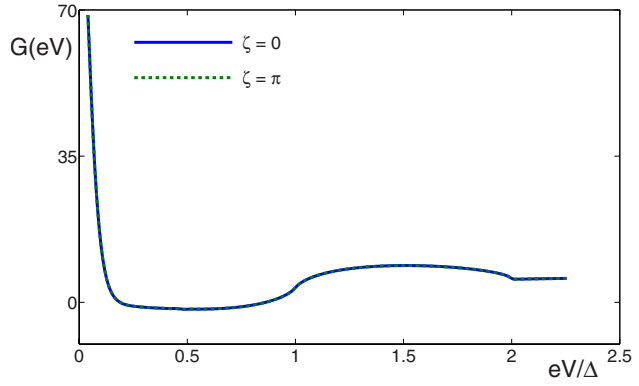

FIG. 3. (Color online) Differential conductance as a function of voltage when $q=0$. For small voltages, the zero bias conductance peak followed by negative differential resistance is due to transport between Andreev bound states on each side. There is no dependence on ζ in this pure triplet case.

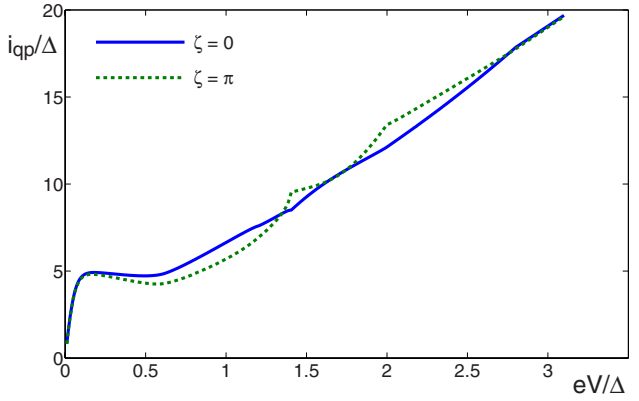

FIG. 4. (Color online) Current-voltage diagram when $q=0.4$. Transport between Andreev bound states dominates for small voltages.

no Andreev bound states. In the differential conductance in Fig. 7, there is a clear difference between $\zeta=0$ and $\zeta=\pi$. See Ref. 24 for a simplified discussion of why this occurs.

Finally, we examine the scenario where the singlet to triplet ratio is $q=2$. At this value, both $\chi_{+,k}$ and $\chi_{-,k}$ are fully gapped and of the same sign. The current-voltage diagram is given in Fig. 8 and the differential conductance in Fig. 9. Above $eV/\Delta=2$, the behavior is similar to the $q=1$ case.

In the cases $q=1$ and $q=2$, we observe that the graphs differ in the region $2(q-1)<eV/\Delta<2(q+1)$. This will also be the case for higher values of q, but the width of this region $[2(q+1)-2(q-1)=4]$ becomes small relative to the voltages at which the graphs differ ($eV/\Delta \approx 2q$). In the limit $q\to\infty$, we are left with the singlet result, with a single step in the current for both $\zeta=0$ and $\zeta=\pi$.

B. Josephson current

We now move on to the Josephson current, given by Eq. (37). This has not been investigated in as much detail as the quasiparticle current. In this section, we only suggest that the critical Josephson junction at zero voltage may depend on

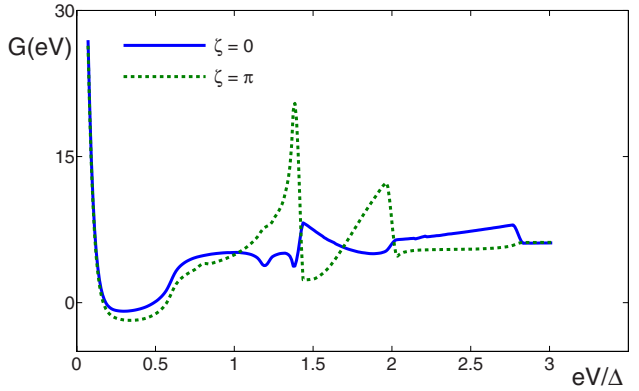

FIG. 5. (Color online) Differential conductance in the case $q=0.4$. Transport between Andreev bound states dominates for small voltages.

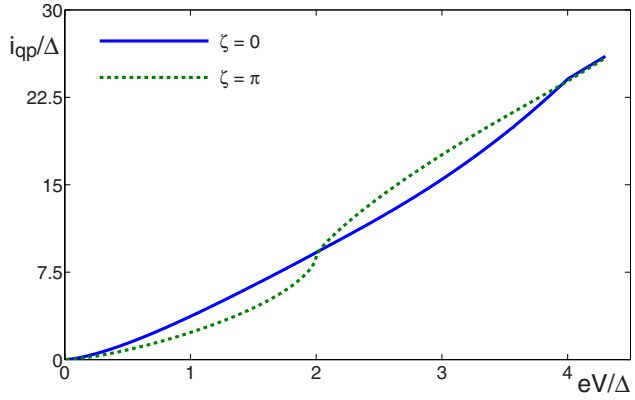

FIG. 6. (Color online) Current-voltage diagram when $q=1$. At this point, there are no Andreev bound states.

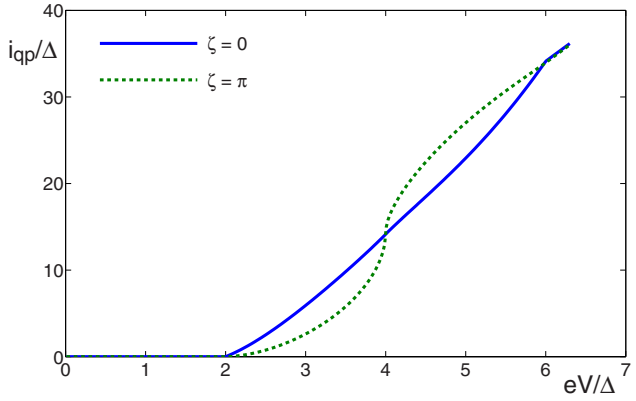

FIG. 8. (Color online) Current-voltage diagram when $q=2$. At this point, both bands are fully gapped.

the angle ζ between the axes of broken inversion symmetry of the crystal. We make no attempt to give any quantitative estimates here, since this depends not only on the particular pairing state of the material in question but also on several other issues, such as the details of the tunneling matrix elements. Only experiments can determine whether this effect really occurs and to what degree.

The critical or maximal Josephson current at $eV=0$, $I_{J,c}(\zeta)$, is defined as the absolute value of the Josephson current at phase difference $\vartheta_B - \vartheta_A = \pm\pi/2$. We still use the Rashba spin-orbit coupling and consider only one pairing state, given by

$$\chi_{+,k} = \text{const}, \quad \chi_{-,k} = 0. \tag{44}$$

This is probably not very realistic but suffices to illustrate the effect.[45] In this case, there are no Andreev bound states.

As mentioned in the previous section, the dependence on ζ disappears when only perpendicular momenta contribute to the current. This is also the case for the Josephson current. We illustrate this by introducing a cutoff in the angle integrals, integrating over $\theta_c < \theta < \pi - \theta_c$ and $-\pi/2 + \phi_c < \phi < \pi/2 - \phi_c$. Here, $\theta_c = \phi_c = 0$ corresponds to integration over the entire semisphere, whereas only perpendicular momenta contributes when $\theta_c = \phi_c \to \pi/2$.

Figure 10 shows the variation of the critical Josephson current with ζ. Note the difference in current for the cases $\zeta=0$ and $\zeta=\pi$. One should also observe that the variation is reduced when the cutoff angle increases, corresponding to a narrowing of the tunneling cone.

Although we have only studied a special scenario, the general message is that a variation of the critical Josephson current with ζ may be expected when the gap is a mixture of singlet and triplet components.

V. CONCLUDING REMARKS

We have investigated both the current-voltage diagram and the critical Josephson current in planar tunnel junctions consisting of two superconductors with antisymmetric spin-orbit coupling. This is relevant for several recently discovered superconductors, where the spin-orbit coupling is a consequence of the crystal lacking inversion symmetry. Expressions for the currents have been derived in the tunneling limit using a general spin-orbit coupling.

Numerical results have been presented in the case of the Rashba spin-orbit coupling. We have investigated the depen-

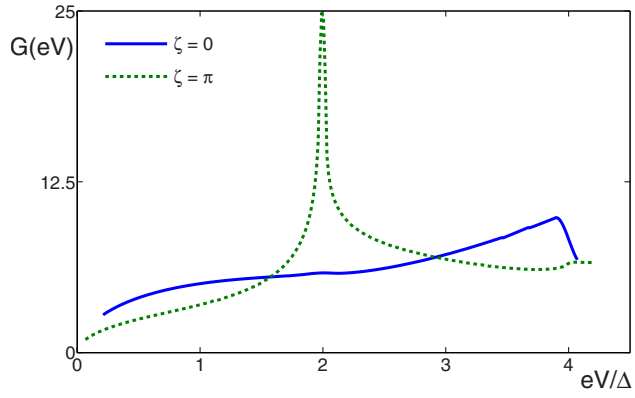

FIG. 7. (Color online) Differential conductance when $q=1$. Note the qualitative difference in the two cases for $eV/\Delta < 4$.

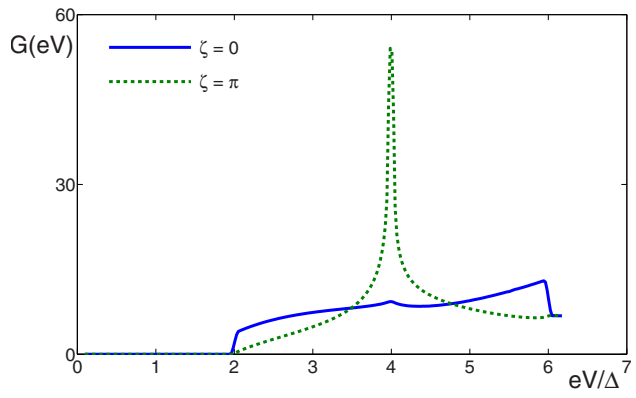

FIG. 9. (Color online) Differential conductance when $q=2$. The two cases of $\zeta=0$ and $\zeta=\pi$ differ significantly when $2 < eV/\Delta < 6$.

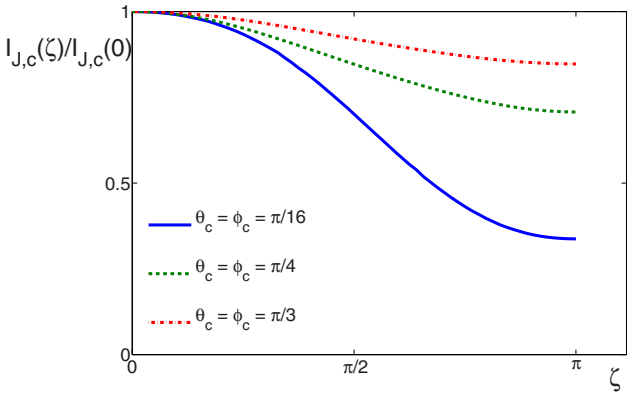

FIG. 10. (Color online) The variation of the critical Josephson current with ζ for three different cutoff angles. Note the difference in the cases $\zeta=0$ and $\zeta=\pi$. The variation diminishes as the tunneling cone is narrowed.

dence on the relative angle between the directions of broken inversion symmetry on each side of the junction. It has been shown that if the gap is a mixture of spin singlet and spin triplet parts, qualitative changes in the differential conductance may be expected when varying this angle. One may also observe quantitative changes in the critical Josephson current. This is a result of the fact that spin is conserved in the tunneling process, whereas the spin structure of the spin-orbit split bands is determined by the direction of broken inversion symmetry. One should note that broken inversion symmetry on both sides of the junction is of importance. As stated earlier, similar conductance variations does not necessarily appear when replacing one of the superconductors with a ferromagnet and varying its magnetization.

The experimental verification of these phenomena requires synthesis of junctions with specific crystallographic orientation on each side. It is worth mentioning that Josephson junctions with controllable crystallographic orientation were essential in proving the d-wave symmetry of the order parameter in the high-T_c cuprates.[18] Furthermore, the roughness of the tunnel barrier should be as small as possible. In addition, the planar tunnel junctions must be thin enough to ensure that momenta with finite parallel components contribute to the current. Finally, it should be pointed out that a difference in the normal phase densities of states of the two bands could give rise to some of the above mentioned effects even for conventional pairing. However, this should be possible to detect by measuring the current-voltage characteristics in the normal phase above T_c.

Many approximations and assumptions have been made in order to produce these results. Thus, the results presented here are expected to be of qualitative value only. The main message is that experiments on Josephson junctions of noncentrosymmetric superconductors may provide a direct connection between the possibly unconventional pairing and the lack of inversion symmetry in the crystal.

ACKNOWLEDGMENTS

The author would like to thank Yukio Tanaka for a very informative electronic mail correspondence. Discussions with Asle Sudbø, Thomas Tybell, and Eskil K. Dahl have also been of great value. This work was supported by the Research Council of Norway, Grant No. 158547/431 (NANOMAT).

APPENDIX A: DERIVATION OF THE HALF-SPACE GREEN'S FUNCTION

First, we note that the momentum space Gor'kov equations in the bulk are

$$\mathcal{A}(\boldsymbol{k},i\omega_n)\mathbb{G}_b(\boldsymbol{k},i\omega_n)=\mathbb{1}, \tag{A1}$$

where

$$\mathcal{A}(\boldsymbol{k},i\omega_n)=\begin{pmatrix}[i\omega_n-(\varepsilon_{\boldsymbol{k}}-\mu)]\mathbb{1}-\boldsymbol{B}_{\boldsymbol{k}}\cdot\sigma & -\Delta_{\boldsymbol{k}}\\ -\Delta_{\boldsymbol{k}}^{\dagger} & [i\omega_n+(\varepsilon_{\boldsymbol{k}}-\mu)]\mathbb{1}-\boldsymbol{B}_{\boldsymbol{k}}\cdot\sigma^{*}\end{pmatrix} \tag{A2}$$

and $\mathbb{G}_b(\boldsymbol{k},i\omega_n)$ are matrices in spin $\times$ particle-hole space. The subscript b denotes bulk. $\omega_n=(2n+1)\pi/\beta$ is a fermion Matsubara frequency. The definition of $\mathbb{G}_b(\boldsymbol{k},i\omega_n)$ and the solution of Eq. (A1) are given in Sec. II A.

We now want to determine the normal and anomalous Green's function when we restrict our system to a half-space, i.e., $x<0$. Contrary to the bulk case, the Green's function will not be diagonal in momentum space. We do, however, assume translational symmetry in the y and z directions, such that the Green's function will be diagonal in $\boldsymbol{k}_\parallel=k_y\hat{\boldsymbol{y}}+k_z\hat{\boldsymbol{z}}$. It is convenient to work in a mixed basis, where we define the Green's functions $\tilde{\mathcal{G}}_{\sigma\sigma'}(x_1,x_2,\boldsymbol{k}_\parallel,\tau)=-\langle T_\tau c_{x_1,\boldsymbol{k}_\parallel,\sigma}(\tau)c^{\dagger}_{x_2,\boldsymbol{k}_\parallel,\sigma'}(0)\rangle$ and $\tilde{\mathcal{F}}_{\sigma\sigma'}(x_1,x_2,\boldsymbol{k}_\parallel,\tau)=\langle T_\tau c_{x_1,\boldsymbol{k}_\parallel,\sigma}(\tau)c_{x_2,-\boldsymbol{k}_\parallel,\sigma'}(0)\rangle$. The Gor'kov equations in the continuum limit are

$$\int_{-\infty}^{0}dx\mathcal{A}(x_1,x,-i\partial_x,\boldsymbol{k}_\parallel,i\omega_n)\tilde{\mathbb{G}}(x,x_2,\boldsymbol{k}_\parallel,i\omega_n)=\delta(x_1-x_2)\mathbb{1} \tag{A3}$$

in spin $\times$ particle-hole space. We have defined

$$\mathcal{A}(x_1,x,-i\partial_x,\boldsymbol{k}_\parallel,i\omega_n)=\begin{pmatrix}[i\omega_n\mathbb{1}-H_{\mathrm{N}}(x,-i\partial_x,\boldsymbol{k}_\parallel)]\delta(x_1-x) & -\Delta(x_1,x,\boldsymbol{k}_\parallel)\\ -\Delta^{\dagger}(x,x_1,\boldsymbol{k}_\parallel) & [i\omega_n\mathbb{1}+H_{\mathrm{N}}^{*}(x,-i\partial_x,-\boldsymbol{k}_\parallel)]\delta(x_1-x)\end{pmatrix} \tag{A4}$$

where Δ and H_N are 2×2-matrices in spin space. The 4×4 Green's function is

$$\tilde{\mathbb{G}}(x,x_2,\boldsymbol{k}_\parallel,i\omega_n)=\begin{pmatrix}\tilde{\mathcal{G}}(x,x_2,\boldsymbol{k}_\parallel,i\omega_n) & -\tilde{\mathcal{F}}(x,x_2,\boldsymbol{k}_\parallel,i\omega_n)\\ -\tilde{\mathcal{F}}^\dagger(x,x_2,\boldsymbol{k}_\parallel,i\omega_n) & -\tilde{\mathcal{G}}^{\mathrm{t}}(x_2,x,-\boldsymbol{k}_\parallel,-i\omega_n)\end{pmatrix} \tag{A5}$$

and should fulfill proper boundary conditions. The equations are valid for $x_1,x_2<0$. The difference from the full space Gor'kov equations is the restriction $x<0$ in the integral. The bulk version of Eq. (A3) reduces to Eq. (A1).

The pair potential $\Delta(x_1,x,\boldsymbol{k}_\parallel)$ in Eq. (A3) should be determined self-consistently. It is well known that it may differ from its bulk value near surfaces.[21,22] However, we will now apply the usual approximation[17] of replacing the pair potential by its bulk value. Although this is a crude approximation, it is expected to give qualitatively correct results.[17,20]

One way of deriving the half-space Green's function is to consider an infinite system and then introduce a wall of infinitely strong nonmagnetic impurities in order to confine the electrons to one side of the system.[32] The wall of impurities must ensure that there is no transport ("hopping") across the wall and no interaction between the two sides. Since we use a continuum model, a single plane of impurities at $x=0$ will provide an impenetrable surface. It will, however, not prevent interaction between the two sides due to the possibly nonlocal nature of the pair potential. Nevertheless, this interaction with "ghosts" on the other side of the impurity wall is tantamount to approximating $\Delta(x_1,x,\boldsymbol{k}_\parallel)$ by its bulk value. In other words, we construct an auxiliary system for $x>0$ such that a particle in x_1 "feels" the pair potential $\Delta_b(x_1,x,\boldsymbol{k}_\parallel)$ from all x as it would in the bulk. Thus, in the approximation stated above, we may extend the x integral in Eq. (A3) to also include positive x and use the bulk pair potential $\Delta_b(x_1,x,\boldsymbol{k}_\parallel)$. However, we must demand that the boundary condition $\tilde{\mathbb{G}}(x_1,x_2,\boldsymbol{k}_\parallel,i\omega_n)=0$ for $x_1=0$ or $x_2=0$ is fulfilled due to the infinitely strong impurities at $x=0$.

Having made the above mentioned approximation, it is easy to show that the ansatz

$$\tilde{\mathbb{G}}(x_1,x_2,\boldsymbol{k}_\parallel,i\omega_n)=\tilde{\mathbb{G}}_b(x_1,x_2,\boldsymbol{k}_\parallel,i\omega_n)-\tilde{\mathbb{G}}_b(x_1,0,\boldsymbol{k}_\parallel,i\omega_n)\times\tilde{\mathbb{G}}_b^{-1}(0,0,\boldsymbol{k}_\parallel,i\omega_n)\tilde{\mathbb{G}}_b(0,x_2,\boldsymbol{k}_\parallel,i\omega_n) \tag{A6}$$

satisfies the boundary conditions and the Gor'kov equations. Thus, we have expressed the half-space Green's function in terms of bulk Green's functions.

Since we desire a description of the system in terms of plane wave states, we are interested in the Fourier representation of the Green's function [Eq. (A5)],

$$\tilde{\mathbb{G}}(x_1,x_2,\boldsymbol{k}_\parallel,i\omega_n)=\int_{-\infty}^{\infty}dk_{1,x}\int_{-\infty}^{\infty}dk_{2,x}\mathbb{G}(\boldsymbol{k}_1,\boldsymbol{k}_2,i\omega_n)\times e^{-ik_{1,x}x_1+ik_{2,x}x_2}. \tag{A7}$$

Using the Fourier representation of the bulk Green's function, $\tilde{\mathbb{G}}_b(x_1,x_2,\boldsymbol{k}_\parallel,i\omega_n)=\int_{-\infty}^{\infty}dk_x\mathbb{G}_b(\boldsymbol{k},i\omega_n)e^{-ik_x(x_1-x_2)}$, we arrive at

$$\mathbb{G}(\boldsymbol{k}_1,\boldsymbol{k}_2,i\omega_n)=[\mathbb{G}_b(\boldsymbol{k}_1,i\omega_n)\delta(k_{1,x}-k_{2,x})-\mathbb{G}_b(\boldsymbol{k}_1,i\omega_n)\tilde{\mathbb{G}}_b^{-1}(0,0,\boldsymbol{k}_\parallel,i\omega_n)\times\mathbb{G}_b(\boldsymbol{k}_2,i\omega_n)]\delta(\boldsymbol{k}_{1,\parallel}-\boldsymbol{k}_{2,\parallel}). \tag{A8}$$

We see that the half-space Green's function differs from the bulk function by the second term, which is nondiagonal in the perpendicular components of the momenta.

APPENDIX B: TRACE CALCULATIONS

In Sec. II B, we defined $\tilde{\sigma}^{\lambda\rho\mu}_{\boldsymbol{k}_1,\boldsymbol{k}_2}=\sigma^{\lambda}_{\hat{\boldsymbol{B}}_{\boldsymbol{k}_1}}\sigma^{\rho}_{\hat{\boldsymbol{b}}_{\boldsymbol{k}_\parallel}}\sigma^{\mu}_{\hat{\boldsymbol{B}}_{\boldsymbol{k}_2}}\equiv\beta^{\lambda\rho\mu}_{\boldsymbol{k}_1,\boldsymbol{k}_2}\mathbb{1}+\boldsymbol{\alpha}^{\lambda\rho\mu}_{\boldsymbol{k}_1,\boldsymbol{k}_2}\cdot\boldsymbol{\sigma}$, where $\sigma^{\lambda}_{\hat{\boldsymbol{B}}_{\boldsymbol{k}}}=\mathbb{1}+\lambda\hat{\boldsymbol{B}}_{\boldsymbol{k}}\cdot\boldsymbol{\sigma}$. Using the algebra of Pauli matrices, one arrives at

$$\beta^{\lambda\rho\mu}_{\boldsymbol{k}_1,\boldsymbol{k}_2}=1+\lambda\rho(\hat{\boldsymbol{B}}^{\mathrm{A}}_{\boldsymbol{k}_1}\cdot\boldsymbol{b}^{\mathrm{A}}_{\boldsymbol{k}_\parallel})+\rho\mu(\boldsymbol{b}^{\mathrm{A}}_{\boldsymbol{k}_\parallel}\cdot\hat{\boldsymbol{B}}^{\mathrm{A}}_{\boldsymbol{k}_2})+\lambda\mu(\hat{\boldsymbol{B}}^{\mathrm{A}}_{\boldsymbol{k}_1}\cdot\hat{\boldsymbol{B}}^{\mathrm{A}}_{\boldsymbol{k}_2})+i\lambda\rho\mu\hat{\boldsymbol{B}}^{\mathrm{A}}_{\boldsymbol{k}_1}\cdot(\boldsymbol{b}^{\mathrm{A}}_{\boldsymbol{k}_\parallel}\times\hat{\boldsymbol{B}}^{\mathrm{A}}_{\boldsymbol{k}_2}),$$

$$\begin{aligned}\boldsymbol{\alpha}^{\lambda\rho\mu}_{\boldsymbol{k}_1,\boldsymbol{k}_2}=&\lambda\hat{\boldsymbol{B}}^{\mathrm{A}}_{\boldsymbol{k}_1}+\rho\boldsymbol{b}^{\mathrm{A}}_{\boldsymbol{k}_\parallel}+\mu\hat{\boldsymbol{B}}^{\mathrm{A}}_{\boldsymbol{k}_2}+i\lambda\rho(\hat{\boldsymbol{B}}^{\mathrm{A}}_{\boldsymbol{k}_1}\times\boldsymbol{b}^{\mathrm{A}}_{\boldsymbol{k}_\parallel})\\&+i\rho\mu(\boldsymbol{b}^{\mathrm{A}}_{\boldsymbol{k}_\parallel}\times\hat{\boldsymbol{B}}^{\mathrm{A}}_{\boldsymbol{k}_2})+i\lambda\mu(\hat{\boldsymbol{B}}^{\mathrm{A}}_{\boldsymbol{k}_1}\times\hat{\boldsymbol{B}}^{\mathrm{A}}_{\boldsymbol{k}_2})\\&+\lambda\rho\mu[(\boldsymbol{b}^{\mathrm{A}}_{\boldsymbol{k}_\parallel}\cdot\hat{\boldsymbol{B}}^{\mathrm{A}}_{\boldsymbol{k}_2})\hat{\boldsymbol{B}}^{\mathrm{A}}_{\boldsymbol{k}_1}+(\hat{\boldsymbol{B}}^{\mathrm{A}}_{\boldsymbol{k}_1}\cdot\boldsymbol{b}^{\mathrm{A}}_{\boldsymbol{k}_\parallel})\hat{\boldsymbol{B}}^{\mathrm{A}}_{\boldsymbol{k}_2}\\&-(\hat{\boldsymbol{B}}^{\mathrm{A}}_{\boldsymbol{k}_1}\cdot\hat{\boldsymbol{B}}^{\mathrm{A}}_{\boldsymbol{k}_2})\boldsymbol{b}^{\mathrm{A}}_{\boldsymbol{k}_\parallel}],\end{aligned} \tag{B1}$$

and similarly for side B, where $\mathrm{A}\to\mathrm{B}$, $\lambda,\rho,\mu\to\gamma,\eta,\nu$, and $\boldsymbol{k}\to\boldsymbol{p}$. We now intend to find the functions $A_i(\boldsymbol{k}_F,\boldsymbol{p}_F)$ defined in Eq. (31), on which both the one-particle current I_{qp} and the two-particle current I_J depend. First, note that

$$\mathrm{Tr}\,\sigma^{\lambda}_{\hat{\boldsymbol{B}}^{\mathrm{A}}_{\boldsymbol{k}}}\sigma^{\gamma}_{\hat{\boldsymbol{B}}^{\mathrm{B}}_{\boldsymbol{p}}}=2[1+\lambda\gamma(\hat{\boldsymbol{B}}^{\mathrm{A}}_{\boldsymbol{k}}\cdot\hat{\boldsymbol{B}}^{\mathrm{B}}_{\boldsymbol{p}})],$$

$$\mathrm{Tr}\,\sigma^{\lambda}_{\hat{\boldsymbol{B}}^{\mathrm{A}}_{\boldsymbol{k}}}\tilde{\sigma}^{\gamma\eta\nu}_{\boldsymbol{p}_1,\boldsymbol{p}_2}=2[\beta^{\gamma\eta\nu}_{\boldsymbol{p}_1,\boldsymbol{p}_2}+\lambda(\hat{\boldsymbol{B}}^{\mathrm{A}}_{\boldsymbol{k}}\cdot\boldsymbol{\alpha}^{\gamma\eta\nu}_{\boldsymbol{p}_1,\boldsymbol{p}_2})],$$

$$\mathrm{Tr}\,\tilde{\sigma}^{\lambda\rho\mu}_{\boldsymbol{k}_1,\boldsymbol{k}_2}\sigma^{\gamma}_{\hat{\boldsymbol{B}}^{\mathrm{B}}_{\boldsymbol{p}}}=2[\beta^{\lambda\rho\mu}_{\boldsymbol{k}_1,\boldsymbol{k}_2}+\gamma(\boldsymbol{\alpha}^{\lambda\rho\mu}_{\boldsymbol{k}_1,\boldsymbol{k}_2}\cdot\hat{\boldsymbol{B}}^{\mathrm{B}}_{\boldsymbol{p}})],$$

$$\mathrm{Tr}\,\tilde{\sigma}^{\lambda\rho\mu}_{\boldsymbol{k}_1,\boldsymbol{k}_2}\tilde{\sigma}^{\gamma\eta\nu}_{\boldsymbol{p}_1,\boldsymbol{p}_2}=2[\beta^{\lambda\rho\mu}_{\boldsymbol{k}_1,\boldsymbol{k}_2}\beta^{\gamma\eta\nu}_{\boldsymbol{p}_1,\boldsymbol{p}_2}+(\boldsymbol{\alpha}^{\lambda\rho\mu}_{\boldsymbol{k}_1,\boldsymbol{k}_2}\cdot\boldsymbol{\alpha}^{\gamma\eta\nu}_{\boldsymbol{p}_1,\boldsymbol{p}_2})], \tag{B2}$$

obtained by using $\mathrm{Tr}\,\mathbb{1}=2$ and $\mathrm{Tr}\,\sigma_i=0$. To simplify the expressions $A_i(\boldsymbol{k}_F,\boldsymbol{p}_F)$, some useful relations are $\hat{\boldsymbol{B}}^{A}_{\boldsymbol{k}_F}\cdot\boldsymbol{b}^{A}_{\boldsymbol{k}_\parallel}=\hat{\boldsymbol{B}}^{A}_{\boldsymbol{k}_F}\cdot\boldsymbol{b}^{A}_{\boldsymbol{k}_\parallel}=|\boldsymbol{b}^{A}_{\boldsymbol{k}_\parallel}|^2$ and $\hat{\boldsymbol{B}}^{A}_{\boldsymbol{k}_F}\cdot\hat{\boldsymbol{B}}^{A}_{\boldsymbol{k}_F}=2|\boldsymbol{b}^{A}_{\boldsymbol{k}_\parallel}|^2-1$. In addition, we are only interested in $A_i(\boldsymbol{k}_F,\boldsymbol{p}_F)$ as appearing in the Fermi surface integrals (30) and (37). This allows further simplifications when using the symmetries $\chi_{\lambda,\boldsymbol{k}}=\chi_{\lambda,\bar{\boldsymbol{k}}}$ and $\hat{\boldsymbol{B}}_{-\boldsymbol{k}}=-\hat{\boldsymbol{B}}_{\boldsymbol{k}}$. Thus, when appearing in the integrals (30) and (37), we have

$$A_1^{\lambda\gamma}(\boldsymbol{k}_F,\boldsymbol{p}_F) = 4[1+\lambda\gamma(\hat{\boldsymbol{B}}^{\mathrm{A}}_{\boldsymbol{k}_F}\cdot\hat{\boldsymbol{B}}^{\mathrm{B}}_{\boldsymbol{p}_F})],$$

$$A_2^{\lambda\gamma\eta\nu}(\boldsymbol{k}_F,\boldsymbol{p}_F) = 4[1+\gamma\nu+\eta(\gamma+\nu)|\boldsymbol{b}^{\mathrm{B}}_{\boldsymbol{p}_\parallel}|^2+\lambda(\gamma+\nu+2\gamma\eta\nu|\boldsymbol{b}^{\mathrm{B}}_{\boldsymbol{p}_\parallel}|^2)(\hat{\boldsymbol{B}}^{\mathrm{A}}_{\boldsymbol{k}_F}\cdot\hat{\boldsymbol{B}}^{\mathrm{B}}_{\boldsymbol{p}_F})+\lambda\eta(1-\gamma\nu)\hat{\boldsymbol{B}}^{\mathrm{A}}_{\boldsymbol{k}_F}\cdot\boldsymbol{b}^{\mathrm{B}}_{\boldsymbol{p}_\parallel}],$$

$$A_3^{\lambda\rho\mu\gamma}(\boldsymbol{k}_F,\boldsymbol{p}_F) = 4[1+\lambda\mu+\rho(\lambda+\mu)|\boldsymbol{b}^{\mathrm{A}}_{\boldsymbol{k}_\parallel}|^2+\gamma(\lambda+\mu+2\lambda\rho\mu|\boldsymbol{b}^{\mathrm{A}}_{\boldsymbol{k}_\parallel}|^2)(\hat{\boldsymbol{B}}^{\mathrm{A}}_{\boldsymbol{k}_F}\cdot\hat{\boldsymbol{B}}^{\mathrm{B}}_{\boldsymbol{p}_F})+\gamma\rho(1-\lambda\mu)\boldsymbol{b}^{\mathrm{A}}_{\boldsymbol{k}_\parallel}\cdot\hat{\boldsymbol{B}}^{\mathrm{B}}_{\boldsymbol{p}_F}],$$

$$\begin{aligned}A_4^{\lambda\rho\mu\gamma\eta\nu}(\boldsymbol{k}_F,\boldsymbol{p}_F) = 4\Big\{&[1+\lambda\mu+\rho(\lambda+\mu)|\boldsymbol{b}^{\mathrm{A}}_{\boldsymbol{k}_\parallel}|^2][1+\gamma\nu+\eta(\gamma+\nu)|\boldsymbol{b}^{\mathrm{B}}_{\boldsymbol{p}_\parallel}|^2]+\{1-\lambda\mu+[2\lambda\mu+\rho(\lambda+\mu)]|\boldsymbol{b}^{\mathrm{A}}_{\boldsymbol{k}_\parallel}|^2\}\\
&\times\{1-\gamma\nu+[2\gamma\nu+\eta(\gamma+\nu)]|\boldsymbol{b}^{\mathrm{B}}_{\boldsymbol{p}_\parallel}|^2\}+[(\lambda+\mu+2\lambda\rho\mu|\boldsymbol{b}^{\mathrm{A}}_{\boldsymbol{k}_\parallel}|^2)(\gamma+\nu+2\gamma\eta\nu|\boldsymbol{b}^{\mathrm{B}}_{\boldsymbol{p}_\parallel}|^2)+\lambda\gamma+\mu\nu](\hat{\boldsymbol{B}}^{\mathrm{A}}_{\boldsymbol{k}_F}\cdot\hat{\boldsymbol{B}}^{\mathrm{B}}_{\boldsymbol{p}_F})\\
&+[(\lambda+\mu+2\lambda\rho\mu|\boldsymbol{b}^{\mathrm{A}}_{\boldsymbol{k}_\parallel}|^2)\eta(1-\gamma\nu)+(\lambda+\mu)\eta(1+\gamma\nu)](\hat{\boldsymbol{B}}^{\mathrm{A}}_{\boldsymbol{k}_F}\cdot\boldsymbol{b}^{\mathrm{B}}_{\boldsymbol{p}_\parallel})+[\rho(1-\lambda\mu)(\gamma+\nu+2\gamma\eta\nu|\boldsymbol{b}^{\mathrm{B}}_{\boldsymbol{p}_\parallel}|^2)+\rho(1+\lambda\mu)\\
&\times(\gamma+\nu)](\boldsymbol{b}^{\mathrm{A}}_{\boldsymbol{k}_\parallel}\cdot\hat{\boldsymbol{B}}^{\mathrm{B}}_{\boldsymbol{p}_F})+[\rho(1-\lambda\mu)\eta(1-\gamma\nu)+\rho(1+\lambda\mu)\eta(1+\gamma\nu)](\boldsymbol{b}^{\mathrm{A}}_{\boldsymbol{k}_\parallel}\cdot\boldsymbol{b}^{\mathrm{B}}_{\boldsymbol{p}_\parallel})+(\lambda\nu+\mu\gamma)(\hat{\boldsymbol{B}}^{\mathrm{A}}_{\boldsymbol{k}_F}\cdot\hat{\boldsymbol{B}}^{\mathrm{B}}_{\bar{\boldsymbol{p}}_F})\\
&-\left[\frac{1}{4}\rho(\lambda-\mu)\eta(\gamma-\nu)+\left(\lambda\mu+\frac{1}{2}\rho(\lambda+\mu)\right)\left(\gamma\nu+\frac{1}{2}\eta(\gamma+\nu)\right)\right](\hat{\boldsymbol{B}}^{\mathrm{A}}_{\boldsymbol{k}_F}\times\hat{\boldsymbol{B}}^{\mathrm{A}}_{\bar{\boldsymbol{k}}_F})\cdot(\hat{\boldsymbol{B}}^{\mathrm{B}}_{\boldsymbol{p}_F}\times\hat{\boldsymbol{B}}^{\mathrm{B}}_{\bar{\boldsymbol{p}}_F})\Big\}.\end{aligned} \tag{B3}$$

APPENDIX C: MATSUBARA SUMS

The fermion Matsubara sums in Eq. (32) and (38) may be converted to contour integrals in the complex plane through the identity

$$\frac{1}{\beta}\sum_{\omega_n}A(i\omega_n-i\omega_\nu)B(i\omega_n) = -\frac{1}{2\pi i}\oint_C dz A(z-i\omega_\nu)B(z)n_F(z), \tag{C1}$$

for general $A(z-i\omega_\nu)$ and $B(z)$. The contour C must encircle the poles of the Fermi-Dirac function $n_F(z)=(1+e^{\beta z})^{-1}$. The functions $A(z-i\omega_\nu)$ and $B(z)$ appearing in Sec. III will have branch cuts and possibly poles on the lines $\mathrm{Im}\, z=i\omega_\nu$ and $\mathrm{Im}\, z=0$, respectively. This must be taken into account when deforming the contour. After the deformation has been performed, we may let $i\omega_\nu\to eV+i0^+$.

The functions entering sums (32) and (38) are

$$g^{\mathrm{B}}_\gamma(z) = -\frac{z}{\sqrt{|\chi^{\mathrm{B}}_{\gamma,\boldsymbol{p}}|^2-z^2}},$$

$$f^{\mathrm{B}}_\gamma(z) = \frac{\chi^{\mathrm{B}}_{\gamma,\boldsymbol{p}}}{\sqrt{|\chi^{\mathrm{B}}_{\gamma,\boldsymbol{p}}|^2-z^2}}e^{i\vartheta^{\mathrm{B}}},$$

$$\Gamma^{\mathrm{B}}_{\gamma\eta\nu}(z) = -\frac{z(\chi^{\mathrm{B}}_{\gamma,\boldsymbol{p}}\chi^{\mathrm{B}}_{\eta,\boldsymbol{p}}+\chi^{\mathrm{B}}_{\eta,\boldsymbol{p}}\chi^{\mathrm{B}}_{\nu,\boldsymbol{p}}-\chi^{\mathrm{B}}_{\gamma,\boldsymbol{p}}\chi^{\mathrm{B}}_{\nu,\boldsymbol{p}}-z^2)\sqrt{|\chi^{\mathrm{B}}_{-d,\boldsymbol{p}}|^2-z^2}}{2(|\chi^{\mathrm{B}}_{c,\boldsymbol{p}}|^2-z)[b^{\mathrm{B}}_{-,\boldsymbol{p}_\parallel}(\chi^{\mathrm{B}}_{+,\boldsymbol{p}}\chi^{\mathrm{B}}_{-,\boldsymbol{p}}-z^2)+b^{\mathrm{B}}_{+,\boldsymbol{p}_\parallel}\sqrt{|\chi^{\mathrm{B}}_{+,\boldsymbol{p}}|^2-z^2}\sqrt{|\chi^{\mathrm{B}}_{-,\boldsymbol{p}}|^2-z^2}]},$$

$$\Lambda^{\mathrm{B}}_{\gamma\eta\nu}(z) = \frac{[\chi^{\mathrm{B}}_{\gamma,\boldsymbol{p}}\chi^{\mathrm{B}}_{\eta,\boldsymbol{p}}\chi^{\mathrm{B}}_{\nu,\boldsymbol{p}}-z^2(\chi^{\mathrm{B}}_{\gamma,\boldsymbol{p}}+\chi^{\mathrm{B}}_{\nu,\boldsymbol{p}}-\chi^{\mathrm{B}}_{\eta,\boldsymbol{p}})]\sqrt{|\chi^{\mathrm{B}}_{-d,\boldsymbol{p}}|^2-z^2}}{2(|\chi^{\mathrm{B}}_{c,\boldsymbol{p}}|^2-z)[b^{\mathrm{B}}_{-,\boldsymbol{p}_\parallel}(\chi^{\mathrm{B}}_{+,\boldsymbol{p}}\chi^{\mathrm{B}}_{-,\boldsymbol{p}}-z^2)+b^{\mathrm{B}}_{+,\boldsymbol{p}_\parallel}\sqrt{|\chi^{\mathrm{B}}_{+,\boldsymbol{p}}|^2-z^2}\sqrt{|\chi^{\mathrm{B}}_{-,\boldsymbol{p}}|^2-z^2}]}e^{i\vartheta^{\mathrm{B}}}, \tag{C2}$$

where we have defined $c=\mathrm{sgn}(\gamma+\eta+\nu)$ and $d=\gamma\eta\nu$.

We choose the branch cuts such that

$$\sqrt{|\chi^{\mathrm{B}}_{\gamma,\boldsymbol{p}}|^2-(E\pm i0^+)^2} = \sqrt{|\chi^{\mathrm{B}}_{\gamma,\boldsymbol{p}}|^2-E^2}\Theta[|\chi^{\mathrm{B}}_{\gamma,\boldsymbol{p}}|-|E|]\mp i\,\mathrm{sgn}(E)\sqrt{E^2-|\chi^{\mathrm{B}}_{\gamma,\boldsymbol{p}}|^2}\Theta[|E|-|\chi^{\mathrm{B}}_{\gamma,\boldsymbol{p}}|], \tag{C3}$$

and similarly for side A.

The functions $g^{\mathrm{B}}_\gamma(\boldsymbol{p},E+i0^+)$ and $\Gamma^{\mathrm{B}}_{\gamma\eta\nu}(\boldsymbol{p},E+i0^+)$ have the property $B(E+i0^+)=B(E-i0^+)^*$. In addition, $\mathrm{Im}\, B(E+i0^+)$ is an even function of E. Using this, one finds that the imaginary part of the sums in Eq. (32) may be expressed as

$$\mathrm{Im}\, S_i(eV + i0^+) = -\frac{\mathrm{sgn}(eV)}{\pi}\int_{-\infty}^{\infty} dE\, \mathrm{Im}[A(E-|eV|+i0^+)]\mathrm{Im}[B(E+i0^+)] \times [n_F(E-|eV|) - n_F(E)]. \quad \text{(C4)}$$

The functions $f_\gamma^{\mathrm{B}}(\boldsymbol{p}, E+i0^+)$ and $\Lambda_{\gamma\eta\nu}^{\mathrm{B}}(\boldsymbol{p}, E+i0^+)$ have the property $\widetilde{B}(E\pm i0^+)=[\widetilde{B}_R(E)\pm i\widetilde{B}_I(E)]e^{i\vartheta^B}$, where the real functions $\widetilde{B}_R(E)$ and $\widetilde{B}_I(E)$ are even and odd in E, respectively. At $eV=0$, this enables us to write the imaginary part of the sums in Eq. (38) as

$$\mathrm{Im}\, \widetilde{S}_i(i0^+) = \frac{\sin(\vartheta^{\mathrm{B}}-\vartheta^{\mathrm{A}})}{\pi}\int_{-\infty}^{\infty} dE[\widetilde{A}_R(E)\widetilde{B}_I(E) + \widetilde{A}_I(E)\widetilde{B}_R(E)][1 - 2n_F(E)]. \quad \text{(C5)}$$

[1] S. Fujimoto, J. Phys. Soc. Jpn. **76**, 051008 (2007).
[2] M. Sigrist, D. F. Agterberg, P. A. Frigeri, N. Hayashi, R. P. Kaur, A. Koga, I. Milat, K. Wakabayashi, and Y. Yanase, J. Magn. Magn. Mater. **310**, 536 (2007).
[3] V. M. Edelstein, Sov. Phys. JETP **68**, 1244 (1989); V. M. Edelstein, Phys. Rev. Lett. **75**, 2004 (1995).
[4] L. P. Gor'kov and E. I. Rashba, Phys. Rev. Lett. **87**, 037004 (2001).
[5] I. Bonalde, W. Brämer-Escamilla, and E. Bauer, Phys. Rev. Lett. **94**, 207002 (2005); M. Yogi *et al.*, J. Phys. Soc. Jpn. **75**, 013709 (2006); K. Izawa, Y. Kasahara, Y. Matsuda, K. Behnia, T. Yasuda, R. Settai, and Y. Onuki, Phys. Rev. Lett. **94**, 197002 (2005).
[6] M. Yogi *et al.*, J. Phys. Soc. Jpn. **75**, 013709 (2006).
[7] K. V. Samokhin, Phys. Rev. B **72**, 054514 (2005).
[8] N. Hayashi, K. Wakabayashi, P. A. Frigeri, and M. Sigrist, Phys. Rev. B **73**, 092508 (2006).
[9] S. Fujimoto, J. Phys. Soc. Jpn. **75**, 083704 (2006).
[10] K. V. Samokhin, E. S. Zijlstra, and S. K. Bose, Phys. Rev. B **69**, 094514 (2004).
[11] R. Eguchi, T. Yokoya, T. Baba, M. Hanawa, Z. Hiroi, N. Kamakura, Y. Takata, H. Harima, and S. Shin, Phys. Rev. B **66**, 012516 (2002).
[12] H. Q. Yuan, D. F. Agterberg, N. Hayashi, P. Badica, D. Vandervelde, K. Togano, M. Sigrist, and M. B. Salamon, Phys. Rev. Lett. **97**, 017006 (2006).
[13] M. Nishiyama, Y. Inada, and G.-Q. Zheng, Phys. Rev. Lett. **98**, 047002 (2007).
[14] O. Vyaselev, K. Arai, K. Kobayashi, J. Yamazaki, K. Kodama, M. Takigawa, M. Hanawa, and Z. Hiroi, Phys. Rev. Lett. **89**, 017001 (2002); M. D. Lumsden, S. R. Dunsiger, J. E. Sonier, R. I. Miller, R. F. Kiefl, R. Jin, J. He, D. Mandrus, S. T. Bramwell, and J. S. Gardner, *ibid.* **89**, 147002 (2002).
[15] T. Shibauchi, L. Krusin-Elbaum, Y. Kasahara, Y. Shimono, Y. Matsuda, R. D. McDonald, C. H. Mielke, S. Yonezawa, Z. Hiroi, M. Arai, T. Kita, G. Blatter, and M. Sigrist, Phys. Rev. B **74**, 220506(R) (2006); Y. Shimono, T. Shibauchi, Y. Kasahara, T. Kato, K. Hashimoto, Y. Matsuda, J. Yamaura, Y. Nagao, and Z. Hiroi, Phys. Rev. Lett. **98**, 257004 (2007).
[16] I. Giaever, Phys. Rev. Lett. **5**, 147 (1960); **5**, 464 (1960).
[17] S. Kashiwaya and Y. Tanaka, Rep. Prog. Phys. **63**, 1641 (2000).
[18] C. C. Tsuei, J. R. Kirtley, M. Rupp, J. Z. Sun, A. Gupta, M. B. Ketchen, C. A. Wang, Z. F. Ren, J. H. Wang, and M. Bhushan, Science **271**, 329 (1996).
[19] T. Yokoyama, Y. Tanaka, and J. Inoue, Phys. Rev. B **72**, 220504(R) (2005).
[20] C. Iniotakis, N. Hayashi, Y. Sawa, T. Yokoyama, U. May, Y. Tanaka, and M. Sigrist, Phys. Rev. B **76**, 012501 (2007).
[21] V. Ambegaokar, P. G. de Gennes, and D. Rainer, Phys. Rev. A **9**, 2676 (1974).
[22] L. J. Buchholtz and G. Zwicknagl, Phys. Rev. B **23**, 5788 (1981).
[23] C. R. Hu, Phys. Rev. Lett. **72**, 1526 (1994).
[24] K. Børkje and A. Sudbø, Phys. Rev. B **74**, 054506 (2006).
[25] S. Graser and T. Dahm, Phys. Rev. B **75**, 014507 (2007).
[26] A. Brinkman, A. A. Golubov, H. Rogalla, O. V. Dolgov, J. Kortus, Y. Kong, O. Jepsen, and O. K. Andersen, Phys. Rev. B **65**, 180517(R) (2002); D. F. Agterberg, E. Demler, and B. Janko, *ibid.* **66**, 214507 (2002).
[27] P. A. Frigeri, D. F. Agterberg, A. Koga, and M. Sigrist, Phys. Rev. Lett. **92**, 097001 (2004).
[28] V. P. Mineev, Int. J. Mod. Phys. B **18**, 2963 (2004).
[29] I. A. Sergienko and S. H. Curnoe, Phys. Rev. B **70**, 214510 (2004).
[30] S. Fujimoto, Phys. Rev. B **72**, 024515 (2005).
[31] P. A. Frigeri, D. F. Agterberg, A. Milat, and M. Sigrist, Eur. Phys. J.: Appl. Phys. **54**, 435 (2006).
[32] A. M. Bobkov, L. Y. Zhu, S.-W. Tsai, T. S. Nunner, Y. S. Barash, and P. J. Hirschfeld, Phys. Rev. B **70**, 144502 (2004).
[33] L. J. Buchholtz and D. Rainer, Z. Phys. B **35**, 151 (1979).
[34] One might expect that this approximation breaks down when $\boldsymbol{k}_{F,x}\to 0$ and that $N^x_{\pm,\boldsymbol{k}_F}\to 0$ in that case, but this will not pose any problem here.
[35] R. E. Prange, Phys. Rev. **131**, 1083 (1963).
[36] G. D. Mahan, *Many-particle Physics* (Kluwer Academic, Dordrecht/Plenum, New York, 2000).
[37] There should also be an index A(B) on the $\tilde{\sigma}$'s, since they depend on $\hat{\boldsymbol{B}}^{\mathrm{A(B)}}_{\boldsymbol{k}(\mathbf{p})}$. We skip this, since the momenta ($\boldsymbol{k}$ or $\boldsymbol{p}$) tell us to which side they belong.
[38] N. R. Werthamer, Phys. Rev. **147**, 255 (1966).
[39] V. Ambegaokar and A. Baratoff, Phys. Rev. Lett. **10**, 486 (1963).
[40] T. Löfwander, V. S. Shumeiko, and G. Wendin, Supercond. Sci. Technol. **14**, R53 (2001).
[41] In the case of a ferromagnet with magnetization $\boldsymbol{M}^{\mathrm{B}}$, combinations such as $\boldsymbol{B}^{\mathrm{A}}_{\boldsymbol{k}_F}\cdot\boldsymbol{M}^{\mathrm{B}}+\boldsymbol{B}^{\mathrm{A}}_{\tilde{\boldsymbol{k}}_F}\cdot\boldsymbol{M}^{\mathrm{B}}=2\boldsymbol{b}^{\mathrm{A}}_{\boldsymbol{k}_\parallel}\cdot\boldsymbol{M}^{\mathrm{B}}$ would not contribute when summing over all $\boldsymbol{k}_\parallel$ and using $\boldsymbol{b}^{\mathrm{A}}_{-\boldsymbol{k}_\parallel}=-\boldsymbol{b}^{\mathrm{A}}_{\boldsymbol{k}_\parallel}$. However, introducing some spatial anisotropy in the densities of states could change this. See also Ref. 46, where a junction between a two-dimensional electron gas with Rashba spin-orbit coupling and a ferromagnet were considered.
[42] The size of t could, of course, depend on ζ, at least if different junctions are used for different ζ. However, the qualitative fea-

tures of the current-voltage diagram would be unaffected by that.

[43] W. H. Press, W. T. Vetterling, S. A. Teukolsky, and B. P. Flannery, *Numerical Recipes in C* (Cambridge University Press, 1999).

[44] This statement depends on the two densities of states in the non-superconducting phase being equal. However, if they are not, this should give observable effects also above T_c.

[45] These particular gaps have the nice property that the energy integrals may be performed analytically, given some reasonable approximations.

[46] L. W. Molenkamp, G. Schmidt, and G. E. W. Bauer, Phys. Rev. B **64**, 121202(R) (2001).

Article III

Instanton correlators and phase transitions in two- and three-dimensional logarithmic plasmas

Physical Review B **71**, 085112 (2005)

Instanton correlators and phase transitions in two- and three-dimensional logarithmic plasmas

K. Børkje,[1,*] S. Kragset,[1,†] and A. Sudbø[1,‡]
[1]*Department of Physics, Norwegian University of Science and Technology, N-7491 Trondheim, Norway*
(Received 22 June 2004; published 14 February 2005)

The existence of a discontinuity in the inverse dielectric constant of the two-dimensional (2D) Coulomb gas is demonstrated on purely numerical grounds. This is done by expanding the free energy in an applied twist and performing a finite-size scaling analysis of the coefficients of higher-order terms. The phase transition, driven by unbinding of dipoles, corresponds to the Kosterlitz-Thouless transition in the 2D *XY* model. The method developed is also used for investigating the possibility of a Kosterlitz-Thouless phase transition in a three-dimensional system of point charges interacting with a logarithmic pair-potential, a system related to effective theories of low-dimensional strongly correlated systems. We also contrast the finite-size scaling of the fluctuations of the dipole moments of the two-dimensional Coulomb gas and the three-dimensional logarithmic system to those of the three-dimensional Coulomb gas.

DOI: 10.1103/PhysRevB.71.085112 PACS number(s): 04.50.+h, 11.25.−w, 98.80.−k

I. INTRODUCTION

Compact $U(1)$ gauge fields in three dimensions are of great interest in condensed matter theory, as they arise in effective theories of strongly correlated two-dimensional (2D) systems at zero temperature.[1–4] Lightly doped Mott-Hubbard insulators, such as high-T_c cuprates, are examples of systems possibly described by such theories, where the compact gauge field emerges from strong local constraints on the electron dynamics.[2,5–7] High-T_c cuprates appear to fall outside the Landau-Fermi-liquid paradigm, and a so-called confinement-deconfinement transition in the gauge theories may be associated with breakdown of Fermi liquid and quasiparticles in 2D at $T=0$.[6–8] Obliteration of electronlike quasiparticles and spin-charge separation in the presence of interactions is well known to occur in one spatial dimension. However, the mechanism operative in that case, namely singular forward scattering, is unlikely to be operative in higher dimensions due to the much less restrictive kinematics at the Fermi surface.[9] Proliferation of instantons of emergent gauge fields show more promise as a viable candidate mechanism. This line of pursuit has recently been reinvigorated in the context of understanding the physics of lightly doped Mott-Hubbard insulators and unconventional insulating states.[10]

The compact nature of a constraining gauge field on a lattice model introduces topological defects defined by surfaces where the field jumps by 2π, forming a gas of instantons (or "monopoles") in $2+1$ dimensions.[11] Considering the gauge sector only, the interactions between these instantonic defects are the same as between charges in a 3D Coulomb gas, i.e., $1/r$-interactions. Such a gas is always in a metallic or plasma phase with a finite screening length,[11,12] and there is no phase transition between a metallic regime and an insulating regime. However, in models where compact gauge fields are coupled to *matter fields*, the interaction between the magnetic monopoles may be modified by the emergence of an anomalous scaling dimension of the gauge field due to critical matter-field fluctuations.[13] This is the case for the compact abelian Higgs model with matter fields in the fundamental representation.[14]

In Refs. 14, it was shown that the introduction of a matter field with the fundamental charge leads to an anomalous scaling dimension in the gauge field propagator.[13] The effect is to alter the interaction potential between the magnetic monopoles from $1/r$ to $-\ln r$. The existence of a confinement-deconfinement transition in the gauge theory is thus related to whether a phase transition occurs in a 3D gas of point charges with logarithmic interactions. However, one should note that the legitimacy of a monopole action based on just pairwise interactions has been questioned, particularly when viewed as an effective description of an effective gauge theory of strongly interacting systems.[15] The 3D logarithmic plasma is however of considerable interest in its own right.

In two dimensions, where $-\ln r$ is the Coulomb potential, it is known that the logarithmic gas experiences a phase transition from a low-temperature insulating phase consisting of dipoles to a high-temperature metallic phase. This is nothing but the Coulomb-gas representation of the Kosterlitz-Thouless transition in the 2D *XY* model. In a 3D logarithmic gas, the existence of a phase transition is still subject to debate.[14,16,17] Renormalization group arguments have been used[14] to demonstrate that a transition may occur, driven by the unbinding of dipoles. Others have claimed that the 3D logarithmic gas is always in the metallic phase.[16] In a recent paper,[18] large scale Monte Carlo simulations indicated that two distinct phases of the 3D-log gas exists; a low-T regime where the dipole moment does not scale with system size and a high-T regime where the dipole moment is system size dependent. Those results do not, however, determine the character of the phase transitions. That will be the main subject of this paper.

The Kosterlitz-Thouless transition in the 2D *XY* model is characterized by the universal jump to zero of the helicity modulus.[19] In the corresponding 2D Coulomb gas, it is the inverse of the macroscopic dielectric constant ϵ that experiences a jump to zero when going from the insulating to the metallic phase. According to Ref. 14, such a universal discontinuity should also take place for ϵ^{-1} in the 3D logarithmic gas associated with the confinement-deconfinement transition. Proving that such discontinuities exist numerically is a

 ©2005 The American Physical Society

subtle task. The discontinuous character of the helicity modulus in the 2D *XY* model is very hard to see in a convincing manner by computing the helicity modulus, due to severe finite-size effects. It was only recently proven on purely numerical grounds that such a discontinuity exists[20] in a simple, but yet clever manner. By imposing a twist across the system and expanding the free energy in this twist to the fourth order, a stability argument was used to show that the second order term in the expansion, the helicity modulus, must be nonzero at T_c. The proof relies on the ability to conclude that the fourth order term is negative in the thermodynamic limit, from which the discontinuity follows immediately. In this paper, we will repeat this procedure, but now in the language of the 2D Coulomb gas. In addition to confirming the results of Minnhagen and Kim, the method which we develop here could be suitable for proving the possibly discontinuous behavior of ϵ^{-1} in the 3D logarithmic gas. This is a main motivation for translating the procedure of Ref. 20 to the vortex language, since the 3D logarithmic gas is not the dual theory of any simple spin model. After having demonstrated the discontinuity in the 2D Coulomb gas, we go on to apply the method on the 3D logarithmic gas. We also compare the scaling with system size of the mean square dipole moment for these logarithmic plasmas, and contrast the results with those of the 3D Coulomb gas. This is important, since the mean square dipole moment does not scale with system size below a certain temperature for the logarithmic plasmas.[18] This indicates that two phases exist, where the low-temperature regime consists of tightly bound pairs. However, the results for the 3D Coulomb gas are qualitatively different, in accordance with the fact that such a low-temperature phase is absent in that case.

II. MODEL

The Hamiltonian of the 2D *XY* model on a square lattice modified with a twist $\mathbf{T}(x,y)$ is

$$H_{XY} = -J\sum_{\langle i,j\rangle} \cos(\theta_i - \theta_j - 2\pi \mathbf{r}_{ij}\cdot\mathbf{T}), \tag{1}$$

where $\mathbf{r}_{ij}$ is the displacement between the nearest neighbor pairs to be summed over. We set the coupling constant J to unity. The volume of the system, i.e., the number of lattice points, is L^2, and the angle θ_i is subject to periodic boundary conditions. In the Villain approximation, a duality transformation leads to the Hamiltonian

$$H = \frac{1}{2}\sum_{i,j} (m + \varepsilon^{\mu\nu}\Delta^\mu T^\nu)_i V_{ij} (m + \varepsilon^{\rho\sigma}\Delta^\rho T^\sigma)_j, \tag{2}$$

where m_i are point charges on the dual lattice, corresponding to vortex excitations in the *XY* model. Δ^μ is a lattice derivative and $\varepsilon^{\mu\nu}$ is the completely antisymmetric symbol. The potential V_{ij} is given by

$$V(|\mathbf{r}_i - \mathbf{r}_j|) = \frac{2\pi^2}{L^2}\sum_{\mathbf{q}} \frac{e^{-i\mathbf{q}\cdot(\mathbf{r}_i - \mathbf{r}_j)}}{2 - \cos q_x - \cos q_y}, \tag{3}$$

which has a logarithmic long-range behavior. Details of the dualization are found in Appendix A. As is well known, Eq. (2) at zero twist describes the two-dimensional Coulomb gas (2D CG). In this representation, the Kosterlitz-Thouless phase transition of the 2D *XY* model is recognized by a discontinuous jump to zero of the inverse macroscopic dielectric constant ϵ^{-1} at T_c. We note that the curl of the twist $\mathbf{T}$ acts as a modification of the charge field in the 2D CG.

The free energy of the system is $F = -T \ln Z$, where the partition function is given by summing the Boltzmann factor over all charge configurations

$$Z = \sum_{\{m\}} e^{-H/T}. \tag{4}$$

Let us write the Hamiltonian in Fourier representation

$$H = \frac{1}{2L^2}\sum_{\mathbf{q}} (m_{\mathbf{q}} + \varepsilon^{\nu\lambda} Q^\nu_{-\mathbf{q}} T^\lambda_{\mathbf{q}}) V_{\mathbf{q}} (m_{-\mathbf{q}} + \varepsilon^{\rho\sigma} Q^\rho_{\mathbf{q}} T^\sigma_{-\mathbf{q}}), \tag{5}$$

where the discrete Fourier transform is defined as in Appendix B and $\Delta^\mu e^{\pm i\mathbf{q}\cdot\mathbf{r}} \equiv e^{\pm i\mathbf{q}\cdot\mathbf{r}} Q^\mu_{\pm\mathbf{q}}$.

III. STABILITY ARGUMENT

From Eq. (1), it is clear that $F(\mathbf{T}) \geqslant F(0)$ in the low-temperature phase, i.e., the free energy is minimal for zero twist. This inequality is also valid at the critical temperature T_c, since the free energy must be a continuous function of temperature. As a consequence, the Taylor expansion

$$F(\mathbf{T}) - F(0) = \sum_\alpha \sum_{\mathbf{q}_1} \left.\frac{\partial F}{\partial T^\alpha_{\mathbf{q}_1}}\right|_{\mathbf{T}=0} T^\alpha_{\mathbf{q}_1} + \sum_{\alpha,\beta}\sum_{\mathbf{q}_1\mathbf{q}_2} \left.\frac{\partial^2 F}{\partial T^\alpha_{\mathbf{q}_1}\partial T^\beta_{\mathbf{q}_2}}\right|_{\mathbf{T}=0} \frac{T^\alpha_{\mathbf{q}_1} T^\beta_{\mathbf{q}_2}}{2} + \cdots \tag{6}$$

cannot be negative for any $T \leqslant T_c$. Expressions for the derivatives of the free energy with respect to a general twist are found in Appendix B. Only terms of even order will contribute to the series, since m_i may take equally many positive and negative values. We are free to *choose* the twist to be

$$\mathbf{T}(x,y) = \frac{\Delta}{L^\eta}\sin\left(\frac{2\pi y}{L}\right)\hat{\mathbf{x}}, \tag{7}$$

where Δ is an arbitrarily small constant and $\eta = 1$ for the two-dimensional Coulomb gas. To the fourth order, this long-wavelength twist turns Eq. (6) into

$$F(\mathbf{T}) - F(0) = \frac{\Delta^2}{4} C_{\mathbf{k}} \left(1 - \frac{V_{\mathbf{k}}}{L^2 T}\langle m_{\mathbf{k}} m_{-\mathbf{k}}\rangle\right) + \frac{\Delta^4}{32}\frac{(C_{\mathbf{k}} V_{\mathbf{k}})^2}{L^4 T^3}\left(\langle m_{\mathbf{k}} m_{-\mathbf{k}}\rangle^2 - \frac{1}{2}\langle (m_{\mathbf{k}} m_{-\mathbf{k}})^2\rangle\right), \tag{8}$$

where $\mathbf{k} = (0, 2\pi/L)$ and $C_{\mathbf{k}} = Q^y_{\mathbf{k}} Q^y_{-\mathbf{k}} V_{\mathbf{k}}$. We recognize the paranthesis in the second order term as the dielectric response function $\epsilon^{-1}(\mathbf{k})$, where $\mathbf{k}$ is now the smallest nonzero wave vector in a finite system. Note that the prefactors in both terms are independent of system size as $L \to \infty$. The crucial argument to use is the same as in Ref. 20. If the

fourth order term approaches a finite negative value at T_c in the limit $L\to\infty$, the second order term, $\epsilon^{-1}(\mathbf{k}\to 0)$, must be positive to satisfy the inequality $F(\mathbf{T})\geqslant F(0)$. Furthermore, since we know that the inverse dielectric constant is zero in the high-temperature phase, it necessarily experiences a discontinuity at T_c. As we shall see, Monte Carlo simulations show that the fourth order term is indeed negative at T_c in the thermodynamic limit.

The argument described above will also apply to a three-dimensional gas of point charges interacting via a pair potential of some sort, as long as the twist raises the free energy in the low-temperature regime. Since the curl of the twist $\mathbf{T}$ is a vector in that case, one may for instance choose the z component of this vector as the perturbing charge in Eq. (2). The two three-dimensional systems we will consider are the logarithmic gas and the Coulomb gas. The expansion (6) is valid for any system size L. However, to make the change in free energy nondivergent as $L\to\infty$, the twist must be chosen such that the terms in the expansion are independent of system size. This is obtained by choosing $\eta=2$ for the logarithmic gas and $\eta=3/2$ for the Coulomb gas. η is defined in Eq. (7). In both cases, the second order term will be proportional to

$$\epsilon^{-1}(\mathbf{k}) = 1 - \frac{V_{\mathbf{k}}}{L^3 T}\langle m_{\mathbf{k}} m_{-\mathbf{k}}\rangle. \tag{9}$$

The fourth order term will be proportional to

$$\epsilon_4(\mathbf{k}) \equiv \frac{1}{T^3}\left(\langle m_{\mathbf{k}} m_{-\mathbf{k}}\rangle^2 - \frac{1}{2}\langle (m_{\mathbf{k}} m_{-\mathbf{k}})^2\rangle\right) \tag{10}$$

in the logarithmic case. In the case of a 3D Coulomb gas, the interesting quantity will be ϵ_4/L^2, which is independent of system size since $\langle m_{\mathbf{k}} m_{-\mathbf{k}}\rangle \sim L$ in that case.

IV. SIMULATION RESULTS

Standard Metropolis Monte Carlo simulations are carried out on the model (2) at zero twist. An $L\times L$ square lattice with periodic boundary conditions is used and the system is kept electrically neutral at all times during the simulations. This is achieved by inserting dipoles with probability according to the Metropolis algorithm: An insertion of a negative or positive charge is attempted at random at a given lattice site, and an opposite charge is placed at one of the nearest-neighbor sites to make the dipole. This is one move, accepted with probability $\exp(-\Delta E/T)=\exp[-(\mathcal{H}_{\text{new}}-\mathcal{H}_{\text{old}})/T]$, and the sequence of trying this for all sites in the system once is defined as one sweep. If a charge is placed on top of an opposite one, the effect is to annihilate the existing one. All simulations are performed going from high to low temperature and after simulating one system size L the sampled data are postprocessed using Ferrenberg-Swendsen reweighting techniques.[21]

A. 2D Coulomb gas

We consider first the 2D Coulomb gas, which is known to suffer a metal-insulator transition via a Kosterlitz-Thouless phase transition. In this case, Monte Carlo data are obtained for $L=4-100$ and for each L up to 200 000 sweeps at each temperature is used.

We start by taking the Hamiltonian (2) and computing the mean square of the dipole moment $\langle s^2\rangle$ as a function of system size and temperature. A mean square dipole moment which is independent of system size indicates the existence of tightly bound dipoles and a dielectric or insulating phase. If the mean square dipole moment scales with system size, this demonstrates the existence of free unbound charges and hence a metallic phase. In other words, we expect in the low-temperature dielectric insulating phase no finite-size scaling of $\langle s^2\rangle$, whereas we should expect $\langle s^2\rangle \propto L^{\alpha(T)}$ with $\alpha(T)\leqslant 2$ at higher temperatures. Using an intuitive low density argument, neglecting screening effects,[22] we can calculate the behavior of $\langle s^2\rangle$ to leading order in L,

$$\langle s^2\rangle \propto \begin{cases} \text{const.}, & T < T_{\text{KT}}, \\ L^{(T-T_{\text{KT}})/T}, & T_{\text{KT}} < T < 2T_{\text{KT}}, \\ L^2, & 2T_{\text{KT}} < T. \end{cases} \tag{11}$$

Hence, $\alpha(T)$ is zero for low temperatures and a monotonically increasing function of temperature just above T_{KT}. Including screening effects in 2D shows that this conclusion still holds, however the temperature at which it occurs is determined by screening.

Details of the simulations may be found in Ref. 18. The result is shown in Fig. 1 where we have the mean square dipole moment for the 2D case both as a function of temperature for various system sizes, and as function of system size for various temperatures. From this we may extract the scaling constant $\alpha(T)$ which is shown in the center panel of Fig. 1. A related method for using dipole fluctuations to measure vortex-unbinding has recently been used in Ref. 23.

Below a temperature $T\approx 1.3$, no scaling of $\langle s^2\rangle$ is seen, consistent with a low-temperature dielectric phase. The temperature at which scaling stops is consistent with the known temperature at which the 2D Coulomb gas suffers a metal-insulator transition.

Simulation results for the inverse dielectric constant are shown for a selection of system sizes in Fig. 2. Since ϵ^{-1} is expected to be discontinuous at T_c in the limit $\mathbf{k}\to 0$, we consider only the smallest possible wave vector in each system, $\mathbf{k}=(0,2\pi/L)$, and we see that the decrease of ϵ^{-1} towards zero with increasing T indeed gets sharper as L grows. It is, however, difficult to decide from these plots alone whether or not the dielectric constant is discontinuous at T_c. The fourth order term in the expansion of the free energy, ϵ_4 defined in Eq. (10), is therefore investigated in a corresponding manner and plotted in Fig. 3.

We note that this quantity has a dip at a temperature which can be associated with the transition temperature. If this dip remains finite and negative as L approaches infinity, ϵ^{-1} must exhibit a jump at T_c. The depth of the dip is shown in Fig. 4 for a variety of system sizes ranging from $L=4$ to $L=100$ and as a function of $1/L$. It clearly decreases with increasing L. However, from the positive curvature of the data in the log-log plot we may conclude that the depth remains nonzero when we extrapolate to $1/L=0$, a conclusion

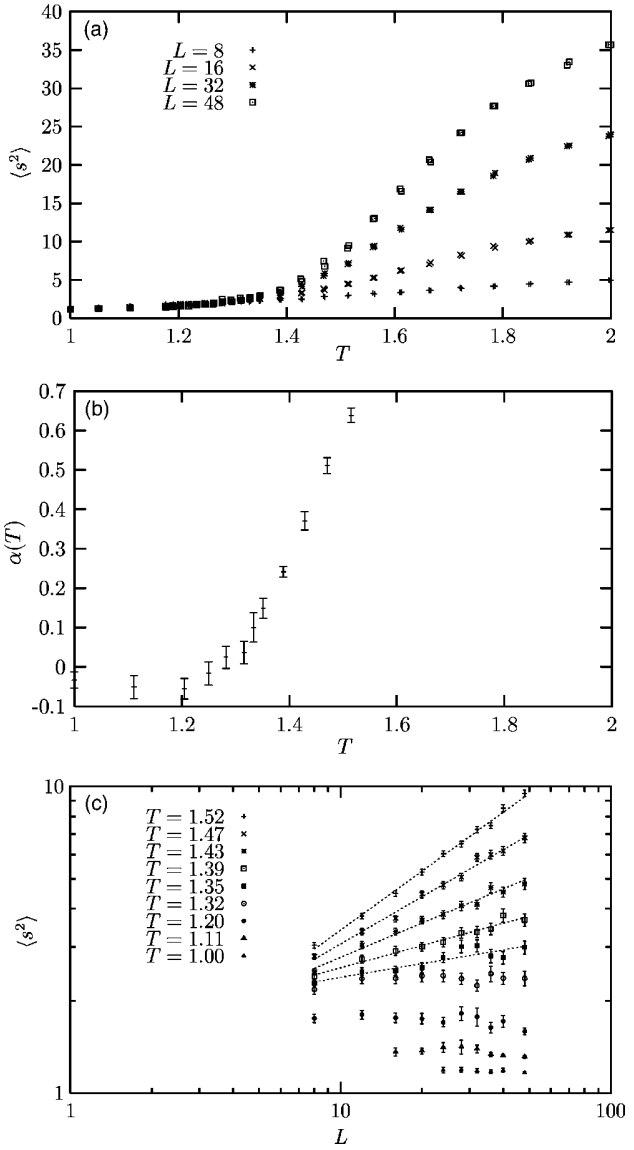

FIG. 1. The mean square dipole moment $\langle s^2\rangle$ as a function of temperature (top panel), and system size (bottom panel) for the 2D Coulomb gas. The middle panel shows the scaling exponent α extracted from $\langle s^2\rangle \sim L^{\alpha(T)}$.

reached by assuming power-law dependence of the depth on L.

We can now subtract from the depth a constant chosen so as to linearize the curve in the log-log plot. This constant consequently corresponds to the depth when extrapolating the data to the thermodynamic limit $1/L=0$, and we find this to be 0.047 ± 0.005.

By plotting the temperature at which the fourth order term has its minimum against $1/L$, we can follow a similar procedure as the above one. This is shown in Fig. 5. We linearize a log-log plot by subtracting a carefully chosen constant and end up with the number 1.36 ± 0.04. This is nothing else than an estimate of the critical temperature of the 2D CG, and compares well to earlier results.[24] The approach towards T_c is however a bit slow, making a precise determination of

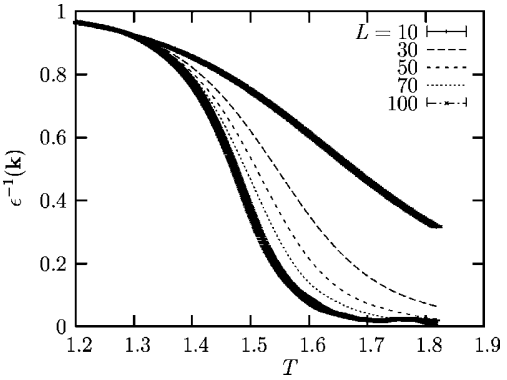

FIG. 2. Inverse dielectric constant taken at the smallest possible wave vector in a finite system $\mathbf{k}=(0,2\pi/L)$ and plotted against temperature T for system sizes $L=10$, 30, 50, 70, and 100 for the 2D Coulomb gas. The decrease of ϵ^{-1} towards zero becomes sharper with increasing L, consistent with the prediction of a discontinuous jump. Errorbars are given in the top and bottom curves, and omitted for clarity in the others.

the critical temperature difficult. This drawback was also noted by Minnhagen and Kim for the corresponding computations on the 2D XY model.[20]

B. 3D logarithmic system

We may carry out the same type of analysis for the mean square dipole moment for a system of point charges interacting via a three-dimensional logarithmic bare pair potential (3D LG). For this system, much less is known. Such a system has recently been considered in the context of studying confinement-deconfinement phase transitions in the $(2+1)$-dimensional Abelian Higgs model.[14] The results are shown in Fig. 6.

Qualitatively and quantitatively the results are the same in the 3D LG as for the 2D case. This strongly suggests that the 3D LG also has a low-temperature dielectric insulating phase

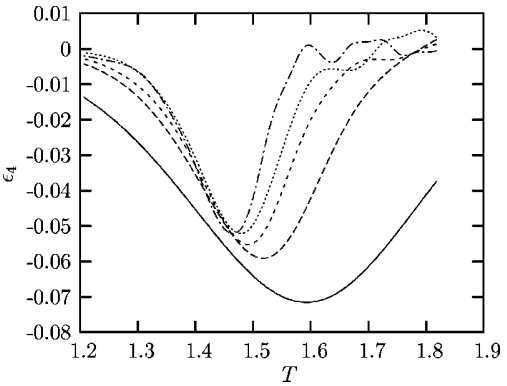

FIG. 3. The coefficient ϵ_4 of the fourth order term of the expansion of the free energy, for the 2D Coulomb gas. The same systems are used in this plot as in Fig. 2, and the depths decrease with increasing L. The important question is whether this dip vanishes at T_c or not. Errorbars are omitted but will be reintroduced in Fig. 4. The oscillation at high T is due to noise from the reweighting.

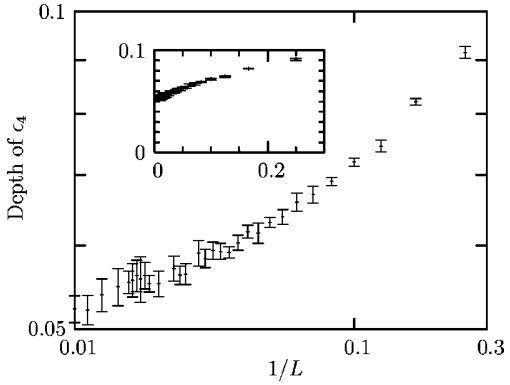

FIG. 4. Depth of the dip in the fourth order term shown in Fig. 3 for the 2D Coulomb gas. The data are obtained from simulations of system sizes ranging from $L=4$ to $L=100$ and plotted both on a linear scale (inset) and on a log-log scale. The positive curvature in the log-log plot clearly indicates a nonzero value of the depth when extrapolating to the limit $L\to\infty$.

separated by a phase transition from a high-temperature phase. In the low-temperature regime the charges of almost all dipoles are bound as tightly as possible, the separation of the charges correspond to the lattice constant. In the high-temperature regime the dipoles have started to separate, reflected by a scaling of $\langle s^2\rangle \sim L^{\alpha(T)}$ with the system size. Since $\alpha(T)=0$ at low temperatures while $\alpha(T)\neq 0$ in the high-temperature regime a non-analytic behavior of $\alpha(T)$ is implied. This necessarily corresponds to a phase transition in the vicinity of $T\approx 0.3$, a temperature which agrees well with Ref. 14 where a critical value of $T_c=1/3$ was obtained.

Note that, although this simple type of analysis of the mean square dipole moment does not by itself suffice to determine the character of these phase transitions either in the case of 3D LG or 2D CG, it does suffice to shed light on the important issue of whether a low temperature insulating phase exists in the 3D LG as well. This is far from obvious, since the screening properties of a three-dimensional system of charges interacting logarithmically is quite different from

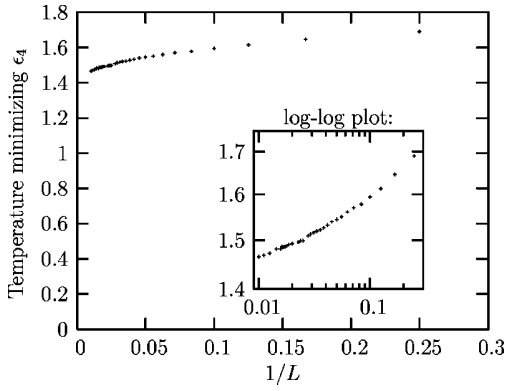

FIG. 5. Temperature minimizing ϵ_4 as a function of inverse system size for the 2D CG. The values are plotted both on a linear scale and on a log-log scale (inset). This temperature reaches a nonzero value at $L\to\infty$ indicated by the positive curvature in the log-log plot. Extrapolation gives $T_c=1.36\pm 0.04$.

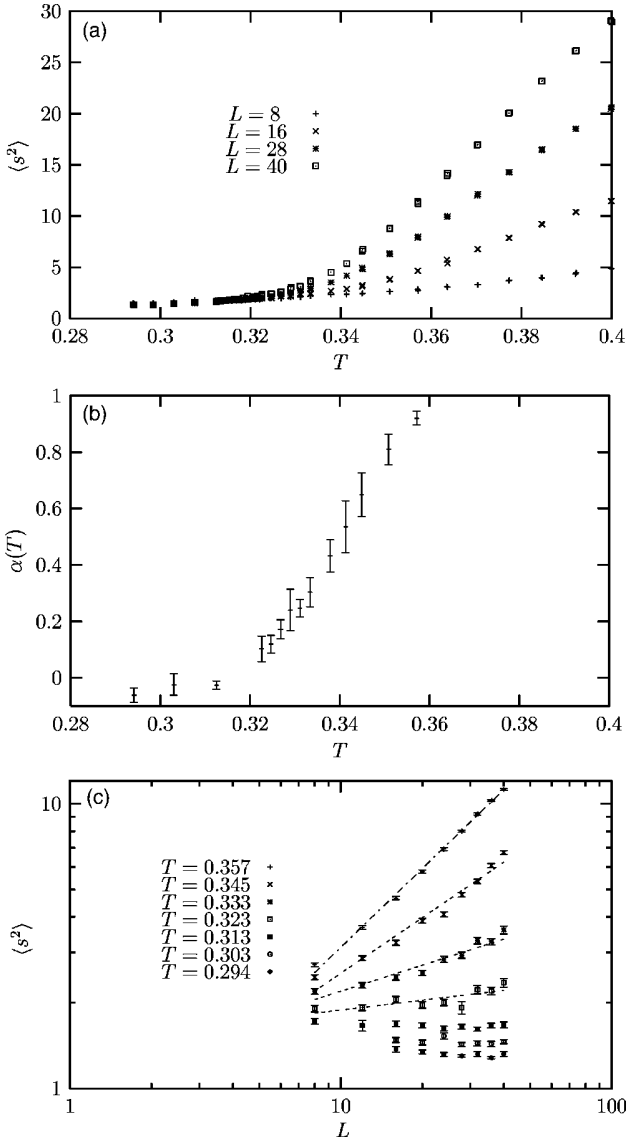

FIG. 6. Mean square dipole moment $\langle s^2\rangle$ as a function of temperature (top panel) and system size (bottom panel) for the 3D system of point charges interacting with a logarithmic bare pair potential (3D LG). The middle panel shows the scaling exponent α extracted from $\langle s^2\rangle \sim L^{\alpha(T)}$.

that of a Coulomb system (in any dimension).[16] It is therefore of considerable interest to repeat the analysis carried out for the 2D Coulomb gas to, if possible, determine the character of a metal-insulator transition in the 3D LG.

In Fig. 7 we show the inverse dielectric constant for the 3D LG as a function of temperature for various system sizes. It shows qualitatively the same behavior as for the 2D CG in that the decrease of ϵ^{-1} towards zero becomes sharper with increasing L. However, the downward drift in the temperature at which the inverse dielectric constant starts decreasing rapidly is more pronounced than in the 2D CG case.

In Fig. 8 we have plotted the fourth order coefficient against temperature for the 3D LG system, and the depth of the dip as a function of system size is shown in Fig. 9. It would clearly have been desirable to be able to access larger

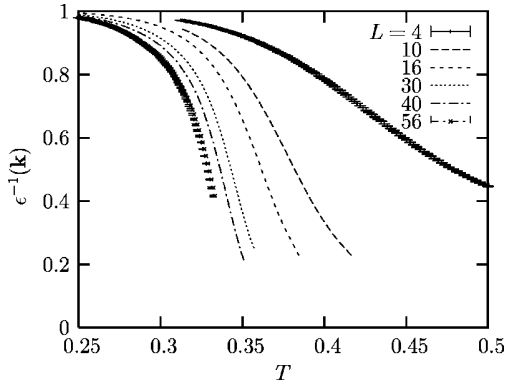

FIG. 7. Inverse dielectric constant taken at the smallest possible wave vector in a finite system, $\mathbf{k}=(0,2\pi/L,0)$, and plotted against temperature T for system sizes $L=4$, 10, 16, 30, 40, and 56, for the 3D LG system. The decrease of ϵ^{-1} towards zero becomes sharper with increasing L, consistent with the prediction of a discontinuous jump. However, the downward drift in the temperature at which the inverse dielectric constant starts decreasing rapidly is more pronounced than in the 2D CG case. Error bars are given in the top and bottom curves, and omitted for clarity in the others.

system sizes than what we have been able to do in the 3D LG case, to bring out a potential positive curvature that was observed in the 2D CG case. From these results, it is unfortunately not possible to tell whether the depth of the dip remains finite and negative as $L\rightarrow\infty$ of if it vanishes. Hence, we are presently not able to firmly conclude that the inverse dielectric constant in the 3D LG experiences a discontinuity.

The temperature locating the minimum in ϵ_4 as a function of system size is shown in Fig. 10 for the 3D LG system. Extrapolation gives $T_c=0.30\pm0.04$.

C. 3D Coulomb gas

In this subsection, we contrast the results of the 2D Coulomb gas and the 3D LG to those of the 3D Coulomb gas. The 3D CG is known to be in a metallic high-temperature

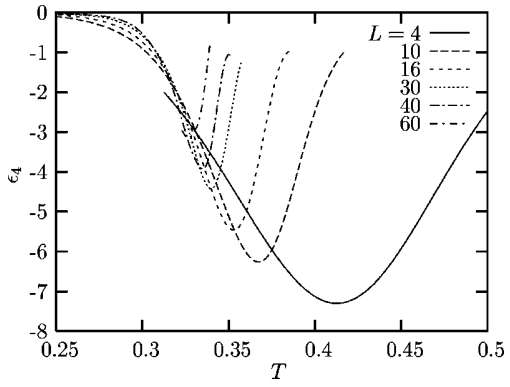

FIG. 8. The coefficient ϵ_4 of the fourth order term of the expansion of the free energy for the 3D LG model. The depths decrease with increasing L, and the important question is whether this dip vanishes at T_c or not. Errorbars are omitted but will be reintroduced in Fig. 9.

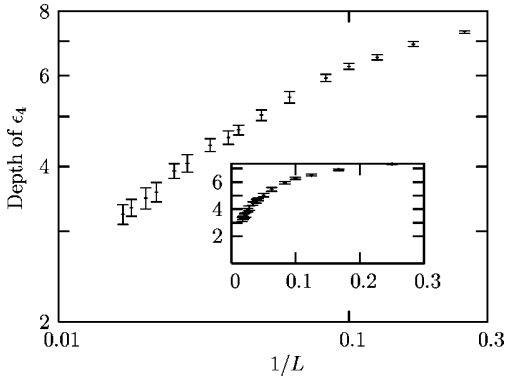

FIG. 9. Depth of the dip in the fourth order term shown in Fig. 8 for the 3D LG. The data are obtained from simulations of system sizes ranging from $L=4$ to $L=60$ and plotted both on a linear scale (inset) and on a log-log scale. The lack of clear positive curvature in the log-log plot that was observed in 2D CG case makes the extrapolation to the limit $L\rightarrow\infty$ more difficult for the system sizes we have been able to access in 3D.

phase for *all* finite temperatures and should exhibit quite different finite-size scaling of $\langle s^2\rangle$ compared to the 2D CG case.[11,14,25] The results are shown in Fig. 11. Note that the temperature dependence of the curves for all different system sizes are qualitatively different in the 3D CG compared to those in the 2D CG and the 3D LG. This becomes particularly apparent upon considering the L dependence of $\langle s^2\rangle$ for various temperatures, where the steepness of the curves increases with decreasing temperature, resulting in a scaling exponent $\alpha(T)$ (from $\langle s^2\rangle\sim L^{\alpha(T)}$) which decreases with increasing temperature. This is quite consistent with what is known for the 3D CG, namely, that it exhibits a metallic state for all finite temperatures, equivalently it corresponds to Polyakov's permanent confinement.[11,14] It is evident that the scaling results for $\langle s^2\rangle$ for the 2D CG and the 3D LG are qualitatively and quantitatively the same, and that they are qualitatively different from those exhibited by the 3D CG. For low temperatures, $\langle s^2\rangle$ seem to be increasing with temperature. This is only a vacuum effect, since vacuum con-

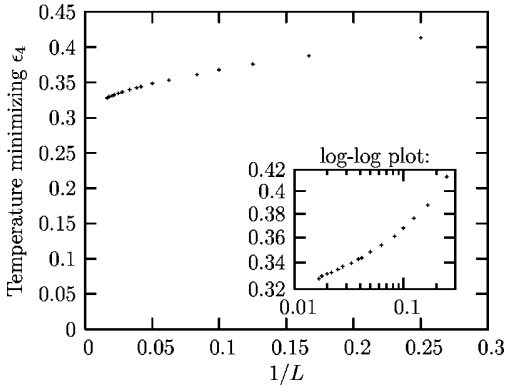

FIG. 10. Temperature minimizing ϵ_4 as a function of inverse system size for the 3D LG system. The values are plotted both on a linear scale and on a log-log scale (inset). This temperature reaches a nonzero value at $L\rightarrow\infty$. Extrapolation gives $T_c=0.30\pm0.04$.

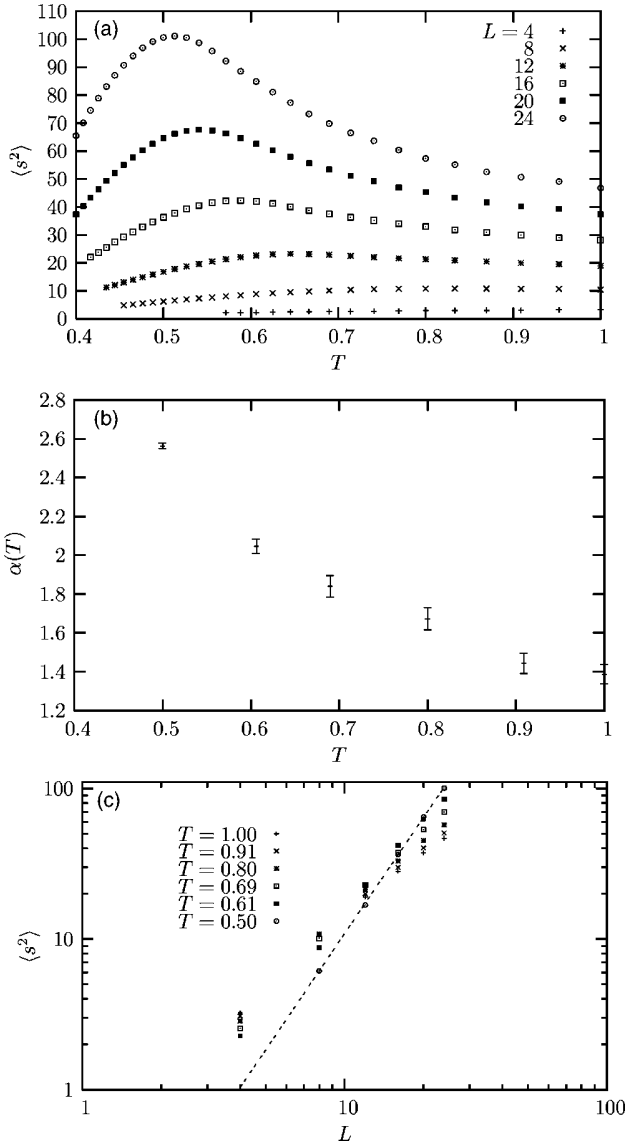

FIG. 11. Mean square dipole moment $\langle s^2\rangle$ as a function of temperature (top panel) and system size (bottom panel) for the 3D Coulomb gas system of point charges interacting with a $1/r$ bare pair potential. The middle panel shows the scaling exponent α extracted from $\langle s^2\rangle \sim L^{\alpha(T)}$.

figurations do not contribute to the measurement of $\langle s^2\rangle$.[18] This means that close to vacuum, only configurations resulting from the insertion of one single dipole at the smallest possible distance will contribute. See also Sec. IV D.

The inverse dielectric constant for the 3D CG is shown as a function of temperature in Fig. 12 with system sizes ranging up to $L=50$. Here also, ϵ^{-1} decreases from unity to zero, but the downward drift in the temperature at which ϵ^{-1} deviates from unity seems to be even stronger than for the 3D LG model. Additionally, the decrease towards zero does not sharpen significantly with increasing L.

We find a similar minimum in the fourth order term in the expansion of the free energy for the 3D CG, ϵ_4/L^2, shown in Fig. 13. However, the dip vanishes as $L\to\infty$ in the current

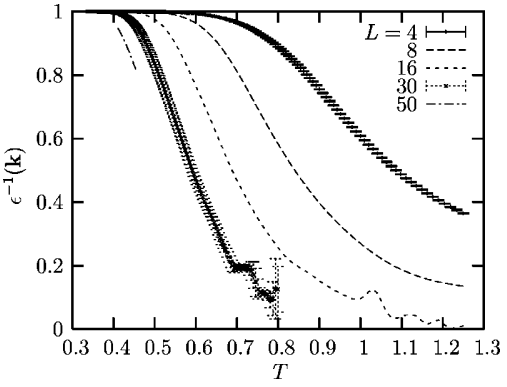

FIG. 12. Inverse dielectric constant taken at the smallest possible wave vector in a finite system, $\mathbf{k}=(0,2\pi/L,0)$, and plotted against temperature T for system sizes $L=4$, 8, 16, 30, and 50, for the 3D CG system. The decrease of ϵ^{-1} towards zero does not sharpen with increasing L, and there is a clear downward drift in the temperature at which ϵ^{-1} deviates from unity. Error bars are given in two of the curves, and omitted for clarity in the others.

model. This is clearly shown in Fig. 14 in contrast to the Figs. 4 and 9 of the other two models.

For completeness we have included in Fig. 15 a plot of the temperature locating the minimum in ϵ_4 as a function of system size also for the 3D CG. There is no phase transition to which this temperature is associated, and the stronger downward drift mentioned above is evident when contrasting this plot to Fig. 10 of the 3D LG. The temperature is reduced by a factor 2 in the largest system considered in the 3D CG compared to the smallest whereas the variation is much smaller in the 3D LG. However, there *is* a weak curvature in the log-log version of Fig. 15. Performing a similar extrapolation as we did for the other two models we end up with a "critical" temperature $T_c=0.24\pm0.04$.

D. Charge density

Finally we present in Fig. 16 the charge density for the three models considered. In all three cases the charge densi-

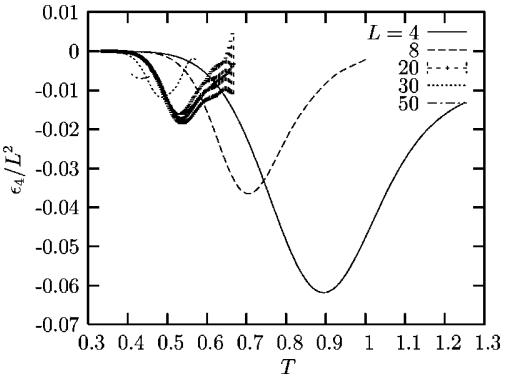

FIG. 13. The coefficient ϵ_4 of the fourth order term of the expansion of the free energy, for the 3D CG. The depths decrease with increasing L and seem to vanish as $L\to\infty$. Errorbars are shown for one of the systems for demonstration.

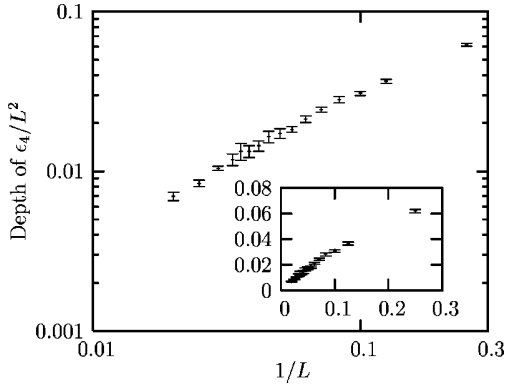

FIG. 14. Depth of the dip in the fourth order term shown in Fig. 13 for the 3D CG. The data are obtained from simulations of system sizes ranging from $L=4$ to $L=50$ and plotted both on a linear scale (inset) and on a log-log scale. It is clear that the dip vanishes in the thermodynamic limit.

ties are independent of L and from these curves we can approximate the average separation r_{mean} between the charges assuming uniform distribution

$$r_{\mathrm{mean}} = \left(\frac{1}{Q_{\mathrm{Sum}}/V} \right)^{1/d}, \tag{12}$$

where d is the dimension. We concentrate on the (L-dependent) temperatures which minimize ϵ_4. In the two logarithmically interacting models, r_{mean} ranges from ~ 4 for the smallest systems and up to ~ 8 for the largest. In the 3D Coulomb gas on the other hand, r_{mean} remains close to L even for the largest system sizes meaning that the systems are close to their vacuum states at these temperatures. This strongly suggests that the features we investigate are only extreme low-density effects in the 3D CG model. Screening, which should take place at all temperatures in a system always being in a metallic state, is not possible in this limit.

In the 2D CG and 3D LG models the situation is different. The interesting temperature domains are smaller and the charge densities are kept close to constant which in turn allows screening for the largest systems.

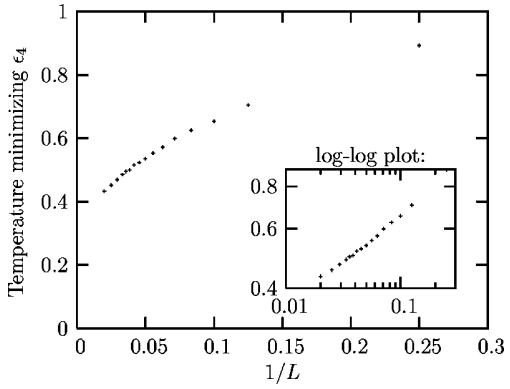

FIG. 15. Temperature minimizing ϵ_4 as a function of inverse system size for the 3D CG system. The values are plotted both on a linear scale and on a log-log scale (inset).

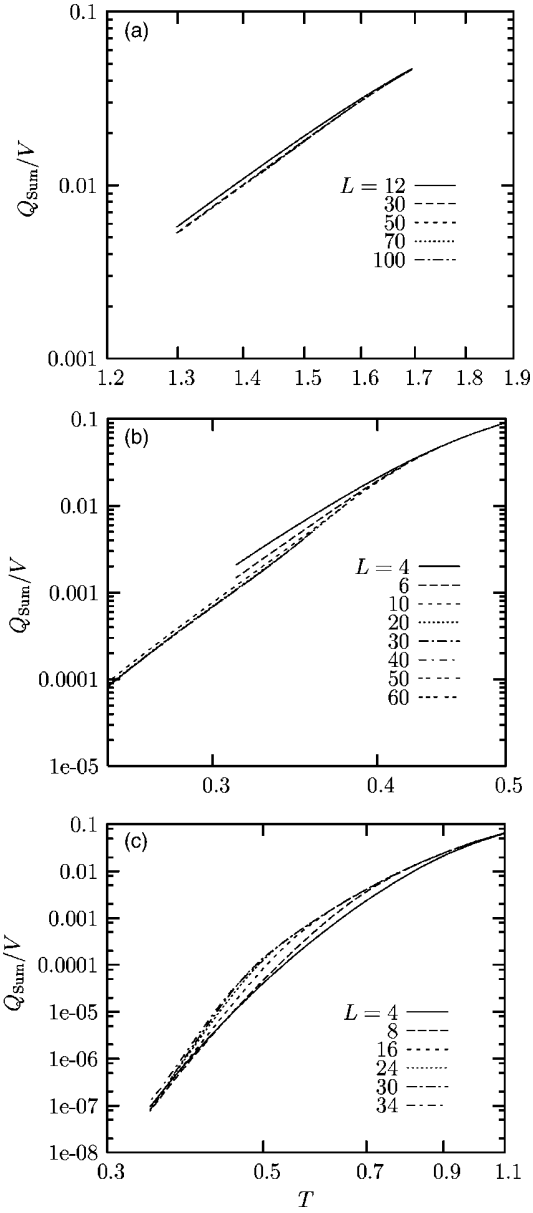

FIG. 16. Charge density Q_{sum}/V plotted vs temperature on log-log scales for the (a) 2D CG, (b) 3D LG, and (c) 3D CG models. The volume V corresponds to the total number of sites L^d. Note that Q_{sum}/V is independent of system size L in all three cases.

V. COMMENTS ON UNIVERSALITY

In the 2D CG, the universal jump to zero of the inverse dielectric constant ϵ^{-1} is given by[19,26]

$$\epsilon^{-1} = \frac{2T_c}{\pi}. \tag{13}$$

Using the estimate for the critical temperature found in section IV A, the value at T_c should, according to Eq. (13), be $\epsilon^{-1}=0.86\pm0.03$. This is in agreement with Fig. 2, since it is in this region the curves seem to split.

In Ref. 20, it was speculated that the finite negative value of the fourth order modulus $\langle \mathrm{Y}_4 \rangle \approx -0.130$ could be associ-

ated with a universal number. In the 2D CG, $V_k \sim L^2$ and $Q_k^y \sim 2\pi/L$ for large L, such that the modification $\Delta \rightarrow \Delta/(\sqrt{2}\pi)$ turns Eq. (8) into

$$F(\mathbf{T}) - F(0) = \frac{\Delta^2}{2}\epsilon^{-1} + \frac{\Delta^4}{4!}3\epsilon_4. \tag{14}$$

This means that if ϵ^{-1} corresponds to the helicity modulus $\langle \Upsilon \rangle$, it is $3\epsilon_4$ that corresponds to the fourth order modulus $\langle \Upsilon_4 \rangle$. It is interesting to notice that $3\epsilon_4 = -0.141 \pm 0.015$ fits nicely with the value found in Ref. 20, speculated to be a universal number. One may therefore speculate that the value of ϵ_4 at T_c is a universal number independent of T_c. Whether this is a sign of a true universality or a mere coincidence requires further investigation.

One should also note that with this modification of Δ, the additional twist term in the *XY* Hamiltonian (1) becomes $\sqrt{2}\Delta \sin(2\pi y/L)/L$. It seems natural to suggest that the net effect of a sine twist is given by its r.m.s. value, i.e., $[1/L\int_0^L \sin^2(2\pi y/L)dy]^{1/2} = 1/\sqrt{2}$. This gives a net twist of Δ across the system, which is the same as in Ref. 20.

The universal jump of ϵ^{-1} in the 3D LG is given by the flow equations derived in Ref. 14. In our units, this jump is predicted to be

$$\epsilon^{-1} = \frac{5T_c}{2}, \tag{15}$$

and by using the critical temperature found in section IV B, this amounts to an ϵ^{-1} in the interval (0.65,0.85). Since the different curves in Fig. 7 do not merge in the low-temperature regime, as they do in the 2D CG case, it is difficult to make a precise determination of the jump in the 3D LG based on these simulations. However, one cannot rule out that the jump lies inside the interval mentioned.

VI. CONCLUDING REMARKS

In this paper we have considered various quantities related to a possible phase transition in systems of point charges interacting with bare logarithmic pair potentials, in 2D and 3D. We have also carried out comparisons with the results obtained in the 3D Coulomb gas in some cases. The quantities we have focused on are the fluctuations of the dipole moment $\langle s^2 \rangle$ and the fourth order coefficient of the free energy expanded in an appropriate twist. We have shown that the dipole moment fluctuations, associated with the polarizability of the charge systems, has a scaling exponent $\alpha(T)$ defined by $\langle s^2 \rangle \sim L^{\alpha(T)}$ which is positive above some temperature and zero below this temperature for the 2D CG and the 3D LG cases, and is an increasing function of temperature. On the other hand, for the 3D CG case $\alpha(T)$ is finite positive for all temperatures we have considered, and is a *decreasing* function of temperature. This in itself strongly suggests that the 3D LG has statistical physics much more akin to the 2D CG than to the 3D CG. For the 2D CG we have demonstrated that the inverse dielectric constant experiences a discontinuous jump to zero at the phase transition. This has been done by investigation of a series expansion of free energy using Monte Carlo simulations. The possibility of a universal value of the fourth order term proposed in Ref. 20 has also been commented on, and a possible agreement with this value has been observed. The method developed in this paper will apply to any gas of vortex loops or point charges with any interaction potential. We have applied it to the 3D LG. Although it would have been desirable to be able to access larger system sizes than what we have been able to in the present paper, the results we obtain for the 3D LG suggest that this model may also undergo a metal-insulator transition with a discontinuity in the inverse dielectric function at the critical point, in agreement with the renormalization group results of Ref. 14.

ACKNOWLEDGMENTS

This work was supported by the Research Council of Norway, Grant Nos. 158518/431, 158547/431 (NANOMAT), and by the Norwegian High Performance Computing Consortium (NOTUR). One of us (S. K.) acknowledges support from the Norwegian University of Science and Technology. We acknowledge useful discussions with F. S. Nogueira and Z. Tesanovic.

APPENDIX A: DUALITY TRANSFORMATION

The partition function for the *XY* model with coupling constant $J=1$ is

$$Z = \Pi_i \int \frac{d\theta_i}{2\pi} e^{\beta \Sigma_{\mathbf{r}} \cos(\nabla\theta - 2\pi\mathbf{T})}, \tag{A1}$$

where the sum is over all links between lattice points $\nabla\theta \equiv \theta_i - \theta_j$ and $\mathbf{T}(\mathbf{r})$ is the twist between the two lattice points sharing the link $\mathbf{r}$. We will consider three spatial dimensions and comment on any differences in 2D. Applying the Villain approximation, we get

$$Z = \int \mathcal{D}\theta \sum_{\{\mathbf{n}\}} e^{-(\beta/2)\Sigma_{\mathbf{r}}(\nabla\theta - 2\pi\mathbf{T} - 2\pi\mathbf{n})^2}. \tag{A2}$$

$\mathbf{n}(\mathbf{r})$ is an integer-valued field taking care of the periodicity of the cosine. By a Hubbard-Stratonovich decoupling, one finds

$$Z = \int \mathcal{D}\theta \mathcal{D}\mathbf{v} \sum_{\{\mathbf{n}\}} e^{-\Sigma_{\mathbf{r}}\left[(1/2\beta)\mathbf{v}^2 + i\mathbf{v}\cdot(\nabla\theta - 2\pi\mathbf{T} - 2\pi\mathbf{n})\right]}. \tag{A3}$$

The summation over $\mathbf{n}$ may now be evaluated using the Poisson summation formula

$$\sum_{n=-\infty}^{\infty} e^{2\pi i n v} = \sum_{l=-\infty}^{\infty} \delta(v - l) \tag{A4}$$

at each dual lattice point, yielding

$$Z = \int \mathcal{D}\theta \sum_{\{\mathbf{l}\}} e^{\Sigma_{\mathbf{r}} 2\pi i \mathbf{l}\cdot\mathbf{T} - i\mathbf{l}\cdot\nabla\theta - (1/2\beta)\mathbf{l}^2}. \tag{A5}$$

The field $\mathbf{l}(\mathbf{r})$ is integer valued. Now, performing a partial summation on the second term in the exponent, the θ integration may be carried out. This produces the constraint that $\mathbf{l}$ must be divergence free, solved by the introduction of another integer-valued field such that $\mathbf{l}=\nabla\times\mathbf{h}$. Note that $\mathbf{h}(\mathbf{r})$ is a scalar in 2D. The partition function is now

$$Z=\sum_{\{\mathbf{h}\}} e^{\Sigma_{\mathbf{r}} 2\pi i(\nabla\times\mathbf{h})\cdot\mathbf{T}-(1/2\beta)(\nabla\times\mathbf{h})^2}, \tag{A6}$$

and we observe that $\mathbf{h}\to\mathbf{h}+\nabla\phi$ is a gauge transformation. In two dimensions, the corresponding gauge transformation is $h\to h+c$, where c is a constant. Using Poisson's summation formula once more, we get

$$Z=\int \mathcal{D}\mathbf{h}\sum_{\{\mathbf{m}\}} e^{\Sigma_{\mathbf{r}} 2\pi i(\nabla\times\mathbf{h})\cdot\mathbf{T}-(1/2\beta)(\nabla\times\mathbf{h})^2+2\pi i\mathbf{h}\cdot\mathbf{m}}, \tag{A7}$$

leaving $\mathbf{h}$ no longer integer valued. The field $\mathbf{m}(\mathbf{r})$ is what corresponds to vortex excitations in the XY model. The gauge invariance of the theory produces the constraint $\Sigma_{\mathbf{r}}\phi(\nabla\cdot\mathbf{m})=0$ for all configurations of $\mathbf{m}$. Choosing for instance $\phi=\nabla\cdot\mathbf{m}$, it is clear that $\mathbf{m}$ must be divergence free, i.e., the field lines are closed loops. In 2D, the corresponding constraint is $\Sigma_{\mathbf{r}} m=0$, indicating an overall charge neutrality in the 2D Coulomb gas or zero total vorticity in the 2D XY model.

By another partial summation, we are now left with a Maxwell term and a coupling term between the gauge field $\mathbf{h}$ and the current $\mathbf{M}(\mathbf{r})\equiv\mathbf{m}+\nabla\times\mathbf{T}$:

$$Z=\int \mathcal{D}\mathbf{h}\sum_{\{\mathbf{m}\}} e^{\Sigma_{\mathbf{r}} 2\pi i\mathbf{h}\cdot\mathbf{M}-(1/2\beta)(\nabla\times\mathbf{h})^2}. \tag{A8}$$

One may now perform a partial integration in the second term and use the gauge where $\nabla\cdot\mathbf{h}=0$, such that $\nabla\times\nabla\times\mathbf{h}=-\nabla^2\mathbf{h}$. Then, by going to Fourier space and completing squares, the $\mathbf{h}$ integration becomes Gaussian. This leaves us with

$$Z=Z_0\sum_{\{\mathbf{m}\}} e^{(2\beta\pi^2/N)\Sigma_{\mathbf{q}}\mathbf{M}_{\mathbf{q}}G_{\mathbf{q}}^{-1}\mathbf{M}_{-\mathbf{q}}}, \tag{A9}$$

where $\nabla^2 e^{\pm i\mathbf{q}\cdot\mathbf{r}}\equiv e^{\pm i\mathbf{q}\cdot\mathbf{r}}G_{\mathbf{q}}$ and Z_0 is a constant. Defining the discrete Laplacian by

$$\Delta^2 f(\mathbf{r})=\sum_{\mu}[f(\mathbf{r}+\hat{e}_\mu)+f(\mathbf{r}-\hat{e}_\mu)-2f(\mathbf{r})], \tag{A10}$$

it is clear that $G_{\mathbf{q}}=-2(d-\Sigma_{\mu=1}^{d}\cos q_\mu)$, denoting the number of space dimensions by d. Returning to real-space representation, we arrive at

$$Z=Z_0\sum_{\{\mathbf{m}\}} e^{-(\beta/2)\Sigma_{\mathbf{r}_i,\mathbf{r}_j}\mathbf{M}(\mathbf{r}_i)V(|\mathbf{r}_i-\mathbf{r}_j|)\mathbf{M}(\mathbf{r}_j)}, \tag{A11}$$

the interaction being given by

$$V(\mathbf{r})=\frac{2\pi^2}{L^2}\sum_{\mathbf{q}}\frac{e^{i\mathbf{q}\cdot\mathbf{r}}}{d-\sum_{\mu=1}^{d}\cos q_\mu}. \tag{A12}$$

APPENDIX B: EXPANSION OF FREE ENERGY

Consider the Hamiltonian

$$H_0=\frac{1}{2}\sum_{i,j}\mathbf{m}_i V_{ij}\mathbf{m}_j, \tag{B1}$$

describing a 3D system of integer-valued currents $\mathbf{m}$ on a lattice interacting via the potential $V_{ij}=V(|\mathbf{r}_i-\mathbf{r}_j|)$. We impose periodic boundary conditions on the system. Perturbing the field $\mathbf{m}$ with a transversal twist turns Eq. (B1) into

$$H=\frac{1}{2}\sum_{i,j}(\mathbf{m}+\nabla\times\mathbf{T})_i V_{ij}(\mathbf{m}+\nabla\times\mathbf{T})_j. \tag{B2}$$

We let the linear system size be L and define the discrete Fourier transform by

$$f_{\mathbf{q}}=\sum_{\mathbf{r}} f(\mathbf{r})e^{i\mathbf{q}\cdot\mathbf{r}}, \tag{B3}$$

where $\mathbf{r}=(n_x,n_y,n_z)$ and $n_i=0,\ldots,L-1$. The inverse transform is

$$f(\mathbf{r})=\frac{1}{N}\sum_{\mathbf{q}} f_{\mathbf{q}}e^{-i\mathbf{q}\cdot\mathbf{r}}, \tag{B4}$$

where $\mathbf{q}=2\pi/L(k_x,k_y,k_z)$ and $k_i=-L/2+1,\ldots,L/2$. N is the number of lattice sites. Let us also define $Q_{\pm\mathbf{q}}^{\nu}$ by $\Delta^\nu e^{\pm i\mathbf{q}\cdot\mathbf{r}}=e^{\pm i\mathbf{q}\cdot\mathbf{r}}Q_{\pm\mathbf{q}}^{\nu}$, where Δ^ν is a lattice derivative. In Fourier representation the Hamiltonian becomes

$$H=\frac{1}{2N}\sum_{\mathbf{q}}(m_{\mathbf{q}}^{\mu}+\varepsilon^{\mu\nu\lambda}Q_{-\mathbf{q}}^{\nu}T_{\mathbf{q}}^{\lambda})V_{\mathbf{q}}(m_{-\mathbf{q}}^{\mu}+\varepsilon^{\mu\rho\sigma}Q_{\mathbf{q}}^{\rho}T_{-\mathbf{q}}^{\sigma}). \tag{B5}$$

For later use, we calculate the derivative of H, which is

$$\frac{\partial H}{\partial T_{\mathbf{q}_1}^{\alpha}}=\frac{1}{N}\varepsilon^{\mu\nu\alpha}Q_{-\mathbf{q}_1}^{\nu}(m_{-\mathbf{q}_1}^{\mu}+\varepsilon^{\mu\rho\sigma}Q_{\mathbf{q}_1}^{\rho}T_{-\mathbf{q}_1}^{\sigma})V_{\mathbf{q}_1}. \tag{B6}$$

We also note that

$$\frac{\partial^2 H}{\partial T_{\mathbf{q}_1}^{\alpha}\partial T_{\mathbf{q}_2}^{\beta}}=\frac{1}{N}\varepsilon^{\mu\nu\alpha}\varepsilon^{\mu\rho\beta}Q_{-\mathbf{q}_1}^{\nu}Q_{\mathbf{q}_1}^{\rho}V_{\mathbf{q}_1}\delta_{\mathbf{q}_1+\mathbf{q}_2,0} \tag{B7}$$

is independent of $\mathbf{m}$ and that all higher order derivatives are zero.

The free energy is given by $F=-T\ln Z$, where the partition function is

$$Z=\sum_{\{\mathbf{m}\}} e^{-H/T}, \tag{B8}$$

summing over all possible configurations of $\mathbf{m}$. By Taylor expansion of the free energy in the twist, we get

$$F(\mathbf{T})-F(0)=\sum_{\alpha}\sum_{\mathbf{r}_1}\left.\frac{\partial F}{\partial T^{\alpha}(\mathbf{r}_1)}\right|_{\mathbf{T}=0}T^{\alpha}(\mathbf{r}_1)+\sum_{\alpha,\beta}\sum_{\mathbf{r}_1,\mathbf{r}_2}\left.\frac{\partial^2 F}{\partial T^{\alpha}(\mathbf{r}_1)\partial T^{\beta}(\mathbf{r}_2)}\right|_{\mathbf{T}=0}T^{\alpha}(\mathbf{r}_1)T^{\beta}(\mathbf{r}_2)+\cdots. \tag{B9}$$

Note that $F(\mathbf{T}=0)$ refers to the free energy of the unperturbed system described by H_0. By writing each term in the series in Fourier representation, one finds the equivalent expansion in Fourier components of the twist, i.e.,

$$F(\mathbf{T}) - F(0) = \sum_{\alpha} \sum_{\mathbf{q}_1} \left. \frac{\partial F}{\partial T^{\alpha}_{\mathbf{q}_1}} \right|_{\mathbf{T}=0} T^{\alpha}_{\mathbf{q}_1} + \sum_{\alpha,\beta} \sum_{\mathbf{q}_1 \mathbf{q}_2} \left. \frac{\partial^2 F}{\partial T^{\alpha}_{\mathbf{q}_1} \partial T^{\beta}_{\mathbf{q}_2}} \right|_{\mathbf{T}=0} \frac{T^{\alpha}_{\mathbf{q}_1} T^{\beta}_{\mathbf{q}_2}}{2} + \cdots . \tag{B10}$$

The first derivative becomes

$$\frac{\partial F}{\partial T^{\alpha}_{\mathbf{q}_1}} = \frac{1}{Z} \sum_{\{\mathbf{m}\}} \frac{\partial H}{\partial T^{\alpha}_{\mathbf{q}_1}} e^{-H/T} \equiv \left\langle \frac{\partial H}{\partial T^{\alpha}_{\mathbf{q}_1}} \right\rangle . \tag{B11}$$

Proceeding, we find

$$\frac{\partial^2 F}{\partial T^{\alpha}_{\mathbf{q}_1} \partial T^{\beta}_{\mathbf{q}_2}} = \frac{1}{T} \left\langle \frac{\partial H}{\partial T^{\alpha}_{\mathbf{q}_1}} \right\rangle \left\langle \frac{\partial H}{\partial T^{\beta}_{\mathbf{q}_2}} \right\rangle + \frac{\partial^2 H}{\partial T^{\alpha}_{\mathbf{q}_1} \partial T^{\beta}_{\mathbf{q}_2}} - \frac{1}{T} \left\langle \frac{\partial H}{\partial T^{\alpha}_{\mathbf{q}_1}} \frac{\partial H}{\partial T^{\beta}_{\mathbf{q}_2}} \right\rangle \tag{B12}$$

for the second derivative and

$$\frac{\partial^3 F}{\partial T^{\alpha}_{\mathbf{q}_1} \partial T^{\beta}_{\mathbf{q}_2} \partial T^{\gamma}_{\mathbf{q}_3}} = \frac{1}{T^2} \left[2 \left\langle \frac{\partial H}{\partial T^{\alpha}_{\mathbf{q}_1}} \right\rangle \left\langle \frac{\partial H}{\partial T^{\beta}_{\mathbf{q}_2}} \right\rangle \left\langle \frac{\partial H}{\partial T^{\gamma}_{\mathbf{q}_3}} \right\rangle + \left\langle \frac{\partial H}{\partial T^{\alpha}_{\mathbf{q}_1}} \frac{\partial H}{\partial T^{\beta}_{\mathbf{q}_2}} \frac{\partial H}{\partial T^{\gamma}_{\mathbf{q}_3}} \right\rangle - \left\langle \frac{\partial H}{\partial T^{\alpha}_{\mathbf{q}_1}} \right\rangle \times \left\langle \frac{\partial H}{\partial T^{\beta}_{\mathbf{q}_2}} \frac{\partial H}{\partial T^{\gamma}_{\mathbf{q}_3}} \right\rangle - \left\langle \frac{\partial H}{\partial T^{\beta}_{\mathbf{q}_2}} \right\rangle \left\langle \frac{\partial H}{\partial T^{\alpha}_{\mathbf{q}_1}} \frac{\partial H}{\partial T^{\gamma}_{\mathbf{q}_3}} \right\rangle - \left\langle \frac{\partial H}{\partial T^{\gamma}_{\mathbf{q}_3}} \right\rangle \left\langle \frac{\partial H}{\partial T^{\alpha}_{\mathbf{q}_1}} \frac{\partial H}{\partial T^{\beta}_{\mathbf{q}_2}} \right\rangle \right] \tag{B13}$$

for the third. We have exploited the fact that third derivatives of H vanishes. The fourth derivative is found to be

$$\begin{aligned} \frac{\partial^4 F}{\partial T^{\alpha}_{\mathbf{q}_1} \partial T^{\beta}_{\mathbf{q}_2} \partial T^{\gamma}_{\mathbf{q}_3} \partial T^{\delta}_{\mathbf{q}_4}} = \frac{1}{T^3} \Bigg\{ & 6 \left\langle \frac{\partial H}{\partial T^{\alpha}_{\mathbf{q}_1}} \right\rangle \left\langle \frac{\partial H}{\partial T^{\beta}_{\mathbf{q}_2}} \right\rangle \left\langle \frac{\partial H}{\partial T^{\gamma}_{\mathbf{q}_3}} \right\rangle \left\langle \frac{\partial H}{\partial T^{\delta}_{\mathbf{q}_4}} \right\rangle - 2 \Bigg[\left\langle \frac{\partial H}{\partial T^{\alpha}_{\mathbf{q}_1}} \right\rangle \left\langle \frac{\partial H}{\partial T^{\beta}_{\mathbf{q}_2}} \right\rangle \left\langle \frac{\partial H}{\partial T^{\gamma}_{\mathbf{q}_3}} \frac{\partial H}{\partial T^{\delta}_{\mathbf{q}_4}} \right\rangle \\ & + \left\langle \frac{\partial H}{\partial T^{\alpha}_{\mathbf{q}_1}} \right\rangle \left\langle \frac{\partial H}{\partial T^{\gamma}_{\mathbf{q}_3}} \right\rangle \left\langle \frac{\partial H}{\partial T^{\beta}_{\mathbf{q}_2}} \frac{\partial H}{\partial T^{\delta}_{\mathbf{q}_4}} \right\rangle + \left\langle \frac{\partial H}{\partial T^{\alpha}_{\mathbf{q}_1}} \right\rangle \left\langle \frac{\partial H}{\partial T^{\delta}_{\mathbf{q}_4}} \right\rangle \left\langle \frac{\partial H}{\partial T^{\beta}_{\mathbf{q}_2}} \frac{\partial H}{\partial T^{\gamma}_{\mathbf{q}_3}} \right\rangle + \left\langle \frac{\partial H}{\partial T^{\beta}_{\mathbf{q}_2}} \right\rangle \left\langle \frac{\partial H}{\partial T^{\gamma}_{\mathbf{q}_3}} \right\rangle \left\langle \frac{\partial H}{\partial T^{\alpha}_{\mathbf{q}_1}} \frac{\partial H}{\partial T^{\delta}_{\mathbf{q}_4}} \right\rangle \\ & + \left\langle \frac{\partial H}{\partial T^{\beta}_{\mathbf{q}_2}} \right\rangle \left\langle \frac{\partial H}{\partial T^{\delta}_{\mathbf{q}_4}} \right\rangle \left\langle \frac{\partial H}{\partial T^{\alpha}_{\mathbf{q}_1}} \frac{\partial H}{\partial T^{\gamma}_{\mathbf{q}_3}} \right\rangle + \left\langle \frac{\partial H}{\partial T^{\gamma}_{\mathbf{q}_3}} \right\rangle \left\langle \frac{\partial H}{\partial T^{\delta}_{\mathbf{q}_4}} \right\rangle \left\langle \frac{\partial H}{\partial T^{\alpha}_{\mathbf{q}_1}} \frac{\partial H}{\partial T^{\beta}_{\mathbf{q}_2}} \right\rangle \Bigg] + \left\langle \frac{\partial H}{\partial T^{\alpha}_{\mathbf{q}_1}} \right\rangle \left\langle \frac{\partial H}{\partial T^{\beta}_{\mathbf{q}_2}} \frac{\partial H}{\partial T^{\gamma}_{\mathbf{q}_3}} \frac{\partial H}{\partial T^{\delta}_{\mathbf{q}_4}} \right\rangle \\ & + \left\langle \frac{\partial H}{\partial T^{\beta}_{\mathbf{q}_2}} \right\rangle \left\langle \frac{\partial H}{\partial T^{\alpha}_{\mathbf{q}_1}} \frac{\partial H}{\partial T^{\gamma}_{\mathbf{q}_3}} \frac{\partial H}{\partial T^{\delta}_{\mathbf{q}_4}} \right\rangle + \left\langle \frac{\partial H}{\partial T^{\gamma}_{\mathbf{q}_3}} \right\rangle \left\langle \frac{\partial H}{\partial T^{\alpha}_{\mathbf{q}_1}} \frac{\partial H}{\partial T^{\beta}_{\mathbf{q}_2}} \frac{\partial H}{\partial T^{\delta}_{\mathbf{q}_4}} \right\rangle + \left\langle \frac{\partial H}{\partial T^{\delta}_{\mathbf{q}_4}} \right\rangle \left\langle \frac{\partial H}{\partial T^{\alpha}_{\mathbf{q}_1}} \frac{\partial H}{\partial T^{\beta}_{\mathbf{q}_2}} \frac{\partial H}{\partial T^{\gamma}_{\mathbf{q}_3}} \right\rangle \\ & + \left\langle \frac{\partial H}{\partial T^{\alpha}_{\mathbf{q}_1}} \frac{\partial H}{\partial T^{\beta}_{\mathbf{q}_2}} \right\rangle \left\langle \frac{\partial H}{\partial T^{\gamma}_{\mathbf{q}_3}} \frac{\partial H}{\partial T^{\delta}_{\mathbf{q}_4}} \right\rangle + \left\langle \frac{\partial H}{\partial T^{\alpha}_{\mathbf{q}_1}} \frac{\partial H}{\partial T^{\gamma}_{\mathbf{q}_3}} \right\rangle \left\langle \frac{\partial H}{\partial T^{\beta}_{\mathbf{q}_2}} \frac{\partial H}{\partial T^{\delta}_{\mathbf{q}_4}} \right\rangle + \left\langle \frac{\partial H}{\partial T^{\alpha}_{\mathbf{q}_1}} \frac{\partial H}{\partial T^{\delta}_{\mathbf{q}_4}} \right\rangle \left\langle \frac{\partial H}{\partial T^{\beta}_{\mathbf{q}_2}} \frac{\partial H}{\partial T^{\gamma}_{\mathbf{q}_3}} \right\rangle \\ & - \left\langle \frac{\partial H}{\partial T^{\alpha}_{\mathbf{q}_1}} \frac{\partial H}{\partial T^{\beta}_{\mathbf{q}_2}} \frac{\partial H}{\partial T^{\gamma}_{\mathbf{q}_3}} \frac{\partial H}{\partial T^{\delta}_{\mathbf{q}_4}} \right\rangle \Bigg\} . \end{aligned} \tag{B14}$$

Remembering that

$$\left. \frac{\partial H}{\partial T^{\alpha}_{\mathbf{q}_1}} \right|_{\mathbf{T}=0} = \frac{1}{N} \varepsilon^{\mu\nu\alpha} Q^{\nu}_{-\mathbf{q}_1} m^{\mu}_{-\mathbf{q}_1} V_{\mathbf{q}_1}, \tag{B15}$$

it is straightforward to write the derivatives at zero twist as **m** correlators. However, in many cases these expressions may be simplified further. If the sum over all possible configurations $\{\mathbf{m}\}$ is symmetric around zero, one finds that all odd-order correlators are zero, resulting in

$$\left. \frac{\partial F}{\partial T^{\alpha}_{\mathbf{q}_1}} \right|_{\mathbf{T}=0} = \left. \frac{\partial^3 F}{\partial T^{\alpha}_{\mathbf{q}_1} \partial T^{\beta}_{\mathbf{q}_2} \partial T^{\gamma}_{\mathbf{q}_3}} \right|_{\mathbf{T}=0} = 0 . \tag{B16}$$

Furthermore, since $V_{ij} = V(|\mathbf{r}_i - \mathbf{r}_j|)$, i.e., we have a translationally invariant system, the even-order correlators are subject to relations such as

$$\langle m^{\mu}_{-\mathbf{q}_1} m^{\nu}_{-\mathbf{q}_2} \rangle = \langle m^{\mu}_{-\mathbf{q}_1} m^{\nu}_{-\mathbf{q}_2} \rangle \delta_{\mathbf{q}_1 + \mathbf{q}_2, 0} \tag{B17}$$

and

$$\langle m^{\mu}_{-\mathbf{q}_1} m^{\nu}_{-\mathbf{q}_2} m^{\kappa}_{-\mathbf{q}_3} m^{\lambda}_{-\mathbf{q}_4}\rangle = \langle m^{\mu}_{-\mathbf{q}_1} m^{\nu}_{-\mathbf{q}_2} m^{\kappa}_{-\mathbf{q}_3} m^{\lambda}_{-\mathbf{q}_4}\rangle \delta_{\mathbf{q}_1+\mathbf{q}_2+\mathbf{q}_3+\mathbf{q}_4,0}. \tag{B18}$$

Thus, we find

$$\left.\frac{\partial^2 F}{\partial T^{\alpha}_{\mathbf{q}_1} \partial T^{\beta}_{\mathbf{q}_2}}\right|_{\mathbf{T}=0} = \frac{\varepsilon^{\mu\sigma\alpha}\varepsilon^{\nu\rho\beta} Q^{\sigma}_{-\mathbf{q}_1} Q^{\rho}_{-\mathbf{q}_2} V_{\mathbf{q}_1} \delta_{\mathbf{q}_1+\mathbf{q}_2,0}}{N} \times\left(\delta^{\mu\nu} - \frac{V_{\mathbf{q}_2}}{NT}\langle m^{\mu}_{-\mathbf{q}_1} m^{\nu}_{-\mathbf{q}_2}\rangle\right) \tag{B19}$$

for the second derivative and

$$\begin{aligned}\left.\frac{\partial^4 F}{\partial T^{\alpha}_{\mathbf{q}_1} \partial T^{\beta}_{\mathbf{q}_2} \partial T^{\gamma}_{\mathbf{q}_3} \partial T^{\delta}_{\mathbf{q}_4}}\right|_{\mathbf{T}=0} &= \frac{\varepsilon^{\mu\sigma\alpha}\varepsilon^{\nu\rho\beta}\varepsilon^{\kappa\tau\gamma}\varepsilon^{\lambda\eta\delta} Q^{\sigma}_{-\mathbf{q}_1} Q^{\rho}_{-\mathbf{q}_2} Q^{\tau}_{-\mathbf{q}_3} Q^{\eta}_{-\mathbf{q}_4} V_{\mathbf{q}_1} V_{\mathbf{q}_2} V_{\mathbf{q}_3} V_{\mathbf{q}_4}}{N^4 T^3} \\ &\times\{\langle m^{\mu}_{-\mathbf{q}_1} m^{\nu}_{-\mathbf{q}_2}\rangle\langle m^{\kappa}_{-\mathbf{q}_3} m^{\lambda}_{-\mathbf{q}_4}\rangle \delta_{\mathbf{q}_1+\mathbf{q}_2,0}\delta_{\mathbf{q}_3+\mathbf{q}_4,0} \\ &+ \langle m^{\mu}_{-\mathbf{q}_1} m^{\kappa}_{-\mathbf{q}_3}\rangle\langle m^{\nu}_{-\mathbf{q}_2} m^{\lambda}_{-\mathbf{q}_4}\rangle \delta_{\mathbf{q}_1+\mathbf{q}_3,0}\delta_{\mathbf{q}_2+\mathbf{q}_4,0} \\ &+ \langle m^{\mu}_{-\mathbf{q}_1} m^{\lambda}_{-\mathbf{q}_4}\rangle\langle m^{\nu}_{-\mathbf{q}_2} m^{\kappa}_{-\mathbf{q}_3}\rangle \delta_{\mathbf{q}_1+\mathbf{q}_4,0}\delta_{\mathbf{q}_2+\mathbf{q}_3,0} \\ &- \langle m^{\mu}_{-\mathbf{q}_1} m^{\nu}_{-\mathbf{q}_2} m^{\kappa}_{-\mathbf{q}_3} m^{\lambda}_{-\mathbf{q}_4}\rangle \delta_{\mathbf{q}_1+\mathbf{q}_2+\mathbf{q}_3+\mathbf{q}_4,0}\}\end{aligned} \tag{B20}$$

for the fourth. These expressions may also be applied to a gas of point charges in 2D or 3D, that is when m is a scalar field. One way to do this is by replacing $\nabla\times\mathbf{T}$ in Eq. (B2) with its z component $\varepsilon^{z\nu\lambda}\Delta^{\nu}T^{\lambda}$, with the consequence that the greek letter summations may be taken over x and y only. For the second derivative, this results in

$$\left.\frac{\partial^2 F}{\partial T^{\alpha}_{\mathbf{q}_1} \partial T^{\beta}_{\mathbf{q}_2}}\right|_{\mathbf{T}=0} = \frac{\varepsilon^{z\sigma\alpha}\varepsilon^{z\rho\beta} Q^{\sigma}_{-\mathbf{q}_1} Q^{\rho}_{\mathbf{q}_1} V_{\mathbf{q}_1} \delta_{\mathbf{q}_1+\mathbf{q}_2,0}}{N} \times\left(1 - \frac{V_{\mathbf{q}_1}}{NT}\langle m_{\mathbf{q}_1} m_{-\mathbf{q}_1}\rangle\right), \tag{B21}$$

where we have applied $V_{\mathbf{q}}=V_{-\mathbf{q}}$. We recognize the paranthesis as the Fourier transform of the inverse dielectric response function $\epsilon^{-1}(\mathbf{q}_1)$ in the low density limit. Note that the factor

$$\varepsilon^{z\sigma\alpha}\varepsilon^{z\rho\beta} Q^{\sigma}_{-\mathbf{q}_1} Q^{\rho}_{\mathbf{q}_1} = Q^{\sigma}_{\mathbf{q}_1} Q^{\sigma}_{-\mathbf{q}_1}\left(1 - \frac{Q^{\alpha}_{\mathbf{q}_1} Q^{\beta}_{-\mathbf{q}_1}}{Q^{\sigma}_{\mathbf{q}_1} Q^{\sigma}_{-\mathbf{q}_1}}\right) \tag{B22}$$

is a projection operator times $Q^{\sigma}_{\mathbf{q}_1} Q^{\sigma}_{-\mathbf{q}_1} \sim q^2_{1x} + q^2_{1y}$, reflecting the transversality of the twist.

To arrive at Eq. (8), we chose the twist (7) and computed the sums appearing in the expansion (B10) for both the second and fourth order term. The sum over direction is trivial, since our twist points in the x-direction. The sum over momenta is also managable, since $T^x_{\mathbf{q}}$ has nonzero values only for $\mathbf{q}=(0,\pm 2\pi/L)$. This sum gives two contributions in the second order term, due to the restriction $\delta_{\mathbf{q}_1+\mathbf{q}_2,0}$. The same argument results in four contributions for the three terms in Eq. (B20) being a product of two second order correlators. The term containing a fourth order correlator will give six contributions due to the restriction $\delta_{\mathbf{q}_1+\mathbf{q}_2+\mathbf{q}_3+\mathbf{q}_4,0}$.

APPENDIX C: HIGHER ORDER TERMS

Using the method described in this paper involves extrapolation to $L\to\infty$ and deciding whether or not the fourth order term in the expansion (B10) goes to zero or to a finite nonzero value. This procedure could in some cases be difficult. However, if the fourth order term had turned out to be zero in the thermodynamic limit, it would *not* necessarily mean that the second order term, the inverse dielectric response function, would have to go continuously to zero. In fact, if one were able to prove that the fourth order term is negative *or* zero, one could go on to investigate the sixth order term instead. If it then turned out that the value of the sixth order term was hard to establish, one could in principle repeat the procedure and go to higher order terms. We therefore include the sixth derivative here. To simplify calculations, we work with a twist in the x direction only:

$$\begin{aligned}\frac{\partial^6 F}{\partial T^x_{\mathbf{q}_1}\partial T^x_{\mathbf{q}_2}\partial T^x_{\mathbf{q}_3}\partial T^x_{\mathbf{q}_4}\partial T^x_{\mathbf{q}_5}\partial T^x_{\mathbf{q}_6}} &= \frac{1}{T^5}\Bigg\{120\left\langle\frac{\partial H}{\partial T^x_{\mathbf{q}_1}}\right\rangle\left\langle\frac{\partial H}{\partial T^x_{\mathbf{q}_2}}\right\rangle\left\langle\frac{\partial H}{\partial T^x_{\mathbf{q}_3}}\right\rangle\left\langle\frac{\partial H}{\partial T^x_{\mathbf{q}_4}}\right\rangle\left[\left\langle\frac{\partial H}{\partial T^x_{\mathbf{q}_5}}\right\rangle\left\langle\frac{\partial H}{\partial T^x_{\mathbf{q}_6}}\right\rangle - 3\left\langle\frac{\partial H}{\partial T^x_{\mathbf{q}_5}}\frac{\partial H}{\partial T^x_{\mathbf{q}_6}}\right\rangle\right] \\ &+ 18\left\langle\frac{\partial H}{\partial T^x_{\mathbf{q}_1}}\frac{\partial H}{\partial T^x_{\mathbf{q}_2}}\right\rangle\left[13\left\langle\frac{\partial H}{\partial T^x_{\mathbf{q}_3}}\right\rangle\left\langle\frac{\partial H}{\partial T^x_{\mathbf{q}_4}}\right\rangle\left\langle\frac{\partial H}{\partial T^x_{\mathbf{q}_5}}\frac{\partial H}{\partial T^x_{\mathbf{q}_6}}\right\rangle - \left\langle\frac{\partial H}{\partial T^x_{\mathbf{q}_3}}\frac{\partial H}{\partial T^x_{\mathbf{q}_4}}\right\rangle\left\langle\frac{\partial H}{\partial T^x_{\mathbf{q}_5}}\frac{\partial H}{\partial T^x_{\mathbf{q}_6}}\right\rangle\right] \\ &+ 2\left\langle\frac{\partial H}{\partial T^x_{\mathbf{q}_1}}\frac{\partial H}{\partial T^x_{\mathbf{q}_2}}\frac{\partial H}{\partial T^x_{\mathbf{q}_3}}\right\rangle\left[5\left\langle\frac{\partial H}{\partial T^x_{\mathbf{q}_4}}\frac{\partial H}{\partial T^x_{\mathbf{q}_5}}\frac{\partial H}{\partial T^x_{\mathbf{q}_6}}\right\rangle - 48\left\langle\frac{\partial H}{\partial T^x_{\mathbf{q}_4}}\right\rangle\left\langle\frac{\partial H}{\partial T^x_{\mathbf{q}_5}}\frac{\partial H}{\partial T^x_{\mathbf{q}_6}}\right\rangle + 60\left\langle\frac{\partial H}{\partial T^x_{\mathbf{q}_4}}\right\rangle\left\langle\frac{\partial H}{\partial T^x_{\mathbf{q}_5}}\right\rangle\right. \\ &\times\left.\left\langle\frac{\partial H}{\partial T^x_{\mathbf{q}_6}}\right\rangle\right] + 15\left\langle\frac{\partial H}{\partial T^x_{\mathbf{q}_1}}\frac{\partial H}{\partial T^x_{\mathbf{q}_2}}\frac{\partial H}{\partial T^x_{\mathbf{q}_3}}\frac{\partial H}{\partial T^x_{\mathbf{q}_4}}\right\rangle\left[\left\langle\frac{\partial H}{\partial T^x_{\mathbf{q}_5}}\frac{\partial H}{\partial T^x_{\mathbf{q}_6}}\right\rangle - 2\left\langle\frac{\partial H}{\partial T^x_{\mathbf{q}_5}}\right\rangle\left\langle\frac{\partial H}{\partial T^x_{\mathbf{q}_6}}\right\rangle\right] + 6\left\langle\frac{\partial H}{\partial T^x_{\mathbf{q}_1}}\right\rangle \\ &\times\left\langle\frac{\partial H}{\partial T^x_{\mathbf{q}_2}}\frac{\partial H}{\partial T^x_{\mathbf{q}_3}}\frac{\partial H}{\partial T^x_{\mathbf{q}_4}}\frac{\partial H}{\partial T^x_{\mathbf{q}_5}}\frac{\partial H}{\partial T^x_{\mathbf{q}_6}}\right\rangle - \left\langle\frac{\partial H}{\partial T^x_{\mathbf{q}_1}}\frac{\partial H}{\partial T^x_{\mathbf{q}_2}}\frac{\partial H}{\partial T^x_{\mathbf{q}_3}}\frac{\partial H}{\partial T^x_{\mathbf{q}_4}}\frac{\partial H}{\partial T^x_{\mathbf{q}_5}}\frac{\partial H}{\partial T^x_{\mathbf{q}_6}}\right\rangle\Bigg\} - \frac{12}{T^4}\frac{\partial^2 H}{\partial T^x_{\mathbf{q}_1}\partial T^x_{\mathbf{q}_2}}\Bigg\{2\left\langle\frac{\partial H}{\partial T^x_{\mathbf{q}_3}}\right\rangle\end{aligned}$$

$$\times \frac{\partial H}{\partial T^x_{\mathbf{q}_4}} \Big\rangle \Big\langle \frac{\partial H}{\partial T^x_{\mathbf{q}_5}} \frac{\partial H}{\partial T^x_{\mathbf{q}_6}} \Big\rangle + 2 \Big\langle \frac{\partial H}{\partial T^x_{\mathbf{q}_3}} \frac{\partial H}{\partial T^x_{\mathbf{q}_4}} \Big\rangle \Big\langle \frac{\partial H}{\partial T^x_{\mathbf{q}_5}} \frac{\partial H}{\partial T^x_{\mathbf{q}_6}} \Big\rangle + \Big\langle \frac{\partial H}{\partial T^x_{\mathbf{q}_3}} \Big\rangle \Big\langle \frac{\partial H}{\partial T^x_{\mathbf{q}_4}} \frac{\partial H}{\partial T^x_{\mathbf{q}_5}} \frac{\partial H}{\partial T^x_{\mathbf{q}_6}} \Big\rangle \Big\}$$

$$+ \frac{12}{T^3} \frac{\partial^2 H}{\partial T^x_{\mathbf{q}_1} \partial T^x_{\mathbf{q}_2}} \frac{\partial^2 H}{\partial T^x_{\mathbf{q}_3} \partial T^x_{\mathbf{q}_4}} \Big\{ \Big\langle \frac{\partial H}{\partial T^x_{\mathbf{q}_5}} \frac{\partial H}{\partial T^x_{\mathbf{q}_6}} \Big\rangle + 2 \Big\langle \frac{\partial H}{\partial T^x_{\mathbf{q}_5}} \Big\rangle \Big\langle \frac{\partial H}{\partial T^x_{\mathbf{q}_6}} \Big\rangle \Big\}. \tag{C1}$$

Note that we are allowed to permute the momenta $\mathbf{q}_1, \ldots, \mathbf{q}_6$, since these are summed over in the free energy expansion. Assuming vanishing odd-order correlators and imposing that m is a scalar field gives

$$\frac{\partial^6 F}{\partial T^x_{\mathbf{q}_1} \partial T^x_{\mathbf{q}_2} \partial T^x_{\mathbf{q}_3} \partial T^x_{\mathbf{q}_4} \partial T^x_{\mathbf{q}_5} \partial T^x_{\mathbf{q}_6}} = \frac{Q^y_{-\mathbf{q}_1} Q^y_{-\mathbf{q}_2} Q^y_{-\mathbf{q}_3} Q^y_{-\mathbf{q}_4} Q^y_{-\mathbf{q}_5} Q^y_{-\mathbf{q}_6} V_{\mathbf{q}_1} V_{\mathbf{q}_2} V_{\mathbf{q}_3} V_{\mathbf{q}_4}}{N^4 T^3} \Big\{ 12 \langle m_{-\mathbf{q}_1} m_{-\mathbf{q}_2} \rangle \Big[1 - \frac{2 V_{\mathbf{q}_5}}{NT} \langle m_{-\mathbf{q}_3} m_{-\mathbf{q}_4} \rangle \Big]$$

$$\times \delta_{\mathbf{q}_1+\mathbf{q}_2,0} \delta_{\mathbf{q}_3+\mathbf{q}_4,0} \delta_{\mathbf{q}_5+\mathbf{q}_6,0} - \frac{V_{\mathbf{q}_5} V_{\mathbf{q}_6}}{N^2 T^2} \Big[\langle m_{-\mathbf{q}_1} m_{-\mathbf{q}_2} m_{-\mathbf{q}_3} m_{-\mathbf{q}_4} m_{-\mathbf{q}_5} m_{-\mathbf{q}_6} \rangle \delta_{\mathbf{q}_1+\mathbf{q}_2+\mathbf{q}_3+\mathbf{q}_4+\mathbf{q}_5+\mathbf{q}_6,0}$$

$$- 3 \langle m_{-\mathbf{q}_1} m_{-\mathbf{q}_2} \rangle \delta_{\mathbf{q}_1+\mathbf{q}_2,0} (5 \langle m_{-\mathbf{q}_3} m_{-\mathbf{q}_4} m_{-\mathbf{q}_5} m_{-\mathbf{q}_6} \rangle \delta_{\mathbf{q}_3+\mathbf{q}_4+\mathbf{q}_5+\mathbf{q}_6,0} - 6 \langle m_{-\mathbf{q}_3} m_{-\mathbf{q}_4} \rangle$$

$$\times \langle m_{-\mathbf{q}_5} m_{-\mathbf{q}_6} \rangle \delta_{\mathbf{q}_3+\mathbf{q}_4,0} \delta_{\mathbf{q}_5+\mathbf{q}_6,0}) \Big] \Big\}. \tag{C2}$$

*E-mail address: kjetil.borkje@phys.ntnu.no
†E-mail address: steinar.kragset@phys.ntnu.no
‡E-mail address: asle.sudbo@phys.ntnu.no

[1] I. Affleck and J. B. Marston, Phys. Rev. B **39**, 11538 (1989).
[2] G. Baskaran and P. W. Anderson, Phys. Rev. B **37**, 580 (1988).
[3] I. Affleck, Z. Zou, T. Hsu, and P. W. Anderson, Phys. Rev. B **38**, 745 (1988); Z. Zou and P. W. Anderson, *ibid.* **37**, 627 (1988).
[4] E. Dagotto, E. Fradkin, and A. Moreo, Phys. Rev. B **38**, 2926 (1988).
[5] L. B. Ioffe and A. I. Larkin, Phys. Rev. B **39**, 8988 (1989).
[6] N. Nagaosa and P. A. Lee, Phys. Rev. B **61**, 9166 (2000).
[7] G. Mudry and E. Fradkin, Phys. Rev. B **49**, 5200 (1994); **50**, 11 409 (1994).
[8] I. Ichinose and T. Matsui, Phys. Rev. B **51**, 11 860 (1995); I. Ichinose, T. Matsui, and M. Onoda, *ibid.* **64**, 104516 (2001).
[9] D. K. K. Lee and Y. Chen, J. Phys. A **21**, 4155 (1988).
[10] T. Senthil and M. P. A. Fisher, Phys. Rev. B **62**, 7850 (2000).
[11] A. M. Polyakov, Nucl. Phys. B **120**, 429 (1977).
[12] J. M. Kosterlitz, J. Phys. C **10**, 1046 (1977).
[13] I. F. Herbut and Z. Tešanović, Phys. Rev. Lett. **76**, 4588 (1996).
[14] H. Kleinert, F. S. Nogueira, and A. Sudbø, Phys. Rev. Lett. **88**, 232001 (2002); Nucl. Phys. B **666**, 361 (2003).
[15] M. Hermele, T. Senthil, M. P. A. Fisher, P. A. Lee, N. Nagaosa, and X.-G. Wen, cond-mat/0404751 (unpublished).
[16] I. F. Herbut and B. H. Seradjeh, Phys. Rev. Lett. **91**, 171601 (2003); I. F. Herbut, B. H. Seradjeh, S. Sachdev, and G. Murthy, Phys. Rev. B **68**, 195110 (2003); M. J. Case, B. H. Seradjeh, and I. F. Herbut, Nucl. Phys. B **676**, 572 (2004).
[17] M. N. Chernodub, E.-M. Ilgenfritz, and A. Schiller, Phys. Lett. B **547**, 269 (2002); **555**, 206 (2003).
[18] S. Kragset, F. S. Nogueira, and A. Sudbø, Phys. Rev. Lett. **92**, 186403 (2004).
[19] D. R. Nelson and J. M. Kosterlitz, Phys. Rev. Lett. **39**, 1201 (1977); P. Minnhagen and G. G. Warren, Phys. Rev. B **24**, 2526 (1981).
[20] P. Minnhagen and B. J. Kim, Phys. Rev. B **67**, 172509 (2003).
[21] A. M. Ferrenberg and R. H. Swendsen, Phys. Rev. Lett. **61**, 2635 (1988); , **63**, 1195 (1989).
[22] J. M. Kosterlitz and D. J. Thouless, J. Phys. C **6**, 1181 (1973).
[23] H. A. Fertig and J. P. Straley, Phys. Rev. B **66**, 201402(R) (2002); H. A. Fertig, Phys. Rev. Lett. **89**, 035703 (2002).
[24] P. Olsson (private communication).
[25] J. M. Kosterlitz, J. Phys. C **10**, 3753 (1977).
[26] P. Minnhagen, Phys. Rev. B **32**, 3088 (1985).

Article IV

Effective theory of fluctuating orbital currents in high-T_c cuprates

preprint (2007)

Effective theory of fluctuating orbital currents in high-T_c cuprates

Kjetil Børkje[1] and Asle Sudbø[1]

[1]*Department of Physics, Norwegian University of Science and Technology, N-7491 Trondheim, Norway*

(Dated: Received January 6, 2008)

We derive an effective dissipative quantum field theory for fluctuating orbital currents in clean CuO_2 sheets of high-T_c cuprates, based on a three-band model. The Coulomb repulsion term between Cu- and O-sites is decoupled in terms of current operators representing horizontal and vertical parts of circulating currents within each CuO_2 unit cell of the lattice. The model has ordering of currents at finite temperatures. The dissipative kernel in the model is of the form $|\omega|/|\mathbf{q}|$, indicating Landau damping. Applications of the effective theory to other models are also discussed.

PACS numbers: 74.20.Rp, 74.50.+r, 74.20.-z

Constructing an effective description of the long-wavelength and low-energy physics of high-T_c superconducting cuprates represents a profound and formidable problem in physics. Such a description must be consistent with experimental observations of several anomalous normal state properties of these systems. Varma has recently proposed that quantum critical fluctuations associated with the breakup of a subtle order, involving circulating currents, could induce the observed anomalous normal state properties of high-T_c superconductors [1]. Essentially, the associated quantum critical fluctuations are suggested to produce a fluctuation spectrum resulting in a Marginal Fermi Liquid [2]. Recently, such a spectrum has been derived from a conjectured effective field theory of circulating currents [3].

The particular form of proposed order involves circulating currents within a CuO_2 unit cell where the currents run horizontally and vertically through a Cu site and close by *direct hopping between O orbitals*, as in Fig. 1. Three other equivalent patterns may be found by reversing the direction of the current through each Cu-site in the horizontal and vertical directions. This results in a pattern of *staggered* orbital

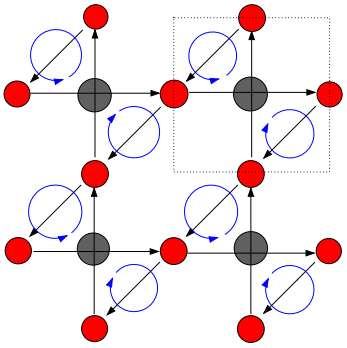

FIG. 1: (Color online) The circulating current phase Θ_{II} [1]. Cu sites are grey circles, O sites are red. The unit cell is shown by the dashed square. A staggered magnetic moment pattern within each unit cell that repeats from unit cell to unit cell (the curl of the blue directed circles) is indicated.

magnetic moments within each unit cell, such that the pattern repeats from unit cell to unit cell. A magnetic intensity of the type associated with the above orbital magnetism has recently been reported [4]. Since no obvious thermodynamic singularities have so far been reported at the pseudogap-line in the cuprates, it is important to investigate whether or not the proposed models for this novel type of order imply the presence or absence of prominent signals in such quantities as specific heat or (indirectly) magnetization. Other staggered orbital magnetic patterns have also been proposed, most notably the extension of the staggered flux phase [5] to finite doping [6].

We derive an effective quantum field theory for fluctuating orbital currents from a microscopic description of clean CuO_2 planes. We are primarily interested in investigating the intrinsic effects such fluctuations have on the physics of the cuprates. We therefore neglect disorder, as was also done in Ref. 3. With ever improving sample quality, we expect that the effective theory we derive should be useful. The starting point is the three-band model $H = \sum_{\mathbf{r},\sigma} \varepsilon_d d^\dagger_{\mathbf{r},\sigma} d_{\mathbf{r},\sigma} + K_{pd} + K_{pp} + H^{(1)}_{\rm int} + H^{(2)}_{\rm int}$, where $K_{pd} = t_{pd} \sum_{\mathbf{r},\sigma} [d^\dagger_{\mathbf{r},\sigma}(p_{x,\mathbf{r}+\frac{a}{2}\hat{\mathbf{x}},\sigma} - p_{x,\mathbf{r}-\frac{a}{2}\hat{\mathbf{x}},\sigma} - p_{y,\mathbf{r}+\frac{a}{2}\hat{\mathbf{y}},\sigma} + p_{y,\mathbf{r}-\frac{a}{2}\hat{\mathbf{y}},\sigma}) + \text{h.c.}]$, $K_{pp} = -t_{pp} \sum_{\mathbf{r},\sigma} [(p^\dagger_{x,\mathbf{r}+\frac{a}{2}\hat{\mathbf{x}},\sigma} - p^\dagger_{x,\mathbf{r}-\frac{a}{2}\hat{\mathbf{x}},\sigma})(p_{y,\mathbf{r}+\frac{a}{2}\hat{\mathbf{y}},\sigma} - p_{y,\mathbf{r}-\frac{a}{2}\hat{\mathbf{y}},\sigma}) + \text{h.c.}]$ and $H^{(2)}_{\rm int} = V \sum_{\mathbf{r},\sigma,\sigma'} n_{d,\mathbf{r},\sigma}(n_{p_x,\mathbf{r}+\frac{a}{2}\hat{\mathbf{x}},\sigma'} + n_{p_x,\mathbf{r}-\frac{a}{2}\hat{\mathbf{x}},\sigma'} + n_{p_y,\mathbf{r}+\frac{a}{2}\hat{\mathbf{y}},\sigma'} + n_{p_y,\mathbf{r}-\frac{a}{2}\hat{\mathbf{y}},\sigma'})$. We work with electron operators and the vacuum is defined as empty $d_{x^2-y^2}$, p_x and p_y orbitals. The $\mathbf{r}$-sum runs over the Cu-lattice. The Cu-O and O-O hopping is governed by the parameters t_{pd} and t_{pp}, respectively, whereas ε_d is the difference in on-site energy between the copper and oxygen orbitals. The term $H^{(1)}_{\rm int}$ represents on-site repulsion terms, for which we make the crude assumption that their effect is to merely renormalize the hopping parameters $t_{pd} \to \bar{t}_{pd} = |x| t_{pd}$, $t_{pp} \to \bar{t}_{pp} = |x| t_{pp}$, where $|x|$ is the deviation from half-filling [1]. We also assume the O-O repulsion to be small. Hence, we only consider explicitly $H^{(2)}_{\rm int}$, the Cu-O-repulsion.

The interaction-term $H^{(2)}_{\rm int}$ can be decoupled [7] in terms of bosonic fields coupling to the bilinear fermion operators $A^{(i)}_{\mathbf{q},\sigma,\sigma'} \equiv N^{-1/2} \sum_{\mathbf{k}} (a^{(i)}_{x,\mathbf{k}-\mathbf{q}} p^\dagger_{x,\mathbf{k}-\mathbf{q},\sigma'} + a^{(i)}_{y,\mathbf{k}-\mathbf{q}} p^\dagger_{y,\mathbf{k}-\mathbf{q},\sigma'}) d_{\mathbf{k},\sigma}$ with $i = 1,..,4$ [1]. Here, N is the number of Cu lattice sites. We define $a^{(1)}_{x,\mathbf{k}} = a^{(2)}_{x,\mathbf{k}} =$

$\sin(k_x a/2) \equiv s_{x,k}$, $a^{(3)}_{x,\mathbf{k}} = a^{(4)}_{x,\mathbf{k}} = \cos(k_x a/2) \equiv c_{x,k}$ and $a^{(1)}_{y,\mathbf{k}} = -a^{(2)}_{y,\mathbf{k}} = s_{y,k}$, $a^{(3)}_{y,\mathbf{k}} = -a^{(4)}_{y,\mathbf{k}} = c_{y,k}$, where a is the Cu-Cu lattice constant. A discussion of $\langle A^{(i)}_{0,\sigma,\sigma'}\rangle$ as translational invariant order parameters in the cuprates is found in [1]. While $i = 2$ transforms as the kinetic energy, $i = 1$ and $i = 3, 4$ *give rise to different current patterns*. Since the observed magnetic signal [4] is consistent with the current patterns of $i = 3, 4$, we keep only this in what follows. An effective model for the $i = 1$-part was considered in [8]. Observe the relation $N^{-1/2}\sum_{\mathbf{k}} c_{x,k-q} p^\dagger_{x,\mathbf{k}-\mathbf{q},\sigma'} d_{\mathbf{k},\sigma} = 1/4\left(\kappa^x_{\mathbf{q},\sigma,\sigma'} + i j^x_{\mathbf{q},\sigma,\sigma'}\right)$, where, in real space,

$$j^x_{\mathbf{r},\sigma,\sigma'} \equiv \frac{i}{2}\left[d^\dagger_{\mathbf{r},\sigma}\left(p_{x,\mathbf{r}+\frac{a}{2}\hat{\mathbf{x}},\sigma'} + p_{x,\mathbf{r}-\frac{a}{2}\hat{\mathbf{x}},\sigma'}\right) - \text{h.c.}\right]. \quad (1)$$

In a unit cell centered on Cu, this is proportional to the current from the left oxygen to the copper *plus* the current from copper to the right oxygen. We define $j^y_{\mathbf{r},\sigma,\sigma'}$ in the same way, but with a minus sign due to the d-wave symmetry of the Cu-orbital. Finite expectation values of $\kappa^{x(y)}_{\mathbf{r},\sigma,\sigma'}$ would correspond to Landau-Pomeranchuk instabilites, believed not to be relevant in the cuprates. Thus, we retain only the decoupling fields that correspond to spin diagonal expectation values of the operators $j^{x(y)}_{\mathbf{r},\sigma,\sigma'}(\tau)$, since $\langle j^{x(y)}_{\mathbf{r},\sigma,\sigma}(\tau)\rangle \neq 0$ in the current pattern depicted in Fig. 1. The fields retained, $J^{x(y)}_{\mathbf{r}}(\tau)$, are real and $\langle J^{x(y)}_{\mathbf{r}}(\tau)\rangle = V\langle j^{x(y)}_{\mathbf{r},\sigma,\sigma'}(\tau)\rangle\delta_{\sigma,\sigma'}$, *i.e.* the fields represent charge currents on horizontal and vertical O-Cu-O-links. The fields $J^{x(y)}_{\mathbf{r}}(\tau)$ and the fermions are coupled by particle-hole excitations of the form $i\sum_{\mathbf{k},\mathbf{q},\sigma}\left(J^x_{-\mathbf{q}} c_{x,k-q}\, p^\dagger_{x,\mathbf{k}-\mathbf{q},\sigma} d_{\mathbf{k},\sigma} - (x \to y) - \text{h.c.}\right)$, where the time dependence was omitted. It is important to keep in mind that the bosonic fields $J^{x(y)}_{\mathbf{r}}(\tau)$ transform as vectors under a change of coordinate system. Note that we could also have chosen the arguments of the $a^{(i)}$'s to be $\mathbf{k}$ and not $\mathbf{k}-\mathbf{q}$ in $A^{(i)}_{\mathbf{q},\sigma,\sigma'}$, corresponding to a decoupling in terms of currents defined on horizontal and vertical Cu-O-Cu-links.

Integrating out the fermion fields, we obtain the partition function as $Z = \int DJ^x DJ^y\ e^{-S}$, where the effective action is given by $S = \frac{1}{2V}\sum_{\mathbf{q},\omega_\nu}\left[J^x_{\mathbf{q}}(i\omega_\nu)J^x_{-\mathbf{q}}(-i\omega_\nu) + J^y_{\mathbf{q}}(i\omega_\nu)J^y_{-\mathbf{q}}(-i\omega_\nu)\right] - \text{Tr}\ln\left[\mathcal{G}_0^{-1} + \Sigma\right]$. Using the gauge transformation $p_{x,\mathbf{k},\sigma} \to i p_{x,\mathbf{k},\sigma}$, $p_{y,\mathbf{k},\sigma} \to -i p_{y,\mathbf{k},\sigma}$, we have

$$\mathcal{G}^{-1}_{0,\mathbf{k}_1\mathbf{k}_2,\sigma_1\sigma_2}(i\omega_{n_1}, i\omega_{n_2}) = \delta_{\mathbf{k}_1,\mathbf{k}_2}\delta_{n_1,n_2}\delta_{\sigma_1,\sigma_2}\begin{pmatrix} -i\omega_{n_1} + \varepsilon_d - \mu & 2t_{pd}s_{x,k_1} & 2t_{pd}s_{y,k_1} \\ 2t_{pd}s_{x,k_1} & -i\omega_{n_1} - \mu & 4t_{pp}s_{x,k_1}s_{y,k_1} \\ 2t_{pd}s_{y,k_1} & 4t_{pp}s_{x,k_1}s_{y,k_1} & -i\omega_{n_1} - \mu \end{pmatrix}, \quad (2)$$

$$\Sigma_{\mathbf{k}_1\mathbf{k}_2,\sigma_1\sigma_2}(i\omega_{n_1}, i\omega_{n_2}) = \frac{\delta_{\sigma_1,\sigma_2}}{\sqrt{\beta N}}\begin{pmatrix} 0 & c_{x,k_2}J^x_{\mathbf{k}_{12}}(i\omega_{12}) & c_{y,k_2}J^y_{\mathbf{k}_{12}}(i\omega_{12}) \\ c_{x,k_1}J^x_{\mathbf{k}_{12}}(i\omega_{12}) & 0 & 0 \\ c_{y,k_1}J^y_{\mathbf{k}_{12}}(i\omega_{12}) & 0 & 0 \end{pmatrix}, \quad (3)$$

where we have defined $\mathbf{k}_{12} \equiv \mathbf{k}_1 - \mathbf{k}_2$ and $\omega_{12} \equiv \omega_{n_1} - \omega_{n_2}$. For $t_{pp} = 0$, the non-interacting part of the problem $\mathcal{G}_0^{-1}$ may easily be diagonalized into three quasiparticle bands $E^{(0)}_{\mathbf{k}} = 0, E^{(\pm)}_{\mathbf{k}} = \varepsilon_d/2 \pm \sqrt{(\varepsilon_d/2)^2 + 4t^2_{pd}(s^2_{x,k} + s^2_{y,k})}$, of which $E^{(0)}_{\mathbf{k}}, E^{(-)}_{\mathbf{k}}$ are full and $E^{(+)}_{\mathbf{k}}$ is partially filled. This picture is not qualitatively altered by $t_{pp} \neq 0$. A nonzero value of t_{pp} is however vital for the realization of the current pattern. It is implicit that $\langle J^{x(y)}_{\mathbf{r}}(\tau)\rangle \to 0$ when $t_{pp} \to 0$ [1].

Expanding the last term [9], odd powers of J vanish, such that $\text{Tr}\ln\left[\mathcal{G}_0^{-1} + \Sigma\right] = \text{Tr}\ln\mathcal{G}_0^{-1} - \frac{1}{2}\text{Tr}\left[\mathcal{G}_0\Sigma\right]^2 + \mathcal{O}(J^4)$, where $-\text{Tr}\ln\mathcal{G}_0^{-1}$ gives the free energy of the non-interacting system, and Σ involves the fluctuating fields J^x and J^y. To second order in the fields $J^{x(y)}$ and in space and imaginary time gradients, we have derived a quantum dissipative effective action $S = S_{\text{C}} + S_{\text{Q}}$, where

$$\begin{aligned} S_{\text{C}} &= \sum_{\mathbf{q},\omega_\nu}\sum_{i,j=x,y} G^{-1}_{\text{C},ij}\, J^i_{\mathbf{q}}(i\omega_\nu)J^j_{-\mathbf{q}}(-i\omega_\nu), \\ S_{\text{Q}} &= \sum_{\mathbf{q},\omega_\nu}\sum_{i,j=x,y} G^{-1}_{\text{Q},ij}\, J^i_{\mathbf{q}}(i\omega_\nu)J^j_{-\mathbf{q}}(-i\omega_\nu), \end{aligned} \quad (4)$$

with $G^{-1}_{\text{C},xx} = \alpha_c + \alpha_l\, q_x^2 + \alpha_t\, q_y^2$, $G^{-1}_{\text{C},yy} = \alpha_c + \alpha_l\, q_y^2 + \alpha_t\, q_x^2$, $G^{-1}_{\text{C},xy} = G^{-1}_{\text{C},yx} = \alpha_{xy}\, q_x q_y$, $G^{-1}_{\text{Q},xx} = \alpha_0\,\omega_\nu^2 + \alpha_d\frac{|\omega_\nu|}{|\mathbf{q}|}\hat{q}_y^2$, $G^{-1}_{\text{Q},yy} = \alpha_0\,\omega_\nu^2 + \alpha_d\frac{|\omega_\nu|}{|\mathbf{q}|}\hat{q}_x^2$ and $G^{-1}_{\text{Q},xy} = G^{-1}_{\text{Q},yx} = -\alpha_d\frac{|\omega_\nu|}{|\mathbf{q}|}\hat{q}_x\hat{q}_y$. Here, $\hat{q}_x = q_x/|\mathbf{q}|$. The dissipation kernel is valid for $|\omega_\nu|/|\mathbf{q}| \ll 1$. The limit $|\omega_\nu|/|\mathbf{q}| \gg 1$ does not contribute to dissipation. The explicit expressions for the coefficients α_i are unwieldy and of limited use. The equality of the diagonal and off-diagonal dissipation coefficients is only correct when $t_{pp} = 0$. Changes when $t_{pp} \neq 0$ are small and unimportant, and are neglected in the following. Note also that this theory might not be applicable to the ordered phase, since the Fermi surface is proposed to be gapped there [1].

However, it is the fluctuation spectrum in the disordered phase which is important in connection with the Marginal Fermi Liquid hypothesis [2].

We have divided the action into a classical (C) and a quantum (Q) part. At finite temperatures, only the classical piece of the action $S_{\rm C}$ needs to be considered as far as critical properties are concerned. The excitation energies of the eigenmodes of $S_{\rm C}$ are given by $\lambda_\pm = \alpha_c + (\alpha_l + \alpha_t)\, q^2/2 \pm \sqrt{(\Delta\alpha)^2 q^4 + \gamma q_x^2 q_y^2}$, where $\Delta\alpha = (\alpha_l - \alpha_t)/2$, and $\gamma = \alpha_{xy}^2 - (2\Delta\alpha)^2$. Hence, for $(\alpha_l, \alpha_t) > 0$, a uniformly ordered state is stable in the classical domain below some critical temperature, provided $\alpha_{xy}^2 < \alpha_l^2 + \alpha_t^2$.

The dissipation kernel essentially gives Landau damping, albeit anisotropic due to the directional nature of the fields. The dissipation is a result of coupling to the gapless particle-hole excitations in the band $E_{\mathbf{k}}^{(+)}$. The singular form $|\omega_\nu|/|\mathbf{q}|$ is correct only if the order in the horizontal and vertical currents are *uniform* and not modulated at some nonzero reciprocal vector. It implies that the dynamical critical exponent $z = 3$ [11]. See however Ref. 9.

Current amplitude fluctuations are expected to be high-energy excitations [1] and will therefore not determine the critical properties of the model. Thus, we treat the fields $J_{\mathbf{r}}^x(\tau)$ and $J_{\mathbf{r}}^y(\tau)$ as *Ising variables*. Reverting to a real space Cu-lattice formulation and setting $a = 1$, we obtain (up to constant terms)

$$S_{\rm C} = -\int_0^\beta d\tau \left[\sum_{\langle \mathbf{r},\mathbf{r}'\rangle} \left(\tilde{\alpha}^x_{\mathbf{r},\mathbf{r}'} J^x_{\mathbf{r}}(\tau) J^x_{\mathbf{r}'}(\tau) + \tilde{\alpha}^y_{\mathbf{r},\mathbf{r}'} J^y_{\mathbf{r}}(\tau) J^y_{\mathbf{r}'}(\tau) \right) + \sum_{\langle\langle \mathbf{r},\mathbf{r}'\rangle\rangle} \tilde{\alpha}^{xy}_{\mathbf{r},\mathbf{r}'} \Big(J^x_{\mathbf{r}}(\tau) J^y_{\mathbf{r}'}(\tau) + J^y_{\mathbf{r}}(\tau) J^x_{\mathbf{r}'}(\tau) \Big) \right], \tag{5}$$

$$S_{\rm Q} = \tilde{\alpha}_0 \int_0^\beta d\tau \sum_{\mathbf{r}} \left[\left(\frac{\partial J^x_{\mathbf{r}}}{\partial \tau} \right)^2 + \left(\frac{\partial J^y_{\mathbf{r}}}{\partial \tau} \right)^2 \right] + \tilde{\alpha}_d \int_0^\beta d\tau\, d\tau' \sum_{\mathbf{r},\mathbf{r}'} \sum_{i,j} \Big(J^i_{\mathbf{r}}(\tau) - J^i_{\mathbf{r}'}(\tau') \Big) \mathbb{K}^{ij}_{\mathbf{r}-\mathbf{r}'}(\tau - \tau') \Big(J^j_{\mathbf{r}}(\tau) - J^j_{\mathbf{r}'}(\tau') \Big).$$

Here, $\langle \mathbf{r}, \mathbf{r}' \rangle$ and $\langle\langle \mathbf{r}, \mathbf{r}' \rangle\rangle$ denote nearest-neighbor and next-nearest-neighbor summations, respectively. For $\mathbf{r} - \mathbf{r}' = \pm\hat{\mathbf{x}}$, $\tilde{\alpha}^x_{\mathbf{r},\mathbf{r}'} = \tilde{\alpha}_l$ and $\tilde{\alpha}^y_{\mathbf{r},\mathbf{r}'} = \tilde{\alpha}_t$, whereas when $\mathbf{r} - \mathbf{r}' = \pm\hat{\mathbf{y}}$, $\tilde{\alpha}^x_{\mathbf{r},\mathbf{r}'} = \tilde{\alpha}_t$ and $\tilde{\alpha}^y_{\mathbf{r},\mathbf{r}'} = \tilde{\alpha}_l$. The parameter $\tilde{\alpha}^{xy}_{\mathbf{r},\mathbf{r}'} = \tilde{\alpha}_{xy}$ when $\mathbf{r} - \mathbf{r}' = \pm(\hat{\mathbf{x}} + \hat{\mathbf{y}})$ and $\tilde{\alpha}^{xy}_{\mathbf{r},\mathbf{r}'} = -\tilde{\alpha}_{xy}$ when $\mathbf{r} - \mathbf{r}' = \pm(\hat{\mathbf{x}} - \hat{\mathbf{y}})$. The coefficient $\tilde{\alpha}_d > 0$ and the positive semidefinite matrix $\mathbb{K}_{\mathbf{r}-\mathbf{r}'}(\tau - \tau') = K_{\mathbf{r}-\mathbf{r}'}(\tau - \tau')\, \hat{\mathbf{g}}_{\mathbf{r}-\mathbf{r}'} \otimes \hat{\mathbf{g}}_{\mathbf{r}-\mathbf{r}'}$, where $\hat{\mathbf{g}}_{\mathbf{r}-\mathbf{r}'} = (\mathbf{r} - \mathbf{r}')/|\mathbf{r} - \mathbf{r}'|$ and $K_{\mathbf{r}}(\tau) = 1/(|\mathbf{r}| \sin^2(\pi\tau/\beta))$. Fluctuations $(J^x_{\mathbf{r}} \to -J^x_{\mathbf{r}}, J^y_{\mathbf{r}} \to J^y_{\mathbf{r}})$ corresponds to going from the depicted current pattern (Fig. 1) to a new one which is obtained by a counterclockwise rotation by $\pi/2$, $(J^x_{\mathbf{r}} \to J^x_{\mathbf{r}}, J^y_{\mathbf{r}} \to -J^y_{\mathbf{r}})$ corresponds to clockwise rotation of $\pi/2$, and $(J^x_{\mathbf{r}} \to -J^x_{\mathbf{r}}, J^y_{\mathbf{r}} \to -J^y_{\mathbf{r}})$ to a rotation of π. It is implied that in the dissipation kernel, we must use a short-distance cutoff in $(\tau, \mathbf{r})$-space, since the expressions are derived in the limit of low $(\omega, \mathbf{q})$.

In general, we have $\tilde{\alpha}_l \neq \tilde{\alpha}_t$. A current living on a horizontal O-Cu-O-link, $J^x_{\mathbf{r}}$, couples to $J^x_{\mathbf{r}\pm\hat{\mathbf{x}}}$ through $\tilde{\alpha}_l$, and to $J^x_{\mathbf{r}\pm\hat{\mathbf{y}}}$ through $\tilde{\alpha}_t$. As seen from Figure 1, there is no reason for these couplings to be similar, and in fact a detailed derivation shows that they are not [13].

At finite temperature, we may ignore the inertial and dissipative terms, which reduces the model to a classical model of two coupled Ising fields. Such a classical model will suffice to study the breakup of the current pattern at finite temperatures, while its quantum critical version can only be accessed via the full dissipative field theory. Note also that the dissipation kernel is *non-local* both in imaginary time and in space. The latter distinguishes this dissipation term from the Caldeira-Leggett type of dissipation appropriate for an array of Josephson junctions [12, 14]. The non-locality in $\mathbf{r}$-space is anisotropic for the same reason as for the nearest-neighbor coupling.

Eq. (5) may be rewritten on the form

$$S_{\rm C} = -\int_0^\beta d\tau \left\{ \sum_{\langle \mathbf{r},\mathbf{r}'\rangle} \Big[\bar{\alpha}\, \cos(\theta_{\mathbf{r},\tau} - \theta_{\mathbf{r}',\tau}) + (\Delta\tilde{\alpha})_{\mathbf{r},\mathbf{r}'}\, \sin(\theta_{\mathbf{r},\tau} + \theta_{\mathbf{r}',\tau}) \Big] + 2 \sum_{\langle\langle \mathbf{r},\mathbf{r}'\rangle\rangle} \tilde{\alpha}^{xy}_{\mathbf{r},\mathbf{r}'}\, \cos(\theta_{\mathbf{r},\tau} + \theta_{\mathbf{r}',\tau}) \right\}, \tag{6}$$

$$S_{\rm Q} = 2\tilde{\alpha}_0 \int_0^\beta d\tau \sum_{\mathbf{r}} \left(\frac{\partial \theta_{\mathbf{r},\tau}}{\partial \tau} \right)^2 + \tilde{\alpha}_d \int_0^\beta d\tau\, d\tau' \sum_{\mathbf{r},\mathbf{r}'} \sum_{i,j} \Big(J^i(\theta_{\mathbf{r},\tau}) - J^i(\theta_{\mathbf{r}',\tau'}) \Big) \mathbb{K}^{ij}_{\mathbf{r}-\mathbf{r}'}(\tau - \tau') \Big(J^j(\theta_{\mathbf{r},\tau}) - J^j(\theta_{\mathbf{r}',\tau'}) \Big),$$

where we have used the parametrization $\cos(\theta_{\mathbf{r},\tau}) = (J^x_{\mathbf{r}}(\tau) + J^y_{\mathbf{r}}(\tau))/2$, $\sin(\theta_{\mathbf{r},\tau}) = (J^x_{\mathbf{r}}(\tau) - J^y_{\mathbf{r}}(\tau))/2$, and

$\theta_{\mathbf{r},\tau} \in (0, \pi/2, \pi, 3\pi/2)$. We have defined $\bar{\alpha} = (\tilde{\alpha}_l + \tilde{\alpha}_t)$, $(\Delta\tilde{\alpha})_{\mathbf{r},\mathbf{r}'} = (\tilde{\alpha}_l - \tilde{\alpha}_t)$ for $\mathbf{r} - \mathbf{r}' = \pm\hat{\mathbf{x}}$ and $(\Delta\tilde{\alpha})_{\mathbf{r},\mathbf{r}'} = -(\tilde{\alpha}_l - \tilde{\alpha}_t)$ for $\mathbf{r} - \mathbf{r}' = \pm\hat{\mathbf{y}}$.

Eqs. (5) and (6) are the main results of this paper. These models describe a phase transition from a disordered bosonic state (a Fermi liquid), into a state with bosonic order in the form of ordered orbital currents.

We next proceed to discuss some qualitative aspects. Consider first this model at finite temperature, where we may use the approximation $S \approx S_{\rm C}$. When $(\tilde{\alpha}_l, \tilde{\alpha}_t) > 0$ and $\tilde{\alpha}_{xy} = 0$, the current pattern in Fig. 1 repeats uniformly from unit cell to unit cell throughout the system in the ordered state. The specific heat has a logarithmic singularity at a critical temperature determined by the condition $\sinh(2\beta_c\tilde{\alpha}_l)\sinh(2\beta_c\tilde{\alpha}_t) = 1$, where $\beta_c = 1/T_c$. Anisotropy in the nearest-neighbor couplings suppresses the critical temperature and critical amplitudes, and narrows the critical region, but does not alter the universality class of the phase transition [15]. When $(\tilde{\alpha}_l, \tilde{\alpha}_t) = 0$ and $\tilde{\alpha}_{xy} \neq 0$, the ground state of the system features a striped phase in the diagonal directions, irrespective of the sign of $\tilde{\alpha}_{xy}$. Note also that when $\mathrm{sign}(\tilde{\alpha}_l) \neq \mathrm{sign}(\tilde{\alpha}_t)$ and $\tilde{\alpha}_{xy} = 0$, one obtains order with a period of twice the lattice constant.

The dissipative term in this model comes from the coupling of the bosonic current fields to particle-hole excitations in the partially filled band $E^{(+)}_{\mathbf{k}}$, *i.e.* an intraband transition. In the above, we defined the currents on horizontal and vertical O-Cu-O-links, living on Cu-sites. We could alternatively have defined the currents on Cu-Cu-links, both in a three-band model and in a one-band model. This definition would be relevant to the study of d-density waves [5, 6]. However, one would expect a different dissipation term in that case, due to the finite modulation vector of the ordered currents. Note also that the ω_ν^2-terms in $S_{\rm Q}$ in Eq. (4), equivalently the inertial terms in Eqs. (5) and (6), are of multiband origin.

The quartic terms in $S_{\rm C}$ that would emerge from the above treatment are of the type $\alpha^{ijlm}_{\mathbf{r}_1\mathbf{r}_2\mathbf{r}_3\mathbf{r}_4} J^i_{\mathbf{r}_1} J^j_{\mathbf{r}_2} J^l_{\mathbf{r}_3} J^m_{\mathbf{r}_4}$. Note that for $i = j = x$, $l = m = y$, these terms include an Ashkin-Teller type of four-spin interaction, used in Ref. 3 to argue that the Ising type of singularity in specific heat would be quenched. $S_{\rm C}$ in Eqs. (5,6) differs from the model of Ref. 3 in several respects. However, a direct comparison is difficult, as it is not clear what physical quantitites the fields in Ref. 3 represent. Firstly, the Ising-exchange coupling terms in Eqs. (5,6) are anisotropic, possibly highly anisotropic, due to the bond-character of the Ising variables. Moreover, the term $\tilde{\alpha}^{xy}_{\mathbf{r},\mathbf{r}'} J^x_{\mathbf{r}} J^y_{\mathbf{r}'}$ in Eqs. (5,6) is absent in Ref. 3. While this term may be perturbatively irrelevant, it is far from clear that $\tilde{\alpha}_{xy}$ is actually small. In addition, there also seems to be a discrepancy between the dissipation kernel $|\omega_\nu|/|\mathbf{q}|$ derived here and the one employed in Ref. 3.

We expect our model to be generically useful in describing thermal and quantum critical fluctuations of directed particle-hole bond variables in fermionic lattice models.

Acknowledgements. This work was supported by the Research Council of Norway Grants No. 158518/431 and No. 158547/431 (NANOMAT), and Grant No. 167498/V30 (STORFORSK). The hospitality of the Center for Advanced Study at The Norwegian Academy of Science and Letters is acknowledged, as well as useful discussions with C. M. Varma and Z. Tesanovic.

[1] C. M. Varma, Phys. Rev. B **73**, 155113 (2006).
[2] C. M. Varma, P. B. Littlewood, S. Schmitt-Rink, E. Abrahams, and A. E. Ruckenstein, Phys. Rev. Lett., **63**, 1996 (1989).
[3] V. Aji and C. M. Varma, Phys. Rev. Lett. **99**, 067003 (2007).
[4] B. Fauque *et al*, Phys. Rev. Lett. **96**, 197001 (2006); H. A. Mook *et al*, Talk at Aspen Center for Physics, August 2007.
[5] I. Affleck and J. B. Marston, Phys. Rev. B **37**, 3774 (1988).
[6] S. Chakravarty, R. B. Laughlin, D. K. Morr, and C. Nayak, Phys. Rev. B **63**, 094503 (2001).
[7] R. L. Stratonovich, Dokl. Akad. Nauk SSSR **2**, 1097 (1957); J. Hubbard, Phys. Rev. Lett., **3**, 77 (1959).
[8] H. C. Lee and H.-Y. Choi, Phys. Rev. B **64**, 094508 (2001).
[9] Note that this procedure [10] of integrating out the fermions and expanding the logarithm in the case of a $|\mathbf{q}| = 0$ order parameter and gapless fermions in general leads to singular coefficients and might not be very suitable for renormalization group analysis. See D. Belitz *et al*, Rev. Mod. Phys. **77**, 579 (2005).
[10] J. A. Hertz, Phys. Rev B **14**, 1165 (1976).
[11] The scaling function for the susceptibility is $\chi(\mathbf{q},\omega) = (Z/T^{(2-\eta)/z})\Phi_\pm\left(\frac{(cq)^z}{T}, \frac{\omega}{T}\right)$, where T is temperature, Z is related to critical amplitudes, z is dynamical critical exponent, and η is the anomalous scaling dimension of the relevant fields. For $z = 3$, the $\mathbf{q}$-dependence of this quantity is weak compared to the ω/T-dependence at low $(\mathbf{q},\omega)$.
[12] A. O. Caldeira and A. J. Leggett, Ann. Phys. (N.Y.) **149**, 374 (1984).
[13] Anisotropy is generic to bond-variables, which, unlike site-variables, have *directionality*. See also A. Melikyan and Z. Tesanovic, Phys. Rev. B **74**, 214511 (2005).
[14] See also P. Werner, K. Völker, M. Troyer, and S. Chakravarty, Phys. Rev. Lett., **94**, 047201 (2005). The dissipative part of the action in this (spatially extended) transverse field Ising-chain is non-local only in time, but local in space, due to the local character of the coupling between the heat-bath oscillators and the Ising spins.
[15] L. Onsager, Phys. Rev. **65**, 117 (1944).